Smart Innovation, Systems and Technologies 191

Roumen Kountchev · Aniket Mahanti · Shen Chong · Srikanta Patnaik · Margarita Favorskaya *Editors*

Advances in Wireless Communications and Applications

Wireless Technology: Intelligent Network Technologies, Smart Services and Applications, Proceedings of 3rd ICWCA 2019

KES International

Springer

Smart Innovation, Systems and Technologies

Volume 191

The Smart Innovation, Systems and Technologies book series encompasses the topics of knowledge, intelligence, innovation and sustainability. The aim of the series is to make available a platform for the publication of books on all aspects of single and multi-disciplinary research on these themes in order to make the latest results available in a readily-accessible form. Volumes on interdisciplinary research combining two or more of these areas is particularly sought.

The series covers systems and paradigms that employ knowledge and intelligence in a broad sense. Its scope is systems having embedded knowledge and intelligence, which may be applied to the solution of world problems in industry, the environment and the community. It also focusses on the knowledge-transfer methodologies and innovation strategies employed to make this happen effectively. The combination of intelligent systems tools and a broad range of applications introduces a need for a synergy of disciplines from science, technology, business and the humanities. The series will include conference proceedings, edited collections, monographs, handbooks, reference books, and other relevant types of book in areas of science and technology where smart systems and technologies can offer innovative solutions.

High quality content is an essential feature for all book proposals accepted for the series. It is expected that editors of all accepted volumes will ensure that contributions are subjected to an appropriate level of reviewing process and adhere to KES quality principles.

**** Indexing: The books of this series are submitted to ISI Proceedings, EI-Compendex, SCOPUS, Google Scholar and Springerlink ****

More information about this series at http://www.springer.com/series/8767

Roumen Kountchev · Aniket Mahanti ·
Shen Chong · Srikanta Patnaik ·
Margarita Favorskaya
Editors

Advances in Wireless Communications and Applications

Wireless Technology: Intelligent Network Technologies, Smart Services and Applications, Proceedings of 3rd ICWCA 2019

Springer

Editors
Roumen Kountchev
Department of Radio Communications
and Video Technologies
Technical University
Sofia, Bulgaria

Shen Chong
College of Information Science
and Technology
Hainan University
Haikou, China

Margarita Favorskaya
University of Science
and Technology
Moscow, Russia

Aniket Mahanti
Department of Computer Science
University of Auckland
Auckland, New Zealand

Srikanta Patnaik
School of Computer Science
and Engineering
SOA University
Bhubaneswar, Odisha, India

ISSN 2190-3018 ISSN 2190-3026 (electronic)
Smart Innovation, Systems and Technologies
ISBN 978-981-15-5878-8 ISBN 978-981-15-5879-5 (eBook)
https://doi.org/10.1007/978-981-15-5879-5

This Springer imprint is published by the registered company Springer Nature Singapore Pte Ltd.
The registered company address is: 152 Beach Road, #21-01/04 Gateway East, Singapore 189721, Singapore

Preface

The fast development of contemporary computers, machine learning, and artificial intelligence opened new horizons and possibilities for the accomplishment of the related methods, algorithms, and network technologies. The major part of the development of these technologies takes intelligent wireless communications, smart services, and the new applications. The papers in Volume 2 of the Proceedings were presented at the **3rd International Conference on Wireless Communications and Applications (ICWCA)** on December 21–23 (2019) in Haikou, Hainan, China. Focusing on applications of the latest smart theories and approaches, and the recent advances in the field, they cover topics such as OFDM and multi-carrier techniques; smart antenna and space-time signal processing; MIMO, multi-user MIMO, and massive MIMO; modulation, coding, and diversity techniques; dynamic spectrum access and cognitive radio; interference management and radio resource allocation; equalization techniques; synchronization, estimation, and detection techniques; and wireless multiple access (e.g., CDMA, OFDMA, NOMA).

Volume 2 "**Devices, Systems and Applications**" of the Proceedings comprises 28 chapters, which could be separated into the following three groups:

First group: Chapters 1–12. These chapters comprise investigations related to the development of new systems, technologies, and applications of the contemporary wireless communication networks as follows: application of 5G communication technology in CATV access network; an overlapping architecture of large-size wide-body aircraft based on cloud sea computing in 5G open grid computing environment; influence of inter-symbol interference for high mobility adaptive OFDM systems in fading channel; performance of low-density parity check codes in 5G communication system; space vector pulse width modulation technology of current source inverter; test method for 5G massive MIMO devices: plane wave generator with planar array antenna; feedback heading control for autonomous underwater vehicle based on reduced-order observer; influence on band gap overlap and Q-factor of the coaxial Bragg structure with double-sinusoidal ripples operating at 0.35 THz; design and implementation of a classic literature reading assist system based on android; vehicular ad hoc networks connectivity strategy in urban scene; analysis of multiple primary users cognitive

radio non-orthogonal multiple access (CR-NOMA) networks under partial relay selection and physical layer security of NOMA system with passive eavesdropping.

Second group: Chapters 13–22. There are various aspects of the design of devices and systems for wireless digital communications and their applications investigated and analyzed: intelligent algorithm which detects compensation capacitor failure; jamming-assisted proactive eavesdropping in decode-and-forward relaying systems; determination of membership degree in risk assessment of transportation process; online monitoring system for the amusement equipment based on wireless sensor network ZigBee; design of intelligent quantitative sealing device based on Internet of things (IoT) technology; analysis on construction and application of special emergency communication systems in the industry; virtual reality platform construction of intangible cultural heritage of Li nationality in Hainan; design of control system for reinforcing bar thread processing equipment; simulation of applying superconducting receiving technology to satellite payload and Python teaching and practice from the perspective of computational ecology.

Third group: Chapters 23–28. In these chapters, investigations are included on various wireless communication devices, systems, and services as follows: detection of compromised devices based on alert logs in the smart grid; design and realization of trunk amplifier at 2.5–2.6 GHz; automated home safety through IoT; study of Sanya tourism income based on fuzzy time series forecasting model; in-time private cloud mobile app-based announcement portal; a Hong Kong case study with broad application for academic, commerce, government, and development and application of multi-functional intelligent robot motion chassis.

All chapters of the proceedings were reviewed and passed the plagiarism check. The editors express their deep gratitude to IRNet for the excellent organization, coordination, and support. Also, we thank the sponsors, the members of the Organizing Committee, the members of the International Program Committee of ICWCA 2019, and all authors for their efforts for the preparation of the proceedings for publishing. We want to express our deepest gratitude to Springer excellent team for their support and expertise, which did the publishing of the book possible.

The book will be useful for researchers, university students (BSc and MSc), PhD students, and lecturers, working in the area of the contemporary wireless communication networks and their applications.

Sofia, Bulgaria — Roumen Kountchev
Auckland, New Zealand — Aniket Mahanti
Haikou, China — Shen Chong
Bhubaneswar, India — Srikanta Patnaik
Krasnoyarsk, Russian Federation — Margarita Favorskaya

Contents

Research and Application of 5G Communication Technology in CATV Access Network 1
Xinyuan Zheng, Xiaohua He, and Yanhua Zhang

An Overlapping Architecture of Large-Size Wide-Body Aircraft Based on Cloud Sea Computing in 5G OGCE 7
Zhi Lü, Mingzhe Yuan, Yi Lü, and Zhongfeng Wang

The Influence of ICI for High Mobility Adaptive OFDM Systems in Nakagami-M Fading Channel 15
Xiuyan Zhang and Qiming Sun

Research on the Performance of LDPC Codes in 5G Communication System 25
Sai Li, Lin Zhou, Shuying Zhang, Chen Chen, Yuqing Fu, and Yucheng He

Research on SVPWM Modulation Technology of Current-Source Inverter 33
Wang Shuaiyi, Qu Yaojun, Zhang Lei, Li Chaochao, Song Yanxia, Kanae Shunshoku, and Bai Jing

A New Test Method for 5G Massive MIMO Devices: Plane Wave Generator with 36 Planar Array Antenna 39
Yu Zhang, Xiang Wu, Xiang Zhang, Yuxin Ren, Chong Pan, and Guiming Wei

Feedback Heading Control for Autonomous Underwater Vehicle Based on Reduced-Order Observer 47
Xiangrong Zhou and Fengzhen Chen

Influence on Band-Gap Overlap and *Q*-Factor of the Coaxial Bragg Structure with Double-Sinusoidal Ripples Operating at 0.35 THz Frequency 55
Xue-Yong Ding, Hong-Rui Su, Yuan Wang, and Lian-Sheng Wang

The Design and Implementation of a Literature Reading-Assist System Based on Android 63
Chang Han, Hui Zhang, Jianfeng Hou, Zihang Zhao, and Yushuang Sui

Research on VANETs Connectivity Strategy in Urban Scene 75
Li Wen Xu and Li Juan Qiao

Performance Analysis of Multiple Primary Users CR-NOMA Networks Under Partial Relay Selection 85
Yuhang Qiao, Yucheng He, Liangmei Zhang, Jianquan Yang, and Lin Zhou

Research on Physical Layer Security of NOMA System with Passive Eavesdropping 93
XiaoHua Lu, Yucheng He, Liangmei Zhang, Jianquan Yang, and Lin Zhou

Intelligent Algorithm Detects Compensation Capacitor Failure 101
Shunran Xue, Dongfeng Xing, Guangwu Chen, Jianqiang Shi, and Yongbo Si

Jamming-Assisted Proactive Eavesdropping in Decode-And-Forward Relaying Systems 111
Yukai Fang, Yucheng He, Liangmei Zhang, Jianquan Yang, and Lin Zhou

Determination of Membership Degree in Risk Assessment of Transportation Process 119
Chaozhou Chen, Guofang Wu, and Guoliang Dong

Online Monitoring System for the Amusement Equipment Based on Wireless Sensor Network ZigBee 127
Jin-e Wang and Lechen Sun

Design of Intelligent Seasoning Quantitative Device Based on Internet of Things Technology 135
Yi Liu, Danhong Chen, Qibing Yan, and Qiuya Song

Analysis on Construction and Application of the Special Emergency Communication Systems in the Industries 143
Haitao Wang, Lihua Song, Jun Liu, and Lijun Liu

Research on the VR Platform Construction of Intangible Cultural Heritage of Li Nationality in Hainan 153
Xi Deng

Design of Control System for Reinforcing Bar Thread Processing Equipment 163
Hongyu Wang and Huijun Sun

Simulation Experiment Research of Applying Superconducting Receiving Technology to Satellite Payload 171
Jun Zhi, Wei Ji, Yu- Dong Pei, and Shan Huang

Python Teaching Research and Practice from the Perspective of Computational Ecology 177
Lina Wang and Ying Ren

Detection of Compromised Devices Based on Alert Logs in Smart Grid 183
Zhengping Jin, Ye Liang, Yifan Zhou, Xueqi Jin, Piaohong Kong, Zhengwei Jiang, and Lisong Shao

Design and Realization of Trunk Amplifier at 2.5–2.6 GHz 195
Shiwen Li and Licong Li

Automated Home Safety Through IoT 205
Sangam Malla, Prabhat Kumar Sahu, Priyam Patnaik, and Srikanta Patnaik

The Forecast Study of Sanya Tourism Income Based on Fuzzy Time Series Forecasting Model F5 213
Wang Haifeng, Hu Yaqi, Li Jinxia, and Wang Hongxu

A Just-In-Time Private-Cloud Mobile-App-Based Announcement Portal (AP): A Hong Kong Case Study with Broad Application for Academic, Commerce, Government 221
Brian Siu

Development and Application of Multi-functional Intelligent Robot Motion Chassis 229
Sun Hao, Liu Yongcheng, Ma Xiaolin, Wang Jing, Wang Mingrui, Chen Tao, and Wang Chao

About the Editors

Prof. Roumen Kountchev, D.Sc., serves at the Faculty of Telecommunications, Department of Radio Communications and Video Technologies, Technical University of Sofia, Bulgaria. He has over 300 papers published in magazines and conference proceedings, 15 books, 46 book chapters, and 20 patents to his credit. He is or has been a member of the Euro Mediterranean Academy of Arts and Sciences; President of the Bulgarian Association for Pattern Recognition; editorial board member of IJBST Journal Group; and an editorial board member of the International Journal of Reasoning-based Intelligent Systems and the International Journal of Broad Research in Artificial Intelligence and Neuroscience.

Dr. Aniket Mahanti is a Senior Lecturer in Computer Science at the University of Auckland, New Zealand. Holding a Ph.D. in Computer Science from the University of Calgary, Dr. Aniket has published over 40 papers in reputed peer-reviewed journals, book chapters, and conference proceedings. Dr. Aniket has more than 15 years of technical experience in the areas of information technology, computer networks, and Internet systems.

Prof. Shen Chong, D.Sc., is Deputy Director of Hainan University Scientific Research Office, China. Holding degrees from the School of Electronic Information of Wuhan University and the University of Strathclyde, he also has 23 patents and has published more than 100 SCI and EI indexed papers. He was the PI of projects funded by the National Natural Science Foundation, Ministry of Education, International Science and Technology Cooperation, etc.

Prof. Srikanta Patnaik serves at the Department of Computer Science and Engineering, Faculty of Engineering and Technology, SOA University, Bhubaneswar, India. He has published over 100 papers in international journals and conference proceedings, 2 textbooks, and 32 edited volumes, and is Editor-in-Chief of the International Journal of Information and Communication Technology, International Journal of Computational Vision and Robotics, and the following book series: Modeling and Optimization in Science and Technology (Springer),

Advances in Computer and Electrical Engineering, and Advances in Medical Technologies and Clinical Practices (IGI-Global).

Prof. Margarita Favorskaya is Head of the Department of Informatics and Computer Techniques at Reshetnev Siberian State University of Science and Technology. She serves as a book editor for Springer; as a reviewer for numerous journals, including Neurocomputing, Knowledge Engineering and Soft Data Paradigms, and Pattern Recognition Letters; and as an Associate Editor for e.g. Intelligent Decision Technologies Journal, the International Journal of Knowledge-Based Intelligent Engineering Systems, and the International Journal of Reasoning-based Intelligent Systems.

Research and Application of 5G Communication Technology in CATV Access Network

Xinyuan Zheng, Xiaohua He, and Yanhua Zhang

Abstract Based on the understanding and research of the mainstream cable TV optical node technology and 5G wireless communication technology, this paper proposes a new type of cable TV access network optical node with 5G wireless signal output, which integrates 5G technology to provide wireless access at the cable network access terminal, expands the access terminal form and optimizes the public service function of the cable television network.

1 Introduction

Cable TV network has always been an important part of the communication network. At present, the number of CATV users in China has reached 230 million. The two-way network reform covers more than 150 million users, and the two-way network reform penetrates more than 80 million users. Optical nodes in CATV access network architecture are getting closer and closer to users. One optical node covering 50 users is the most typical application structure.

The 5G mobile communication (the fifth-generation mobile communication standard, also known as the fifth-generation mobile communication technology) is the further development and extension of the 4G mobile communication [1]. If 4G is the era of video, 5G will usher in the era of virtual reality and interconnection of all things and will also realize the intelligent interconnection between people, people and things, things and things. Enhanced mobile broadband (eMBB), massive machine communication (mMTC) and ultra reliable and low delay (URLLC) are the three major application scenarios of 5G defined at the 3GPP conference [2]. eMBB is mainly used for large-volume mobile broadband services such as 3D/UHD video; mMTC is mainly for large-scale Internet of things business; URLLC is mainly for driverless, industrial self-service. Mobilization and other services require low latency and high reliability [3].

X. Zheng (✉) · X. He · Y. Zhang
Communication University of Zhejiang, Hangzhou 310018, Zhejiang, China
e-mail: zhengxy123456@163.com

R. Kountchev et al. (eds.), *Advances in Wireless Communications and Applications*,
Smart Innovation, Systems and Technologies 191,
https://doi.org/10.1007/978-981-15-5879-5_1

In order to further accelerate the development and application of 5G technology, there is an urgent need for 5G cross-border integration, and to strengthen the research of deep cross-integration between wireless communication technology and IoT, high-speed optical communication, advanced computing and large data technology. The optical node of high-speed optical communication in CATV access network has been closed to the client, forming FTTB network. This project mainly studies the cross-integration technology of digital TV optical node and 5G communication. It integrates 5G technology to provide wireless access at the access end of cable network, expands the access terminal form and optimizes the public service function of digital TV network.

The optical node technology of CATV and 5G communication technology are studied separately, and the cross-integration technology of them is further studied to form a 5G access digital TV optical node technology scheme, which will provide technical support for the next 5G technology application in radio and television access network.

2 Research on Optical Node Receiving Technology of Cable TV

At present, there are two main types of optical nodes in CATV, one is DOCSIS-based bidirectional optical workstation [4], and the other is EPON + EOC.

The former is shown in Fig. 1. The downstream optical receiving module, AGC module and downstream amplification module make up the photoelectric conversion and radio frequency processing of downstream channel of CATV and realize the output of radio frequency signal in the frequency range of 87–1000 MHz; the upstream amplification module and the optical transmitting module make up the 5–65 MHz radio frequency processing and optical transmitting output of the upstream channel; the bidirectional filter is real frequency division multiplexing of Uplink and downstream radio frequency signals. At present, the transmission system based on DOCSIS3.0 technology standard application has the highest transmission rate

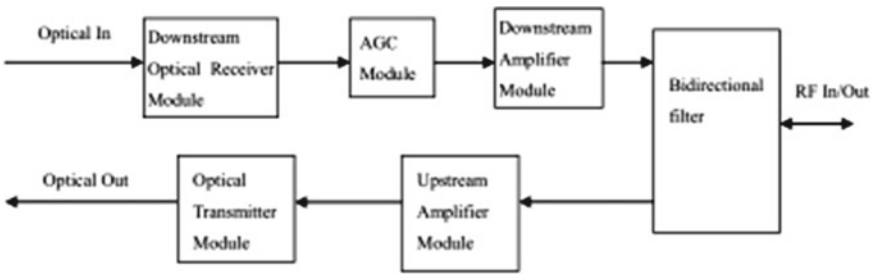

Fig. 1 Principle block diagram of bidirectional optical workstation

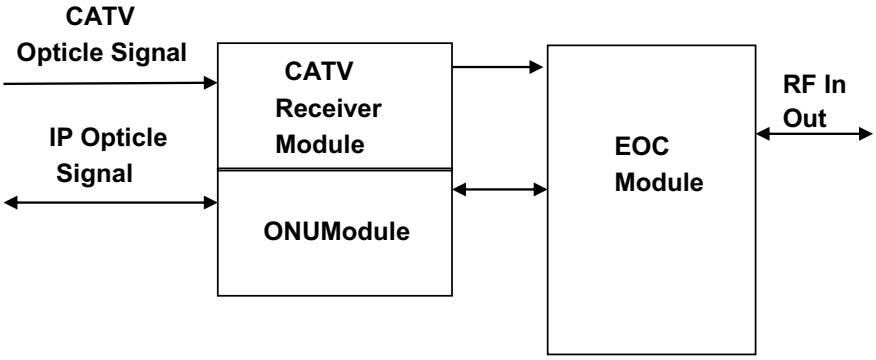

Fig. 2 Principle block diagram of EPON + EOC optical workstation

up to gigabit [5]. In the future, the transmission system based on DOCSIS3.1 technology standard will have a transmission rate of 10,000 megabytes, which is more suitable for the demand of 5G high bandwidth and high speed. We are going to further track and study the optical workstation technology adapted to DOCSIS3.1 technology standard, including the expansion of spectrum bandwidth, the upgrading of frequency division points and so on.

The EPON + EOC optical node is shown in Fig. 2. CATV receiving module realizes downstream channel optoelectronics and outputs 87–860 MHz radio frequency signal; ONU module realizes EPON optical network signal reception and IP signal output; EOC module realizes IP signal modulation and frequency division multiplexing of CATV radio frequency signal, EOC modulation is divided into high frequency modulation and low frequency modulation, and high frequency modulation is usually frequency modulation. The spectrum ranges from 950 to 1500 MHz, and low frequency modulation usually ranges from 5 to 65 MHz. At present, the transmission system based on EPON technology standard application has the highest transmission rate up to 1.25 Gbps. In the future, the transmission system based on 10GEPON technology standard will have a transmission rate of 10,000 megabits, which is more suitable for the demand of 5G high bandwidth and high speed. We will track the transmission technology of 10GEPON, especially ONU module technology.

3 Research on 5G Wireless Communication Base Station

Large-scale MIMO technology used by 5G improves spectrum efficiency; millimeter wave communication technology enlarges capacity and efficiency; D2D communication technology improves user experience and data transmission quality and solves the problem of large traffic consumption caused by data transmission in cellular network. The SON technology used in network technology will save a lot of network maintenance and deployment costs. The use of this technology makes 5G mobile

communication gradually toward intelligent direction. Software Definition Network (SDN) technology makes equipment simpler, conforms to the characteristics of efficient and economical Internet, it is simple to use, and the user's operation process is large. Moreover, 5G will bring faster speed, lower power consumption, smaller latency, larger bandwidth, stronger stability and can support more users.

The structure of 5G base station has changed greatly, and the trend of active antenna is obvious. The 4G macro base station consists of three parts: antenna, radio frequency unit RRU and baseband processing unit BBU deployed in the computer room. The 5G network tends to adopt the new wireless access network architecture of AAU + CU + DU. The antenna and RF unit RRU will be combined into a new unit active antenna unit (AAU). AAU will include not only the RF function of RRU but also the processing function of some physical layer. In 5G era, the increasing number of antenna channels and the active antenna put forward higher requirements for antenna design. Miniaturization and lightweight are the foundation. The increasing demand for radio frequency components will greatly enhance the market space of base station radio frequency industry. The highly integrated demand will also promote the further upgrading of radio frequency components such as filters and power amplifiers, and the products will be more miniaturized.

4 Research on Cross-Fusion Technology

Combining the optical receiving technology of digital TV optical node and 5G wireless communication base station technology, a new type of optical node of digital TV network is constructed, as shown in Fig. 3. At the same time of realizing radio frequency output in line mode, 5G wireless mode output is realized.

As shown in Fig. 4 based on the new optical node DOCSIS3.1, optical transceiver module realizes the conversion of up-down optical signal and radio frequency signal; CM module, namely cable modem module, realizes the conversion of radio frequency signal and IP signal; 5G module realizes the conversion of IP signal and 5G wireless signal. The transmission system based on DOCSIS 3.1 technology standard has a transmission rate of 10,000 megabytes, which is more suitable for the requirement of 5G high bandwidth and low delay. The new optical node not only realizes the wired access of radio frequency signal but also realizes the access of 5G wireless signal,

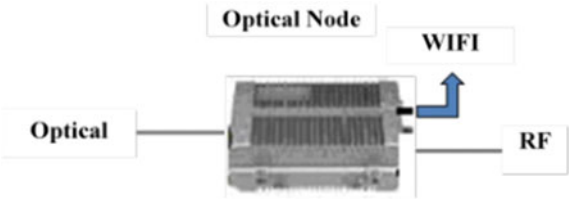

Fig. 3 New optical node model

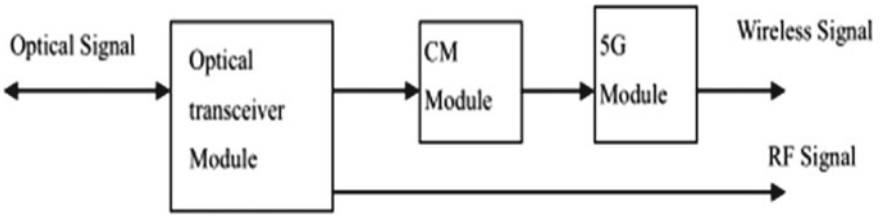

Fig. 4 New optical node based on DOCSIS3.1

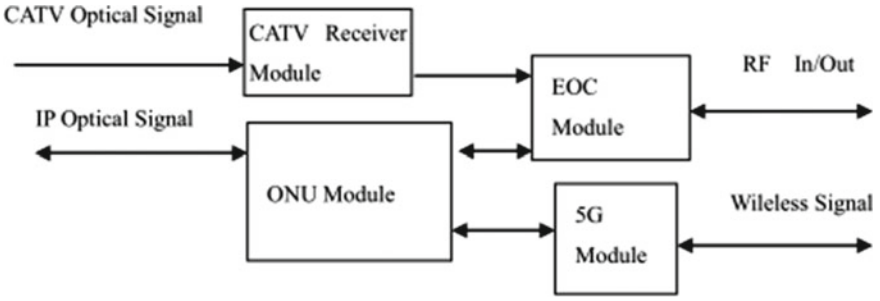

Fig. 5 New optical node based on 10GEPON

enriches the access channels of information and expands the public service scope of digital television network.

As shown in Fig. 5, based on the new optical node of 10GEPON, CATV receiving module realizes the photoelectric conversion of downstream channel and outputs radio frequency signal; ONU module realizes the reception of 10GEPON optical network signal and outputs IP signal; EOC module realizes the modulation of IP signal and frequency division multiplexing of CATV radio frequency signal, and EOC modulation is divided into high frequency modulation and low frequency modulation. Frequency modulation, high frequency modulation usually has a spectrum range of 950–1500 MHz, low frequency modulation usually has a spectrum range of 5–65 MHz; 5G module realizes the conversion of IP signal and 5G wireless signal. Optical transmission system based on 10GEPON technology standard has a transmission rate of 10,000 megabits, which is more suitable for the requirements of high bandwidth and low delay in 5G wireless communication.

5 Concluding Remarks

Based on the understanding and research of optical transceiver technology based on DOCSIS3.1 standard, ONU receiving technology based on 10GEPON network and 5G wireless communication technology, this project proposes a new type of

digital TV network optical node with 5G wireless signal output, which integrates 5G technology to provide wireless access at the access end of wired network, expands the access terminal form, optimizes the access terminal and improves the public service function of digital television network.

References

1. Recommendation ITU-R M.2083-0 IMT Vision-Framework and Overall Objectives of the Future Development of IMT for 2020 and Beyond [R].[S.I.]: ITU-R, Sept
2. IMT-2020(5G) Propulsion Group. 5G White Paper on Vision and Demand [EB/OL] (2014-05). https://www.imt-2020.org.cn/zh/documents/download/12015
3. IMT-2020(5G) Propulsion Group. 5G White Paper on Vision and Demand [EB/OL] (2015-02). https://www.imt-2020.org.cn/zh/documents/download/2
4. Xinyuan, Z., Genliang, Z., Jiefang, Z.: Research on OBIfree technology based on C-DOCSIS+RFoG network. Procedia Comput. Sci. **107**, 545–549 (2017)
5. Xinyuan, Z., Chen, Y.: A new C-DOCSIS network system, radio and television. Information **294**, 22–25 (2016)

An Overlapping Architecture of Large-Size Wide-Body Aircraft Based on Cloud Sea Computing in 5G OGCE

Zhi Lü, Mingzhe Yuan, Yi Lü, and Zhongfeng Wang

Abstract Based on the fifth generation of mobile communication (5G), 5G open grid computing environment (5G OGCE), in order to avoid the accident of commercial passenger aircraft caused by the engine fire, cloud sea computing (CSC) model, and an overlapping fault-tolerant large-size wide-body (large passenger) aircraft architecture based on CSC are presented in this paper. The new overlapping architecture (or configuration) consists of a coupling robot (CR), a flying wing structure (blended wing body (BWB)) regarded as a load-carrying carrier aircraft (host), and a commercial passenger aircraft with two semi-embedded rear propulsion engines regarded as a passenger cabin. A passenger-cabin passenger plane, a swept-back wing host aircraft, and a coupling robot (CR) combine and form an overlapping fault-tolerant structure's large passenger aircraft. The CR can tightly couple with the carrier aircraft (host) and the passenger-cabin aircraft (boarding aircraft). The CR consists of a grasping hand type robot (GHTR) and so on. A 5G/6G control cloud of cloud sea computing (CSC) model in 5G OGCE controls the operation of CR and flying and the disassembly of an overlapping fault-tolerant large-size wide-body aircraft. When the engine failure of the load-carrying (carrier) aircraft occurs, passenger-cabin aircraft is launched and ejected from the overlapping fault-tolerant large passenger aircraft (OFTLPA) by the grasping hand of GHTR of CR under the control of the control cloud and the pilot, OFTLPA breaks up. The passenger-cabin aircraft flies away from the load-carrying aircraft and realizes safe flight.

Z. Lü (✉)
School of IT and Engineering, Tianjin University of Technology and Education, Tianjin 300222, China
e-mail: lvzhi@tute.edu.cn

M. Yuan · Y. Lü · Z. Wang
Shenyang Institute of Automation, Chinese Academy of Sciences, Shenyang 110016, China

R. Kountchev et al. (eds.), *Advances in Wireless Communications and Applications*,
Smart Innovation, Systems and Technologies 191,
https://doi.org/10.1007/978-981-15-5879-5_2

1 Introduction

More than 60 years after Boeing 707 appeared, Boeing 737 Max 8 also crashed (March 10, 2019). What is more thought-provoking is that Airbus 380 also suffered engine fire. The engine failure of the Airbus 380, at the peak of its fleet development, has cast another shadow over the development of large airliners with the traditional tube-and-swept wing configuration. Nevertheless, combined with fuel and airline operating costs, has led to get ready to closed the production lines of the Airbus 380, a large passenger jet with 550 passenger.

Liebeck [1] proposed the design of blended wing body (BWB) structure. The structure layout of the second generation BWB, the baseline configuration structure of Boeing BWB-450, and the propulsion and structure of aerodynamics are given, and the internal space structure of Boeing BWB-450 and Airbus 380 is compared. Faggiano et al. [2] proposed an aerodynamic design of a flying V aircraft model. From the perspective of structural dynamics, Airbus 380 is still superior to these two structural designs, which can be seen from the successful development of GE-9X [3] large turbofan engine by General Electric.

According to bionics, the flight principles of hummingbird and the movement posture and structure of the Blue shark (*Prionace glauca*) are explained in [4, 5], and the traditional tube-and-swept wing configuration is still the most suitable large passenger aircraft model.

This paper presents a method for solving such a problem of engine accident and flying security, an overlapping large passenger aircraft architecture and a coupling robot (CR) system are presented, and a CR and Joint Robot (JR) also can be shown in Lü et al. [6], and the structure of another overlapping structure for safe flight of commercial large airliners is shown in Lü et al. [7], which are our previous study on safe flight of large airliners.

The rest of this paper is organized as follows: Sect. 2 gives a model of the coupling robot and grasping (and shaking) hand type robot (GHTR) structure, whose main structure is connected to the main structure of the flight power passenger aircraft carrying passenger-cabin aircraft. Section 3 discusses the structure and system of systems (SoS). A large power load-carrying aircraft and the clasping-hand structure of GHTR of CR in case of an air crash release the open clasping hands and launch and eject the passenger-cabin aircraft, and the passenger-cabin aircraft flies away from the carrying aircraft that has an accident and disaster. And a subsonic and hypersonic carrier aircraft are discussed. Section 4 presents open cloud sea computing (CSC) in 5G OGCE and discusses software architecture and the control cloud of CSC in commercial large aircrafts connected by GHTR of the coupling robot (CR). Finally, Sect. 5 is about conclusion of this paper.

2 Modeling and Approach

Coupling robot (CR) is composed of coupling frame structure, clasping-hand structure and grasping (and shaking) hand type robot (GHTR), and frame connector. CR is a connecting robot, the lower part of the robot's frame structure, which is a lower concave bottom, is connected to the "main structure of the load-carrying power aircraft." This is a chassis structure that connects to the main structure of the flight power passenger plane that carries the passenger-cabin passenger plane.

The upper part of the frame structure of CR is located under the abdomen of the aircraft that acted as the passenger-cabin aircraft. The upper part of the structure is composed of the frame structure, the connecting rod, and sensors.

Figure 1 shows the structure model of CR and its GHTR. A large number of control signals are transmitted by the controller, the open hand tasks and launching and ejecting action executed by CR and GHTR, and a copy of the information signal is sent to the airport command and control (C2) center, and under the control of control cloud based on CSC in 5G OGCE, an OFTLPA can continue to fly or land safely. Thus, we have definitions and propositions as follows,

Definition (Coupling Robot (CR), or, called connecting robot (CR)) 1. A CR is a form of 9-tuple:

$$\begin{aligned} \mathrm{CR} = < & \text{Coupled sense active concurrent agent (CS-ACA), Base frame,} \\ & \text{top frame, Grasping (Grapple and grip) hand type robot,} \\ & \text{holding rod of top frame, Seamless docking edge robot, Programmable} \\ & \text{logic controllers (PLCs), Interface of communication} \\ & \text{networks (CN-interface), Performance indication (Pi)} > \end{aligned} \tag{1}$$

The number of grippers of GHTR is determined by the number of webs and flanges of aluminum alloy of the frame in the main frame structure of large passenger plane. Generally, each web and flange, that is, a round rib has a pair of grippers. If the number of ribs is $L = n$, the number of grippers will be $H = 2n$. The number of grippers will be $H < 2n$ if the webs and flanges with high load pressure is used.

Definition (Grasping hand type robot or GHTR) 2. A GHTR is a form of 6-tuple:

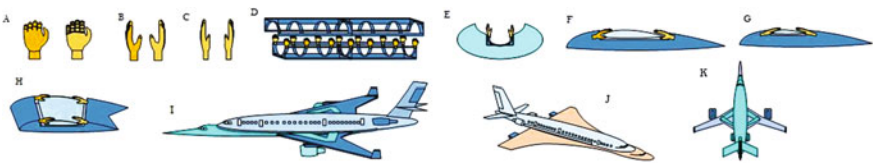

Fig. 1 Structure of CR and GHTR, an OFTLPA consists of them. **a** The clasping-hand. **b** A state of hand. **c** Another state of hand. **d** CR. **e** Sectional view of lower part of CR. **f** Root airfoil of wing of OFTLPA. **g** Middle airfoil of wing. **h** Root and middle and tip airfoil on planform. **i** Side view of OFTLPA. **j** Side overlooking view of OFTLPA. **k** Planform of OFTLPA

$$\text{GHTR} = < \text{Grasping Hands, Hand state, synchronization, Programmable logic controller (PLCs), Interface of communication networks (CN - interface), Performance indication (Pi)} > \quad (2)$$

The overlapping passenger plane is a combinatorial system of a passenger aircraft and a load-carrying power aircraft (LCPA), which realizes a complete flight function and structure of the passenger plane through the combination of components. Moreover, the overlapped propulsion mode generated by multiple engines can be generated through the combinatorial system of multiple aircraft. Namely, we have,

Definition (Overlapping Aircraft or OA) 3. An OA is a form of 3-tuple:

$$\text{OA} =< \text{Combinatorial Connecting Robot, Aircraft, Multi-Propulsion} > \quad (3)$$

The functions of CR are a combinatorial and integrated functions of fuselage and wing. The wing function and the flight power system of an overlapping structure aircraft are divided into two independent systems. CR connects two separate systems, making them a separable, integrated system.

Thus, the passenger cabin of OFTLPA turns into a passenger-cabin aircraft. When an engine accident occurs, a large commercial passenger airplane disintegrates into a load-carrying power aircraft and passenger-cabin aircraft. At this point, the CR is located on the load-carrying power aircraft (LCPA) to launch and eject the passenger-cabin aircraft. Figure 1 illustrates the structure of an OFTLPA.

Proposition (Synchronization behavior of GHTR) 1. If an even number of grippers grip the bar on the upper frame, or if an even number of grippers release and pop the bar, then each gripper must behave synchronously.

Proposition (Symmetry of Structure of GHTR) 2. Each pair of grippers is of palm symmetry if an even number of grippers are to hold and lock the grippers on the upper frame.

3 Structure and System of Systems

Figure 2 shows the structural model of an overlapping commercial large passenger aircraft (OCLPA) or called OFTLPA with CR as an overlapped coupling system for a coupled load-bearing aircraft and a passenger-cabin aircraft.

An overlapping fault-tolerant large passenger aircraft (OFTLPA) is a system of systems (SoS). According to definition 3 in this paper, the cluster of gripper of GHTR constitutes a local SoS. LCPA and the passenger-cabin aircraft (PCA) by using CR constitute an SoS. According to the principles of open system, the system of a system needs to exchange energy, materials, and information with the outside world.

Thus, a cloud sea computing (CSC) is required to realize the various exchanges of open systems. In this way, for large passenger aircraft and air traffic control

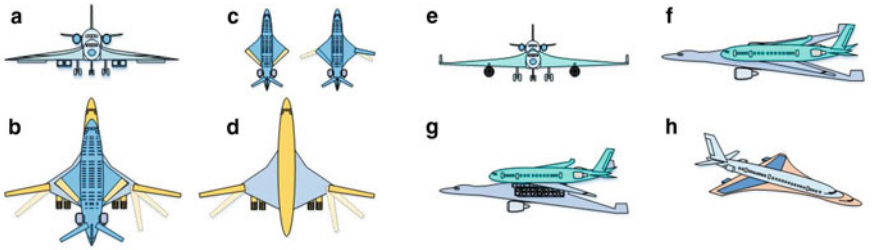

Fig. 2 Structure of an overlapping commercial large passenger aircraft (OCLPA) based on Tupolev tu-160 in 5G OGCE. **a** An elevation of an overlapping commercial airliner (OCA) based on two Tupolev tu-160. **b** Top view of an OCA. **c** Top view of the passenger aircraft. **d** Top view of a LCPA based on Tupolev tu-160. **e** An elevation of an OCA. **f** Flight attitude of an OCA. **g** Docking state of an OCA. **h** Flight attitude of an OCA based on a supersonic LCPA

systems, CSC is required to implement an approach to SoSE. Based on the self-governance principle and open interface principle of open system, this paper presents an OFTLPA. This structure satisfies the principle of synergism and reconfiguration.

The safety and reliable structure design of commercial large airliners has always been a complicated NP-hard. The overlapping commercial jumbo aircraft based on Tupolev tu-160 can achieve subsonic and supersonic cruise. Subsonic commercial flight can be achieved if the design is based on Airbus 380 or Airbus Beluga XL overlapped commercial jumbo aircraft.

4 Cloud Sea Computing Model in 5G OGCE

Cloud computing is a service-oriented architecture. Like other computing models in parallel distributed computing system, there are also some problems of vector computing and complex control engineering solution in cloud computing. Thus, a cloud sea computing (CSC) model is presented in this paper. The aim of which is to solve complex problems in SoSE. For commercial large passenger aircraft, it has been a difficult problem that a cloud computing-based air traffic control system is able to solve the safety of aviation of flights of the airlines flying on air route every day. Thus, we have.

Definition (Cloud Sea Computing or CSC) 4. Cloud sea computing is a collection and a model of a form of 18-computing-tuple:

$$\begin{aligned} \mathrm{CSC} = < & \text{Cloud-Fog-Mist-Edge, Corrosion-photochemistry-electrochemistry,} \\ & \text{Fields-tides, flow-waves, Diffusion-decomposing-aggregation,} \\ & \text{Concurrency, Synchronization, Asynchronization, Exchange, Convection,} \\ & \text{Transparency, Transition, Transport, Domains, Organization,} \\ & \text{Reconfiguration, Calculus, Channel} > \end{aligned} \tag{4}$$

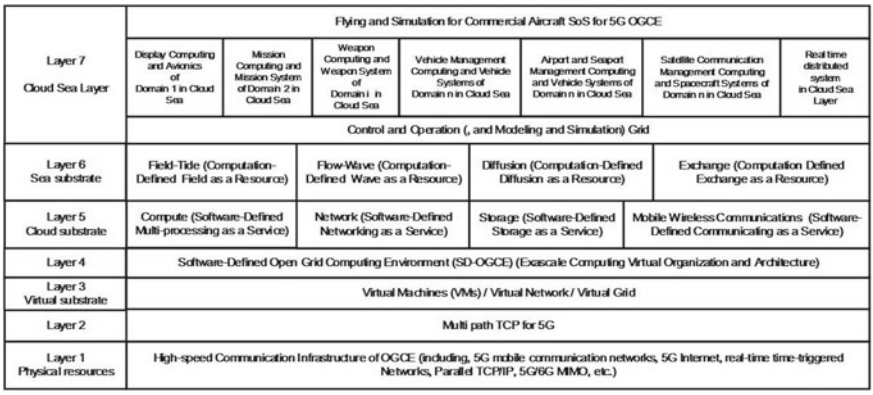

Fig. 3 Command and control (C2) software architecture of OFTLPAs and air traffic control systems based on cloud sea computing in 5G OGCE

Figure 3 shows a software architecture flying of a commercial large-size wide-body aircraft commanded and controlled by using air traffic control systems supported by a software architecture based on cloud sea computing in 5G OGCE. In fact, cloud sea computing is more suitable for the computing supported by 5G/6G Network, especially the polarization channel and polar code structure in 5G Networks, which are more suitable for cloud sea computing mode. The control of coupling robot (CR) and grasping hand type robot (GHTR) is expressed and controlled in vector form, and the software system of PLCs is constructed based on DNA molecule and DNA sequence in bioinformatics.

5 Conclusions

An overlapping fault-tolerant large passenger aircraft or structural model of an overlapping commercial large passenger aircraft is presented in this paper, which includes passenger aircraft, CR, and GHTR, the physical characteristics of which are a two-row parallel gripper cluster of GHTR structure, controlled by a software based on DNA sequence of control cloud of CSC. In aircraft flying for long periods of time, will encounter a variety of weather and climate environment, and therefore, CSC model is presented. Through the support of the open CSC and control cloud, an overlapping commercial large passenger aircraft can be disintegrated rapidly in flying in case of engine failure and accident, in order to avoid crash and passenger jet crashed, realize the passenger-cabin aircraft flying safely trustworthy and reliable.

Acknowledgements This work was supported by the National High-Tech R&D ("863/CIMS") Program of China (Contract No. 2014AA041801).

References

1. Liebeck, R.H.: Design of the blended wing body subsonic transport. J. Air-Craft **41**(1), 10–25 (2004)
2. Faggiano, F., Vos, R., Baan, M., van Dijk, R.: Aerodynamic design of a flying V aircraft. In: 17th AIAA Aviation Technology, Integration, and Operations Conference, pp. 1–25. AIAA AVIATION Forum, Denver, Colorado (2017)
3. GE-9X Homepage. https://www.geaviation.com/commercial/engines/ge9x-commercial-aircraft-engine, 24 Nov 2019
4. Hummingbird Homepage. https://wikipedia.moesalih.com/Hummingbird. 20 Nov 2019
5. Blue shark Homepage. https://wikipedia.moesalih.com/Blue_shark. 20 Oct 2019
6. Lü, Z., Wang, Z.F., Lü, Y., Yuan, M.Z.: Joint robot and aircraft carriers combinatorial systems in the sea in 5G OGCE. In: Proceedings of the 3rd International Conference on Robotics and Automation Engineering (ICRAE), pp. 76–81. IEEE, Guangzhou, China (2018). https://doi.org/10.1109/ICRAE.2018.8586754
7. Lü, Z., Wang, Z.F., Lü, Y., Yuan, M.Z.: An architecture of system of systems (SoS) for commercial flight security in 5G OGCE. In: Proceedings of 5th International Conference on Systems and Informatics (ICSAI), pp. 288–293. IEEE, Nanjing, China (2018). https://doi.org/10.1109/icsai.2018.8599363

The Influence of ICI for High Mobility Adaptive OFDM Systems in Nakagami-M Fading Channel

Xiuyan Zhang and Qiming Sun

Abstract Orthogonal frequency division multiplexing (OFDM) has been the leading multi-carrier modulation technology for radio communication. In this article, we studied the impact of power transmission and rate adaptive modulation on the average spectral efficiency (ASE) of OFDM systems by using square M-ary QAM (MQAM) under instantaneous bit error rate (BER) and average power constraints in Nakagami multipath fading (NMF) channel. We obtained closed-form expressions for the capacity when this adaptive scheme is used in NMF channel and inter-carrier interference (ICI) at the high mobility. Simulation result has indicated that the adaptive modulation has optimistic increase in ASE versus the non-adaptive modulation.

1 Introduction

OFDM has become the core technology of 4G and will continue to be used in 5G because of the low complexity method to eliminate inter-symbol interference (ISI). However, ICI is inevitable in high-speed environment [1], so high mobility communication has become a research difficult problem in high-speed environment.

In terms of the traditional OFDM, the same modulation scheme is used for all OFDM subcarriers. The BER is dominated by severely fading subcarrier. However, adaptation technology can effectively improve the performance of OFDM systems. In the past two decades, many scholars have studied the adaptive modulation technology of OFDM. Since Andrea J. Goldsmith proposed the optimal adaptive technology [2] of the time-domain water filling theorem, many scholars have improved it. Ye et al. [3] studied the impact of imperfect CSI on adaptive technology and proposed a channel estimation method based on multi-information to improve the spectral efficiency degradation caused by estimation error. Sun and Wu [4] studied pilot symbol adaptive modulation (PSAM) in high-speed environment and proposed its

X. Zhang · Q. Sun (✉)
College of Electrical and Information Engineering, Northeast Petroleum University, Daqing 163318, China
e-mail: qming_sun@163.com

R. Kountchev et al. (eds.), *Advances in Wireless Communications and Applications*,
Smart Innovation, Systems and Technologies 191,
https://doi.org/10.1007/978-981-15-5879-5_3

lower limit. But they did not consider the impact of ICI on high-speed environments. Dong et al. [5] proposed the influence of ICI on Rayleigh multipath fading [6] channel in high-speed environment and compared the influence of ICI on spectrum efficiency between different speeds. However, most of the current studies are based on Rayleigh multipath fading, while a few studies are focused on the adaptation of NMF [7] channels, especially at high speed. Owing to NMF can represent various channel features, such as $m = 1$ is Rayleigh fading channel and $m \to \infty$ transform into addictive white Gaussian noise (AWGN), it is very meaningful to study.

The mind contribution of this paper is in analyzing the influence of rate and power adaptation on the ASE of OFDM systems through using square MQAM subject to average transmit power and instantaneous BER in the NMF channels. We obtained close-form expressions for ASE of OFDM system when this adaptive scheme is used in the NMF channel and existing ICI at the high mobility. Numerical and simulation results indicate that adaptive modulation has significantly improved in ASE over non-adaptive modulation. We find that together with the increase of the value of m, or when the speed drops, the influence of ICI will also drop.

The layout of this article is as follows. We introduce the system model of OFDM in Sect. 2—fast fading channel and the existing ICI, which were caused by the channel. In Sect. 3, the capacity of NMF channel for the optimal adaptation scheme is derived. In Sect. 4, we enumerate some numerical examples comparing the NMF channel capacity with different speeds, and the conclusion driven in Sect. 5.

2 System Model

In this article, we used the wide-sense stationary uncorrelated scattering (WSSUS) model for the wireless communication channel [8]. Therefore, the kth OFDM subcarrier at the receiver can be written as

$$Y_k = d_k H_k + I_k + W_k \tag{1}$$

where

$$H_k = \frac{1}{N} \sum_{n=0}^{N-1} H_k(n) \tag{2}$$

$$I_k = \frac{1}{N} \sum_{m=0, m \neq k}^{N-1} \sum_{n=0}^{N-1} d_m H_m(n) \exp(j 2\pi n(m-k)/N) \tag{3}$$

where d_k is the frequency-domain signal transmitted over the kth subcarrier. Assume $H_k(n)$ is the Fourier transform for channel gain at time n, and W_k defined as complex additive white Gaussian noise (AWGN). Note that $E\left\{H_k(n_1) H_k^*(n_2)\right\} = J_0(2\pi f_d T_s(n_1 - n_2)/N)$ and $H_k(n)$ are a complex Gaussian random distribution,

$H_k(n) \sim \mathcal{CN}(0, 1)$. The OFDM symbol duration stands for T_s, where $T_s = \frac{N}{B} + \frac{L_{CP}}{B}$. Let B stands for received signal bandwidth, and L_{CP} is the length of cyclic prefix (CP). In this paper, we neglect the effect of CP, and from the article [7], we know that the CP will reduce the spectral efficiency by about 10–20% in practical OFDM systems. The function $J_0(\cdot)$ stands for the 0th-order Bessel function of the first kind. And frequency f_d is the Doppler frequency, where expressed as $f_d = \frac{v}{c} f_c$. The mobile terminal velocity is v (km/h), c is the light speed, and f_c is the carrier frequency. For expression (3), the ICI power of the kth OFDM subcarrier should be written as

$$P_{\mathrm{ICI}}^{k} = E\left\{|I_k|^2\right\} = \sum_{m=0, m\neq k}^{N-1} \overline{S}\phi_{k,m} \tag{4}$$

where $\phi_{k,m} = \frac{1}{N}\left(N + 2\sum_{n=1}^{N-1}(N-n)J_0\left(2\pi f_d T_s \frac{n}{N}\right)\cos(2\pi n(k-m)/N)\right)$, and $\overline{S}$ stands for the average transmitted power, which is defined as $\overline{S} = E\left\{|d_k|^2\right\}$. Now, assume the data is uncorrelated on each OFDM subcarrier and the ICI power is independent of each OFDM subcarrier index k, so ICI power can be written as

$$P_{\mathrm{ICI}} = \overline{S}\left(1 - \frac{1}{N^2}\left(N + 2\sum_{n=1}^{N-1}(N-n)J_0\left(2\pi f_d T_s \frac{n}{N}\right)\right)\right) \tag{5}$$

The normalized ICI power P_N is used for simplifying the problem, where $P_N = \frac{P_{\mathrm{ICI}}}{\overline{S}}$. From WSSUS model [9], the following property regarding H_k follows directly: H_k is a complex Gaussian random distribution, $H_k \sim \mathcal{CN}(0, \rho)$. Where

$$\rho_0 = E\left\{|H_k|^2\right\} = \frac{\left(N + 2\sum_{n=1}^{N-1}(N-n)J_0\left(2\pi f_d T_s \frac{n}{N}\right)\right)}{N^2} = 1 - P_N \tag{6}$$

From [10], the upper bound of P_N can be obtained as $P_N \leq \frac{1}{24}(2\pi f_d T_s)^2$. As shown in Fig. 1, we can find that is a tightness approximation at the time of $f_d T_s \leq 0.3$.

3 Adaptive OFDM Scheme

For adaptive OFDM modulation scheme, the optimal adaptation [2] is variable rate and variable transmit power under the instantaneous BER and average power constrain. The instantaneous BER of each subcarrier is [8]

$$\mathrm{BER}(\gamma[k]) \approx C_1 \exp\left(\frac{-C_2\gamma[k]\frac{s(\gamma[k])}{\overline{S}}}{\left(2^{\beta(\gamma[k])} - 1\right)\left(P_N^{(k)}\overline{\gamma} + 1\right)}\right) \tag{7}$$

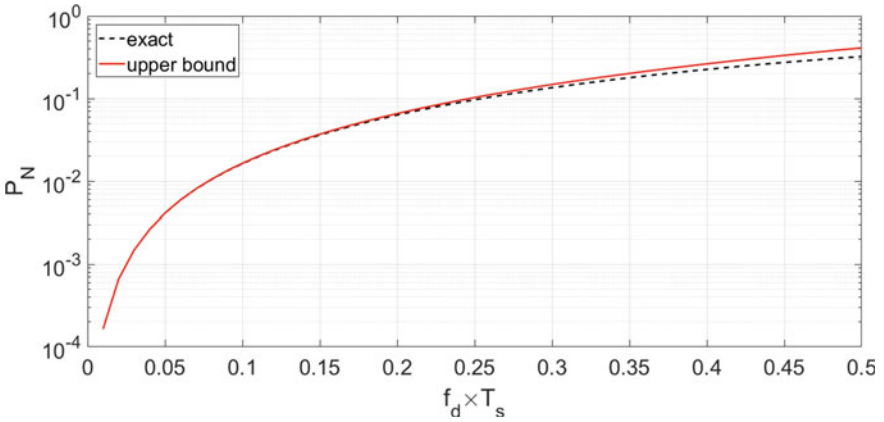

Fig. 1 Exact ICI power versus upper bound with $N = 1024$

where $C_1 = 0.2, C_2 = 1.6$. $\gamma[k]$ is the instantaneous SNR of each subcarrier. $\beta(\gamma[k])$ is bit load for each OFDM subcarrier, $s(\gamma[k])$ stands for the transmitted power, and $\overline{S}$ is average transmitted power. $P_N^{(k)}$ is the normalized ICI power of the kth OFDM subcarrier, from (4), it is got:

$$P_N^{(k)} = \sum_{m=0,m\neq k} \frac{s(\gamma[k])}{\overline{S}} \phi_{k,m} \tag{8}$$

It is very difficult to obtain the exact $P_{N\_\mathrm{ICI}}^{(k)}$ as the transmit powers of each subcarrier change dynamically. But, if we use an upper bound for the largest transmit normalized power $s_{\max} = \max_m \left\{ \frac{s(\gamma[k])}{\overline{S}} \right\}$, then we can easily obtain $P_N^{(k)} = s_{\max} P_N$. Therefore, the upper bound of the instantaneous BER for each subcarrier is obtained as [9]

$$\mathrm{BER}(\gamma[k]) \leq C_1 \exp\left(\frac{-C_2 \gamma[k] \frac{s(\gamma[k])}{\overline{S}}}{\left(2^{\beta(\gamma[k])} - 1\right)(s_{\max} P_N \overline{\gamma} + 1)} \right) \tag{9}$$

where P_N is the normalized ICI power as each subcarrier carries the same average power, as it can be found from (4). Then, by inverting (9) with $\mathrm{BER}(\gamma[k]) = \varepsilon$, the maximum bit load for each OFDM subcarrier can be expressed as

$$\beta(\gamma[k]) \leq \log_2 \left(1 + \frac{\varphi \gamma[k] \frac{s(\gamma[k])}{\overline{S}}}{s_{\max} P_N \overline{\gamma} + 1} \right) \tag{10}$$

where $\varphi = -\frac{C_2}{\ln \varepsilon / C_1}$ is a constant. Expression (10) is a lower bound for each OFDM subcarrier because we use the maximum ICI power. To obtain optimal adaptive

modulation scheme for OFDM system, the optimization problem can be expressed as

$$\mathrm{ASE} = \max_{s(\gamma[k])} \int \beta(\gamma[k]) P_{\gamma[k]}(\gamma[k]) d(\gamma[k]) \tag{11a}$$

subject to

$$E_{\gamma[k]}\{s(\gamma[k])\} \leq \overline{S} \quad \forall k \in N \tag{11b}$$

$$s(\gamma[k]) \geq 0 \quad \forall k \in N \tag{11c}$$

$$\mathrm{BER}(\gamma[k]) \leq \varepsilon \quad \forall k \in N \tag{11d}$$

where $E_x\{\cdot\}$ is the expectation. Therefore, for the optimization problem can be obtained

$$\begin{aligned} J\{s(\gamma[k])\} = & \int \log_2\left(1 + \frac{\varphi\gamma[k]\frac{s(\gamma[k])}{\overline{S}}}{s_{\max} P_N \overline{\gamma} + 1}\right) P_{\gamma[k]}(\gamma[k]) d(\gamma[k]) \\ & - \lambda\left(\int s(\gamma[k]) P_{\gamma[k]}(\gamma[k]) d(\gamma[k]) - \overline{S}\right) \end{aligned} \tag{12}$$

where λ is the Lagrange multiplier. The optimal transmit power adaptive modulation scheme can be obtained by assuming

$$\frac{\partial J\{s(\gamma[k])\}}{\partial s(\gamma[k])} = 0 \tag{13}$$

Therefore, we can find the optimal power adaptation by solving (13)

$$\frac{s(\gamma[k])}{\bar{S}} = \begin{cases} \frac{1}{\lambda \ln 2\bar{S}} - \frac{s_{\max} P_N \bar{\gamma} + 1}{\varphi\gamma[k]}, & \gamma_0 < \gamma[k] \\ 0, & \gamma_0 > \gamma[k] \end{cases} \tag{14}$$

where $\gamma_0 = \frac{(s_{\max} P_N \overline{\gamma} + 1)}{\varphi}$ is the cutoff threshold for $\gamma[k]$. When the signal-to-noise ratio (SNR) drops below γ_0, the subcarrier is not used. This threshold can be found by ensuring that (14) is positive. From [5], we can get $s_{\max} = \lim_{\gamma[k]\to\infty} \frac{s(\gamma[k])}{\bar{S}} = \frac{1}{\lambda \ln 2\overline{S}}$. Substituting (14) into (10), the optimal rate adaptation can be obtained as

$$\beta(\gamma[k]) = \max\left(0, \log_2\left(\frac{\varphi\gamma[k]}{(\lambda \ln 2\overline{S})(s_{\max} P_N \overline{\gamma} + 1)}\right)\right) \tag{15}$$

The maximum average spectral efficiency (ASE) of an adaptation scheme is determined through averaging $\beta(\gamma[k])$. Therefore, it can be computed from

$$\mathrm{ASE} = \int_{\gamma_0}^{+\infty} \log_2\left(\frac{\varphi\gamma[k]}{\left(\lambda \ln 2\overline{S}\right)(s_{\max} P_N \overline{\gamma} + 1)}\right) P_{\gamma[k]}(\gamma[k]) d(\gamma[k]) \tag{16}$$

In order to solve expression (16) by simple numerical process, we can use the probability distribution function (PDF) of $P_{\gamma[k]}(\gamma[k])$, obtained as in [7]

$$P_{\gamma[k]}(\gamma[k]) = \left(\frac{m}{\overline{\gamma[k]}}\right)^m \frac{\gamma[k]^m}{\Gamma(m)} \exp\left(-m\frac{\gamma[k]}{\overline{\gamma[k]}}\right) \quad \gamma \geq 0 \tag{17}$$

where $\overline{\gamma[k]} = \overline{\gamma} E\left\{|H_k|^2\right\} = \overline{\gamma}\rho_0$ is the average SNR for receiver as no ICI, m stands for the NMF parameter ($m \geq 1/2$), and $\Gamma(\cdot)$ is the gamma function. And ρ_0 can be found from expression (6). Therefore, from (16), we can obtain the approximation expression:

$$\mathrm{ASE} = \begin{cases} \log_2(e) E_1\left(\frac{m\gamma_0}{\overline{\gamma}\rho}\right), & m = 1 \\ \log_2(e)\left(E_1\left(\frac{m\gamma_0}{\overline{\gamma}\rho}\right) + \sum_{i=1}^{m-1} \frac{P_i(m\gamma_0/\overline{\gamma}\rho)}{i}\right), & m \geq 2 \end{cases} \tag{18}$$

where $E_1(x) = \int_x^\infty e^{-t}/t d(t)$ is the exponential integral, and $P_i(\cdot)$ is Poisson distribution defined by

$$P_i(x) = \exp(-x) \sum_{j=0}^{i-1} \frac{x^j}{j!} \tag{19}$$

4 Simulation and Numerical Results

In this part, the previous theoretical results were examined by MATLAB simulation. In all simulations presented here, the parameters correspond to IEEE 802.11a to outdoor speed environments [9]. Assuming a total bandwidth of OFDM systems B is 5 MHz and divided into $N = 1024$ subchannels. The carrier frequency is $f_c = 2$ GH, the target BER is $\varepsilon = 10^{-3}$, and the mobility is $v = \{100, 200, 300, 400, 500\}$ km/h.

For the case of $\overline{\gamma[k]} = 30$ dB, the performance of the optimal power adaptations $s(\gamma[k])/\overline{S}$ is simulated, and result is shown in Figs. 2 and 3. Figure 2 is Rayleigh fading channel ($m = 1$), we can discover the similar trends, and as the speed increases, more transmit power is needed and larger cutoff value. In practice, the ICI power is larger when the speed increases. Figure 3 is NMF channel for different values of $m = \{1, 2, 4\}$. Easily, we can find when the m increases, less transmit power is

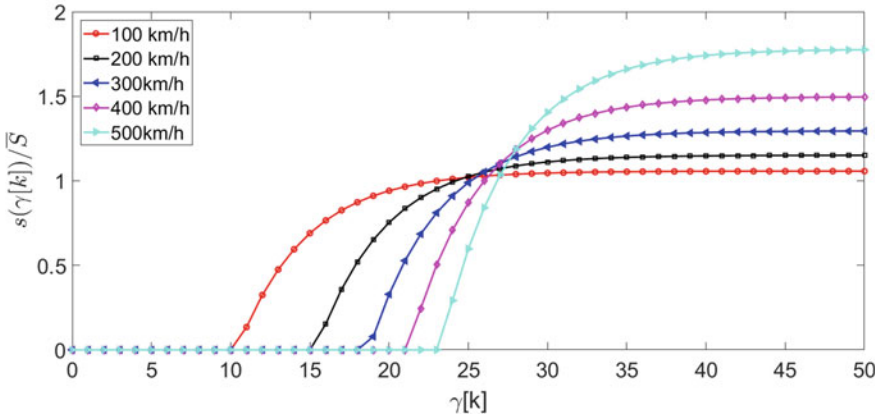

Fig. 2 $\frac{s(\gamma[k])}{\overline{S}}$ for MQAM in Rayleigh fading channel

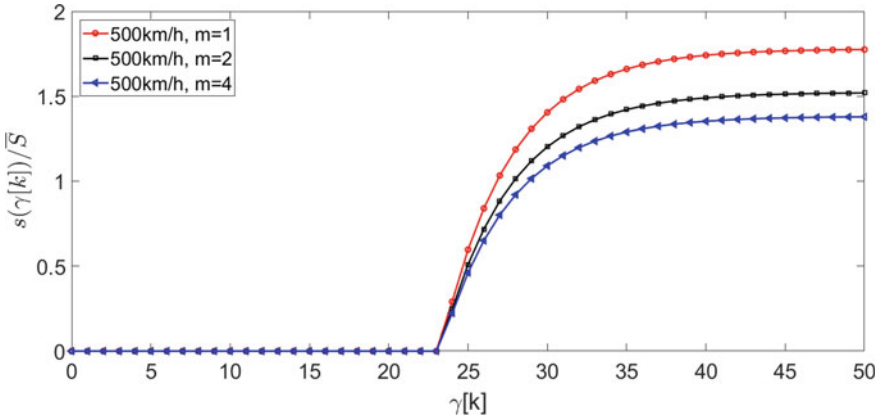

Fig. 3 $\frac{s(\gamma[k])}{\overline{S}}$ for MQAM in NMF channel

needed. Due to the value of m increase, the fading channel influence is no more remarkable.

Figure 4 shows the ASE of adaptation scheme compared with non-adaptation scheme for different speeds. In Fig. 4, it is obvious that high speed results in lower ASE and the adaptive versus the non-adaptive scheme have an optimistic ASE increase. More detailed numerical values can be found from Table 1: it indicates that adaptive versus non-adaptive scheme has about 1.5–4 bps/Hz ASE gain (the gain increases with the speed decrease). The reason for this phenomenon is also due to the high mobility leads to larger ICI power, and the influence of fading channel also results in ASE trend certain level. The different value of m for the influence of OFDM system is plotted in Fig. 5. From Fig. 5, we can discover that as the m

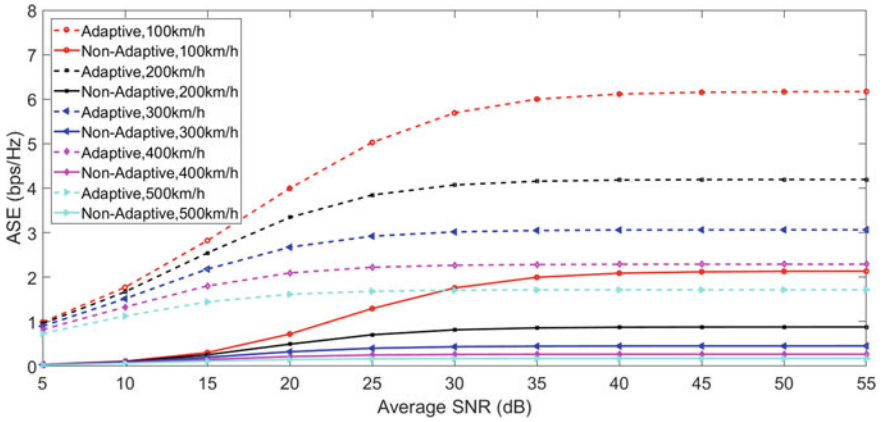

Fig. 4 ASE versus average SNR in Rayleigh fading channel

Table 1 Comparison of the ASE of five different speeds ($\overline{\gamma} = 50$ dB)

ASE	100 km/h	200 km/h	300 km/h	400 km/h	500 km/h
Adaptive	6.165	4.193	3.064	2.289	1.717
Non-adaptive	2.13	0.8802	0.4535	0.2682	0.1736

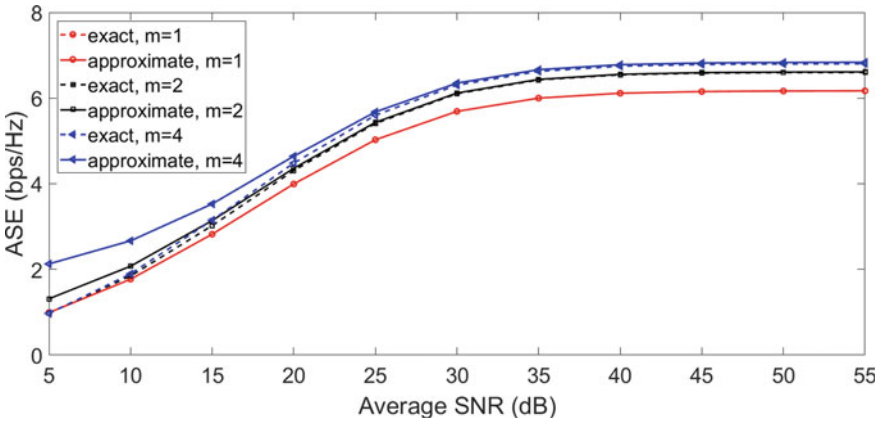

Fig. 5 The influence of m in NMF channel at the speed 100 km/h

increases, the ASE also increases because the m increase stands for fading channel trend flat results in reducing the influence of ICI power. And we also found that the approximation is very close to exact expression subject to high average SNR.

5 Conclusion

In this article, optimum rate and power adaptive OFDM systems have been studied for maximum ASE with square MQAM subject to instantaneous BER and average power in the NMF channel. Especially, we obtained close-form expressions for the capacity when this adaptive scheme is used in NMF channel with existing ICI at high mobility. By comparing different velocities under the average SNR constrain, the simulation results indicated that adaptive modulation scheme has optimistic gain in ASE versus non-adaptive modulation. Numerical results proved that the ASE of OFDM systems will increase when the speed decreases and/or the value of m drops, due to the ICI power.

References

1. Fan, P., Zhao, J., Chih-Lin, I.: 5G high mobility wireless communications: challenges and solutions. China Commun. **13**, 1–13 N/A (2016)
2. Goldsmith, A.J., Varaiya, P.P.: Capacity of fading channels with channel side information. IEEE Trans. Inf. Theory J. **43**(6), 1986–1992 (1997)
3. Ye, S., Blum, R.S., Cimini, L.J.: Adaptive OFDM systems with imperfect channel state information. IEEE Trans. Wirel. Commun. J. **5**(11), 3255–3265 (2006)
4. Sun, N., Wu, J.: Maximizing spectral efficiency for high mobility systems with imperfect channel state information. IEEE Trans. Wirel. Commun. J. **13**(3), 1462–1470 (2014)
5. Dong, Z., Fan, P., Panayirci, E., Mathiopoulos, P.T.: Effect of power and rate adaptation on the spectral efficiency of MQAM/OFDM system under very fast fading channels. EURASIP J. Wirel. Commun. Netw. J. **2012**(1), 208 (2012)
6. Sklar, B.: Rayleigh fading channels in mobile digital communication systems. I. Characterization. IEEE Commun. Mag. J. **35**(7), 90–100 (1997)
7. Aalo, V.A.: Performance of maximal-ratio diversity systems in a correlated Nakagami-fading environment. IEEE Trans. Commun. J. **43**(8), 2360–2369 (1995)
8. Choi, Y.-S., Voltz, P.J., Cassara, F.A.: On channel estimation and detection for multicarrier signals in fast and selective Rayleigh fading channels. IEEE Trans. Commun. J. **49**(8), 1375–1387 (2001)
9. Chung, S.T., Goldsmith, A.J.: Degrees of freedom in adaptive modulation: a unified view. IEEE Trans. Commun. J. **49**(9), 1561–1571 (2001)
10. Li, Y., Cimini, L.J.: Bounds on the interchannel interference of OFDM in time-varying impairments. IEEE Trans. Commun. J. **49**(3), 401–404 (2001)

Research on the Performance of LDPC Codes in 5G Communication System

Sai Li, Lin Zhou, Shuying Zhang, Chen Chen, Yuqing Fu, and Yucheng He

Abstract With the development of the Internet of Things technology, the fourth-generation mobile communication system cannot meet the needs of the Internet of Things (IOT). In order to provide higher transmission rate, smaller delay, and more powerful device connection capabilities, turbo codes are replaced by low-density parity-check (LDPC) codes in enhanced mobile broadband (eMBB) scenarios of fifth-generation wireless systems (5G). The check matrixes of LDPC codes in the 5G standard have two important characteristics. One is that they are all extended from high code rate check matrices to support the LDPC codes in different code rates and the incremental redundancy hybrid automatic repeat request (IR-HARQ) scheme. The other is that there are both dual-diagonal sub-matrix and identity sub-matrix in each check matrix to reduce the encoding complexity. This paper first details the structures and characteristics of LDPC codes in 5G standard, and then, the performance of 5G LDPC codes with different code lengths and code rate in the additive white Gaussian noise (AWGN) channel is proposed.

1 Introduction

LDPC codes which are a kind of linear block codes with sparse check matrix are proposed by Gallager in 1962 [1, 2]. The further research in [3, 4] shows that the performance of LDPC codes with confidence propagation algorithm can approach Shannon limit. The proposal of quasi-cyclic low-density parity-check (QC-LDPC) codes in [5] achieves a breakthrough in hardware implementation for LDPC codes. The Richardson–Urbanke (RU) algorithm greatly reduces the coding complexity, but

S. Li · L. Zhou (✉) · S. Zhang · C. Chen · Y. Fu · Y. He
Xiamen Key Laboratory of Mobile Multimedia Communications, College of Information Science and Engineering, Huaqiao University, Xiamen 361021, Fujian, China
e-mail: linzhou@hqu.edu.cn

L. Zhou · Y. He
State Key Laboratory of Integrated Services Networks, Xidian University, Xi'an 710071, Shaanxi, China

R. Kountchev et al. (eds.), *Advances in Wireless Communications and Applications*,
Smart Innovation, Systems and Technologies 191,
https://doi.org/10.1007/978-981-15-5879-5_4

the matrix inversion operation involved in the RU algorithm will destroy the sparsity of matrix and increase the operation times [6]. The coding complexity can be further reduced by designing the block sub-matrices as single-diagonal or dual-diagonal structure. Gallager introduces sum-product algorithm (SPA) in his doctoral dissertation, which has the best performance with highest complexity and is also known as the belief propagation (BP) algorithm [7]. The min-sum algorithm (MSA) reduces the complexity of SPA by transforming the large number of multiplication operations into fetching sign and comparison operations of log-likelihood ratio (LLR), but it brings a degree of performance loss. The reason of the performance loss is that the amplitude of the external information output of check nodes (CN) in the MSA algorithm is greater than the SPA algorithm, so the normalized min-sum algorithm and the offset min-sum algorithm introduce a weighting or scaling factor individually to approximate the performance of SPA [8–10].

2 The Structure of 5G LDPC Codes

The 5G LDPC code is a kind of QC-LDPC codes which matrix H are composed of many $z \times z$ sub-matrixes; it can be extended from two base matrices BG1 and BG2. There are only 0 and 1 elements in BG1 and BG2, the 0 elements correspond to zero $z \times z$ sub-matrixes and the 1 elements relate to non-zero $z \times z$ sub-matrixes in H. The size of BG1 and BG2 is 46×68 and 42×52, respectively, and the factor z is called expansion factor or lifting size.

BG1 and BG2 relate to cyclic-shift matrixes PG1 and PG2 of the same size, respectively. They use -1 and specific right cyclic-shift value x to represent the corresponding sub-matrix in H as a zero matrix or an identity matrix circularly right shifted by x bits.

The structure of the cyclic-shift matrixes is shown in Fig. 1a; each block matrix corresponds to a region of the check matrix H. Sub-matrices A and C are composed of cyclic-shift matrices and zero matrices. The sub-matrix B satisfies (1), $\mathbf{b}_1$ is a 4-dimensional vector with three none -1 elements, and two of them are $b(1)$ and

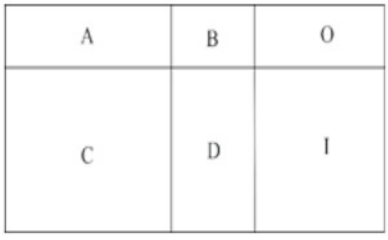

(a) Overall structure of base matrices

0	0	-1	-1
-1	0	0	-1
1	-1	0	0
0	-1	-1	0

(b) Structure of sub-matrix B

Fig. 1 Structure of the cyclic-shift matrices in 5G standard

$b(3)$. $\mathbf{B}_2$ is a 4×3 dual-diagonal matrix, which means that if the rows and columns of $\mathbf{B}_2$ are represented by i and j, respectively, the $z \times z$ sub-matrix is associated with the positions $i = j$ and $i = j + 1$ which are identity matrices and the remaining positions are zero matrices. The sub-matrix $\mathbf{O}$ is a zero matrix, and the sub-matrix $\mathbf{I}$ is an identity matrix.

$$\mathbf{B} = \left[(\mathbf{b}_1)_{4\times 1} \middle| (\mathbf{B}_2)_{4\times 3} \right] \tag{1}$$

The structure of sub-matrix B in PG2 (the definition is shown above) is shown in Fig. 1b.

3 Rate Matching in 5G

To achieve efficient and reliable transmission in factual channel, it is necessary to design a set of LDPC codes with different code rates to match the channel resource allocated by the base station. High code rate LDPC codes are used at high SNR to improve transmission efficiency, and low-rate LDPC codes are used at low SNR channel conditions to ensure reliable signal transmission. The check matrix $\mathbf{H}$ of 5G LDPC codes is expanded from high code rate check matrices, and the low code rate codes are obtained by serially concatenating parity bits behind the high code rate codes. The block [**A B**] in Fig. 1 actually corresponds to a high code rate LDPC codes, and the block [**C D I**] associates with some extended redundant bits. There are multiple cyclic-shift matrices, and expansion factors are designed in 5G standard to adapt to different information bit lengths and support multiple code rates, but the information bits and code rate directly supported by check matrix are still limited.

Shortening and puncturing are used to support 1-bit particle size of information bits and match different channel resource allocation resolutions. Information bit shortening refers to filling zeros at the end of information bits as needed to achieve the required length, while parity bit punching deletes redundant check bits in the end to the allocated channel resource. In addition, the first two columns of $\mathbf{H}$ are high weight columns and the information bits associated with these columns should also be punctured.

The number of information and parity puncturing bits and information shortening bits is denoted as N_{punc1}, N_{punc2} and N_{padd} which are calculated by (2)–(4), respectively. The number of columns in base matrices related to information bit length K and code bit length N is represented by k_b and n_b.

$$N_{\text{punc1}} = 2z \tag{2}$$

$$N_{\text{punc2}} = n_b \times z - 2z - N - N_{\text{padd}} \tag{3}$$

$$N_{\text{padd}} = k_b \times z - K \tag{4}$$

4 The Simulation Performance of 5G LDPC Codes

In order to investigate the decoding performance of LDPC codes with different code lengths and code rates, a software simulation platform is first built and a large number of simulations are performed. The complete simulation platform mainly includes source, encoding unit, modulation unit, channel, demodulation unit and decoding unit, as shown in Fig. 2.

Let $S = \{s_1, s_2, \ldots, s_k\}$ denotes the original information symbol, and after encoding, the coded n symbols $C = \{c_1, c_2, \ldots, c_n\}$ modulate with BPSK ($0 \rightarrow 1, 1 \rightarrow -1$) in the modulation unit to obtain the symbols $V = \{v_1, v_2, \ldots, v_n\}$ waiting for transmission through Gaussian channel. The disturbed symbols $Y = \{y_1, y_2, \ldots, y_n\}$ will be received at the receiver and can be calculated by (5), while $n_i : N(0, \sigma_n^2)$ is a Gaussian random variable.

$$y_i = v_i + n_i \tag{5}$$

After demodulating and decoding, the performance of 5G LDPC codes is measured by comparing the BLER between decoded information sequence and original information sequence.

The decoding algorithm in our simulation platform is SPA. Let $L_{j\rightarrow i}$ denote the extrinsic information from variable nodes VN j to check nodes CN i, and $L_{i\rightarrow j}$ denote the extrinsic information from CN i to VN j. $N(j)$ represents the check nodes connected to the variable node j, and the value of LLR calculated from y_i is denoted by L_j, and the element in base matrix at row i and column j is represented by h_{ij}. The main steps of SPA are as follows.

(1) Initialization

$$L_j = L(v_j|y_j) = 2y_i/\sigma^2 \tag{6}$$

$$L_{j\rightarrow i} = L_j \quad (h_{ij} = 1) \tag{7}$$

(2) Extrinsic information updated in VN

$$L_{i\rightarrow j} = 2\tanh^{-1}\left(\prod_{j'\in N(i)-\{j\}} \tanh\left(\frac{1}{2}L_{j'\rightarrow i}\right)\right) \tag{8}$$

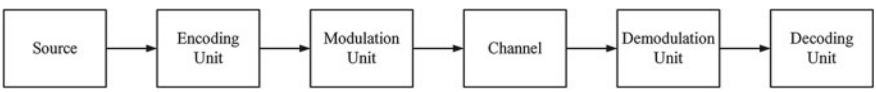

Fig. 2 Communication simulation system 5G LDPC decoding

(3) Extrinsic information updated in CN

$$L_{j\to i} = L_j + \sum_{i'\in N(j)-\{i\}} L_{i'\to j} \tag{9}$$

(4) The sum of LLR

$$L_j^{\text{total}} = L_j + \sum_{i\in N(j)} L_{i\to j} \tag{10}$$

The termination criterion for iteration:

The decoded information sequence $\hat{\mathbf{v}}$ is calculated by (11). If $\hat{\mathbf{v}}\mathbf{H}^{\mathrm{T}} = 0$ or the maximum iteration is reached, the iteration process will be terminated; otherwise, it will go to step 2.

$$\hat{v}_j = \begin{cases} 1, \text{ when } L_j^{\text{total}} < 0 \\ 0, \text{ else} \end{cases} \quad (j = 0, 1, \ldots, n-1) \tag{11}$$

In 5G standard, BG1 is mainly for long code and high code rate, and BG2 is for short code and low code rate. We simulate the performance of two different base matrices at different code lengths and code rates to the overall performance of 5G LDPC codes. The $K = 4224$ LDPC codes of BG1 with three different code rates 2/3, 3/4 and 5/6 are shown in Fig. 3a. Simulation results prove that compared to the LDPC codes with the code rate $R = 3/4$ and $R = 5/6$, the $R = 2/3$ LDPC code has the best performance and achieves 0.5 dB and 1.2 dB gains compared with $R = 3/4$ and $R = 5/6$ L. Simulation results prove that the LDPC code with the code rate R =2/3 achieves 0.5 dB and 1.2 dB gain, respectively, compared with R =3/4 and R =5/6 over the AWGN channel with the BLER =10^{-4}. The $K = 1040$ LDPC codes have a similar simulation result as shown in Fig. 3b. The LDPC code with a code rate of 1/3

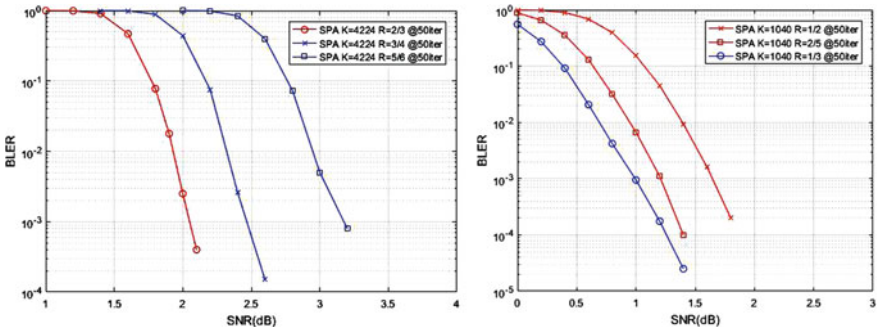

(a) for K=4224 LDPC codes of BG1 (b) for K=1040 LDPC codes of BG2

Fig. 3 BER performance comparison of different code rates

tends to converge around SNR = 1.4 dB, while the $R = 1/2$ LDPC code approaches convergence until SNR = 1.8 dB. This is mainly because the LDPC code with a low bit rate transmits more parity bits, and more check nodes are used in decoding, so that it can converge quickly and have a better performance at lower SNR. However, low-rate LDPC codes will consume more energy during transmission and need a higher complexity decoder.

5 Conclusion

In the 5G communication system, LDPC code as the channel code in data channel has extremely excellent performance. On the one hand, this paper introduces the special structure in the check matrices of 5G LDPC codes and explores the relationship between matrix structure and the flexibility and encoding complexity. On the other hand, a complete simulation system is established, which simulates the performance of 5G LDPC codes with different code lengths and code rates in additive white Gaussian noise (AWGN) channel using SPA algorithm and obtains the specific relationship between code rate and performance.

Acknowledgements This paper was funded in part by the National Natural Science Foundation of China (61901182, 61302095), The Natural Science Foundation of Fujian Province of China (2018J01096, 2018J05105), Quanzhou City Science & Technology Program of China (2018C108R) and the Graduate Students Foundation of National Huaqiao University (18013082032).

References

1. Shannon, C.E.: Communication theory of secrecy systems. Bell Syst. Tech. J. **28**(4), 656–715 (1948)
2. Gallager, R.: Low-density parity-check codes. IRE Trans. Inf. Theory **8**(1), 21–28 (1962)
3. MacKay, D.J.C., Neal, R.M.: Near Shannon limit performance of low density parity check codes. Electron. Lett. **33**(6), 457–458 (1997)
4. Spielman, D.A.: Linear-time encodable and decodable error-correcting codes. IEEE Trans. Inf. Theory **42**(11), 1723–1731 (1996)
5. Fossorier, M.: Quasi-cyclic low density parity check codes. In: IEEE International Symposium on Information Theory, p. 150. IEEE Press, Yokohama, Japan (2003)
6. Richardson, T.J., Urbanke, R.L.: Efficient encoding of low-density parity-check codes. IEEE Trans. Inf. Theory **47**(2), 638–656 (2001)
7. McEliece, R., Mackay, D.J.C., Cheng, J.F.: Turbo decoding as an instance of Pearl's 'Belief Propagation' algorithm. IEEE J. Sel. Areas Commun. **16**(2), 140–152 (1998)
8. Zhang, L., Huang, J., Cheng, L.L.: Reliability-based high-efficient dynamic schedules for belief propagation decoding of LDPC codes. In: IEEE 11th International Conference on Signal Processing, pp. 1388–1392. IEEE Press, Beijing (2012)

9. Chang, Y.M., Casado, A.I.V., Chang, M.C.F.: Lower-complexity layered belief-propagation decoding of LDPC codes. In: IEEE International Conference on Communications, pp. 1155–1160. IEEE Press, Beijing (2008)
10. Wang, Z., Cui, Z.: Low-complexity high-speed decoder design for quasi-cyclic LDPC codes. IEEE Trans. Very Large Scale Integr. (VLSI) Syst. **15**(1), 104–114 (2007)

Research on SVPWM Modulation Technology of Current-Source Inverter

Wang Shuaiyi, Qu Yaojun, Zhang Lei, Li Chaochao, Song Yanxia, Kanae Shunshoku, and Bai Jing

Abstract Aiming at the problem of large output harmonics of high-performance current-source inverter, a space vector pulse width modulation technology is proposed. By selecting a sawtooth wave as the carrier wave, the sideband harmonics generated by the modulation sequence can be moved away to the right to reduce the effects of low-order harmonics, the simulations, and experiments that prove the feasibility and effectiveness of the control strategy. The objective of this paper is related to nonlinear system control field.

1 Introduction

Current-source inverters (CSI) are widely used in high-power applications due to their advantages such as large power, four-quadrant operation, good load voltage waveform, reliable short-circuit protection, and reduced system cost. Current-source inverters have been researched in the fields of medium- and high-voltage motor speed modulation, superconducting energy storage, induction heating, micro-grid, active power filtering, electric vehicles, and photovoltaic grid connection.

At present, the pulse width modulation (PWM) algorithm for CSI is only divided into sine pulse width modulation (SPWM) [1] and SVPWM [2–5]. In 2015, S. Dusmez, a senior engineer from Texas Instruments in order to avoid noise content in transient current response [6], presents a new SVPWM scheme by replacing null

W. Shuaiyi · Z. Lei · S. Yanxia · B. Jing (✉)
Beihua University, Jilin 132013, People's Republic of China
e-mail: jlbyj@163.com

Q. Yaojun
China Petroleum JiLin Chemical Engineering Co., Ltd., Electric Control Room, Shenyang, China

L. Chaochao
State Grid Yingshang County Electric Power Supply Company, Fuyang, China

K. Shunshoku
Junshin Gakuen University, Fukuoka 815-8510, Japan

R. Kountchev et al. (eds.), *Advances in Wireless Communications and Applications*,
Smart Innovation, Systems and Technologies 191,
https://doi.org/10.1007/978-981-15-5879-5_5

vectors with complementary active vectors such that the added vectors effectively cancel out each other, and the applied resultant voltage remains the same as in the conventional SVPWM. The proposed scheme reduces the system error caused by the dead time of the switches with enlarged pulse widths, enabling low-speed drive [7]. In 2016, K. Rajashekara, a professor at the University of Texas at Dallas, presents a new space vector pulse width modulation scheme to reconstruct phase currents using neutral point current sensing in three-level T-type converters (TLTTCs). The scheme greatly reduced switching losses and low-frequency noise [8]. China's research on current-source inverters is mainly based on scientific research institutions and key laboratories. There are no cases of practical application and mostly theoretical research and experimental prototypes. Professor Jin Ke of Nanjing University of Aeronautics and Astronautics has proposed an improved SVPWM algorithm on the issue of maintaining transformer volt-second balance [9]. Zhejiang University has a lot of research on multi-level current-source inverters and modulation algorithms. At the same time, it has matured research on strategies such as direct current control, indirect current control, and improved model predictive control. A variety of experimental prototypes and mature devices have been developed [10, 11]. Because the traditional SVPWM algorithm is too complicated to calculate, it is difficult to apply [12–17]. Professor Tan Guojun of China University of Mining and Technology proposed an SVPWM algorithm based on line voltage coordinates on this issue. Through the coordinate transformation, the steps of determining the basic vector and the solution of the action time corresponding to the basic vector are simplified [18].

2 Current-Source Inverter

The main circuit structure of AC-DC-AC type inverter is shown in Fig. 1. The intermediate DC link in the main circuit of this type of inverter uses large inductance filtering to make the DC waveform relatively straight, so the internal impedance of

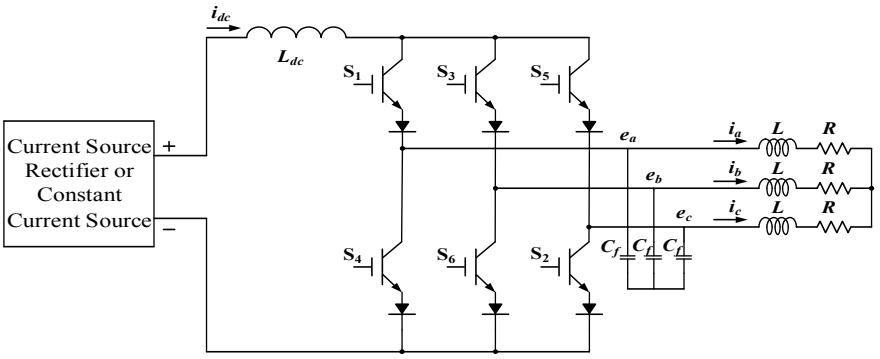

Fig. 1 Topology structure of three-phase CSI circuit

the power supply is very large, which is basically a constant current source for the load.

Due to the development of superconducting magnetic energy storage technology, large-capacity CSI has been developed. The current-source inverter CSI adopts PWM control mode, which has a significant effect on improving the current waveform (making it close to a sine wave) at low frequency. Compared with the voltage-source inverter VSI, its characteristics are as follows:

(1) The current-source inverter is a constant current source, and the system has a slow response to load current changes, so it is suitable for single motor transmission, but it can meet the requirements of quick start-up, braking, and reversible operation. VSI is a constant voltage source and is suitable as a variable-frequency power supply for multiple motors running synchronously.
(2) The current-source inverter has four-quadrant operation capability without any additional power switching devices; however, a voltage-source inverter must have an active inverter attached to the grid side. When the power is large, a sine wave filter needs to be added to the output.
(3) Due to the ability of the current-source inverter to change the polarity of the DC voltage quickly, the dynamic response of the current-source variable-frequency speed regulation system is faster than that of the voltage-source variable-frequency speed regulation system.
(4) Current-source inverter needs a minimum load connected for normal operation. Voltage-source inverter can run under no-load condition.
(5) Current-source inverters are generally used in large-capacity occasions. It uses gate turn-off thyristor (GTO), silicon controlled rectifier (SCR), or integrated gate-commutated thyristor (IGCT) components in series to achieve direct high-voltage frequency conversion. The voltage can reach 10 kV. Because the DC link uses inductance element, which is not sensitive enough to the current, so it is not easy for an overcurrent fault to happen; the inverter is also very reliable, and the protection performance is good.

3 The Simulation of Three-Phase CSI System

According to the working principle of CSI shown in Fig. 1, a three-phase CSI Simulink universal simulation model is built in the MATLAB environment. The model diagram of the entire system is shown in Fig. 2.

Set the simulation sampling time to 5e−6 s, the switching frequency to 7500 Hz, the modulation depth to 1, the system output expected frequency is 50 Hz, the output filter inductance is 5 mH, the DC is 100 A, the load is a 1 Ω pure resistive load, the output filter capacitor is 30 μF, and simulation time is taken as 0.2 s. After the simulation operation is completed, the waveform of the a-phase voltage waveform after stabilization is shown in Fig. 3, with good sinusoidal degree.

Figure 4 shows the phase A voltage waveform when the inverter outputs 50 Hz and 35 Hz. It can be seen from the figure that the inverter output has a good sine.

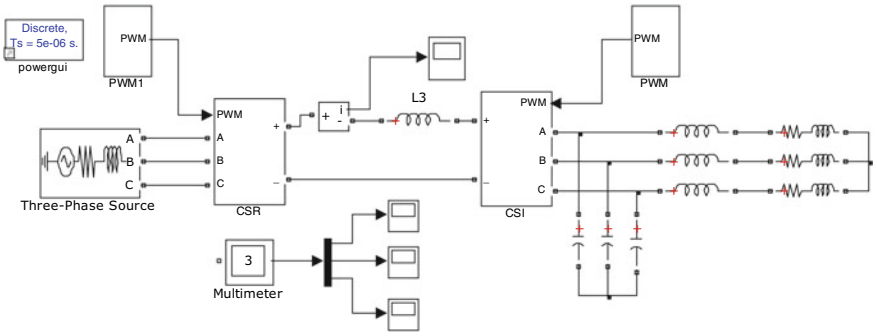

Fig. 2 Simulation diagram of a three-phase CSI universal system

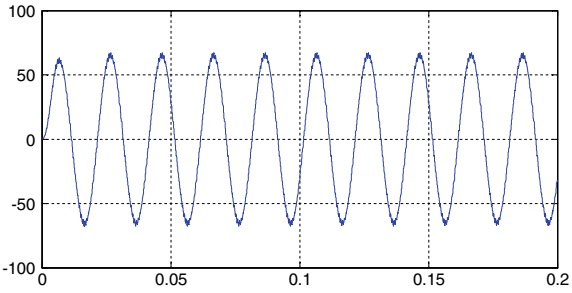

Fig. 3 A-phase output voltage waveform with SVPWM modulation

When the A-phase load is abruptly changed to half of the original, the frequency of the modulation wave is changed in the DSP program at the same time.

It can be seen from Fig. 4 that although the waveform of the inverter output has a good sine degree, there are still large harmonics. This is because the resistive analog load used in this article limits the selection of filter inductance parameters. At the same time, for safety reasons, the current level of the system is small, and the current ripple is large compared to the fundamental wave.

4 Conclusions

From the perspective of space vector, SVPWM directly controls the output current vector of the system. It is a widely used online modulation method with fast dynamic response, high current utilization rate, and low harmonic level under low-frequency switching conditions, which lays a foundation for the future engineering application of current converter.

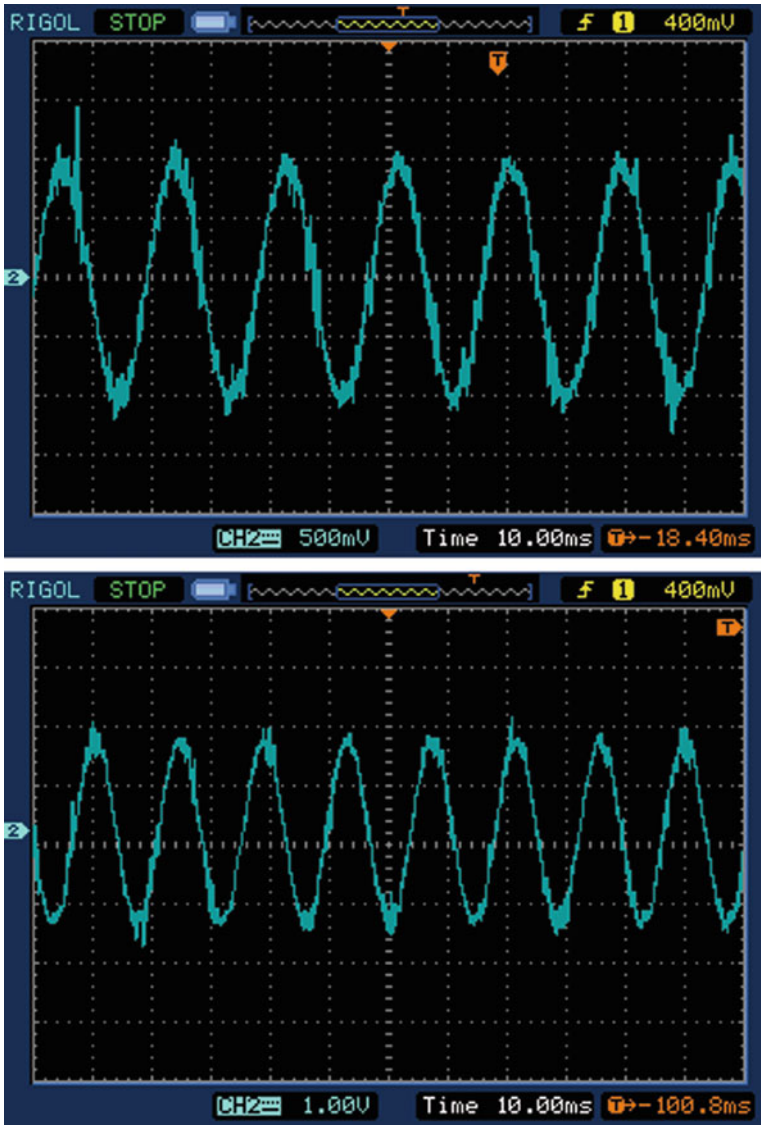

Fig. 4 Voltage waveform when the phase A on the inverter side outputs 50 and 35 Hz

Acknowledgements This research was supported by the science and technology project in Jilin Province (20180312009ZX).

References

1. Jin, T., Liu, P.: Design and verification method of multi-channel SPWM waveform generator. J. Instrum. **39**(07), 208–216 (2018)
2. Liu, T.T., Tan, Y., Wu, G.: Simulating of high speed PMSM control system based on SVPWM. Power Syst. Prot. Control **37**(12), 11–19 (2009)
3. Lu, B., Liu, W.: Simulation of three-phase SPWM inverter based on Matlab/Simulink. Electron. Des. Eng. **21**(1), 132–134 (2013)
4. Tan, G., Liu, Z., Ye, Z.B.: Research on SVPWM algorithm of ANPC-5L inverter based on line voltage coordinate system. Chin. J. Electr. Eng. **33**(30), 26–33 (2016)
5. Wang, W., Luo, A., Li, Y., Xu, X.Y.: A new SVPWM algorithm for active power filters. Chin. J. Electr. Eng. **32**(18), 52–58 (2012)
6. Ozturk, S.B., Akin, B., Toliyat, H.A.: Low-cost direct torque control of permanent magnet synchronous motor using Hall-effect sensors. In: Proceedings of IEEE. APEC, pp. 1–7 (2006)
7. Dusmez, S., Qin, L., Akin, B.: A new SVPWM technique for DC negative rail current sensing at low speeds. IEEE Trans. Industr. Electron. **62**(2), 826–831 (2015)
8. Li, X., Dusmez, S.: A new SVPWM for the phase current reconstruction of three-phase three-level T-type converters. IEEE Trans. Power Electron. **31**(3), 2627–2637 (2016)
9. Gu, L., Jin, K.: A three-phase isolated bidirectional AC/DC converter and its modified SVPWM algorithm. IEEE Trans. Power Electron. **30**(10), 5458–5468 (2015)
10. Xiong, Y., Wang, P.R., Bao, J.Y.: A new split-phase control three-phase current-source five-level inverter. Chin. J. Electr. Eng. **25**(16), 13–16 (2005)
11. Wang, K.R., Wu, Y.X., Li, Y.L.: Digital implementation of PWM modulation for a current-source three-phase inverter. Power Electron. Technol. **4**, 76–78 (2011)
12. Wu, X.J., Xiong C.L., Hou, N.F., Xiao, Y.: A simplified multilevel SVPWM algorithm suitable for any three-phase cascaded H-bridge converter. Chin. J. Electr. Eng. **36**(10), 2753–2761 (2016)
13. Ma, M., He, X., Williams, B.W.: Hybrid PWM strategy of SVPWM and VSVPWM for NPC three-level voltage-source inverter. IEEE Trans. Power Electron. **25**(12), 3026–3036 (2010)
14. Wu, X.J., Xiong, C.L., Feng, X.Y.: A general multilevel space vector PWM algorithm suitable for single-phase cascaded H-bridge converters. Trans. China Electrotech. Soc. **32**(14), 127–136 (2017)
15. Xiong, C.L., Diao, F., Wu, X.J., Feng, X.Y.: Simplified multi-level SVPWM algorithm for single-phase converters. J. Motors Control **23**(04), 56–66 (2019)
16. Dai, P., Wu, B., Su, L.C., Yang, T.P.: Research on common mode voltage suppression strategy of NPC/H bridge five-level inverter based on new SVPWM. J. Electr. Eng. Control **19**(02), 20–25 (2015)
17. Wang, G., Wang, X.D., Ma, J.J., Bai, Y.L.: Research on a fast SVPWM algorithm and its over modulation strategy. Power Syst. Prot. Control **47**(03), 136–145 (2019)
18. Liu, Z., Wang, Y., Tan, G., Li, H.: A novel SVPWM algorithm for five-level active neutral-point-clamped converter. IEEE Trans. Power Electron. **31**(5), 3859–3866 (2016)

A New Test Method for 5G Massive MIMO Devices: Plane Wave Generator with 36 Planar Array Antenna

Yu Zhang, Xiang Wu, Xiang Zhang, Yuxin Ren, Chong Pan, and Guiming Wei

Abstract With the development of communication technology, 4G antenna and 5G massive multiple-input multiple-output (MIMO) devices need the over-the-air test in the anechoic chamber. Due to the size and high working frequency, large distances between the transmitter and receiver are required to measure the device in a real far-field environment, which will largely increase the area and cost of the test system. This paper presents a simulation of the plane wave generator (PWG), which could synthesize a plane wave in the near field and largely minimize the size and cost. The PWG anechoic chamber was usually consisted of a plane wave generator, a turntable, and a whole chamber. Inside the chamber, the sidewalls, floor, and ceiling are covered with high-quality absorbers to reduce the reflected energy level. The chamber was designed and simulated using the commercial package named "EAST WAVE". The quality of the quiet zone for this chamber was verified at 3.5 GHz through finite-difference time-domain (FDTD) method. During the simulation modeling, the dielectric and permeability of the absorber have also been taken into account, and the perfect matched layer conditions are applied to limit the computation domain. The simulation result shows that good amplitude and phase uniformity throughout the quiet zone (QZ) have been achieved.

1 Introduction

Antenna test is an important and interesting topic in the over-the-air (OTA) test of 4G and 5G devices, and many different solutions based on far-field ranges, compact antenna test ranges, and near-field ranges have been adopted [1]. High investment, large antenna anechoic chamber, and long construction period are shortcomings of these solutions. In this paper, a new method to synthesize a plane wave in the near field is introduced, the plan wave generator (PWG) system, with few probes achieving

Y. Zhang · X. Wu (✉) · X. Zhang · Y. Ren · C. Pan · G. Wei
China Academy of Information and Communications Technology, CAICT, No. 52 Hua Yuan Bei Road, Haidian District 10091, Beijing, China
e-mail: wuxiang@caict.ac.cn

R. Kountchev et al. (eds.), *Advances in Wireless Communications and Applications*,
Smart Innovation, Systems and Technologies 191,
https://doi.org/10.1007/978-981-15-5879-5_6

similar quiet zone (QZ) performance like the far-field chamber. Compared with the other systems, the PWG has considerably smaller size at lower frequency, which reduces the investment and the area of the anechoic chamber.

As shown in Fig. 1, a PWG system usually consists of an anechoic chamber, a plane wave generator, and a turntable. Inside the chamber, the sidewalls, floor, and ceiling are covered with high-quality absorbers to reduce the reflected energy level [2]. There are different geometrical shapes for the absorbers, such as wedge and pyramid. Pyramidal shaped electromagnetic wave absorbers have wide frequency and wide incident angle characteristics to efficiently absorb incoming electromagnetic wave from the test devices in the anechoic chambers [3]. In order to investigate the amplitude and phase uniformity throughout the quiet zone of the PWG chamber before construction, design and simulations are needed. To save the money and time, a full-waveform simulation is developed and demonstrated in this paper [4].

For anechoic chamber simulation, various kinds of methods in the frequency domain have been developed; for now, the method of moments (MOM), finite element method (FEM), and finite-difference time-domain (FDTD) method are most commonly used [5]. Unlike other methods, the FDTD method is a time-domain full-waveform technique which has been modified and developed through the last decades, and it can directly compute the impulse response of an electromagnetic system in a single simulation, and the FDTD method is adopted to simulate multi-frequencies efficiently.

In this paper, a plane wave generator with 36 planar array antennas has been studied and gets a good performance in the anechoic chamber. The ability to provide

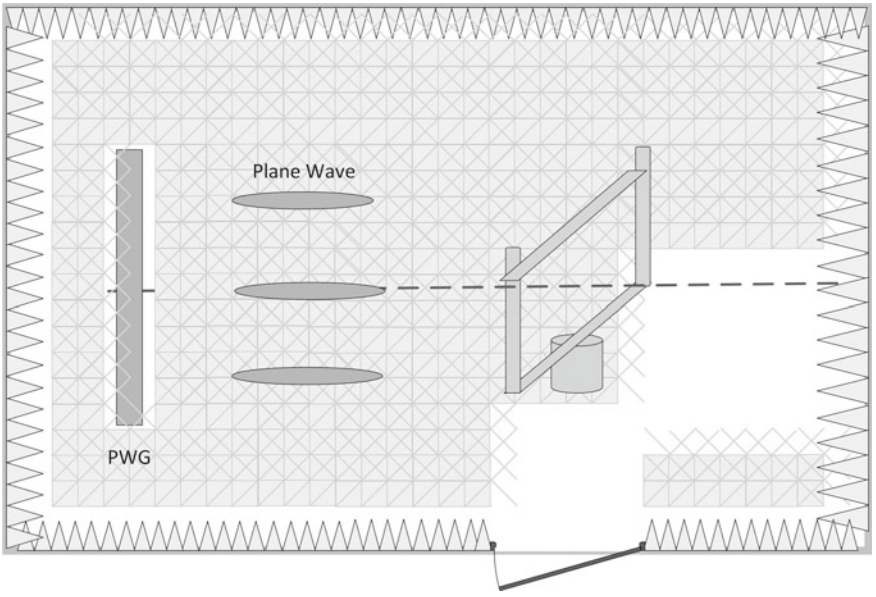

Fig. 1 Overview of the objects in the chamber

good quality of quiet zone will be introduced through simulation and the real test data in the following sections. The FDTD method is employed to establish the design criteria for the PWG system through the commercial package named "EAST WAVE" released by Dong Jun Technology Software.

2 Design Theory

For antenna measurements, a constant amplitude and phase must be generated across an area which is larger than the device under test (DUT). Focusing concentrates on the field plane wave generation attempts to minimize the amplitude and phase deviations. In this paper, a method to design a linear array that creates an approximate plane wave over a prescribed area at a short distance will be presented [6]. This method significantly reduces the separation distance between the transmit antenna and the antenna under test (AUT) and largely reduced the anechoic chamber area. Next, as shown in Fig. 2, a 36-element array at the distance 20λ to approximate a plane

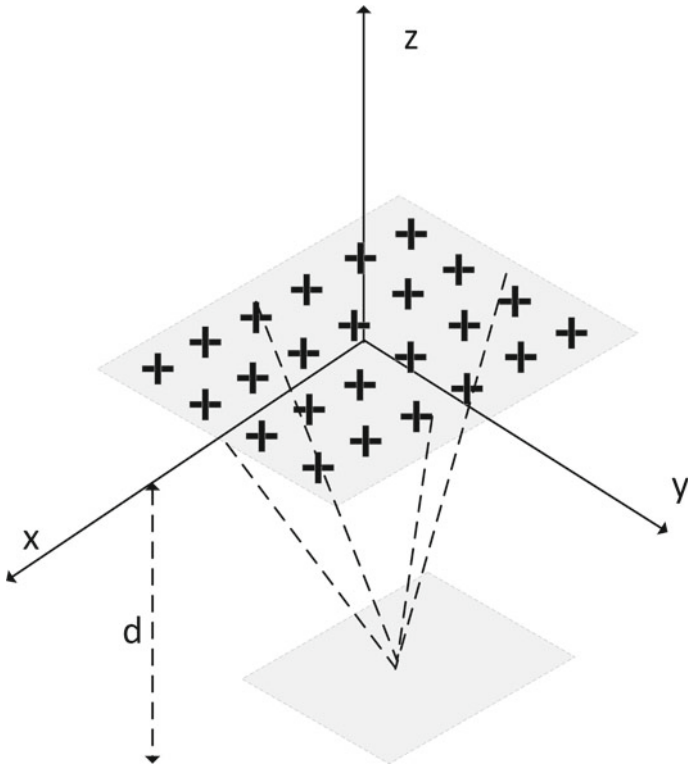

Fig. 2 Rectangular geometry model for the PWG

wave over the QZ will be introduced. And the size and quality of QZ are decided by the number of the array and the element locations [7]; increasing the numbers and optimizing the locations will get a better result.

The mathematic formulation of the radiation pattern of a linear array is given by (1):

$$E(x_m, y_m, z) = \sum_{n=1}^{N} w_n \frac{e^{jkR_{mn}}}{4\pi R_{mn}} \tag{1}$$

where N is the number of elements in the array, w_n is the complex weight of elements n, $k = 2\pi/\lambda$, λ is the wavelength, R_{mn} = distance from element n to the field point (x_m, y_m, z) on the plane wave, and z = distance from array to the plane wave.

The quality of the QZ performance is decided by the numbers of elements, element locations, and element weights. Adjusting these parameters could get a suitable QZ size for our test system. In this paper is used a 50 cm QZ size chamber simulation which is implemented by 36 orthogonal antenna elements at 2 m distance.

3 Chamber Modeling

A PWG system usually consists of an anechoic chamber, a plane wave generator, a turntable, and absorbers. In order to validate the PWG system, the absorber performance and position of the turntable should be taken into consideration seriously. In this paper, a 4.5 m * 4 m * 4 m anechoic chamber will be simulated, with −40 dB pyramidal absorber filled, the turntable located at 2 m away from the PWG, and the PWG system is designed and simulated with FDTD method. The QZ performance simulation result will be introduced next. The anechoic chamber is set with dimensions of 4 m high, 4 m width, and 4.5 m long. A planar source antenna with 36 electrical antennas is chosen as the transmitter source [8].

The quiet zone performance was evaluated through FDTD method by the commercial package "EAST WAVE". Inside the PWG chamber, the sidewalls, floor, and ceiling are covered with high-quality pyramidal absorbers; the pyramidal structure and the block beneath it are made of the same material. At the bottom of the pyramid and block, there is a layer of highly conductive material (perfect electric conductor) which is used to block the interference signal from outside the chamber; above the perfect electric conductor, the perfect matched layer (PML) boundary conditions are employed [9].

Another important element in the chamber is the PWG array, which is located 1 m away from the front wall; the PWG consists of 36 planar array antennas in an area of 2 m * 2 m; the array antenna is a dual-polarized antenna which could be used in 800 MHz to 6 GHz frequency range. The array antenna is an important factor in the PWG system, which is designed with wide bandwidth and small physical size. The turntable (the position of the device under test) is 2 m away from the PWG array,

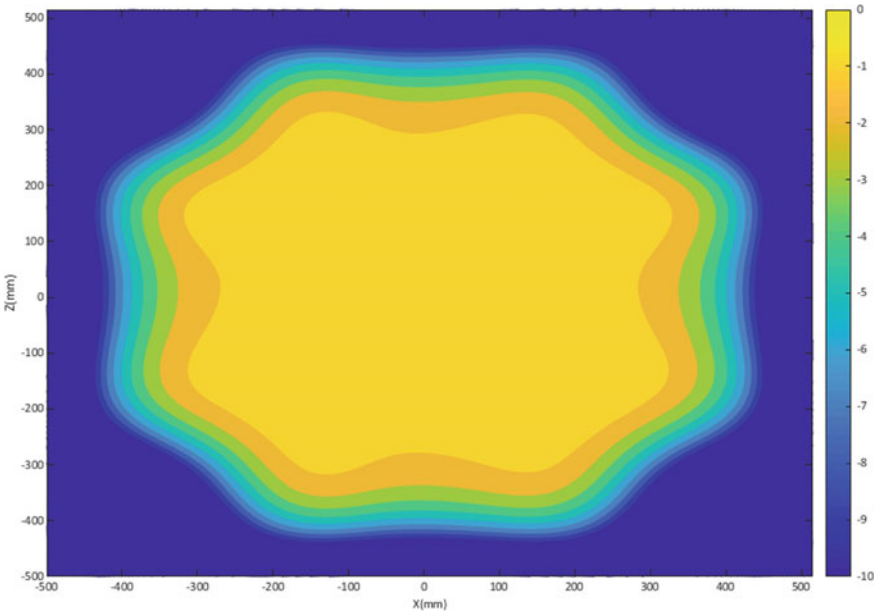

Fig. 3 *E*-field amplitude map of QZ center at 3.5 GHz

and the PWG generates a plane wave at a very close distance which could largely decrease the size of the chamber. The space between the pyramid absorber and PWG array is filled with air to simulate the real condition in the chamber. In order to get the chamber performance in a wide frequency range, a Gaussian pulse function is chosen as the transmitter source. Simulation center frequency 3.5 GHz and the quiet zone electric field distributions are simulated over the position span from −0.5 to 0.5 m.

Using data from the FDTD forward modeling, the quality of the chamber is searched. The quiet zone amplitude and phase field distribution generated by the PWG are shown in Figs. 3 and 4, respectively. As expected, in the designed quiet zone 0.5 m * 0.5 m, the worst-case amplitude variation in the quiet zone region is lower than ±0.4 dB at 3.5 GHz, and phase variation is lower than ±3°, which could meet our test requirements.

4 Conclusions

In this paper, the FDTD method is developed and implemented for the PWG chamber simulation. The PWG system usually consists of an anechoic chamber, a plane wave generator, and a turntable. To test the performance of the chamber, the system was modeled and simulated through the commercial software “EAST WAVE”; PML

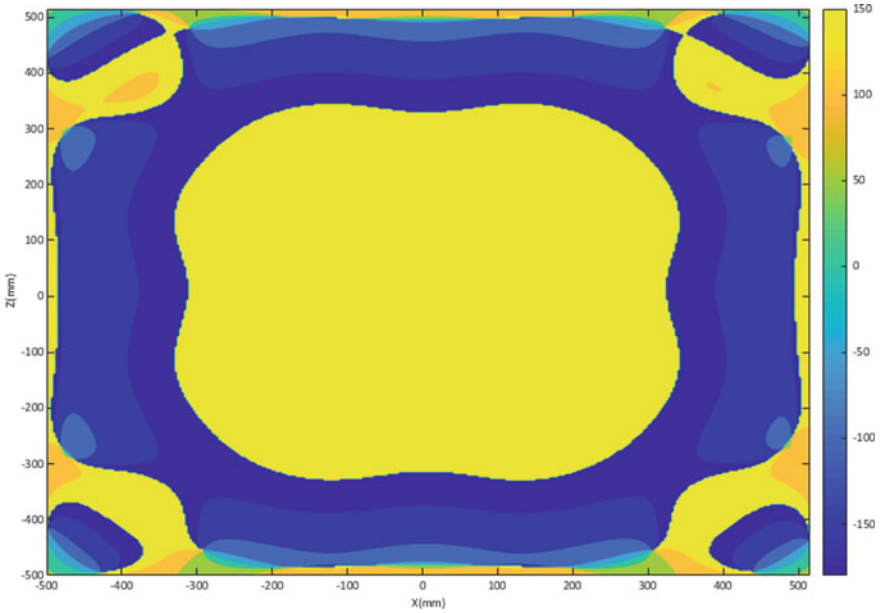

Fig. 4 *E*-field phase map of QZ center at 3.5 GHz

boundary conditions and full-waveform simulation were employed for the numerical modeling. For further validation, an anechoic chamber with the designed PWG is designed and simulated. The simulation result of the model on QZ uniformity shows that good amplitude and phase uniformity throughout the QZ have been achieved. Adjusting the location of the turntables and optimizing the element locations improve the quality of the plane wave; finally, a suitable model was achieved. The QZ performance of the PWG system was validated through simulation, and the result shows that good amplitude and phase uniformity throughout the QZ have been achieved.

Acknowledgements This work was supported by the National Major Science and Technology Projects (No. 2018ZX03001028).

References

1. Kotterman, W.: New challenges in over-the-air testing. In: The 11th European Conference on Antennas and Propagation, pp. 3676–3678. IEEE, Paris (2017)
2. Bucci, O.M.: Plane-wave generators: design guidelines, achievable performances and effective synthesis. IEEE Trans. Antennas Propag. **61**(4), 2005–2018 (2013)
3. Severin, H.: Nonreflecting absorbers for microwave radiation. IRE Trans. Antennas Propag. **4**(3), 385–392 (1956)
4. Li, B.J.: Analysis of far-field patterns of micro disk resonators by the finite-difference time-domain method. IEEE J. Quantum Electron. **33**(9), 1489–1491 (1997)

5. Bhobe, A.: Meander delay line challenge problem: a comparison using FDTD, FEM and MoM. In: IEEE International Symposium on Electromagnetic Compatibility. IEEE, Canada (2001)
6. Buonanno, A.: Reducing complexity in indoor array testing. IEEE Trans. Antennas Propag. **58**(8), 2781–2784 (2010)
7. Bucci, O.: An effective algorithm for the synthesis of a plane wave generator for linear array testing. In: Antennas and Propagation Society International Symposium (APSURSI). IEEE, Chicago (2012)
8. Marti-Canales, J.: Performance analysis of a compact range in the time domain. IEEE Trans. Antennas Propag. **50**(4), 511–516 (2002)
9. Kuester, E.F.: A low-frequency model for wedge or pyramid absorber arrays-I: theory. IEEE Trans. Electromagn. Compat. **36**(4), 300–306 (1994)

Feedback Heading Control for Autonomous Underwater Vehicle Based on Reduced-Order Observer

Xiangrong Zhou and Fengzhen Chen

Abstract Heading control is one fundamental functionality of motion control for autonomous underwater vehicle (AUV). However, the control performance is affected by the disturbance of surrounding environment and the unknown uncertainties of AUV. A novel reduced-order observer is proposed to estimate the state variables of AUV. A continuous-time nonlinear model-based feedback control is designed to enhance the heading control of AUV. The simulation results have shown that the control scheme for heading control proposed in this paper has good performance.

1 Introduction

The autonomous underwater vehicle (AUV) has been applied in many areas nowadays. So, the motion control of AUV has received more and more attentions in recent years. However, the effective motion control algorithm needs development to realize its applications. But its motion attitude is severely affected by environmental disturbance. The motion control of AUV in an unknown environment is a very difficult problem, especially when AUV must react to changes in time by using its full maneuvering capabilities [1–3]. The heading control capability plays an important part for AUV to complete multifarious missions. An improved dynamic fuzzy sliding mode control is designed to improve the depth tracking control performance [4]. The nonlinear dynamic controller combined with Fourier series expansion is proposed to achieve the depth tracking objective [5]. The multi-objective genetic algorithm-based self-tuning proportion–integral–derivative controller is represented to optimize the performance index which is designed and has the added resistance consumption [6]. An improved algorithm is proposed in order to conduct the path of optimal energy consumption [7]. In this paper, feedback heading control with reduced-order observer

X. Zhou · F. Chen (✉)
Department of Information Engineering, Meizhouwan Vocational Technology College, Putian, China
e-mail: fengzhen110@126.com

R. Kountchev et al. (eds.), *Advances in Wireless Communications and Applications*,
Smart Innovation, Systems and Technologies 191,
https://doi.org/10.1007/978-981-15-5879-5_7

is designed to generate the control signal according to the current system states and to make AUV track the desired heading attitude with steady state, settling time and small arrival time.

The rest of the article consists of the following parts. Section 2 describes the nonlinear kinematics and dynamics of AUV. The AUV model linearization and design method of feedback controller based on reduced-order observer are proposed in Sect. 3. The simulation result of AUV is represented to verify the effectiveness of the proposed approach in Sect. 4.

2 Kinematic and Dynamic Model of AUV

There are always two coordinate systems for AUV general motion [1]: One is the body-fixed coordinate system and the other is the inertia coordinate system. The expression of the general dynamics of AUV in the body-referenced frame is shown as follows:

$$\begin{cases} m[(\dot{u} - vr + wq) - x_G(q^2 + r^2) + y_G(pq - \dot{r}) + z_G(pr + \dot{q})] = X \\ m[(\dot{v} - wp + ur) - y_G(r^2 + p^2) + z_G(qr - \dot{p}) + x_G(qp + \dot{r})] = Y \\ m[(\dot{w} - uq + vp) - z_G(p^2 + q^2) + x_G(rp - \dot{q}) + y_G(rq + \dot{p})] = Z \\ I_x\dot{p} + (I_z - I_y)qr + m[y_G(\dot{w} + pv - qu) - z_G(\dot{v} + ru - pw)] = K \\ I_y\dot{q} + (I_x - I_z)rp + m[z_G(\dot{u} + qw - rv) - x_G(\dot{w} + pv - qu)] = M \\ I_z\dot{r} + (I_y - I_x)pq + m[x_G(\dot{v} + ru - pw) - y_G(\dot{u} + qw - rv)] = N \end{cases} \tag{1}$$

where m is AUV mass; x_G, y_G, z_G are the locations of AUV center of mass; I_x, I_y, I_z are rotational inertia of AUV mass; u, v, w, $\dot{u}$, $\dot{v}$, $\dot{w}$ are AUV velocity and acceleration in x-axis, y-axis and z-axis; p, q, r, $\dot{p}$, $\dot{q}$, $\dot{r}$ are AUV angle velocity and angle acceleration of roll, pitch and yaw. The general kinematics of AUV is written as follows

$$\begin{bmatrix} \dot{\chi} \\ \dot{y} \\ \dot{z} \end{bmatrix} = J(\eta_2) \begin{bmatrix} u \\ v \\ w \end{bmatrix} \tag{2}$$

$$\eta_1 = [\chi, y, z]^{\mathrm{T}} \tag{3}$$

$$\eta_2 = [\varphi, \theta, \psi]^{\mathrm{T}} \tag{4}$$

where $\chi, y, z, \dot{x}, \dot{y}, \dot{z}$ are locations and velocities of AUV in x-axis, y-axis and z-axis of the inertia coordinate system, respectively; φ, θ, ψ are the roll angle, pitch angle and yaw angle of AUV, respectively; η_1, η_2 are location vector and attitude angle vector;

$$J(\eta_2) = \begin{bmatrix} \cos\varphi\cos\theta & -\sin\psi\cos\varphi + \cos\psi\sin\theta\sin\varphi & \sin\psi\sin\varphi + \cos\psi\sin\theta\cos\varphi \\ \sin\psi\cos\theta & \cos\psi\cos\varphi + \sin\psi\sin\theta\sin\varphi & -\cos\psi\sin\varphi + \sin\psi\sin\theta\cos\varphi \\ -\sin\theta & \cos\theta\sin\varphi & \cos\theta\cos\varphi \end{bmatrix}$$

3 Design of Feedback Controller Based on Observer

The design structure for AUV is shown in Fig. 1, based on MATLAB.

(1) *kinematic model linearization*

According to the relation between the attitude angle and the angle velocity, the equation is described as follows:

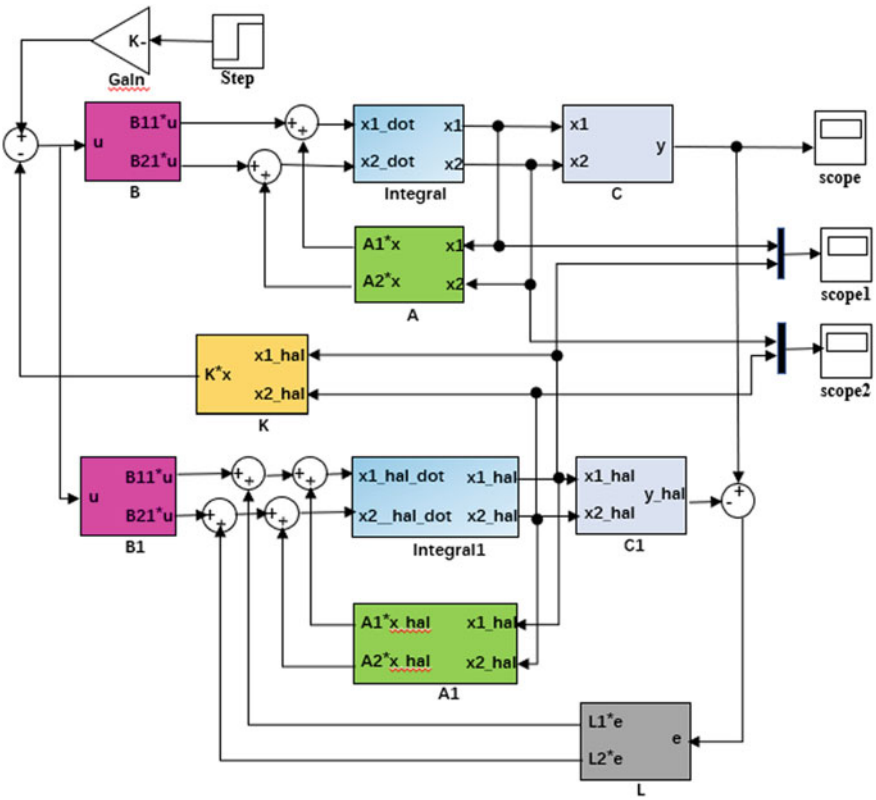

Fig. 1 System frame of feedback control with observer

$$\begin{bmatrix} \dot{\varphi} \\ \dot{\theta} \\ \dot{\psi} \end{bmatrix} = J'(\eta_2) \begin{bmatrix} p \\ q \\ r \end{bmatrix} \tag{5}$$

$$J'(\eta_2) = \begin{bmatrix} 1 & \sin\varphi\tan\theta & \cos\varphi\tan\theta \\ 0 & \cos\varphi & -\sin\varphi \\ 0 & \sin\varphi/\cos\theta & \cos\varphi/\cos\theta \end{bmatrix} \tag{6}$$

Equations (5) and (6) are used in Eq. (2) and then are obtained:

$$\begin{cases} \dot{x} = u\cos\psi - v\sin\psi \\ \dot{y} = u\sin\psi + v\cos\psi \\ \dot{\psi} = r \end{cases} \tag{7}$$

The Euler's expansion formulas are given as follows

$$\begin{cases} \sin\psi = \psi - \frac{\psi^3}{3!} \\ \cos\psi = 1 - \frac{\psi^2}{2!} \end{cases} \tag{8}$$

Equation (8) is used in Eq. (7); for the AUV heading control, one of the most important interference factors is surge, so here, we only consider the impact of surge. Then,

$$\begin{cases} \dot{x} = u - v\psi \\ \dot{y} = U\psi + v \\ \dot{\psi} = r \end{cases} \tag{9}$$

where U is the steady-state surge velocity.

(2) *dynamic model linearization*

The horizontal plane model of AUV is linearized, and the equation is given as follows

$$\begin{cases} m[\dot{u} + \dot{r}y_G] = X \\ m[\dot{v} + Ur + \dot{r}x_G] = Y \\ I_{zz}\dot{r} + m[x_G(\dot{v} + Ur) - y_G\dot{u}] = N \end{cases} \tag{10}$$

where

$$\begin{cases} X = X_{\dot{u}}\dot{u} + X_u u + X_r r + X_{\text{prop}} \\ Y = Y_{\dot{v}}\dot{v} + Y_v v + Y_{\dot{r}}\dot{r} + Y_{\delta_r}\delta_r \\ N = N_v v + N_{\dot{v}}\dot{v} + N_r r + N_{\dot{r}}\dot{r} + N_{\delta_r}\delta_r \end{cases};$$

$X_{\dot{u}}$, $Y_{\dot{v}}$ and $N_{\dot{v}}$ are acceleration coefficients; X_u, Y_v and N_v are velocity coefficients; X_r, Y_r, Y_{δ_r}, N_{δ_r}, N_r are angle velocity coefficients; $Y_{\dot{r}}$ and $N_{\dot{r}}$ are angle acceleration coefficients; δ_r is the rudder angle.

All higher order terms are rejected out in Eq. (10), and Eq. (9) is used in Eq. (1); then, we can get the equation as follows

$$\begin{cases} (m - Y_{\dot{v}})\dot{v} - Y_r\dot{r} + (mU - Y_r)r - Y_v v = Y_{\delta_r}\delta_r \\ (I_{zz} - N_{\dot{r}})\dot{r} - N_{\dot{v}}\dot{v} - N_r r - N_v v = N_{\delta_r}\delta_r \\ \dot{\psi} = r \end{cases} \tag{11}$$

The matrix equation of motion with 3DOF can be given as follows

$$\begin{bmatrix} m - Y_{\dot{v}} & -Y_{\dot{r}} & 0 \\ -N_{\dot{v}} & I_{zz} - N_{\dot{r}} & 0 \\ 0 & 0 & 1 \end{bmatrix} \begin{bmatrix} \dot{v} \\ \dot{r} \\ \dot{\psi} \end{bmatrix} - \begin{bmatrix} Y_v & Y_r & 0 \\ N_v & N_r & 0 \\ 0 & 1 & 0 \end{bmatrix} \begin{bmatrix} v \\ r \\ \psi \end{bmatrix} = \begin{bmatrix} Y_{\delta_r} \\ N_{\delta_r} \\ 0 \end{bmatrix} [\delta_r] \tag{12}$$

The matrix equation of moth with 2 DOF for simulation can be given as follows

$$\begin{bmatrix} I_{zz} - N_{\dot{r}} & 0 \\ 0 & 1 \end{bmatrix} \begin{bmatrix} \dot{r} \\ \dot{\psi} \end{bmatrix} - \begin{bmatrix} N_r & 0 \\ 1 & 0 \end{bmatrix} \begin{bmatrix} r \\ \psi \end{bmatrix} = \begin{bmatrix} N_{\delta_r} \\ 0 \end{bmatrix} [\delta_r] \tag{13}$$

For notational simplicity, the matrix Eq. (13) is denoted by

$$M\dot{x} - C_d x = Du \tag{14}$$

The state-space equations are given as follows

$$\begin{cases} \dot{x} = Ax + Bu \\ y = Cx \end{cases} \tag{15}$$

where $\begin{cases} A = M^{-1}C_d \\ B = M^{-1}D \end{cases}$.

(3) *observer design*

$$\dot{\hat{x}} = A\hat{x} + Bu + L(y - C\hat{x}) \tag{16}$$

where $\hat{x}$ is the estimation of system state vector x.

Let $\tilde{x} = x - \hat{x}$, we get

$$\dot{\tilde{x}} = (A - LC)\tilde{x} \tag{17}$$

4 Simulation Results

The moment of inertia origin at the center of buoyancy is $I_{zz} = 3.46$ kgm^2. The cross-flow added mass is given as $N_{\dot{r}} = -4.88$ kgm^2 and $N_r = -7$ kgm^2/s. The Fin moment is $N_{\delta_r} = -54.53$ kgm^2/s^2. The surge steady-state velocity is $U = 2$ m/s. The system matrices are

$$A = \begin{bmatrix} -0.8403 & 0 \\ 1 & 0 \end{bmatrix}, \quad B = \begin{bmatrix} -6.5462 \\ 0 \end{bmatrix}, \quad C = \begin{bmatrix} 1 \\ 0 \end{bmatrix}, \quad L = \begin{bmatrix} 386.2524 & 40.1597 \end{bmatrix};$$

the system state is $x_0 = \begin{bmatrix} 0 & 1 \end{bmatrix}^{\mathrm{T}}$ and $\hat{x}_0 = \begin{bmatrix} 0 & 0 \end{bmatrix}^{\mathrm{T}}$.

The simulation results of yaw angle ψ and yaw angle velocity r used in the method proposed in this paper are shown in Figs. 2 and 3.

The comparison simulation results of the angle ψ and the yaw angle velocity r with observer and without observer are shown in Fig. 4. The comparison simulation results of the system output are shown in Fig. 5. From the simulation results, the method proposed in this paper has got better results.

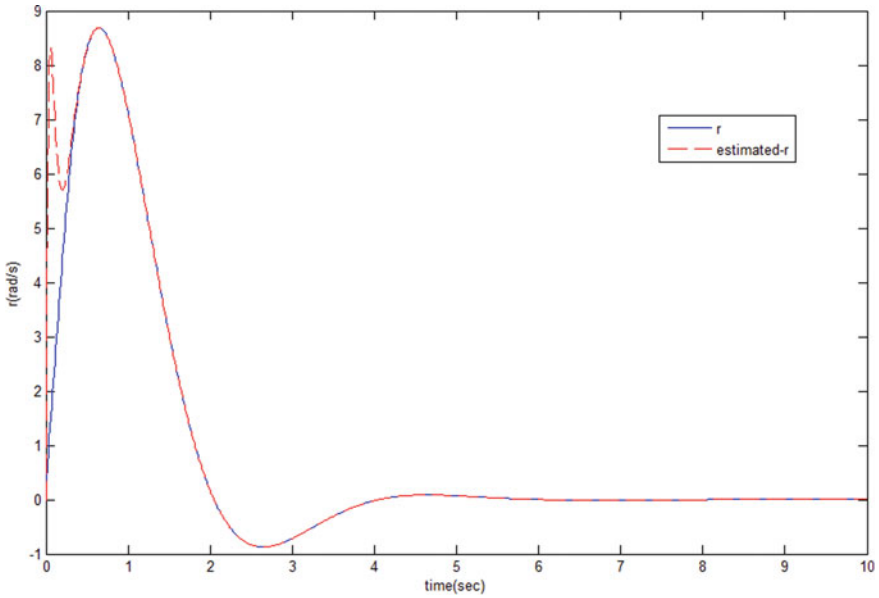

Fig. 2 Simulation r and estimation of r

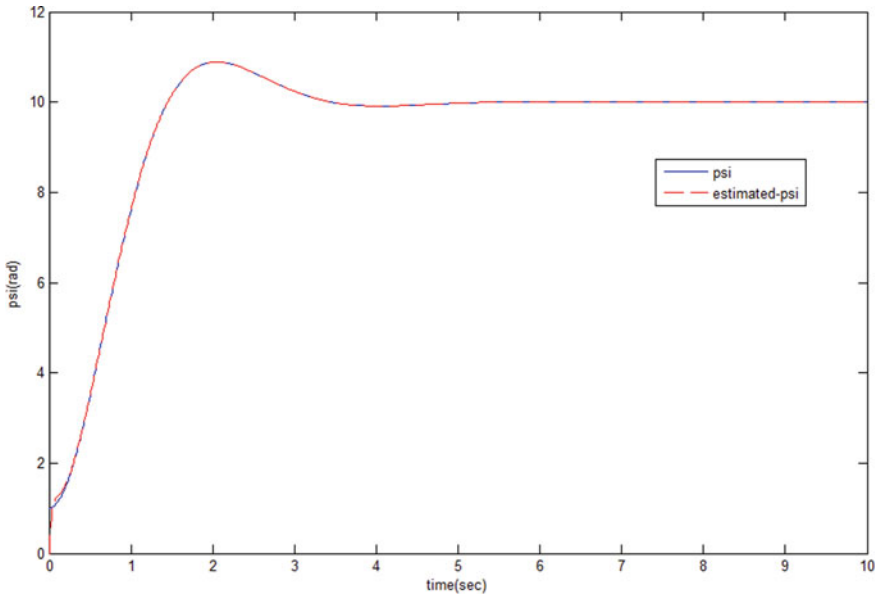

Fig. 3 Simulation ψ and estimation of ψ

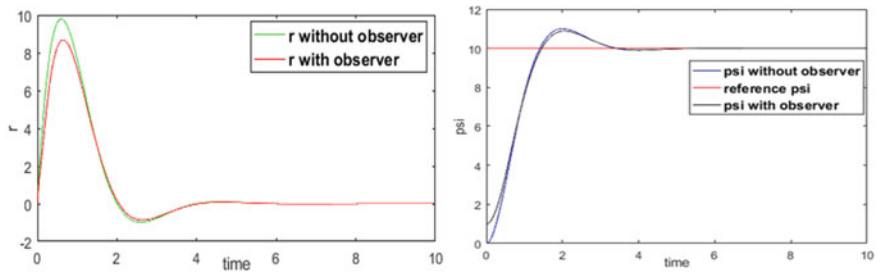

Fig. 4 Comparison of r and ψ with observer and without observer

Fig. 5 Comparison of system output with observer and without observer

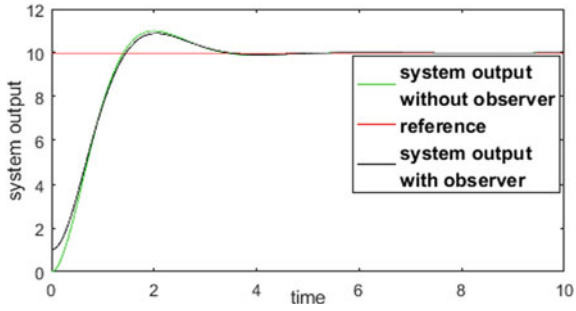

5 Conclusions

In this paper, the method of feedback control with observer is proposed. The simulation and experiment results validate the feasibility and stability of the proposed method in AUV heading control.

Acknowledgements This work is supported by education and scientific research project for young teachers in Education Department of Fujian Province of China (Project Number: JZ181032).

References

1. Frazzoli, E.: Robust hybrid control for autonomous vehicle motion planning. In: IEEE Conference on Decision & Control, vol. 1, pp. 821–826 (2000)
2. Alt, C.: Autonomous underwater vehicles. Autonomous Underwater Lagrangian Platforms and Sensor Workshop, vol. 3 (2003)
3. Yan, Z., Yu, H., Hou, S.: Diving control of underactuated unmanned undersea vehicle using integral-fast terminal sliding model control. J. Central South Univ. **23**(5), 1085–1094 (2016)
4. Lakhekar, G.V., Waghmare, L.M., Londhe, P.S.: Enhanced dynamic fuzzy sliding mode controller for autonomous underwater vehicles. In: Proceedings of the IEEE Underwater Technology (UT'15). IEEE, Chennai, India, Feb 2015
5. Adhami-MIrhosseini, A., Yazdanpanah, M.J., Aguiar, A.P.: Autonomous bottom-following for underwater robotic vehicles. Automatica **50**(8), 2155–2162 (2014)
6. Liu, Z., Jin, H.: Extended radiated energy method and its application to a ship roll stabilization control system. Ocean Eng. **72**, 25–30 (2013)
7. Liang, X., Hua, X., Su, L., Li, W., Zhang, J.: Energy conservation control strategy of autonomous underwater vehicle for ocean search. J. Coastal Res. **73**, 589–593 (2015)

Influence on Band-Gap Overlap and *Q*-Factor of the Coaxial Bragg Structure with Double-Sinusoidal Ripples Operating at 0.35 THz Frequency

Xue-Yong Ding, Hong-Rui Su, Yuan Wang, and Lian-Sheng Wang

Abstract Based on the mode-coupling method, a comparative study is carried out for the frequency response of the double-sinusoidal ripples structure operating at 0.35 THz frequency. The results show that compared to the single-sinusoidal ripples structure, the bandwidth of the competing mode and the operating mode are narrowed by employing the double-sinusoidal ripples, and the *Q*-factor becomes greater. These peculiarities are favorable to constructing a single higher-order mode and high-*Q* resonator operating at THz frequency.

1 Introduction

The Bragg structure is widely used in optoelectronics, microwave electronics, and terahertz technology, especially in the cyclotron resonance maser (CARM) and free-electron laser (FEL) [1–4]. Recently, the attractive peculiarities of the coaxial Bragg structures have been paid much attention [1–11]. The study on the sinusoidal coaxial Bragg structure shows that the structure not only facilitates processing and cooling of reflectors, but also helps to improve the pattern selectivity and purity of the operating mode [11].

In this paper, on the basis of the existing sinusoidal coaxial Bragg structure, the sinusoidal distribution with the same opening depth and a smaller period is added. In order to explore a new type of coaxial Bragg structure with better performance, the characteristics of the double-sinusoidal Bragg structure are simulated and compared.

X.-Y. Ding (✉) · H.-R. Su · Y. Wang · L.-S. Wang
Sanya University, Sanya 572022, Hainan, People's Republic of China
e-mail: ding2008ding@163.com

R. Kountchev et al. (eds.), *Advances in Wireless Communications and Applications*,
Smart Innovation, Systems and Technologies 191,
https://doi.org/10.1007/978-981-15-5879-5_8

2 Theory Model

Different from the sole sinusoidal ripple structure [7], this paper envisaged to etch cycle smaller auxiliary sine distribution in the structure of the wall surface, and form the double-sinusoidal ripples as shown in Fig. 1, where a_0 and b_0 are the average radius, and l_{out} and l_{in} are the corrugation depth of the outer wall and the inner conductor, p_b and p_{in} are the main corrugation period and the embedded auxiliary corrugation, and L is the total length, φ_{out} and φ_{in} are the phase of the outer wall and the inner conductor.

In Fig. 1, the outer-wall radius R_{out} and the inner conductor radius R_{in} can be expressed as a function of the change in the longitudinal position z:

$$R_{\text{out}}(z) = a_0 - l_{\text{out}}[m_a \cos(k_B z + \varphi_{\text{out}}) + m_b \cos(k_A z + \varphi_{\text{out}})] \tag{1}$$

$$R_{\text{in}}(z) = b_0 - l_{\text{in}}[m_a \cos(k_B z + \varphi_{\text{in}}) + m_b \cos(k_A z + \varphi_{\text{in}})] \tag{2}$$

where $k_A = 2\pi/p_{\text{in}}$, $k_B = 2\pi/p_b$, $m_a + m_b = 1$, and the $K_{\text{am}} = \frac{m_b}{m_a}$ is called amplitude proportional coefficient. In general, $k_A = Nk_B$ and $l_{\text{out}} \cdot m_b$ and $l_{\text{in}} \cdot m_b$ represent the embedded auxiliary corrugation depth. When the amplitude scale coefficient $K_{\text{am}} = 0$, the coaxial Bragg structure with double-sinusoidal ripples returns sole sinusoidal ripples [7]. The angles θ_{out} and θ_{in} are expressed as:

$$\tan\theta_{\text{out}} = \frac{\mathrm{d}R_{\text{out}}}{\mathrm{d}z} = l_{\text{out}}[m_a k_B \sin(k_B z + \varphi_{\text{out}}) + m_b k_A \sin(k_A z + \varphi_{\text{out}})] \tag{3}$$

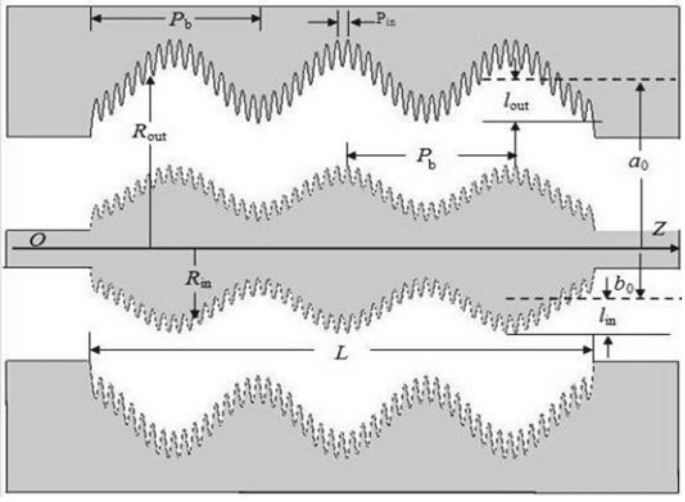

Fig. 1 Longitudinal-section profile of the double-sinusoidal ripples structure

$$\tan\theta_{\text{in}} = \frac{\mathrm{d}R_{\text{in}}}{\mathrm{d}z} = l_{\text{in}}[m_a k_B \sin(k_B z + \varphi_{\text{in}}) + m_b k_A \sin(k_A z + \varphi_{\text{in}})] \tag{4}$$

The transmission of the electromagnetic field in the reflector is solved by wave differential equations [7]. Using the eigenvector method, we can use the following $2N$ characteristic vector superposition represented in the form of a general solution of the equations.

$$\boldsymbol{f} = \left(\boldsymbol{r}_1 \mathrm{e}^{\lambda_1 z}, \boldsymbol{r}_2 \mathrm{e}^{\lambda_2 z}, \ldots, \boldsymbol{r}_{2N-1} \mathrm{e}^{\lambda_{2N-1} z}, \boldsymbol{r}_{2N} \mathrm{e}^{\lambda_{2N} z}\right) \boldsymbol{C} \tag{5}$$

The matrix form is:

$$\begin{pmatrix} f_1^+ \\ f_1^- \\ \vdots \\ f_N^+ \\ f_N^- \end{pmatrix} = \begin{pmatrix} r_{1,1}\mathrm{e}^{\lambda_1 z} & r_{2,1}\mathrm{e}^{\lambda_2 z} & \cdots & r_{2N-1,1}\mathrm{e}^{\lambda_{2N-1} z} & r_{2N,1}\mathrm{e}^{\lambda_{2N} z} \\ r_{1,2}\mathrm{e}^{\lambda_1 z} & r_{2,2}\mathrm{e}^{\lambda_2 z} & \cdots & r_{2N-1,2}\mathrm{e}^{\lambda_{2N-1} z} & r_{2N,2}\mathrm{e}^{\lambda_{2N} z} \\ \vdots & \vdots & \ddots & \vdots & \vdots \\ r_{1,2N-1}\mathrm{e}^{\lambda_1 z} & r_{2,2N-1}\mathrm{e}^{\lambda_2 z} & \cdots & r_{2N-1,2N-1}\mathrm{e}^{\lambda_{2N-1} z} & r_{2N,2N-1}\mathrm{e}^{\lambda_{2N} z} \\ r_{1,2N}\mathrm{e}^{\lambda_1 z} & r_{2,2N}\mathrm{e}^{\lambda_2 z} & \cdots & r_{2N-1,2N}\mathrm{e}^{\lambda_{2N-1} z} & r_{2N,2N}\mathrm{e}^{\lambda_{2N} z} \end{pmatrix} \begin{pmatrix} C_1 \\ C_2 \\ \vdots \\ C_{2N-1} \\ C_{2N} \end{pmatrix} \tag{6}$$

where $\boldsymbol{C} = (C_1, C_2, \ldots, C_{2N-1}, C_{2N})^{\mathrm{T}}$ is an arbitrarily complex constant vector, $\lambda_u (u = 1, 2, 3, \ldots, 2N)$ is for the complex eigenvalues, and the corresponding eigenvectors are $\boldsymbol{r_u} = \left(r_{u,1}, r_{u,2}, \ldots, r_{u,2N-1}, r_{u,2N}\right)^{\mathrm{T}}$. The $2N$ eigenvalues and corresponding eigenvectors are satisfied with the following characteristic equation:

$$(\boldsymbol{K} - \lambda \boldsymbol{I})\boldsymbol{r} = 0 \tag{7}$$

where $\boldsymbol{I}$ is an unit matrix $2N \times 2N$.

According to boundary conditions, $2N$ equations can be obtained as follows:

$$f_1^+\big|_{z=0} = \sum_{p=1}^{2N} C_p r_{p,1} = f_0 \tag{8}$$

$$f_i^+\big|_{z=0} = \sum_{p=1}^{2N} C_p r_{p,2i-1} = 0, \quad (i = 2, 3, 4, \ldots, N) \tag{9}$$

$$f_i^-\big|_{z=L} = \sum_{p=1}^{2N} C_p r_{p,2i} \mathrm{e}^{\lambda_p L} = 0, \quad (i = 1, 2, 3, \ldots, N) \tag{10}$$

The fourth-order Runge–Kutta method is used to solve differential Eqs. (8)–(10), and using the QR algorithm can be calculated all the matrix eigenvalues and corresponding eigenvectors, the LU decomposition of the complex coefficient matrix equations of the right, and the linear equations are solved with high-precision using an iterative improvement algorithm. The specific distribution of the electromagnetic

field can be obtained by the numerical simulation software, and then is solved the reflectivity of each mode:

$$R_i = \left| \frac{f_i^{-(1)}\big|_{z=0}}{f_0} \right|^2 = \left| \frac{\sum_{p=1}^{2N} C_p r_{p,2i}}{f_0} \right|^2, \quad (i = 1, 2, 3, \ldots, N) \tag{11}$$

and the cavity quality factor Q:

$$Q = \omega \frac{W}{P_l}, \tag{12}$$

where W is the stockpile energy, P_l is the loss energy, and ω is the angular frequency.

Based on the equations, we wrote the Fortran code to simulate the reflectivity characteristics of the double-sinusoidal Bragg structure. The good agreement of the Fortran language program code theory with the experiment is demonstrated for various situations in Ref. [10].

3 Influence on Band-Gap Overlap and *Q*-factor of the Double-Sinusoidal Tapered Structure

When the phase difference is set to be π, the band-gap overlap can be separated [8]. It can be further separated by using double-sinusoidal ripples Bragg structure. For better comparison, we use the following parameters in Table 1.

Figure 2 shows the frequency response of the new structure with double-sinusoidal ripples comparing with the sole sinusoidal ripples of the involved modes. We can see from Fig. 2 that not only the bandwidth of the operating mode TE_{61}, but the competing mode TM_{62} become narrowed, and the maximum of reflectivity is bigger

Table 1 Main parameters of the structure with double-sinusoidal ripples

Title	Numerical value
Operating frequency	0.35 THz
Operating mode	TE_{61}, TM_{62}
Outer-wall radius, a_0	10.0 mm
Inner conductor radius, b_0	7.0 mm
The main corrugation amplitude $l_{\text{out}} = l_{\text{in}}$	0.02 mm
The main ripple period p_b	0.43 mm
The embedded auxiliary corrugation period p_{in}	0.027 mm
Length of the cavity	85.621 mm
The phase difference $\varphi_{\text{out}} - \varphi_{\text{in}}$	π

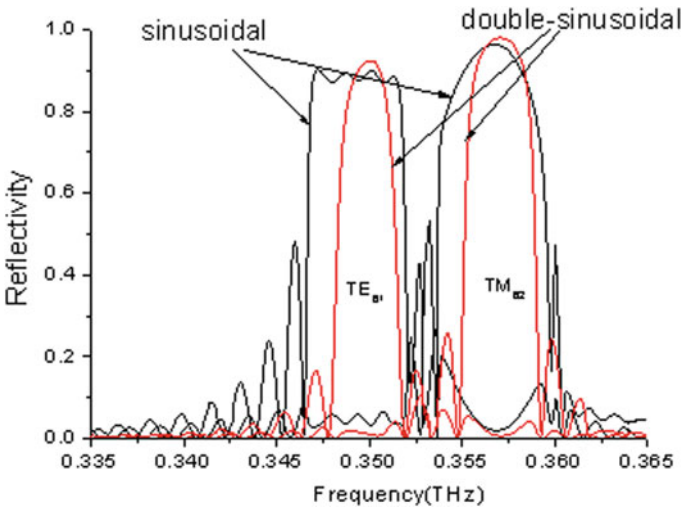

Fig. 2 Frequency response of the new structure with double-sinusoidal ripples comparing with the sole sinusoidal ripples where $K_{\mathrm{am}} = 1$

than the structure with sole sinusoidal ripples, so the model selectivity has been further improved. Furthermore, the competing mode TM_{62} moves away the operating mode TE_{61}, and the band-gap overlap also is efficiently separated.

We can see from Fig. 3 that the *Q*-factor versus the frequency of the existing sinusoidal ripples structure and double-sinusoidal ripples that the central frequency being 0.35 THz corresponds to the operating mode TE_{61} and the central frequency being 0.362 THz corresponds to the main competing mode TM_{62}. From Fig. 3, we can see that the *Q*-factor increased no matter the operating mode TE_{61} or the main competing mode TM_{62} when the coaxial Bragg structure with double-sinusoidal ripples.

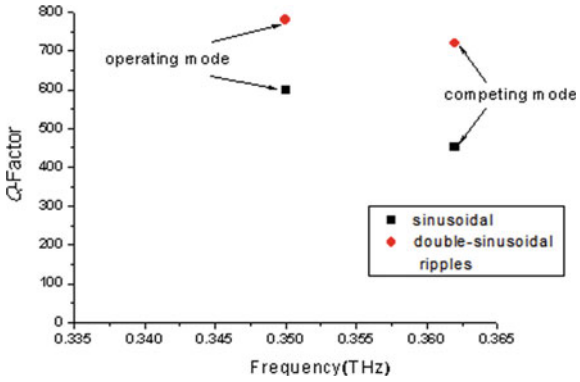

Fig. 3 *Q*-factor versus the frequency of the structure with the existing ripples and double-sinusoidal ripples

It should be pointed out that the sinusoidal curve is a smooth continuous curve; therefore, auxiliary sine distribution surface is smooth and continuous sinusoidal slot, and it is different from the rough surface machining burrs to make additional loss and reduce the Q value. On the contrary, due to the auxiliary sine slot properly changed boundary conditions, which is improved the field distribution, and the Q value increased. The results are shown in Fig. 3.

4 Conclusions

In this paper, we can draw two conclusions:

The bandwidth is narrowed and the maximum of reflectivity is bigger by employing the new structure, which is good for the model selectivity and the band-gap overlap efficiently separation. The single-mode operation with high power and high frequency can be realized.

The Q-factor is improved and the frequency selectivity is enhanced with the new structure.

Acknowledgements This work is supported by the provincial educational reform project funds of Hainan (Hnjg2019ZD-23) and the provincial Natural Science Foundation of Hainan (119MS074).

References

1. Barroso, J.J., Leite Neto, J.P.: Design of coaxial Bragg reflectors. IEEE Trans. Plasma Sci. **34**, 666–672 (2006)
2. McCowan, R.B., Fliflet, A.W., Gold, S.H., Granatstein, V.L., Wang, M.C.: Design of a waveguide resonator with rippled wall reflectors for a 100 GHz CARM oscillator experiment. Int. J. Electron. **65**, 463–475 (1988)
3. Ginzburg, N.S., Peskov, N.Y., Sergeev, A.S., Phelps, A.D.R., Cross, A.W., Konoplev, I.V.: The use of a hybrid resonator consisting of one-dimensional and two-dimensional Bragg reflectors for generation of spatially coherent radiation in a coaxial free-electron laser. Phys. Plasmas **9**, 2798–2802 (2002)
4. Konoplev, I.V., McGrane, P., Cross, A.W., Ronald, K., Phelps, A.D.R.: Wave interference and band control in multiconductor one-dimensional Bragg structures. J. Appl. Phys. **97**, 073101 (2005)
5. Ding, X.Y., Wang, L.L., Lv, Z.S.: Comparative study of coaxial Bragg structure with hybrid ripples shape. Chin. J. Radio Sci. (in Chinese) **30**(6), 1228–1234 (2015)
6. Lai, Y.X., Zhang, S.C.: Coaxial Bragg reflector with a corrugated inner rod. IEEE Microwave Wirel. Compon. Lett. **17**, 328–331 (2007)
7. Lai, Y.X., Zhang, S.C.: Multiwave interaction formulation of a coaxial Bragg structure and its experimental verification. Phys. Plasmas **14**, 113301 (2007)
8. Lai, Y.X., Zhang, S.C.: Separation of band-gap overlap in a coaxial Bragg structure operating in higher-order mode at Terahertz frequency. Phys. Plasmas **15**, 033301 (2008)
9. Ding, X.Y., Wang, L.L.: Comparative study of numerical simulations in coaxial Bragg reflector with the new tapered ripples. Chin. J. Radio Sci. **26**(1), 55–61 (2012)

10. Ding, X.Y., Li, H.F., Lv, Z.S.: Effect of ripple taper on band-gap overlap in a coaxial Bragg structure operating at terahertz frequency. Phys. Plasmas **19**, 092105 (2012)
11. Ding, X.Y., Zhang, S.C.: Effect of ripple shape and taper on frequency response of reflectivity and transmission in a coaxial Bragg structure. J. Phys. D Appl. Phys. **42**, 085104 (2009)

The Design and Implementation of a Literature Reading-Assist System Based on Android

Chang Han, Hui Zhang, Jianfeng Hou, Zihang Zhao, and Yushuang Sui

Abstract In order to encourage people to use the fragmented time to read Chinese and foreign literature classics, absorb the essence of masterpiece, share reading experience, and obtain effective information, we built an Android-based mobile reading-assist system, including reading module, sharing and interaction module, Q&A modules, user avatar module, etc. The system selects 15 classic Chinese and foreign literary classics, collects reading-assist resources, and achieves accurate recommendation of reading, providing readers with a platform that accumulates literary knowledge and cultivates cultural sentiments.

1 Introduction

With the development of all kinds of electronic reading terminal device including mobile phone and e-readers, e-reading behavior, which is informative, convenient, environmentally friendly, economical, and practical, has been pervaded among public. Not only is it high interactive, but also it has the strong and all-round function of videos, voice reading, and the big data search and analysis of an intelligence [1]. According to the survey, the e-reading rate of our nation is rising significantly.

Thoreau, a famous American writer in the nineteenth century, said that classic literatures are the noblest records of human thought. The reason why classic literatures are classics lies in their profound theme, speculative height, and keen insights. Reading classic literatures repeatedly can make people think keenly, have broad vision and noble sentiment. It is also difficult for ordinary books to compete with the improvement of personality and the cultivation of interest. At the same time, it can cultivate patriotism in reading [2].

C. Han · J. Hou (✉) · Z. Zhao · Y. Sui
School of Information, North China University of Technology, Beijing, China
e-mail: houjianfeng@ncut.edu.cn

H. Zhang
Beijing No. 10 Middle School, Beijing, China

R. Kountchev et al. (eds.), *Advances in Wireless Communications and Applications*,
Smart Innovation, Systems and Technologies 191,
https://doi.org/10.1007/978-981-15-5879-5_9

Classic literatures have many advantages, but their obscure words and historical background which are out of touch with today's society have become a stumbling block in the way of reading classic literatures. Based on the popularity of electronic reading and a survey result, nearly 50% of students are willing to use mobile phones as a supplement to classroom learning [3]; we cannot ignore the necessity of the Android-based system of reading-assist for classic literatures. The system data is stored on the server side by MySQL (a relational database management system) and supported on the mobile side by Web service. This paper does not include the content of the development of sever.

Based on Android system and using Java development language, this paper implements a mobile phone application which includes the functions of classic literature reading, precise push of the content of reading-assist, sharing of reading experience, question and answer, and portrait of readers.

The system design originates from the national key topic of educational information technology research in 2018, "Research and development and application of classic literatures reading-assist APP with functions of precise push, plug-in annotation and online question and answer." Precise push is used to deal with information overload. The significance and value of precise push depend on the degree of information overload. The core of precise push is a set of recommendation mechanism [4], which can analyze the reader's behavior data and recommend the content of reading-assist to the reader who will like it.

2 Key Technology

The mobile terminal uses Android Studio for development, using Model–View–Presenter (MVP) mode to separate the view from the logic. Due to the complexity of the logic, the reading-assist matching, data dynamic loading, and caching functions use multi-threading technology in conjunction with network requests.

2.1 Multi-threading Technology

Since the updating operation of the interface of the android system is completed in the main thread, in order to avoid jamming, all the time-consuming operations are completed in the sub-thread. After the time-consuming operation is completed, the main thread will be notified to update the interface. Flexible switching between threads is extremely important. In this paper, we use ReactiveX to implement asynchronous operations, which provide a clear and accurate way to deal with asynchronous problems [5]; the multi-level nesting problem caused by time-consuming operation callbacks can be avoided.

We use ReactiveX in Android Studio and import RxJava development package. The processing idea is called observer mode. The two main logic executers are

observable and observer, and observable handles time-consuming operations. If an error occurs during procession, the observable will send a message to the observer. The observer deals the rest of the operation (including page update, etc.) according to the processing result. The observable and the observer can specify their execution thread through the interface. The operations of observable are generally completed in non-main thread, and the observer updates the page after receiving processing result in main thread.

2.2 Data Caching and Dynamic Loading Technology

The system data mainly includes the original text, read-helping information, Q&A list, user information, etc., in which the data is cached for the original text, and the rest of the data is loaded in real time through the network. In order to facilitate the management of the cached data, SQLite is used in Android for data storing. SQLite is a lightweight relational database. It is very fast and resource-saving, which is very suitable for local persistent storage [6]. To implement CRUD (create, retrieve, update, delete) for SQLite, we use greenDAO, an open-source Android object/relational mapping (ORM, as shown in Fig. 1) development library that uses a simple object-oriented application programming interface (API) to store, update, delete, and query data, which can greatly save the development time of database-related content [7].

While reading books, querying the original text of the local database to confirm whether the text is loaded by the chapter order through the network. If it is loaded from the network successfully, it will be stored in the local SQLite database, and the original data will be loaded locally for later reading. All requests are loaded in real time through the network. The network request is a time-consuming operation that requires multi-threading technology. In order to implement the function of network request, the system adopts the Retrofit development library, which is further encapsulation of okHttp (an android network framework), and supports synchronous and asynchronous, multiple data parsing [8]. We use Gson (an Java serialization/deserialization library to convert Java objects into JSON and back) in this paper.

Fig. 1 Object relational mapping model diagram

2.3 *Reading-Assist Precision Matching Technology*

The precise matching has two meanings. The first is personalized recommendation. The user's historical behavior data is mathematically modeled to mine the user's interests and preferences, to filter the information that the user may be interested in [9]. Specifics of the system are based on the user's reading habits, reading experience sharing, and other behavior analysis and recommend relevant reading information for the user, including the historical background of famous works and famous appreciation. Secondly, the collected reading information is matched according to the content of the famous books and is divided into three categories: hot spot annotation, chapter topic, and reading-assist channel.

The hot spot annotation is a kind of reading information for the specific words. When reading the text, it is displayed on the reading page in a dotted underline by position calculating. The chapter topic is aimed at a particular chapter in this famous book. The user can get it instantly by clicking the button during reading. The reading-assist channel has abundant content. It is a kind of tangible reading-assist information for a certain book, including video, audio, and other more concrete reading information, which is mainly presented in the form of a webpage in the application.

3 System Function Design and Implementation

The system is mainly formed by five modules: user management, reading module, reading-assist module, Q&A module, and reader avatar, and the overall functional module diagram as shown in Fig. 2.

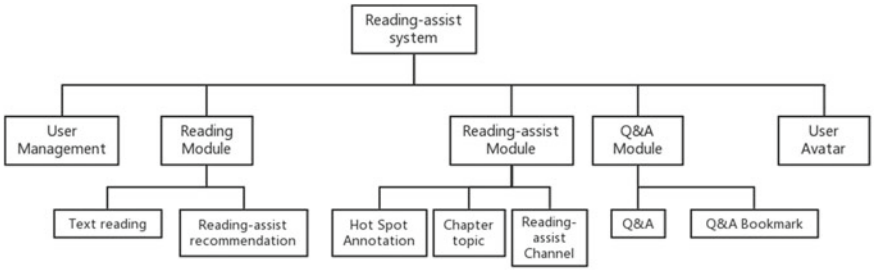

Fig. 2 System architecture chart

3.1 Reading-Assist Module

The reading-assist module is mainly formed by hot spot annotation, chapter topic, and reading-assist channel (see Fig. 3).

While reading passages, user can see some words which have annotation. The hot spot annotation is divided into expert annotations and user annotations. Different kinds of annotations will be displayed differently. Most of the expert annotations are from historical materials, which are some comments or analysis from experts made for this passage. User annotations are from different users, which are the reader's insights or ideas generated during reading. User annotations can be shared, and the interactions are presented under the annotations tab; users can bookmark, like, and comment on these annotations. Experts have the permission to top, classify, and recommend the user comments. If the user's annotations are good, they can become expert annotation after being recommended by experts (see Fig. 4).

The chapter topic is some passages relate to this chapter, which can be extended to the introduction of the historical background and the analysis of experts of this chapter.

There are many modules in reading-assist channel to help users read and understand the content. There are annotations, translations, and analysis of the article, as well as introductions, character relationships, drawings, reading methods and instructions, audio and video, and other reading information.

Fig. 3 Hot spot annotation, annotation page, and annotation channel

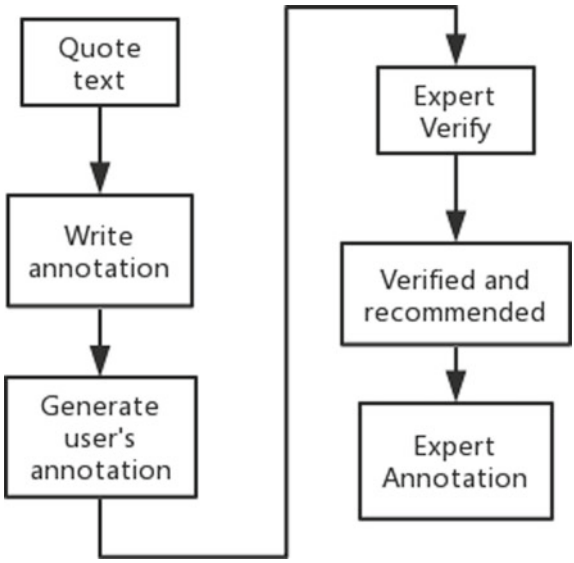

Fig. 4 Annotation flowchart

3.2 Reading System

The reading system is mainly formed by book library and reading (see Fig. 5).

The book library is generated by loading the book information of 15 Chinese and foreign masterpieces from server, which have been edited. The book library page displays all the books. After sending reading request, it will judge whether the content of the chapter is cached. If there is no local cache, the network request is required to get the text (see Fig. 6).

In addition to the text, the reading interface will show a dotted line below sentence with annotation. The book's catalog consists of a custom RecyclerView widget with a search box at the top to search all the text. The reading interface also supports font settings, background color settings, brightness settings, volume key page turning setting, etc.

3.3 Q&A Module

The Q&A module mainly consists of question list and detail page of questions (see Fig. 7).

Any questions that reader encounters during reading can be posted in the Q&A system, and the questions posted will be answered by other users. The question must be for the literature, and users can ask questions by chapter or whole book. All questions and answers in the Q&A module are stored in the server and dynamically loaded when used. After the users post a question, they can invite other users or

Fig. 5 Library page and reading page

experts to answer. The questions with high quality in the question list can be topped. The quality assessment is mainly based on the user's participation. The answer can be liked by the user, and they will be sorted by the number of likes. Users can also collect and comment on questions and answers (see Fig. 8).

3.4 User Avatar

This application expands in units of middle schools, and each school individually sets up server. The maximum number of users generally does not exceed 2000, and the number of books currently includes 15 literatures closely related to middle school reading. The data requested by a single user is mainly text (a small amount). By recording the using behavior and classifying the user's annotations, a pie chart is generated to depict what type of user is. Each piece of information in the pie chart represents a different label, and each label has a different proportion and finally forms the complete pie chart (see Fig. 9).

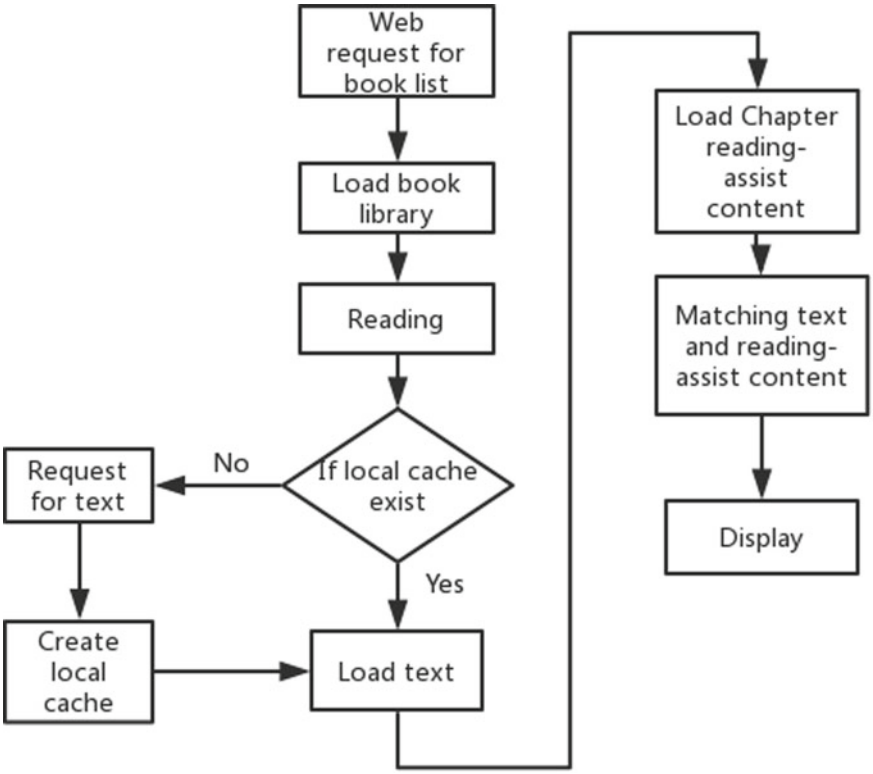

Fig. 6 Reading system flowchart

4 Conclusion

Based on the Android system, this paper uses multi-threading technology, data caching and dynamic loading technology, and reading-assist matching technology to implement a application with friendly user interface and a wealth of features, providing a reading and sharing platform, which makes reading the literature no longer a boring and obscuring thing. We hope to use the relevant methods of machine learning to continuously improve the data analysis process and provide users with more scientific and intelligent reading recommendations afterward.

Fig. 7 Q&A page and Q&A detail page

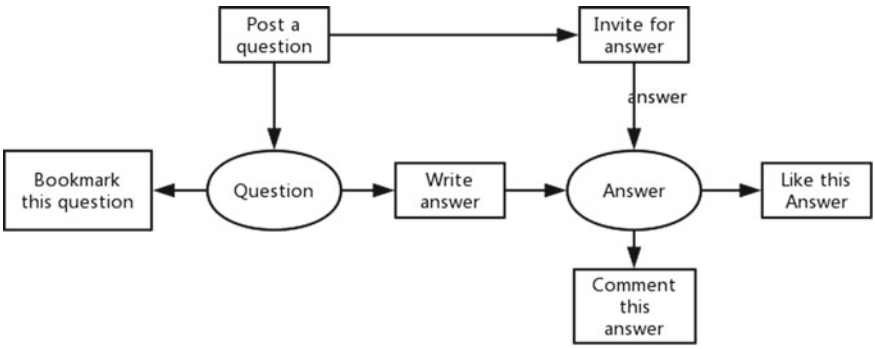

Fig. 8 Q&A flowchart

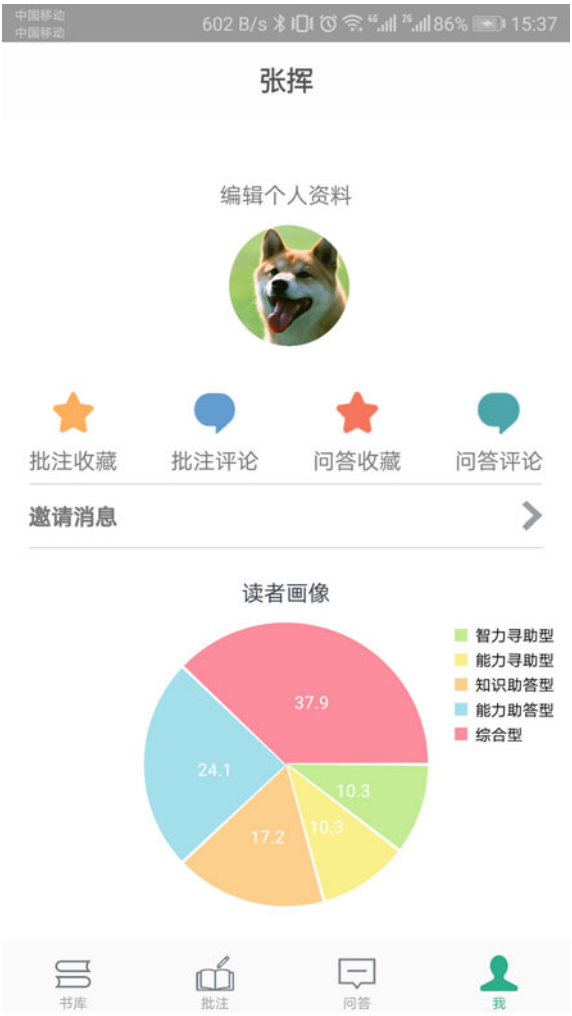

Fig. 9 Use avatar

References

1. LiuQing, F.: On paper books and electronic books development. Chin. Foreign Entrepreneurs **20**, 116 (2019)
2. ZhangJing, F.: A brief analysis of the significance and methods of reading classics. Educ. Teach. Forum **35**, 46–47 (2019)
3. LuBei, F.: Research on the application of smart-phone app in teaching. Occupation **22**, 122–123 (2018)
4. ZhangHui, F., ZouYusong, S.: Analysis of information push application. Chin. J. ICT Educ. **5**(10), 94–96 (2019)
5. ReactiveX. https://reactivex.io/
6. GuoLin, F.: First Line of Code (Android), 2nd edn. Posts & Telecom Press (2016)
7. greenDAO: Android ORM for your SQLite database. https://greenrobot.org/greendao/

8. DingYong, F., ZhuChangshui, S.: A Book reading recommendation system based on android platform. Comput. Sci. **43**, 523–525 (2016)
9. Retrofit. https://square.github.io/retrofit/

Research on VANETs Connectivity Strategy in Urban Scene

Li Wen Xu and Li Juan Qiao

Abstract Connected vehicle connectivity strategies are one of the hot topics of current research. This paper proposes a parked vehicle cluster connectivity network (PVCCN) strategy in a connected car environment. PVCCN forms a data transmission backbone network by parking vehicles on the side of urban roads or off-roads. A mathematical model of optimal data routing from the source vehicle node to the destination vehicle node is established. The simulation proves that the PVCCN strategy in this paper improves the success rate of data transmission at the lowest cost, reduces the delay of data transmission, and enhances the robustness of network connectivity.

1 Introduction

Vehicular ad hoc networks (VANETs) are an important part of intelligent transportation systems (ITS). Its application of communication and control technology enables close collaboration between vehicles, roads, and people to achieve safety, efficient, energy-saving, and comfortable road transportation [1]. Among them, secure information transmission is one of the core issues of VANETs. VANETs have the characteristics of high-speed movement and uneven distribution of nodes. At the same time, there are problems such as the limited channel bandwidth and the transmission delay. Therefore, high requirements are placed on information transmission.

This paper establishes a parked vehicle cluster connectivity network (PVCCN) strategy based on VANETs' V2I communication. In a limited range, vehicle nodes parked on-road parking spaces or non-parking spaces constitute a maximum length parking cluster. *N* parking clusters are established as the backbone of urban traffic—the efficiency and optimal path of multi-hop data transmission. The connected routing strategy of the relay node makes it a good substitute for the expensive road-side

L. W. Xu (✉) · L. J. Qiao
College of Computer Science and Technology, Tropical Ocean University, Sanya 572022, Hainan, China
e-mail: lwenxu@qq.com

R. Kountchev et al. (eds.), *Advances in Wireless Communications and Applications*, Smart Innovation, Systems and Technologies 191,
https://doi.org/10.1007/978-981-15-5879-5_10

unit (RSU) device. Simulations show that the strategy improves the performance of transmission delay and transmission overhead, effectively improving the success rate of data transmission, and data connectivity.

2 Connectivity Strategy

First of all, the calculation and communication module, GPS and electronic map are loaded on the set parked vehicles, and all work normally in the parking state. The parked vehicles are willing to share wireless communication and computing functions. The buffer area of the vehicle nodes is large enough to meet a large amount of data storage, and the intersections are within the effective communication radius. According to the function of the network composed of vehicle nodes, the vehicle network is divided into physical layer, link layer, network and transmission layer, and application layer [2].

2.1 Cluster Management of Parked Vehicles

A large number of parking positions are delimited on both sides of urban roads, which can completely constitute a data link layer of an on-board self-organizing network, but there are special cases where some parked vehicles are too far away from other parked vehicles to communicate with each other. Vehicles moving on the road can be used as auxiliary relay nodes in this special case to realize data connection sessions between vehicles. The parking vehicles on both sides of the same road and off-road are organized into parking clusters for effective management [3].

2.1.1 Parking Cluster Head Selection

The parking cluster is shown in Fig. 1. The parked vehicles $H1$ and $H2$ are the two cluster heads of the road, and $M1$–$M10$ are members of this cluster. The selection of the parking cluster head is set to park vehicle nodes at both ends of the road, so that a parking cluster of sufficient length can be formed so that moving vehicles entering or leaving can communicate with one of the parking cluster heads. After the cluster head is determined, the cluster head is responsible for maintaining the cluster resources and managing the forwarding of member data in the entire cluster. Therefore, each cluster member vehicle node periodically broadcasts its own geographic location, ID number, and remaining storage space so that the cluster head can process the entry, leaving vehicle nodes. In order to improve the robustness of the parking cluster, the parking nodes closest to the two cluster heads in the cluster are set as backup cluster head nodes to park the vehicles. The backup cluster heads are QH1 and QH2 in Fig. 1. It always operates the cluster head to collect information. The backup of the cluster

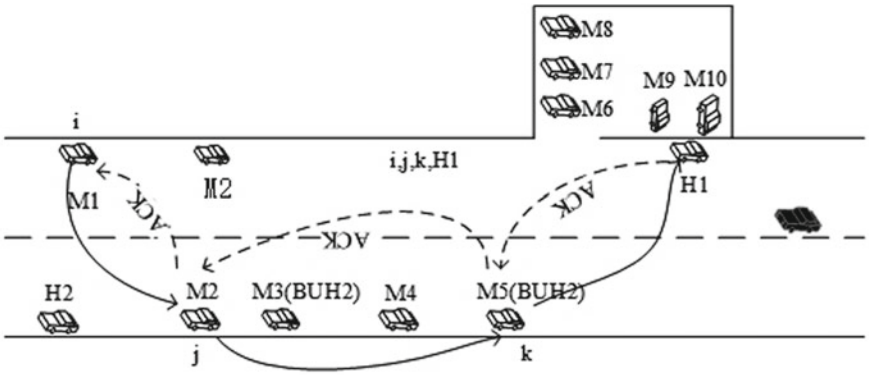

Fig. 1 Inter-cluster communication

head triggers the selection of a new cluster head when the parked vehicle leaves the parking cluster and the old cluster head forward the collected information to the new cluster head [4].

2.1.2 Inter-cluster Communication

In the inter-cluster member communication, if a cluster member that can directly communicate with the cluster head broadcasts its information to the cluster head. If direct communication with the cluster head is not allowed, each hop of the broadcast information will record the ID number of the hop node, and then when the cluster head receives the broadcast information, it will receive the same broadcast message from the source node and receive the first arrival in order. Of the n copies of the broadcast information, and the transmission paths of the n copies are marked as the best path, the next best path, the nth best path, the cluster head is based on the replica information. Along the best path, an acknowledgment (ACK) message with the n path information is returned to the member node. The best path is performed as the best path for the node to periodically report information to the cluster head and the cluster head to send information to the members. Until the n paths do not exist, a new round of broadcast is initiated. As shown in Fig. 1, node i is a cluster member node, $H1$ is a cluster head node, and the path (i, j, k, $H1$) is the best path from i to the cluster head. When the existing isolated cluster member node communicates with the cluster head vehicle, the vehicle that moves to the vehicle and selects the direction of movement toward the data transmission direction is used as the next-hop transmission node, and the vehicle node transmits the data to the destination node through the store-and-forward method. If the cluster head does not receive information about a node after a period of time, the member node is considered to have left the family and deleted it.

2.2 Stop Vehicle Connectivity Strategy

First, we assume that there are only parked vehicle nodes on this road and that they follow a Poisson distribution with parameter λ_1. Therefore, it can be known that the time interval when a moving vehicle encounters a parked vehicle obeys an exponential distribution with a parameter λ_1. We assume that the speed at which a vehicle enters a parking lot is ν. Let $\mu = \lambda_1 \nu$, the distance d between parked vehicles follows an exponential distribution with a parameter of μ. The probability density function of the distribution is:

$$f(d, \mu) = \begin{cases} \mu e^{-\mu d}, d \geq 0 \\ 0, d < 0 \end{cases} \tag{1}$$

Then, let the probability p be the probability that the road is connected by the vehicle node. Then, when $p < 0.5$, the road network connectivity is poor; when $p \geq 0.5$, the road network connectivity is the strongest. Let the communication radius of the vehicle be R, then the probability that the vehicle can communicate is:

$$p(d < R) = \int_0^R f(d, \mu) \mathrm{d}d = \int_0^R \mu \mathrm{d}d = 1 - e^{-\mu R} \tag{2}$$

By setting the total length of the road to L, there are $m = L/R$ communication units in total. If the vehicle density of each communication unit is ρ, the probability p of the unit network connection is:

$$P = \prod_{k-1}^{m} P(d < R) = \left(1 - e^{\rho R}\right) \tag{3}$$

If and only if

$$p = (1 - e^{pR})^m \geq 0.5 \tag{4}$$

At this time, the density of the vehicle node network on the road showing strong connectivity ρ must meet:

$$\rho \geq \frac{-\ln\left(1 - \sqrt[m]{1/2}\right)}{R} \tag{5}$$

Secondly, if the parked vehicle nodes cannot satisfy the Formula (5), it is necessary to use a moving vehicle node to assist the transmission to realize the network connection of the parking cluster. Assume that the moving vehicle nodes entering the parking cluster obey the Poisson distribution of the parameter λ_2, where the speed of moving vehicles entering the parking cluster υ, and the total length of the road is L, and then the number of vehicle nodes N entering the parking cluster is:

$$N = \sum_{i=1}^{\infty} \int_{0}^{\frac{L}{v}} i e^{-\lambda_2 t} \frac{(\lambda_2 t)^i}{i dL/v_2} \tag{6}$$

From Formulas (5) and (6), the density ρ_s of the parked vehicle nodes and the density ρ_m of the mobile vehicle nodes are $\rho_s = \mu$ and $\rho_m = N/L$, respectively. Then, the strong connection of the parking cluster network must be satisfied:

$$\rho_s + \rho_m = \mu + \frac{N}{L} = \rho \geq -\frac{\ln\left(1 - \sqrt[m]{1/2}\right)}{R} \tag{7}$$

Derived from Eqs. (6, 7):

$$\lambda_2 \geq \left(-\frac{\ln\left(1 - \sqrt[m]{1/2}\right)}{R} - \mu\right) v \tag{8}$$

In other words, if the parking nodes in the parking cluster are insufficiently connected, the arrival rate of the mobile vehicle node when entering the parking cluster satisfies the Formula (8), and the network can show a strong connection.

3 Performance Analysis

In this paper, PVCCN is compared with opportunistic dissemination (OP) strategy, mobile distribution-aware data dissemination (MDA) strategy, and election mechanism of mobile node election.

3.1 Simulation Settings

In the NS2 simulation environment, parked vehicles are randomly distributed on the roadside parking spaces or parked in off-street parking spaces according to the density as shown in Fig. 1. The average parking time of each vehicle node is about 41.4 min (standard deviation is 27.17). The NS2 simulator uses the IEEE 802.11 MAC protocol. Vehicle nodes randomly select any vehicle node as the destination of the message and form a parking cluster. Other related parameters are shown in Table 1.

Table 1 Simulation parameters

Parameter	Defaults
Highway length L	1000 m
Communication radius R	250 m
Vehicle nodes	200
Vehicle speed	40–80 kph
Vehicle average generation information period	30 s
Information maintenance cycle	60 s
Data information size	1 kb
Simulation time	1 h

3.2 Stop Vehicle Density Performance Analysis

Figure 2 illustrates the relationship between network connectivity and communication unit density. That is, when the vehicle density increases, the network connectivity will increase; when the road length increases, the vehicle density required for the network to reach a strong connection state will also increase. For example, when the road length is $I = 5R = 1250$ m, when the communication unit density $\rho =$ 10 vehicles/km, the network connectivity is 65.2%; when $\rho = 14$ vehicles/km, the network connectivity ρ increases to 85.8%. When the road length $I = 3R$, the network

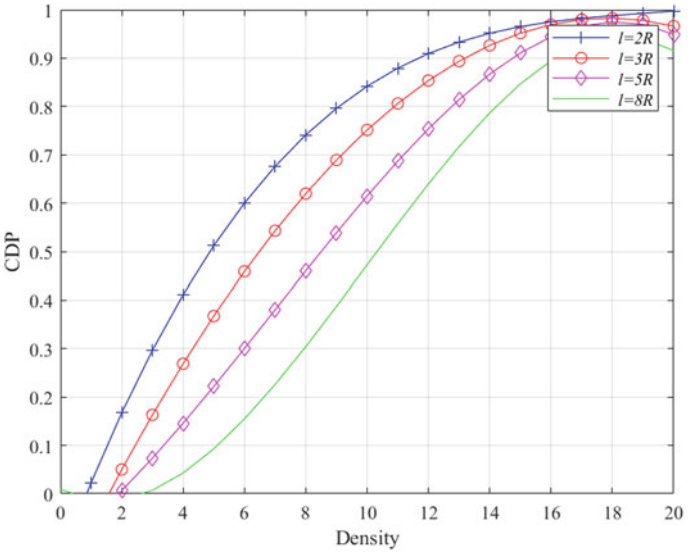

Fig. 2 Connectivity of vehicle density

reaches strong connectivity, and the communication unit vehicle density is 7 vehicles/km. When the road length $l = 5R$, the network reaches strong connectivity, and the communication unit vehicle density is 9 vehicles/km.

3.3 Delay Analysis of Moving Vehicles

The robustness of network transmission is determined by the main factors such as average transmission success rate, average transmission delay, and transmission cost. The experiment uses the PVCCN strategy and three other strategies to study the impact of different vehicle node densities on the performance of the network composed of parking clusters. The situation is shown in Fig. 3a–c.

Figure 3a illustrates that as the density of vehicle nodes increases, the transmission success rate of the PVCCN strategy in the sparse phase of vehicle nodes is higher than the other three strategies. It shows that with the increase of vehicle node density, the network connectivity of PVCCN is strongly connected, ensuring that the data can be transmitted to the parking cluster by choosing the correct path. However, for OP, connectivity is improved during the sparse phase. This is when the vehicle node receives the information and rebroadcasts this information. When a certain procedure is triggered, the message floods and the data are transmitted. MDA indicates that the number of vehicle nodes increases. At a certain level, such as 300–400 vehicle nodes, the network data transmission becomes stable at this time, and the impact of the MDA strategy is limited; when election is the most sparse, the data is difficult to maintain in the mobile node in the target area, so the successful transmission rate is low, and when the number of vehicle nodes increases, the data maintenance increases and the data transmission success rate increases as well.

Figure 3b shows that, with the increase of vehicle node density, the four strategies reduce the transmission delay to a certain extent. OP decreases first and then increases.

Figure 3c shows that with the increase of the vehicle nodes density, the OP strategy has the largest cost due to the heavy traffic load on the network, as each vehicle node participates in spreading the messages, which results in a heavy network transmission load. The PVCCN, MDA, and election strategies have been designed to limit the spread of messages. The traffic growth is linear, which effectively controls the network load. The PVCCN strategy in this article does not require frequent data transfers and reduces redundant traffic, so that the network to have the most reasonable load.

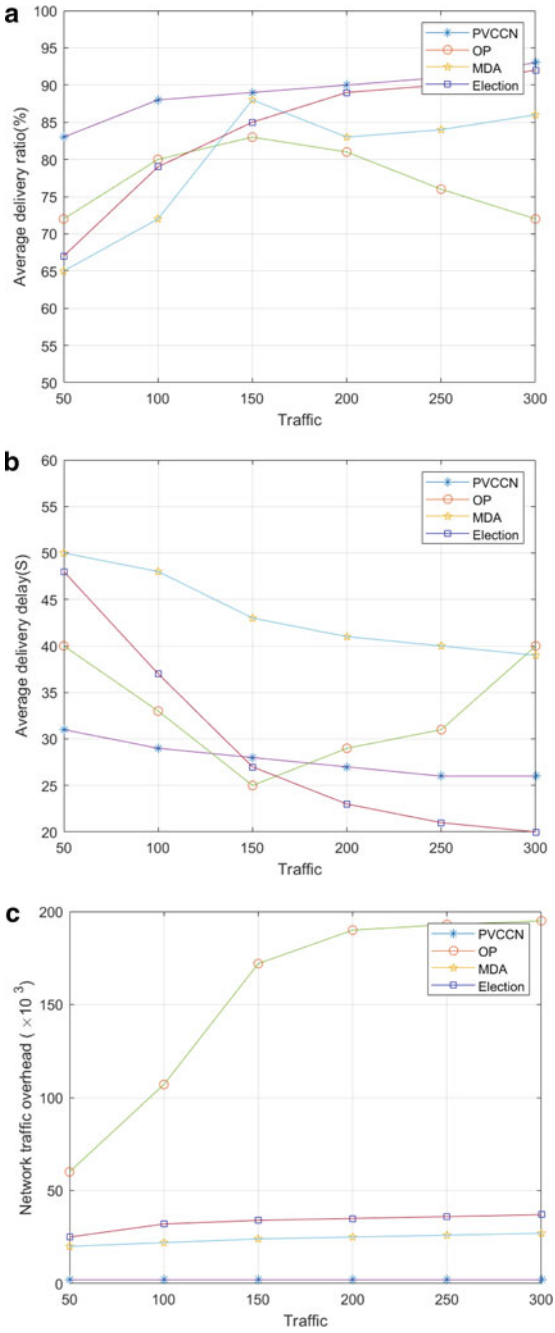

Fig. 3 **a** Average transmission success rate. **b** Average transmission delay. **c** Average transmission cost

3.4 Performance Analysis with RSU

In practical applications, installing a small number of RSU nodes on the road to the Internet of vehicles can bring substantial improvements to the network, and the number of RSUs will determine the network performance. As shown in Fig. 4, this article sets 1, 4, 10, and 20 RSU nodes on the road to test the impact of different numbers of RSU nodes on the can deliver protocol. It shows that the network performance of the PVCCN strategy is better than installing 4 RSU nodes, but weaker than the network performance of installing more than 10 RSU nodes, which is reasonable and is an effective solution for reducing the RSU nodes and increasing the investment cost.

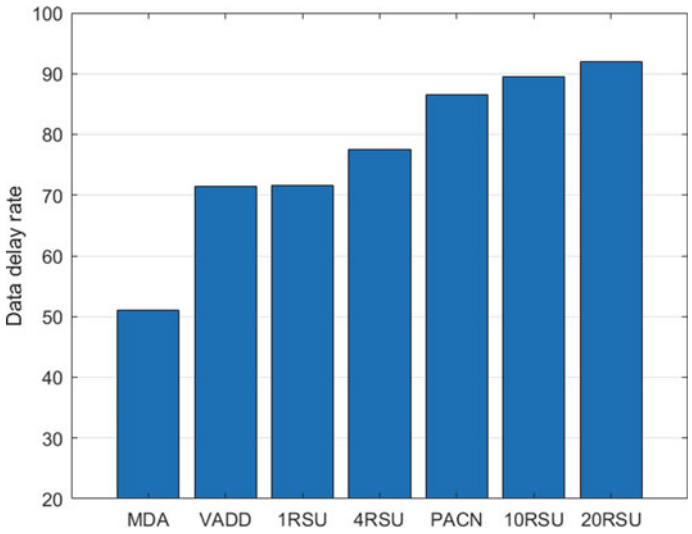

Fig. 4 Impact of the number of RSU

4 Conclusion

This article replaces RSU by parked vehicles on the road to form a stable communication link for connected vehicles. Data is transmitted according to the best data route from the source vehicle node to the destination vehicle node. The minimum cost increases the data transmission success rate and reduces the data transmission time which enhances the robustness of network connectivity. In our future work, we shall analyze and solve the problems that may occur in the data transmission of vehicle nodes based on experimental tests.

Acknowledgement This project won the Hainan Higher Education Science Research Project (Hnky2017-50) and the Hainan Natural Science Foundation Project (618MS075,117150).

References

1. Wu, L.-B., Liu, B.-Y., Nie, L. et al.: Research on selection of safety message broadcast relay in VANET-cellular. Chin. J. Comput. **40**(4), 1004–1016
2. Zhu, J.Q., Ma, C.M., Liu, M., Chen, G.H., Gong, H.G., Liu, B.: Data delivery for vehicular ad hoc networks based on parking backbone. Ruan Jian Xue Bao/J. Softw. **27**(2), 432–450 (2016)
3. Liwen, Xu, Lijuan, Q., Jie, C.: Clustering routing algorithm based on a modified K-means VANET. Comput. Technol. Dev. **28**(3), 15–19 (2018)
4. Nzouonta, J., Rajgure, N., Wang, G., Borcea, C.: Vanet routing on city roads using real-time vehicular traffic information. IEEE Trans. Vehic. Technol. **58**(7), 3609–3626 (2009)

Performance Analysis of Multiple Primary Users CR-NOMA Networks Under Partial Relay Selection

Yuhang Qiao, Yucheng He, Liangmei Zhang, Jianquan Yang, and Lin Zhou

Abstract This paper studies the application of non-orthogonal multiple access (NOMA) technology and relay selection technology in cognitive radio (CR) networks. A downlink cooperative communication model in which a secondary source in multiple primary users (PUs) CR network sends messages to two secondary users (SUs) using the NOMA protocol and spectrum sharing technology is considered. When the channel state information is known and perfect, the link with the maximum instantaneous channel gain from the source node to the relay node is selected by using the partial relay selection strategy. The selected optimal relay and secondary source use the same fixed power allocation scheme without considering dynamic power distribution. In the whole communication process, optimal relay provides decoding and forwarding services for secondary users. For the cognitive radio non-orthogonal multiple access (CR-NOMA), we derive closed expressions for each secondary user. In addition, the numerical results obtained by Monte Carlo simulation verify the correctness of the analysis results.

1 Introduction

NOMA is an effective way to improve spectrum efficiency and approach the multi-user channel capacity boundary [1]. The existing research shows that NOMA cannot only further increase the spectral efficiency, but also an effective method to approach the user channel capacity boundary [2, 3]. The outage performance of cooperative NOMA network in which the relay use amplification-and-forward (AF) protocol has been studied and an optimal scheme based on partial relay selection is proposed in

Y. Qiao · Y. He (✉) · L. Zhang · J. Yang · L. Zhou
Xiamen Key Laboratory of Mobile Multimedia Communications, National Huaqiao University, Xiamen Fujian 361021, China
e-mail: Yucheng.he@hqu.edu.cn

Y. He · L. Zhou
State Key Laboratory of Integrated Services Networks, Xidian University, Xi'an shaanxi 710071, China

R. Kountchev et al. (eds.), *Advances in Wireless Communications and Applications*,
Smart Innovation, Systems and Technologies 191,
https://doi.org/10.1007/978-981-15-5879-5_11

[4, 5]. A suboptimal solution to the problem of cooperative NOMA relay selection is proposed in [6], the selected relay satisfies the user's quality of service by using the max–min relay selection strategy. At the same time, the remaining relays continue receiving signals for opportunities. A relay selection scheme which selects the nth best relay in cooperative NOMA networks is proposed in [7], as well as the simultaneous wireless information and power transfer (SWIPT) can effectively reduce power consumption of relay battery.

Cognitive radio spectrum sharing technology is a potential solution to the shortage of spectrum resources. The outage performance of the CR-NOMA system with DF protocols under the Nakagami-m channel has been researched in [8]. A scheme for strong user to assist weak user to communicate has been proposed in [9], and the closed-form expressions of outage probability and progressive traversal capacity have been derived. Study [10] has considered the CR-NOMA networks with a primary user, and they have shown that the system outage performance can be greatly improved by relay selection sachem. A partial relay selection scheme in CR-NOMA hybrid system is proposed in this paper, which can get better system performance compared to traditional cooperative CR-NOMA model.

2 System Model

As illustrated in Fig. 1, a downlink collaborative CR-NOMA network with alternative multi-relays is considered, which is made up of L primary users $Q_l (l = 1, ..., L)$, a secondary network source S, N cognitive relays $R_n (n = 1, ..., N)$, and two secondary users (D_1 and D_2). It is assumed that each node has only one antenna and can only receive or send messages in a time slot, the decode-and-forward protocol is used with all cognitive relays. All of the channels are assumed to undergo quasi-static flat Rayleigh fading and that all channels are independent of each other. The channel coefficients are h_m,$h_m \sim CN(0, \lambda_m)(m \in \{SR_n, SQ_l, R_nQ_l, R_nD_1, R_nD_2\})$. Without loss of generality, assume $\left|h_{R_nD_2}\right|^2 > \left|h_{R_nD_1}\right|^2$. Due to the long distance or obstruction, it is assumed that the source cannot communicate directly with the destination.

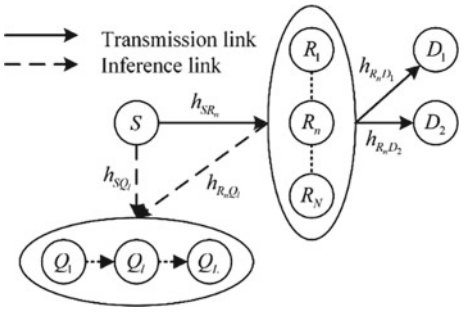

Fig. 1 System model

In the phase I, the SU source node broadcasts superimposed signal $\sqrt{P_S\alpha_1 x_1} + \sqrt{P_S\alpha_2 x_2}$ to all cognitive relay, where α_i denotes the power allocation factors of D_i, with $\alpha_1 + \alpha_2 = 1$ and $\alpha_1 > \alpha_2$, x_i represent the message to be sent to D_i, and the expectation of x_i is 1. When the primary user is free from harmful interference, the secondary network can use the same spectrum resources as the primary network. So the source transmission power is limited:

$$P_S = \min\left\{ P_S^M, Q \Big/ \max_{l=1,\ldots,L} \left\{ \left|h_{SQ_l}\right|^2 \right\} \right\} \tag{1}$$

where P_S^M is the maximum transmit power and Q is interference temperature constraint (ITC).

The partial relay selection strategy selects the optimal relay with the maximum instantaneous channel gain of link $S \rightarrow R_n$. The optimal relay selected by the partial relay selection strategy can be expressed as

$$R_b = \arg\max_{n=1,\ldots,N} \left\{ \left|h_{SR_n}\right|^2 \right\} \tag{2}$$

In the phase II, the cognitive relay uses successive interference cancelation (SIC) technology to detect and decode signals of two secondary users, therefore, the SINR of the signals x_1 and x_2 can be expressed as

$$\gamma_{R_b,x_1} = \rho_S\alpha_1 \left|h_{SR_b}\right|^2 \Big/ \left(\rho_S\alpha_2 \left|h_{SR_b}\right|^2 + 1\right) \tag{3}$$

$$\gamma_{R_n,x_2} = \rho_S\alpha_2 \left|h_{SR_b}\right|^2 \tag{4}$$

where $\rho_S = P_S \big/ \sigma^2$ denotes the transmit signal-to-noise ratio (SNR) at the source.

The cognitive relay uses superposition coding to recode the signal and forward superimposed signal $\sqrt{P_{R_n}\alpha_1 x_1} + \sqrt{P_{R_n}\alpha_2 x_2}$ to secondary users, if decode the superimposed signal successfully. Similar to the source, the relay transmission power is limited:

$$P_{R_b} = \min\left(P_{R_b}^M, Q \Big/ \max_{l=1,\ldots,L} \left|h_{RQ_l}\right|^2 \right) \tag{5}$$

The SINR for D_i to decode x_1 is expressed as

$$\gamma_{D_i,x_1} = \frac{\rho_{R_b}\alpha_1 \left|h_{R_bD_i}\right|^2}{\rho_{R_b}\alpha_2 \left|h_{R_bD_i}\right|^2 + 1} \tag{6}$$

The SINR for D_2 to decode x_2 is expressed as

$$\gamma_{D_2,x_2} = \rho_{R_b}\alpha_2 \left|h_{R_nD_2}\right|^2 \tag{7}$$

3 Performance Analysis

According to the decode-and-forward protocol and SIC principle, the outage probability of D_1 and D_2 is as shown below

$$P_{D_1}^{\text{out}} = 1 - P\left\{\gamma_{R_b,x_1} > \xi_1, \gamma_{R_b,x_2} > \xi_2, \gamma_{D_1,x_1} > \xi_1\right\} \tag{8}$$

$$P_{D_2}^{\text{out}} = 1 - P\left\{\gamma_{R_b,x_1} > \xi_1, \gamma_{R_b,x_2} > \xi_2, \gamma_{D_2,x_1} > \xi_1, \gamma_{D_2,x_2} > \xi_2\right\} \tag{9}$$

where $\xi_i = 2^{R_i} - 1$, R_i is the target rate for D_i. According to the Formulas (1–6), $P_{D_1}^{\text{out}}$ can be rewritten as

$$\begin{aligned} P_{D_1}^{\text{out}} = 1 - P&\left\{\left|h_{SR_b}\right|^2 > \frac{\mu_3}{\rho_S^M}, \frac{\rho_Q\left|h_{SR_b}\right|^2}{\mu_3} > \max_{l=1,\ldots,L}\left|h_{SQ_l}\right|^2\right\} \\ &\times P\left\{\left|h_{R_bD_1}\right|^2 > \frac{\mu_1}{\rho_R^M}, \frac{\rho_Q\left|h_{R_bD_1}\right|^2}{\mu_1} > \max_{l=1,\ldots,L}\left|h_{R_bQ_l}\right|^2\right\} \end{aligned} \tag{10}$$

where $\mu_1 = \xi_1/(\alpha_1 - \xi_1\alpha_2)$, $\mu_2 = \xi_2/\alpha_2$, $\mu_3 = \max\{\mu_1, \mu_2\}$. The cumulative distribution function (CDF) of the $\max_{l=1,\ldots,L}\left|h_{SQ_l}\right|^2$ and the probability density function (PDF) of the $\left|h_{SR_b}\right|^2$ are given by

$$F_{\max\limits_{l=1,\ldots,L}\left|h_{SQ_l}\right|^2}(x) = \sum_{l=0}^{L} C_L^l(-1)^l e^{-\frac{lx}{\lambda_{SQ}}} \tag{11}$$

$$F_{\max\limits_{l=1,\ldots,L}\left|h_{RQ_l}\right|^2}(x) = \sum_{l=0}^{L} C_L^l(-1)^l e^{-\frac{lx}{\lambda_{RQ}}} \tag{12}$$

$$f_{\left|h_{SR_b}\right|^2}(x) = \sum_{n=0}^{N} C_N^n(-1)^{n+1}\frac{n}{\lambda_{SR}}\exp\left[-\frac{nx}{\lambda_{SR}}\right] \tag{13}$$

According to probability theory, $P_{D_1}^{\text{out}}$ can be rewritten as

$$\begin{aligned} P_{D_1}^{\text{out}} = 1 - &\int_{\frac{\mu_3}{\rho_S^M}}^{\infty} F_{\max\limits_{l=1,\ldots,L}\left|h_{SQ_l}\right|^2}\left(\frac{\rho_Q x}{\mu_3}\right) f_{\left|h_{SR_b}\right|^2}(x)\mathrm{d}x \\ &\times \int_{\frac{\mu_1}{\rho_R^M}}^{\infty} F_{\max\limits_{l=1,\ldots,L}\left|h_{RQ_l}\right|^2}\left(\frac{\rho_Q x}{\mu_1}\right) f_{\left|h_{R_bD_1}\right|^2}(x)\mathrm{d}x \end{aligned}$$

$$= \Phi\left(\mu_1, \lambda_{RD_1}\right) \tag{14}$$

where

$$\Phi(x, y) = 1 - \sum_{n=0}^{N} \sum_{l=0}^{L} C_L^l C_N^n (-1)^{l+n+1} \frac{n\mu_3\lambda_{SQ}}{\left(l\rho_Q\lambda_{SR} + n\mu_3\lambda_{SQ}\right)} e^{-\frac{\left(l\rho_Q\lambda_{SR} + n\mu_3\lambda_{SQ}\right)}{\rho_S^M\lambda_{SQ}\lambda_{SR}}} \times \sum_{l=0}^{L} C_L^l (-1)^l \frac{x\lambda_{RQ}}{l\rho_Q y + x\lambda_{RQ}} e^{-\frac{l\rho_Q y + x\lambda_{RQ}}{\lambda_{RQ}\rho_R^M y}}$$

Similar to the calculation of $P_{D_1}^{\text{out}}$, $P_{D_2}^{\text{out}}$ can be written as

$$P_{D_2}^{\text{out}} = \Phi\left(\mu_3, \lambda_{RD_2}\right) \tag{15}$$

4 Numerical Results

In order to evaluate the system performance, we use the numerical results obtained by Monte Carlo simulation to analyze the impact of key parameters on system performance. Expect special declaration, the default parameter is set to $L = 10$, $\lambda_{SR} = 1$, $\lambda_{SQ} = \lambda_{RQ} = 0.5$, $\lambda_{RD_1} = 1$, $\lambda_{RD_2} = 2$, $\alpha_1 = 0.8$, $R_1 = 0.8$ bitS/s/Hz, $R_2 = 2$ bitS/s/Hz and $\rho_R^M = 30$ dB.

Figure 2 shows the relation between outage probability and transmission SNR of source when $\rho_Q = 30$ dB. First of all, we can see that the outage probability of secondary users decrease as the number of relay increase and finally tended to a certain value because of ITC. On the other hand, it can be noticed that the increase rate of outage performance will be not noticeable as the quantity of the cognitive relays is greater than three. The relationship between outage probability and power allocation factor is shown in Fig. 3, in the case of $N = 10$, $\rho_S^M = 30$ dB. It is noticed that the outage probability of D_1 and D_2 equal to 1, if $\alpha_1 - \xi_1\alpha_2 < 0$. The trend decrease and then increase when $\alpha_1 - \xi_1\alpha_2 > 0$. The reason is that the relay needs to successfully decode both message x_1 and x_2, the bigger α_1 is, the easier it is to decode x_1, but the more difficult it is to decode x_2. Therefore, there is an optimal power distribution factor for better outage performance.

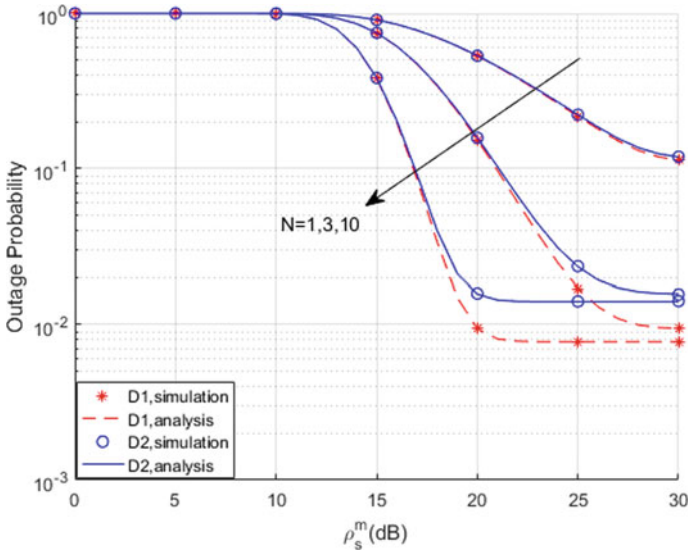

Fig. 2 Comparison of system interrupt performance under different relay numbers

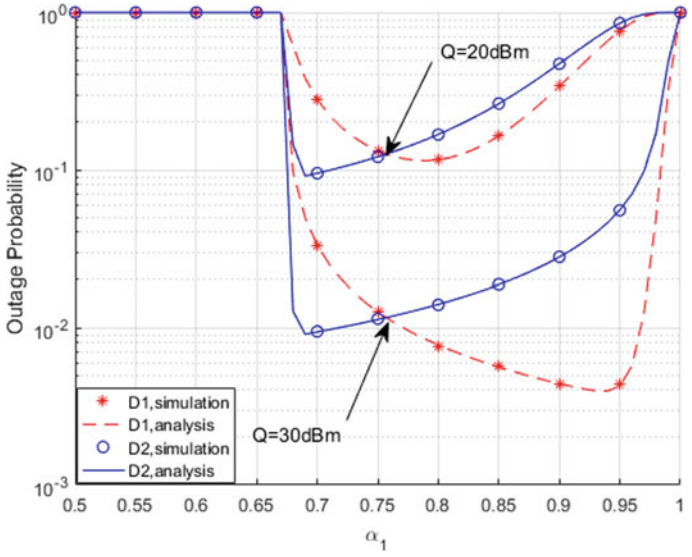

Fig. 3 Influence of power allocation factor on system outage performance under different ITC

5 Conclusions

We have researched the outage performance of CR-NOMA networks which include multiple primary users in this paper. Partial relay selection scheme (PRSS) was used to improve system outage performance. The influence of variable factors in the system on the outage probability of secondary users has been analyzed, such as the number of relays, power allocation factor, and interference temperature constraint. In addition, the closed-form expressions of outage probability of secondary users have been derived. The result shows that increasing the number of relays and using optimal power allocation are effective means to improve system interruption performance in a CR-NOMA network with relay selection.

Acknowledgement This paper was funded in part by the Natural Science Foundation of Fujian Province (2018J01096) and the Subsidized Project for Cultivating Postgraduates' Innovative Ability in Scientific Research of Huaqiao University (18013082031).

References

1. Ding, Z., Lei, X., Karagiannidis, K., Schober, R., Yuan, J., Bhargava, V.: A survey on non-orthogonal multiple access for 5G networks: research challenges and future trends. IEEE J. Sel. Areas Commun. **35**(10), 2181–2195 (2017)
2. Islam, S.M.R., Avazov, N., Dobre, O.A., Kwak, K.: Power-domain non-orthogonal multiple access (NOMA) in 5G systems: potentials and challenges. IEEE Commun. Surv. Tutorials **19**(2), 721–742 (2017)
3. Dai, L., Wang, B., Ding, Z., Wang, Z., Chen, S., Hanzo, L.: A survey of non-orthogonal multiple access for 5G. IEEE Commun. Surv. Tutorials **20**(3), 2294–2323 (2018)
4. Jameel, F., Wyne, S., Nawaz, S.J., Chang, Z., Ristaniemi, T.: Outage analysis of relay-aided non-orthogonal multiple access with partial relay selection. In: 2018 IEEE Globecom Workshops (GC Wkshps), pp.1-6. IEEE Press, Abu Dhabi, United Arab Emirates
5. Li, Y., Li, Y., Chu, X., Ye, Y., Zhang, H.: Performance analysis of relay selection in cooperative NOMA networks. IEEE Commun. Lett. **23**(4), 760–763 (2019)
6. Ju, J., Duan, W., Sun, Q., Gao, S., Zhang, G.: Performance analysis for cooperative NOMA With opportunistic relay selection. IEEE Access **7**(1), 131488–131500 (2019)
7. Liu, X., Yang, L., Chen, J., Zheng, F.: On the performance of nth best relay selection scheme for NOMA-based cooperative relaying networks with swipt. In: 2019 IEEE 89th Vehicular Technology Conference (VTC2019-Spring), pp.1–5. IEEE Press, Kuala Lumpur, Malaysia (2019)
8. Nauryzbayev, G., Arzykulov, S., Tsiftsis, T.A., Abdallah, M.: Performance of cooperative underlay CR-NOMA networks over Nakagami-m Channels. In: 2018 IEEE International Conference on Communications Workshops (ICC Workshops), pp.1–6. IEEE Press, Kansas City, MO (2018)
9. Chu, Y., Champagne, B., Zhu, W.: NOMA-based cooperative relaying for secondary transmission in cognitive radio networks. IET **23**(12), 1840–1851 (2019)
10. Li, C., Guo, D., Guo, K., Qin, Y., Xu, R.: Outage performance of partial relay selection in underlay CR-NOMA Networks. In: IEEE Press. 2019 28th Wireless and Optical Communications (WOCC), pp.1–5. Beijing, China (2019)

Research on Physical Layer Security of NOMA System with Passive Eavesdropping

XiaoHua Lu, Yucheng He, Liangmei Zhang, Jianquan Yang, and Lin Zhou

Abstract This paper investigates the performance of NOMA users collaborative communication system, where there exists a passive eavesdropper that try to eavesdrop the information of center user. A new cooperative NOMA scheme is proposed, in which center user can act as relays to assist cell-edge user in forwarding signals, while cell-edge user employs full-duplex technology to send interference signals to the eavesdropper, which improves the security of communication links and the quality-of-service (QoS). The legitimate receiver decodes the various signals from the superposition signals by successive interference elimination (SIC) technology. The closed expressions of the security outage probability and outage probability of two users are derived respectively under the condition that the wiretap channel statistics channel state information (CSI) is known, and it is verified by Monte Carlo simulation. Both the theoretical analysis and numerical simulations show that the performances of cooperative NOMA scheme are better than the non-cooperative scheme.

1 Introduction

The non-orthogonal multiple access (NOMA) technology is one of the key technologies of the fifth-generation (5G) wireless communication system [1]. With the use of superposition coding and successive interference cancelation (SIC) techniques, multiple users can be simultaneously served in the same resource block (i.e., time/frequency/code), and massive connectivity can be realized efficiently by NOMA. As a result, their users know the messages intended to other weaker users, and

X. Lu · Y. He (✉) · L. Zhang · J. Yang · L. Zhou
Xiamen Key Laboratory of Mobile Multimedia Communications, National Huaqiao University, Xiamen 361021, Fujian, China
e-mail: yucheng.he@hqu.edu.cn

Y. He · L. Zhou
State Key Laboratory of Integrated Services Networks, Xidian University, Xi'an 710071, Shaanxi, China

R. Kountchev et al. (eds.), *Advances in Wireless Communications and Applications*,
Smart Innovation, Systems and Technologies 191,
https://doi.org/10.1007/978-981-15-5879-5_12

hence they can improve the performance of weaker users by resending the decoded information. So it can meet the requirements of low latency and high reliability of heterogeneous, and can support large-scale connection by providing high throughput and better spectral efficiency [2]. However, due to the broadcast characteristics of wireless channel, NOMA technology can improve the spectrum efficiency and the fairness of users, but it cannot preventing eavesdropping [3].

In this context, there have been many research results about the security configuration of NOMA system. In [4], a new transmission interruption constraint scheme is proposed against eavesdropping the NOMA system. In [5] and [6], the artificial noise confidential beamforming of NOMA was studied. In [7], the outage probability and ergodic sum rate are derived in a downlink non-orthogonal multiple access system with two users, but it did not consider the issue of system security. In this paper, we apply relay collaboration and full-duplex technology to the NOMA system in order to improve system security and the quality-of-service (QoS).

In this paper, we proposed a new NOMA user collaboration scheme. The concept of cooperation is achieved by the system's strong users acting as relays to relay weak user signals, and weak users send interference signals to eavesdroppers. Thus, there is not actual relay.

2 System Model

Figure 1 shows the NOMA-equipped cellular system, in which there is a base station denoted by S, simultaneously communicates with a center user A and a cell-edge user B. And there is a malicious eavesdropper trying to eavesdrop on user A's information. The node S, node A, and eavesdropping node E are equipped with a single antenna and work in half-duplex (HD) mode. Node B is equipped with dual antennas and uses full-duplex technology to send or receive information. This article assumes

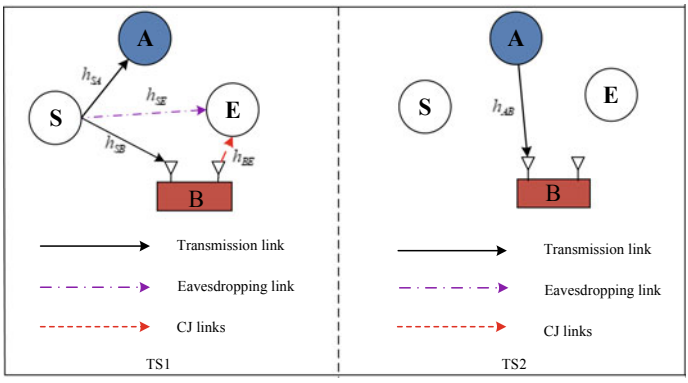

Fig. 1 System model

that the self-interference caused by full-duplex has been eliminated by analog cancelation and digital cancelation techniques completely. We assume that all channels are quasi-static flat Rayleigh fading channels with perfect reciprocity. The channel coefficients of the communication links $S \rightarrow A$, $S \rightarrow B$, $S \rightarrow E$, $A \rightarrow B$, and $B \rightarrow E$ are respectively expressed as h_{ij} $(ij \in \{SA, SB, SE, AB, BE\})$, and the corresponding channel gains $|h_{ij}|^2 (ij \in \{SA, SB, SE, AB, BE\})$ follow the exponential distribution of the mean λ_{ij} $(ij \in \{SA, SB, SE, AB, BE\})$. The transmission of this network is completed in two phases. The transmission process is described in detail as follows.

In the first time slot, the base station S broadcasts superimposed signal $x = \sqrt{\alpha_A P_S} x_A + \sqrt{\alpha_B P_S} x_B$ to user A and user B, where α_A and α_B denote the power allocation coefficients for the messages x_A and x_B of user A and user B, respectively. According to the principle of NOMA, we assume that $|h_{SA}|^2 > |h_{SB}|^2, 0 < \alpha_A < \alpha_B$ and $\alpha_A + \alpha_B = 1$ [8]. While E tries to eavesdrop the x_A from the superimposed signals S at the same time. And user B employs the full-duplex technology to send an interference signal to E for confuse the eavesdropper.

In the second time slot, user A acts as a cooperative relay to forward information x_B of the user B's signal. The legal receiver uses SIC technology to decode the signal. Follow the principle of NOMA, the SIC decoding of each receiver always starts from a weak signal and develops toward a strong signal.

For simplicity of calculation, let $\gamma_i = P_i/\sigma^2 (i \in \{S, A, B\})$, where P_i $(i \in \{S, A, B\})$ and σ^2 denote transmit power and the noise power of the note S, A and B, respectively. Thus, the signal-to-interference-and-noise ratio (SINR) of user A and user B can be described as follows.

(1) At user A: User A to decode x_B can be obtained as

$$\gamma_{SA}^{x_B} = \frac{\alpha_B \gamma_S |h_{SA}|^2}{\alpha_A \gamma_S |h_{SA}|^2 + 1} \tag{1}$$

and the SINR at user A to decode x_A can be expressed as

$$\gamma_{SA}^{x_A} = \alpha_A \gamma_S |h_{SA}|^2 \tag{2}$$

(2) At user B: node B decodes x_B directly by treating the other signals as interference signals in the direct link $S \rightarrow B$.

$$\gamma_{SB}^{x_B} = \frac{\alpha_B \gamma_S |h_{SB}|^2}{\alpha_A \gamma_S |h_{SB}|^2 + 1} \tag{3}$$

The SINR of user B in TS2 can be written as

$$\gamma_{AB} = \gamma_A |h_{AB}|^2 \tag{4}$$

User B employs the selective combining (SC) technique for the received signals of two time slots. After the combining, the receiving SINR is

$$\gamma_B = \max\left\{\gamma_{SB}^{x_B}, \min\left\{\gamma_{SA}^{x_B}, \gamma_{AB}\right\}\right\} \tag{5}$$

(3) At eavesdropper E: Similar to the literature [9], considering the worst-case eavesdropper has strong analysis capabilities and signal extraction capabilities, the eavesdropper can decoded x_A from superimposed signal x with the interference of user B.

$$\gamma_{SE1}^{x_A} = \frac{\alpha_A \gamma_S |h_{SE}|^2}{\gamma_B |h_{BE}|^2 + 1} \tag{6}$$

3 Performance Analysis

In this section, we will derive the closed-form of user A's security outage probability (SOP) and the outage probability (OP) of user B under two schemes. According to literature [10], when the instantaneous data transmission rate of the legal channel link is lower than the minimum data transmission rate, an interrupt occurs. Depending on whether or not there is an eavesdropping, it can be divided into security interrupt event or interrupt event. And the corresponding probability is security outage probability or outage probability.

3.1 Cooperative Scheme

(1) At user A: When user A fails to decode the signal x_B successfully or user A successfully decodes signal x_B that is the SINR of user A decoded signal x_B is higher than the threshold γ_{thB} in the first time slot, but its security capacity is lower than the given threshold value R_{SA}. There $T_{SA} = 2^{R_{SA}}$. A security interrupt event will occur, which can be expressed as

$$\begin{aligned} P_{\text{SOP}}^{A} &= \Pr\left(\frac{1+\gamma_{SA}^{x_A}}{1+\gamma_{SE1}^{x_A}} < 2^{R_{SA}}\right) \Pr\left(\gamma_{SA}^{x_B} \geq \gamma_{thB}\right) + \Pr\left(\gamma_{SA}^{x_B} < \gamma_{thB}\right) \\ &= \frac{T_{SA}\lambda_{SE}}{\lambda_{BE}\lambda_{SA}\gamma_B}\left[-\mathrm{e}^{\frac{T_{SA}\lambda_{SE}+\lambda_{SA}\lambda_{SA}}{\lambda_{BE}\lambda_{SA}\gamma_B}} Ei\left(-\frac{T_{SA}\lambda_{SE}+\lambda_{SA}\lambda_{SA}}{\lambda_{BE}\lambda_{SA}\gamma_B}\right)\right]\mathrm{e}^{\left(-\frac{\gamma_{thB}}{\gamma_S\lambda_{SA}(\alpha_B-\alpha_A\gamma_{thB})}\right)} \end{aligned}$$

$$+\left(1-\mathrm{e}^{\left(-\frac{\gamma_{thB}}{\gamma_S\lambda_{SA}(\alpha_B-\alpha_A\gamma_{thB})}\right)}\right) \tag{7}$$

(2) At user B: User B's outage events occur when the instantaneous data transmission rate of the legal channel link is lower than the minimum data transmission rate $R_{\min B}$, which can be expressed as

$$\begin{aligned} P_{\text{out}}^{B} &= \Pr\left(\frac{1}{2}\log_2\left(1+\max\left\{\gamma_{SB}^{x_B}, \min\left\{\gamma_{SA}^{x_B}, \gamma_{AB}\right\}\right\}\right) < R_{\min B}\right) \\ &= \left(1-\mathrm{e}^{\left(-\frac{T_{\min B}}{\gamma_S\lambda_{SB}(\alpha_B-\alpha_A T_{\min B})}\right)}\right)\left[1-\mathrm{e}^{\left(-\frac{T_{\min B}}{\gamma_S\lambda_{SA}(\alpha_B-\alpha_A T_{\min B})}\right)}\mathrm{e}^{\left(-\frac{T_{\min B}}{\gamma_A\lambda_{AB}}\right)}\right] \end{aligned} \tag{8}$$

where $T_{\min B} = 2^{2R_{\min B}} - 1$.

3.2 Non-cooperative Scheme

In this scheme, the user A does not assist the user B to forward its signal x_B and the user B no longer sends artificial noise to the eavesdropper E. Therefore, the SINR of eavesdropper E is expressed as $\gamma_{SE2}^{x_A} = \alpha_A\gamma_S|h_{SE}|^2$.

(1) At user A: As can be seen in Sect 3.1, the SOP of user A can be derived as

$$\begin{aligned} P_{\text{SOP}}^{a} &= \Pr\left(\log_2\left(\frac{1+\gamma_{SA}^{x_A}}{1+\gamma_{SE2}^{x_A}}\right) < R_{SA}\right)\Pr\left(\gamma_{SA}^{x_B} \geq \gamma_{thB}\right) + \Pr\left(\gamma_{SA}^{x_B} < \gamma_{thB}\right) \\ &= \left(1-\frac{1}{T_{SA}\lambda_{SE}+1}\mathrm{e}^{\left(\frac{1-T_{SA}}{\alpha_A\gamma_S\lambda_{SA}}\right)}\right)\mathrm{e}^{\left(-\frac{\gamma_{thB}}{\gamma_S\lambda_{SA}(\alpha_B-\alpha_A\gamma_{thB})}\right)} + \left(1-\mathrm{e}^{\left(-\frac{\gamma_{thB}}{\gamma_S\lambda_{SA}(\alpha_B-\alpha_A\gamma_{thB})}\right)}\right) \end{aligned} \tag{9}$$

(2) At user B: The OP of user B can be derived as

$$P_{\text{out}}^{b} = \Pr\left(\log_2\left(1+\gamma_{SB}^{x_B}\right) < \gamma_{\min B}\right) = 1-\mathrm{e}^{\left(-\frac{T_{thB}}{\gamma_S\lambda_{SB}(\alpha_B-\alpha_A T_{thB})}\right)} \tag{10}$$

where $T_{\text{th}B} = 2^{R_{\min B}} - 1$.

4 Numerical Results

In this section, we verify the analysis results of the different scheme by Monte Carlo simulations. In the simulation, we set that $\lambda_{SA} = \lambda_{AB} = 1, \lambda_{\mathrm{SB}} = 1/10, \lambda_{SE} = 1/30$, $\lambda_{BE} = 1$. Furthermore, we assume $P_S/\sigma^2 = P_A/\sigma^2 = P_B/\sigma^2 = 20$ dBm, and the target data rate $R_{SA} = 1.5\ bit/s/Hz$, $r_{\mathrm{thB}} = 1$, $R_{\mathrm{min}B} = 1$ bit/s/Hz.

Figure 2 compares the SOP performance of user A versus the transmitted power Ps in different schemes. We observe that as Ps increases, the user A's SOP performance of the cooperative scheme is better than the non-cooperative scheme.

Figure 3 compares the OP performance of user B versus the transmitted power Ps in the different scheme. We observe that as Ps increases, the user B's OP performance of the cooperative scheme is better than the non-cooperative scheme.

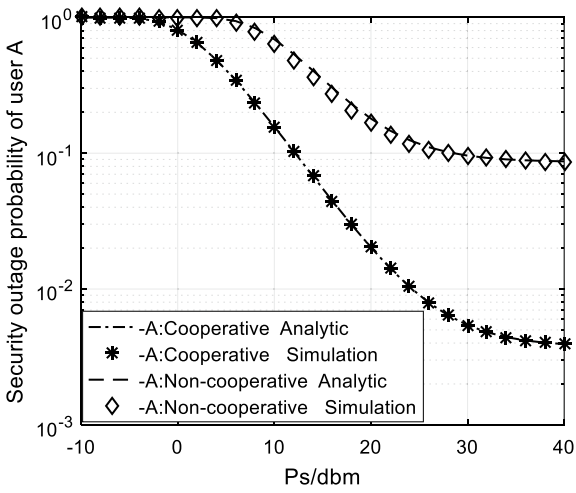

Fig. 2 User A's SOP versus Ps for two schemes

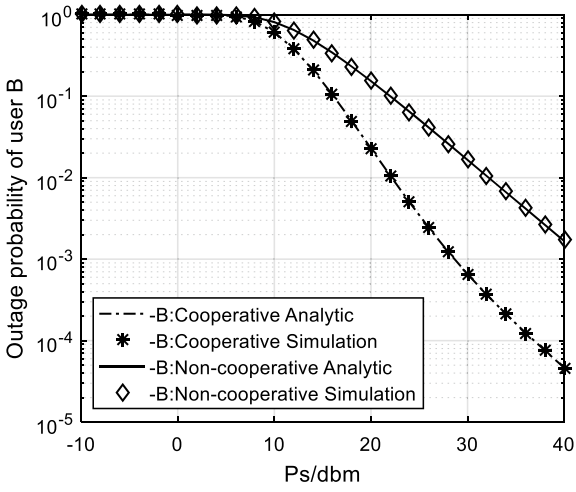

Fig. 3 User B's OP versus Ps for two schemes

5 Conclusion

Based on the inherent coordination characteristics of the NOMA system, this paper studies the physical layer security of a dual-user system in which a strong user acts as a weak user's relay, and a weak user employs full-duplex technology to interference the eavesdropper. Assuming that a passive eavesdropper exists in the system, the closed-form expressions of the SOP of the center user and the outage probability OP of the cell-edge user are derived. The simulation results show that the analysis results are basically consistent with the simulation results. The superiority of the proposed cooperation scheme is verified. This scheme provides new ideas for researching the security of NOMA networks in the future.

Acknowledgement This paper was funded in part by the Natural Science Foundation of Fujian Province (2018J01096) and the Subsidized Project for Cultivating Postgraduates' Innovative Ability in Scientific Research of Huaqiao University (18014082029).

References

1. Ding, Z., Lei, X., Karagiannidis, G.K.: A survey on non-orthogonal multiple access for 5G networks: Research challenges and future trends. IEEE J. Sel. Areas Commun. **35**(10), 2181–2195 (2017)
2. Chen, Z., Ding, Z., Dai, X.: An optimization perspective of the superiority of noma compared to conventional OMA. IEEE Trans. Sig. Process. **65**(19), 5191–5202 (2017)
3. Zheng, B., Wen, M., Wang, C.X.: Secure NOMA based two-way relay networks using artificial noise and full duplex. IEEE J. Sel. Areas Commun. **36**(7), 1 (2018)
4. Lv, L., Ding, Z., Chen, J.: Design of secure NOMA against full-duplex proactive eavesdropping. IEEE Wireless Commun. Let. **8**(4), 1 (2019)
5. Lv, L., Ding, Z., Ni, Q.: Secure MISO-NOMA transmission with artificial noise. IEEE Trans. Veh. Technol. **67**(7), 6700–6705 (2018)
6. Feng, Y., Yan, S., Yang, Z.: Beamforming design and power allocation for secure transmission with NOMA. IEEE Trans. Wireless Commun. **18**(5), 2902–2906 (2019)
7. Zhang, L., Liu, J., Xiao, M.: Performance analysis and optimization in downlink NOMA systems with cooperative full-duplex relaying. IEEE J. Sel. Areas Commun. **35**(10), 1 (2017)
8. Zheng, Y., Ding, Z., Fan, P.: Outage performance for dynamic power allocation in hybrid non-orthogonal multiple access systems. IEEE Commun. Lett. **20**(8), 1 (2016)
9. Brante, G., Alves, H., Souza, R.D.: Secrecy analysis of transmit antenna selection cooperative schemes with no channel state information at the transmitter. IEEE Trans. Commun. **63**(4), 1330–1342 (2015)
10. Shannon, C.E.: Communication theory of secrecy systems. Bell Syst. Tech. J. **28**(4), 656–715 (1949)

Intelligent Algorithm Detects Compensation Capacitor Failure

Shunran Xue, Dongfeng Xing, Guangwu Chen, Jianqiang Shi, and Yongbo Si

Abstract In the future, the railway's information transmission will be through the wireless communications. The non-insulated track circuit is an important railway equipment in China. It is widely used. The track circuit fault diagnosis is an important guarantee for railway transportation safety. The compensation capacitor is an important component of the track circuit, which can effectively guarantee the transmission distance and the signal quality. In recent years, the fault diagnosis of the non-insulated track circuit is mostly focused on the fault diagnosis of the compensation capacitor. The method of capacitor failure points out the entry points, the advantages and disadvantages of each method, and provides reference and help for later scholars.

1 Introduction

The wireless communication is already a necessary communication method in CTCS-3 level train control system. The track circuit is installed outdoors, which is vulnerable to environmental impacts. Once a fault occurs, it will greatly affect the safety of railway transportation. The compensation capacitor is an important component device, which reduces the inductive impedance of the rail and improves the effective transmission distance and receiving quality of the signal. Once a fault occurs, it directly affects the transmission of the track signal. The reception of the locomotive signal will lead to series of red bands such as the track circuit. The fault check of the compensation capacitor that greatly affects the safety of the track is an important part of diagnosing the fault of the track circuit.

S. Xue (✉) · D. Xing · G. Chen · J. Shi · Y. Si
Institute of Automatic Control, Lanzhou Jiaotong University, Lanzhou 730070, China
e-mail: 229002702@qq.com

Key Laboratory of Gansu Province Plateau Traffic Information Engineering and Control, Lanzhou 730070, China

R. Kountchev et al. (eds.), *Advances in Wireless Communications and Applications*,
Smart Innovation, Systems and Technologies 191,
https://doi.org/10.1007/978-981-15-5879-5_13

2 Compensation Capacitor Principle

ZPW-2000A-type track circuit outdoor equipment is complicated, as shown in Fig. 1. The electrical signal sent by the transmitter is transmitted via the cable, and the tuning area is sent along the rail and received by the receiver. The compensation capacitor is located between the two rails. Due to the sensibility of the rail, the transmission of information is attenuated, which cannot meet the long-distance transmission requirements. Therefore, a compensation capacitor is added between the two rails to neutralize the inductivity of the rail and ensure that the signal can be effectively transmitted.

There are two types of faults in the compensation capacitor: the disconnection and the capacitance decrease. Among them, the damage of the broken wire is the biggest, which will cause the rail surface voltage to fluctuate. The fault capacitance is bounded, there is no abnormality near the transmitting end, and the attenuation speed is faster near the receiving end. The original wave shape disappears at the fault position. The downward trend for homeopathic is shown in Fig. 2. The drop in the capacitance value generally only has a significant effect if it falls below the normal value of 60%, and the effect is similar to the broken line. The voltage drop near the receiving end easily leads to the appearance of the red band of the track

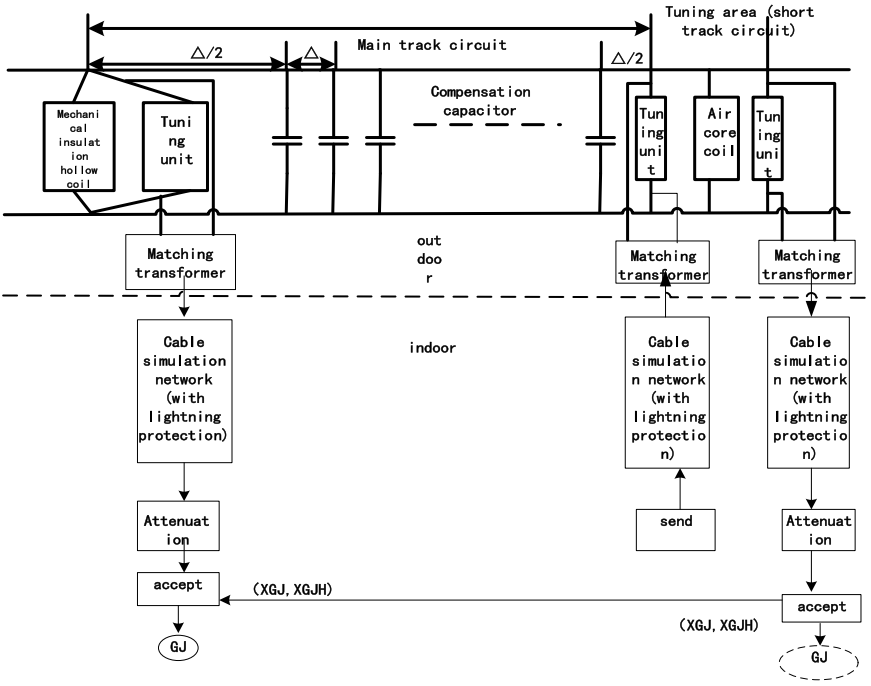

Fig. 1 Track circuit equipment diagram

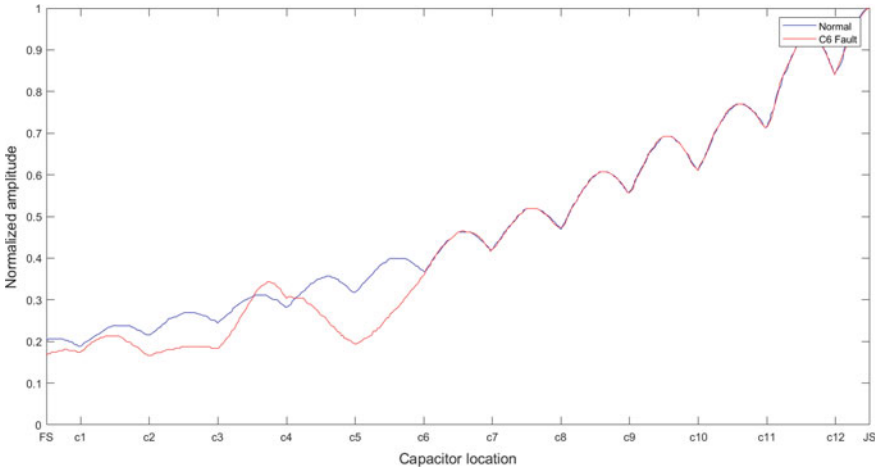

Fig. 2 C6 fault image

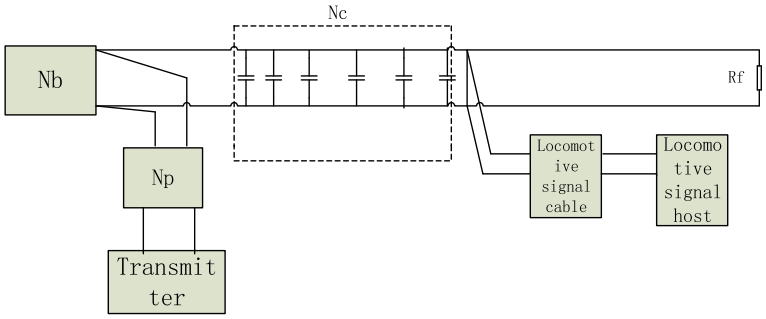

Fig. 3 Induction voltage amplitude modeling

circuit, affecting the normal use of the track circuit, and the attenuation of the signal makes the information of the track circuit not fully acquired, and the safety is not guaranteed (Fig. 3).

3 Compensation Capacitor Fault Modeling

At present, most of the compensation capacitor fault detection sites are used for professional electrical inspection vehicle timing detection. The sensors are sent by the vehicle sensors and are received by the receiver through electromagnetic induction. The state of the compensation capacitor is obtained through computer analysis. Although this method has high accuracy, it does not have timeliness. Failures in

the maintenance cycle cannot be detected and dealt with in time, and the maintenance cost is increased, which cannot meet the requirements of railway transportation safety. At present, the models applied to the compensation capacitor fault detection are relatively simple, and all are based on the transmission line four-terminal network model. The track circuit is mainly composed of a main track and a tuning area. The compensation capacitor is disposed in the main track section and installed according to a prescribed step length. The main track can be regarded as a series of n compensation capacitor units NC, and the entire track circuit can be regarded as it is made up of different parts cascaded.N_l is the main rail model, N_c is the compensation capacitance, $N_g(\mathrm{l}_g/2)$ is a half-step orbit model, N_{F1} and N_{F2} are the tuning region model, N_{SVA} is the air-core coil model, N_P is the transmitter cable model, N_b is the transmitter matches the tuning region model, the modeling of the induced amplitude voltage and the short-circuit current and the rail surface voltage can be completed by establishing each part of the model, and the fault diagnosis is performed in the model through the change of the model simulation curve at the time of failure.

$$N_l = N_C^n \tag{1}$$

$$N_C = N_g\left(l_g/2\right) \times N_{CC} \times N_g\left(l_g/2\right) \tag{2}$$

$$N_{CC} = \begin{bmatrix} 1 & 0 \\ j2\pi f C & 1 \end{bmatrix} \tag{3}$$

$$N_g(\mathrm{l}_g/2) = \begin{bmatrix} \mathrm{ch}\left(r_g \frac{l_g}{2}\right) & Z_c \mathrm{sh}\left(r_g \frac{l_g}{2}\right) \\ \mathrm{sh}\left(r_g \frac{l_g}{2}\right)/Z_c & \mathrm{ch}\left(r_g \frac{l_g}{2}\right) \end{bmatrix} \tag{4}$$

$$N_T = N_{F1} \times N_g(\mathrm{l}_t/2) \times N_{\mathrm{SVA}} \times N_g\left(\mathrm{l}_g/2\right) \times N_{F2} \tag{5}$$

$$N_{F1} = \begin{bmatrix} 1 & 0 \\ Z_{\mathrm{ba1}} + Z_{\mathrm{ca}} & 1 \end{bmatrix} \tag{6}$$

$$N_{F2} = \begin{bmatrix} 1 & 0 \\ Z_{\mathrm{ba2}} + Z_{\mathrm{ca}} & 1 \end{bmatrix} \tag{7}$$

$$N_{\mathrm{SVA}} = \begin{bmatrix} 1 & 0 \\ Z_{\mathrm{SVA}} + Z_{\mathrm{ca}} & 1 \end{bmatrix} \tag{8}$$

$$\begin{cases} A_{\mathrm{cv}}(x) = a_1 a_2 A_{\mathrm{fs}} / \left| N_{\mathrm{sf11}}(x) R_f + N_{\mathrm{sf12}}(x) \right| \\ N_{\mathrm{sf}} = \begin{bmatrix} N_{\mathrm{sf11}} & N_{\mathrm{sf12}} \\ N_{\mathrm{sf21}} & N_{\mathrm{sf22}} \end{bmatrix} = N_P \times N_b \times N_l \end{cases} \tag{9}$$

4 Intelligent Algorithm Based on Curve Fitting Analysis

Due to the obvious difference between the compensation capacitor and the fault image, the foreign scholars Latifa can use the Hilbert–Huang transform (HHT) combined with the Dempster evidence theory to solve the fault of the compensation capacitance trend analysis by fitting the curve and analyzing the parameter changes. Curve fitting each volatility using the mathematical formula $ax^2 + bx + c$, then use the classifier to process the parameters of the formula, analyze the fault, and have a higher correct rate, but the data used in the verification process is based on the simulation experiment, does not have strong persuasive power, and needs to verify the validity through the field data. Moreover, the mathematical formula can only represent the volatility and cannot express the overall attenuation, and the algorithm has high complexity. It requires a large amount of data to establish a corresponding neural network for each capacitor in the line. The workload is huge, and the applicability is not high. Based on the characteristics of the image curve, Alexandra's partial least squares regression (PLS) is combined with the transmission confidence model (TBM) and neural network to simulate the field data. The mathematical formula is used to segment the image. The parameters in the formula are selected as the feature vector to judge the fault. The complexity of the algorithm is still high. It is necessary to establish different networks for different lines, and the workload is large and the implementation is difficult. The literature [1] also fits the curve, using mathematical formulas.

$|f(x)| = a_1 \exp(a_2 x) + (a_3 \exp(a_4 x) - a_1 \exp(a_2 x)) \cos(a_5 x + a_6)$, where $a_1 \exp(a_2 x)$ replaces the total attenuation, $\cos(a_5 x + a_6)$ replaces the overall volatility, $(a_3 \exp(a_4 x) - a_1 \exp(a_2 x))$ represents the range of fluctuations. Such a setting is more in line with the actual situation, omitting the modeling process for each compensation capacitor, reducing the complexity of the algorithm. The *L–M* algorithm is used to eliminate the attenuation term, and the deleted expression is used as the input signal of the GST signal processing to obtain the instantaneous frequency change. The point of the mutation is marked as fault by the Formulas (1) and (2). m_i is the instantaneous frequency mean, f_j is the instantaneous frequency, x_i is the capacitance position, and the fault is judged by whether k_i is abrupt. The feasibility of the method is verified by the field data, but the diagnosis of multiple compensation capacitor faults is lacking, and the process of noise reduction is lacking. The signal processing process is susceptible to noise and other environmental factors such as turnout resistance are not considered.

$$m_i = \begin{cases} \dfrac{1}{x_1 + L_T/2} \displaystyle\sum_{j=0}^{x_1 + L_T/2} f_j, i = 1 \\ \dfrac{1}{x_i - x_{i-1}} \displaystyle\sum_{j=x_{i-1}+L_T/2}^{x_1 + L_T/2} f_j, i = 2, 3, \ldots, n \end{cases} \tag{10}$$

$$k_i = \left| 1 - \frac{m_i}{f_i} \right| \tag{11}$$

In [2], the phase space reconstruction method is used to diagnose the compensation capacitor from the phase change of the signal at the fault time. The idea of phase space reconstruction is to transform a one-dimensional time series projection into other coordinate systems. Some features are more obvious under other coordinates. After obtaining the delay time and the embedded dimension, the coordinates of the projection are tested and the fault is selected. The most obvious coordinate the projection of the feature vector from the normal time. After the real data is verified, the result is consistent with the actual situation, and the pseudo-phase diagram cannot only find out whether the fault diagnosis of the disconnection, but also the fault of the compensation capacitor value drop, and the loose connection fault has a good diagnosis result. However, the simultaneous diagnosis of multiple compensation capacitors has not been diagnosed, especially in the case of adjacent capacitor failures, and the effects on the changes in turnout resistance and shunt resistance have not been considered.

Similarly, according to the regularity change of the fault image, the method of extracting the characteristic curve of the induced voltage amplitude is started by the monotony of the mathematics, the boundary value, and the angle of the first derivative of the fault point. According to the fault feature of the image [3], the monotony of the fault point capacitance will change, from parabolic-like waveform to monotonically decreasing or increasing. The graph is segmented with the position of the capacitor as a point. For each segment of the curve, the left and right boundary values are taken, the maximum and minimum values in the segment are segmented and calculated as feature vectors, and when there are two adjacent capacitors simultaneously In the event of a fault, it is necessary to determine whether the first-order derivatives on the left and right sides of the capacitor are the same. If they are the same, they are simultaneously faulty and vice versa. Through the on-site data verification method, the obtained result is the same as the actual one and not only can detect the fault condition of multiple capacitors, but also can detect the capacitance value of the capacitor. For the two capacitors close to the receiving end, when the capacitance decreases, it can be detected up to 50%; it can be detected when other capacitances drop to 75%, the algorithm is time-sensitive, and the diagnosis is completed with only 0.0214 s, the accuracy is higher, the false alarm rate and the false alarm rate are compared. Now, it has been applied to the TCR remote detection system and has a good effect (Figs. 4 and 5).

$$\begin{cases} Q_{cv}^{i} = \dfrac{A_{mx}^{i} - A_{rg}^{i} + A_{lf}^{i} - A_{mi}^{i}}{2\left(A_{mx}^{i} - A_{mi}^{i}\right)} \\ A_{mx}^{i} = \max\left(A_{cv}^{i}(x)\right) \\ A_{mi}^{i} = \min\left(A_{cv}^{i}(x)\right) \\ A_{lf}^{i} = \begin{cases} A_{cv}^{1} = 0, i = 1 \\ A_{cv}^{i}(x_{c(i-1)}), i \neq 1 \end{cases} \\ A_{rg}^{i} = A_{cv}^{i}(x_{Ci}) \end{cases} \tag{12}$$

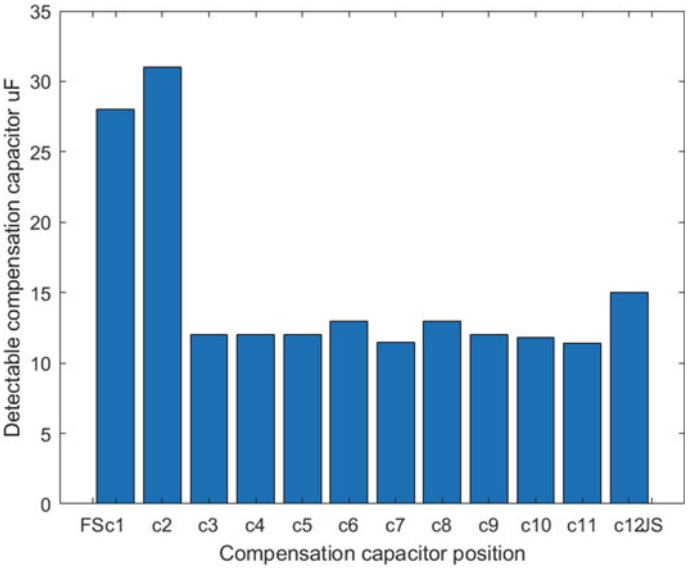

Fig. 4 Detectable compensation capacitor range

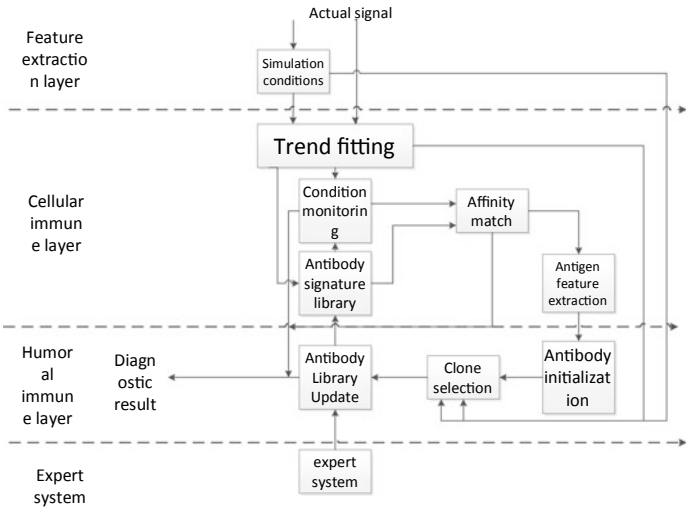

Fig. 5 Layered immune structure

$$\frac{\mathrm{d}A_{cv}^{i}\left(x=x_{ci}^{-}\right)}{\mathrm{d}x}=\frac{\mathrm{d}A_{cv}^{i}\left(x=x_{ci}^{+}\right)}{\mathrm{d}x} \tag{13}$$

5 Frequency Domain Analysis Failure

Generally, the graph of the compensation capacitor is the amplitude curve of the short-circuit current or the amplitude curve of the rail surface voltage. Both of them are nonlinear time-varying signals. From the perspective of signal processing, the signal can be decomposed and converted from the time domain. The fault is analyzed in the frequency domain, and the frequency domain component of the fault time is obtained and compared with the component parameters of the normal time to perform fault diagnosis.

In [4], the HHT method is used to decompose the short-circuit current signal. According to the instantaneous frequency change of the signal, the phase change effectively diagnoses the fault compensation of the track circuit, but there is noise, and the component after decomposition has a large influences. On the basis of this paper, [5] combines B-spline discrete binary wavelet transform (DBWT) with HHT, and uses DBWT to "polish" the signal. "Filtering" suppresses the noise amplitude to the lowest, enhances the amplitude of the effective signal, and weakens the attenuation of the signal. Then, the empirical mode decomposition (EMD) operation is performed on the signal and the decomposed intrinsic mode function (IMF) is summed. As shown in Formula (3), such an improvement can prevent the amplitude-frequency close to the receiving end from being lower than the normal value when the compensation capacitor is faulty, affecting the simulation. Accuracy. The accumulated IMF phase information is discriminated, and if a phase change occurs, it is determined that a failure has occurred. The effectiveness of the method is verified by field data. The verification results show that the method is highly feasible. However, this method does not consider the situation of multiple compensation capacitors at the same time and does not consider the influence of other factors such as turnout resistance on the signal.

$$\begin{cases} s_1(t) = d_1(t) \\ s_2(t) = s_1(t) + d_2(t) \\ \cdots \\ s_n(t) = s_{n-1}(t) + d_n(t) \end{cases} \tag{14}$$

$$\varphi_i(t) = \arctan\left(\overline{s_i(t)}/s_i(t)\right) \tag{15}$$

In the same way, the literature [6] decomposes the induced voltage amplitude envelope signal (IVECS), performs EMD decomposition on the normal signal, and performs curve-fitting on the IMF1 and residual component obtained by the decomposition. The mathematical Formula (5) constructs the IVECS regression model. Through the model, the period of the track circuit without faults, the fixed frequency f and other information can be obtained. When the compensation capacitor fault occurs, the original model cycle is destroyed, and a new fault frequency appears. Based on this, the compensation capacitor fault is judged. Firstly, the IVECS is

normalized to eliminate the influence of some unrelated parameters. Then the DBWT is used to remove the influence of noise in the signal. The processed signal is used as the input signal, and the AOK-TFR adaptive optimal kernel time–frequency representation link is input to extract the fault information. The frequency corresponding to the capacitor is extracted and compared with the corresponding original fixed frequency for fault diagnosis. Due to the high resolution of AOK-TFR, it can effectively suppress cross-interference and can effectively identify local features, making this method more robust and adaptable, and only need actual data to complete the detection, and the timeliness is high, at low cost. However, the paper does not consider multiple capacitor faults, especially when two capacitors fail simultaneously. When two consecutive capacitors fail at the same time, they will affect the frequency of each other and even the frequency of adjacent capacitors.

$$f(x) = a_1 e^{a_2 x}|\cos(a_3 x + a_4)| + a_8 e^{a_9 x} + a_{10} e^{a_{11} x}(|\cos(a_{12} x + a_{13})| + a_{14}) \times [u(x) - u(x - c_i)] \tag{16}$$

$$f = \frac{2a_3}{2\pi} = \frac{N}{L} \tag{17}$$

$$f_w = \frac{2a_{12}}{2\pi} = \frac{2a_3/(2\pi)}{3} = \frac{N}{3L} \tag{18}$$

The above literature decomposition signals use the EMD method. The literature [7] analyzes the advantages and disadvantages of EMD and complementary ensemble empirical mode decomposition (CEEMD). CEEMD solves the modal aliasing of EMD and the redundant noise of ensemble empirical mode decomposition (EEMD) by adding positive and negative two opposite white noise signals. The IMF analysis obtained by EMD, EEMD, and CEEMD decomposition of the rail surface voltage can be obtained. CEEMD can reconstruct the signal better, the correlation is better than EMD, EEMD, and CEEMD is used as the method of extracting characteristic information and the component after decomposition. The energy calculation is performed as a feature vector, input into the neural network, and the fault is identified by training the neural network.

6 Summary

In the future, the railway's information transmission will be wireless communication. The research results of this paper will be used in the future railway wireless information fault diagnosis. Through the research summary of compensation capacitors by scholars at home and abroad in recent years, most scholars use the transmission line four-terminal network to model, through the curve analysis of the rail surface voltage, short-circuit current, and induced amplitude voltage, from the properties of the curve itself. Only a small number of methods taken into account, the failure conditions of

multiple compensation capacitors and can take into account the effects on the curve due to changes in turnout resistance and shunt point groups. (1) Since the capacitance value decreases, it will also have a certain influence on the track circuit. In addition to the diagnosis of the compensation capacitor fault, the next-stage study should also consider the state monitoring of the compensation capacitor. (2) The compensation capacitors on both sides of the main track are only half a step away from each other. Therefore, there are only half waveforms on the waveform. How to handle the half waveform requires further research.

Acknowledgements This work was supported by the National Natural Science Foundation of China (61863024), funded by scientific research projects of higher education institutions in Gansu Province (2018C-11, 2018A-22) and Gansu Natural Science Foundation (17JR5RA089, 18JR3RA130).

References

1. Zhao, L., Xu, J., Liu, W.: Fault detection of compensation capacitors for non-insulated track circuits based on Levenberg-Marquardt algorithm and generalized S-transformation. Control Theory Appl. **27**(12), 1663–1668 (2010)
2. Sun, S., Zhao, H.: A method for compensation capacitance detection of non-insulated track circuits based on phase space reconstruction. J. China Railw. Soc. **10**, 79–84 (2012)
3. Xu, W., Zhao, L.: A fast diagnosis method for multi-fault compensation of non-insulated track circuits. J. China Railw. Soc. **40**(02), 67–72 (2018)
4. Li, Y., Dong, W., Nan, J.: Fault diagnosis of compensation capacitance of non-insulated track circuit based on CEEMD feature extraction. Comput. Measur. Control **23**(02), 378–381 (2015)
5. Qiu, K., Zhao, L., Cai, B.: A method for fault diagnosis of compensation capacitor in non-insulated track circuit based on HHT and DBWWT. J. China Railw. Soc. **33**(3), 49–54 (2011)
6. Zhao, L., Mu, J.: Fault diagnosis method of track circuit based on AOK-TFR. J. Southwest Jiaotong Univ. **46**(1), 84–91 (2011)
7. Zhao, L., Pei, Y., Mu, J.: A comprehensive diagnosis method for faults of uninsulated track circuits based on genetic algorithm. China Railw. Sci. **31**(3), 107–114 (2010)
8. Meng, J., Hou, Y.: Analysis of failure mode of compensation capacitance of track circuit. China Railw. **07**, 93–95+107 (2018)
9. Guo, H., Zhao, L., Feng, D., Li, C.: Research on adjacent section interference protection method for non-insulated track circuits. J. China Railw. Soc. **40**(11), 70–76 (2018)
10. Zhao, L.-H., Zhang, C.-L., Qiu, K.-M., Li, Q.-L.: A fault diagnosis method for the tuning area of jointless track circuits based on a neural network. In: Proceedings of the Institution of Mechanical Engineering, vol. 4 (2013)
11. Zhao, L.-H., Wu, J.-P., Ran, Y.-K.: Fault diagnosis for track circuit using AOK-TFRs and AGA. Control Eng. Practice **12** (2012)
12. Debiolles, A., Oukhellou, L., Denoeux, T., et al.: Output coding of spatially dependent subclassifiers in evidential framework application to the diagnosis of railway track/vehicle transmission system. In: 9th International Conference on Information Fusion (2006)
13. Debiolles, A., Oukhellou, L., Aknin, P.: Combined use of partial least squares regression and neural network for diagnosis tasks. In: Proceedings of the 17th International Conference on Pattern Recognition, vol. 2 (2004)
14. Zhang, W.: Development and application of railway electric vehicle inspection vehicle. Railw. Comput. Appl. **18**(3), 46–48 (2009)

Jamming-Assisted Proactive Eavesdropping in Decode-And-Forward Relaying Systems

Yukai Fang, Yucheng He, Liangmei Zhang, Jianquan Yang, and Lin Zhou

Abstract With the increasing threat of lawbreakers to public security, proactive eavesdropping and supervision begin to play an important role in the commercial and military fields. This paper proposes a proactive monitoring scheme for jamming first and then eavesdropping for suspicious communication in decode-and-forward (DF) relay network. After the suspicious user is jammed, in order to maintain a constant outage probability, it is forced to change the transmission rate of the suspicious users. By converting the relationship between the suspicious transmission rate and the jamming power, the expression of optimal suspicious communication rate that maximizes the average eavesdropping rate under certain limiting conditions is obtained; in that way, the expression of optimal jamming power is obtained. Comparing this optimal jamming scheme with passive eavesdropping and proactive eavesdropping under constant jamming power, both of the results of expression and simulation show that the average eavesdropping rate under this optimal scheme significantly outperforms the other two schemes.

1 Introduction

Different from the illegal eavesdropping in the traditional physical layer security research, proactive eavesdropping is mainly aimed at suspicious communication systems that may exist for crimes. The concept of proactive eavesdropping was first proposed by Xu in [1]. The full-duplex (FD) proactive eavesdropper in this system actively sends interference to suspicious receivers. Suspicious transmitter is forced

Y. Fang · Y. He (✉) · L. Zhang · J. Yang · L. Zhou
Xiamen Key Laboratory of Mobile Multimedia Communications, National Huaqiao University, Xiamen 361021, Fujian, China
e-mail: yucheng.he@hqu.edu.cn

Y. He · L. Zhou
State Key Laboratory of Integrated Services Networks, Xidian University, Xi'an 710071, Shaanxi, China

R. Kountchev et al. (eds.), *Advances in Wireless Communications and Applications*,
Smart Innovation, Systems and Technologies 191,
https://doi.org/10.1007/978-981-15-5879-5_14

to reduce the transmission rate in order to maintain a constant outage probability, which makes the performance of eavesdropping better.

In the early research of proactive eavesdropping, the system assumed that the self-interference (SI) caused by FD was completely eliminated. This ideal assumption is very hard to achieve in practice whether it uses the technology of analog or digital elimination of self-interference, there will have residues [2]. Taking self-interference into consideration, [3] adopts multiple antennas to mitigate the effects of self-interference and discusses the joint design of interference power and transmit/receive beamforming vectors when the eavesdropping non-outage probability is optimal under four different modes. At the same time, the concept of spoofing relay was proposed in [4, 5], and the spoofing rate of proactive eavesdroppers and the power optimization design of jammers with multiple spoofing relays were respectively studied.

Furthermore, in [6, 7], they proposed three different half-duplex (HD) proactive eavesdropping modes and carried out research on their non-outage probability and proactive eavesdropping rate, respectively. Based on one of these three modes, [8] considers a model of suspicious communication with amplify-and-forward (AF) relay network and uses the method in [1] to optimize its jamming power. In this paper, we propose the optimization of another half-duplex proactive eavesdropping mode when the suspicious relay adopts DF protocol. We obtain the expression of its optimal jamming power and the comparison of performance simulation.

2 System Model

As shown in Fig. 1, we consider a proactive eavesdropping scenario, where the proactive eavesdropper E attempts to send signal of jamming to the suspicious DF relay R in the first time slot and eavesdrop in the next time slot. Besides of the suspicious relay, the suspicious communication system consists of a suspicious transmitter S and a suspicious receiver D. All of the users are equipped with a single antenna, and we assume that the direct link from suspicious transmitter to suspicious receiver is sufficiently weak to be ignored due to the long-distance path loss or obstacles.

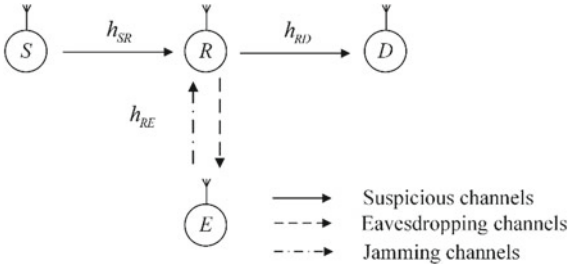

Fig. 1 System model

In the first time slot, E tries to send interference to R which is receiving signals from S at the same time. And it eavesdrops signals sent by R in the second time slot. The Rayleigh fading channel gain of links $S \to R$, $R \to D$, $R \to E$ were denoted by $|h_{SR}|^2$, $|h_{RD}|^2$, $|h_{ER}|^2$ which are modeled as independent exponential distributed random variables whose means were denoted by λ_{SR}, λ_{RD}, λ_{ER}. We consider that S transmits with a constant power P_S and the R transmits with P_R, while E employs a jamming power Q_J to interfere with R to facilitate the simultaneous eavesdropping. Thus, the achievable data rates of suspicious links and eavesdropping links are

$$r_0 = \frac{1}{2}\log(1 + \min(\gamma_R, \gamma_D)) \tag{1}$$

$$r_1 = \frac{1}{2}\log(1 + \gamma_E) \tag{2}$$

respectively, where

$$\gamma_R = \frac{P_S|h_{SR}|^2}{Q|h_{ER}|^2 + \sigma^2} \tag{3}$$

$$\gamma_D = \frac{P_R|h_{RD}|^2}{\sigma^2} \tag{4}$$

$$\gamma_E = \frac{P_R|h_{RE}|^2}{\sigma^2} \tag{5}$$

And σ^2 denotes the noise power. Then, the outage probability of D and E could be expressed as:

$$p_0^{\text{out}} = \Pr\{r_0 < R_S\} \tag{6}$$

$$p_1^{\text{out}} = (\Pr r_1 < R_S) \tag{7}$$

where R_S denote the fixed rate of suspicious transmission. In this paper, we define the average eavesdropping rate as expressed in [1]:

$$R_{\text{ave}} = R_S\left(1 - p_1^{\text{out}}\right) \tag{8}$$

As assumed in other papers, we consider that suspicious users cannot recognize the existence of eavesdropper. In that way, the suspicious transmitter will adjust its transmission rate R_S to remain p_0^{out} fixed, i.e., $p_0^{\text{out}} = \delta$. Thus, our next step is to find an optimal jamming power to maximize the average eavesdropping rate, R_{ave}. And the problem is formulated as follows:

$$(P1): \max_{Q_J, R_S} R_{\text{ave}} = R_S\left(1 - p_1^{\text{out}}\right) \tag{9}$$

$$\text{s.t. } p_0^{\text{out}} = \delta, \tag{10}$$

$$0 \le Q_J \le Q_J^{\max} \tag{11}$$

where $Q_J^{\max}$ denotes the max jamming power of proactive eavesdropper.

3 Optimal Jamming Design

In this section, we study the optimal jamming design of the optimization problem ($P1$). At first, we derive the relationship of R_S and Q_J by (10).

According to [9], the cumulative distribution function (CDF) of γ_R is defined as:

$$F_{\gamma_R}(x) = 1 - \frac{\mathrm{e}^{-\frac{\sigma^2 x}{P_S \lambda_{SR}}}}{1 + \frac{Q_J \lambda_{ER}}{P_S \lambda_{SR}} x} \tag{12}$$

And we can easily obtain the expression of p_0^{out}, then combining with (10), we have the one-to-one relationship between R_S and Q_J as follows:

$$Q = \psi(R_S) = \frac{\lambda_{RD} P_R}{\left(2^{2R_S} - 1\right)\lambda_{ED}} + \frac{\lambda_{RD} P_R \exp\left(-\left(2^{2R_S} - 1\right)\left(\frac{\sigma^2}{\lambda_{RD} P_R} + \frac{\sigma^2}{\lambda_{SR} P_S}\right)\right)}{\left(2^{2R_S} - 1\right)(1 - \delta)\lambda_{ED}} \tag{13}$$

Obviously, $\psi(\cdot)$ is a monotonically decreasing function of R_S. Substituting (13) into (11), we have

$$\psi^{-1}\left(Q_J^{\max}\right) < R_S < \psi^{-1}(0) \tag{14}$$

where $\psi^{-1}(\cdot)$ denote the inverse function of $\psi(\cdot)$. After mathematical manipulation, $\psi^{-1}(Q_J)$ can be expressed as:

$$\begin{aligned} \psi^{-1}(Q_J) = & \frac{-\sigma^2 \lambda_{RD}^2 P_R^2 - \sigma^2 \lambda_{RD} \lambda_{SR} P_S P_R + \lambda_{ED} \lambda_{RD} \lambda_{SR} P_S P_R Q_J}{\sigma^2 \lambda_{ED} \lambda_{RD} P_R Q_J + \sigma^2 \lambda_{ED} \lambda_{SR} P_S Q_J} \\ & \times W\left(-\frac{\sigma^2 (\lambda_{RD} P_R + \lambda_{SR} P_S) \exp\left(\frac{\sigma^2 (\lambda_{RD} P_R + \lambda_{SR} P_S)}{\lambda_{ED} \lambda_{SR} P_S Q_J}\right)}{\left(2^{2R_S} - 2\right)\lambda_{ED} \lambda_{SR} P_S Q_J}\right) \end{aligned} \tag{15}$$

where $W(\cdot)$ denotes the Lambert W function [10]. Since combing with (2), (3), and (7), we will get $p_1^{\text{out}} = 1 - \exp\left(-\sigma^2\left(2^{2R_S} - 1\right)/P_R \lambda_{RE}\right)$, so the problem ($P1$) will be equivalently rewritten as:

$$(P2): \max_{Q_J, R_S} R_{\text{ave}} = R_S \exp\left(\frac{-\sigma^2\left(2^{2R_S}-1\right)}{P_R \lambda_{RE}}\right) \tag{16}$$

$$\text{s.t. } (14) \tag{17}$$

According to [1], we have the maximum average eavesdropping rate while R_s^* is denoted as follows:

$$R_s^* = \frac{W\left(P_R \lambda_{RE}/\sigma^2\right)}{2\ln(2)} \tag{18}$$

Furthermore, the optimal suspicious communication rate the optimal jamming power to (P1) is

$$R_s^{\text{opt}} = \max\left(\min\left(\psi^{-1}(0), R_s^*\right), \psi^{-1}(Q_J^{\max})\right) \tag{19}$$

$$Q_J^{\text{opt}} = \psi\left(R_{\text{opt}}\right) = \min\left(\max\left(0, \psi^{-1}(R_S^*)\right), Q_J^{\max}\right) \tag{20}$$

4 Numerical Results

In this section, we present numerical results to validate the performance of the optimal proposed proactive strategy and the comparison with other strategies. In the simulation, we set that $\lambda_{SR} = \lambda_{RD} = 1$, $\lambda_{ER} = 1/40$, if not specified. This is because the channel between R and E is a secondary channel as for suspicious channels. Furthermore, we assume $P_S/\sigma^2 = P_R/\sigma^2 = 20$ dB, $Q_J^{\max}/\sigma^2 = 30$ dB and the target suspicious outage probability $\delta = 0.05$.

Figure 2 depicts the average eavesdropping rate R_{ave} versus the jamming SNR Q_J/σ^2. We observe that as Q_J/σ^2 increases, the average eavesdropping rate increases first and then decreases which shows an optimal jamming power to maximize average eavesdropping rate at about 14 dB. We plot the average eavesdropping rate R_{ave} versus the average channel power gains of $R \to E$ link in Fig. 3 by assuming constant jamming power is $Q_J^{\max}$, and the result shows that the optimal jamming scheme has a better average eavesdropping rate compared to the scheme of passive eavesdropping or eavesdropping with a constant jamming power.

5 Conclusion

This paper considered the issue of proactive eavesdropping in a dual-hop DF relaying system. For this system, we propose an optimal jamming scheme to maximize the average eavesdropping rate and derive the expression of the optimal suspicious

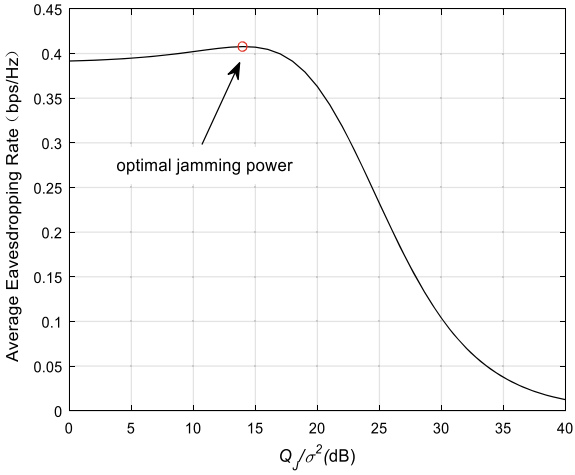

Fig. 2 Average eavesdropping rate versus the jamming SNR

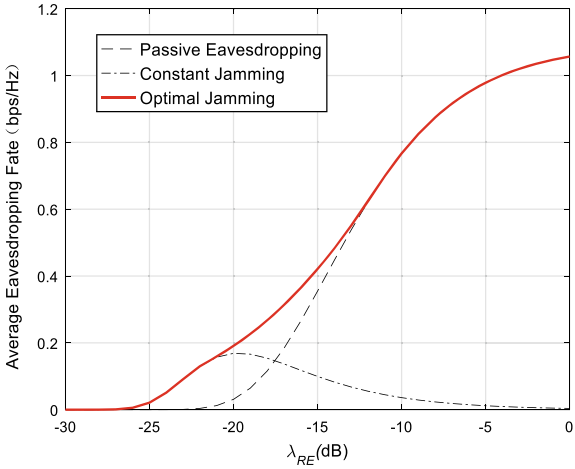

Fig. 3 Average eavesdropping rate versus the average channel power gains of $R \rightarrow E$ link

communication rate the optimal jamming power in this case. The mathematical and simulation results indicate that the performance of optimal jamming scheme outperforms the traditional passive eavesdropping and proactive eavesdropping with a constant jamming power.

Acknowledgement This paper was funded in part by the Natural Science Foundation of Fujian Province (2018J01096) and the Subsidized Project for Cultivating Postgraduates' Innovative Ability in Scientific Research of Huaqiao University (18014082023).

References

1. Xu, J., Duan, L., Zhang, R.: Proactive eavesdropping via jamming for rate maximization over rayleigh fading channels. IEEE Wireless Commun. Lett. **5**(1), 80–83 (2016)
2. Ahmed, M., Tho, L.: Self-interference cancellation limits in full-duplex communication systems. In: 2016 IEEE Global Communications Conference (GLOBECOM), pp. 1–6. IEEE Press, Washington, USA (2016)
3. Zhong, C., Jiang, X., Qu, F., Zhang, Z.: Multi-antenna wireless legitimate surveillance systems: design and performance analysis. IEEE Trans. Wireless Commun. **16**(7), 4585–4599 (2017)
4. Xu, J., Duan, L., Zhang, R.: Fundamental rate limits of physical layer spoofing. IEEE Wireless Commun. Lett. **6**(2), 154–157 (2017)
5. Jihwan, M., Hoon, L., Changick, S.: Relay-assisted proactive eavesdropping with cooperative jamming and spoofing. IEEE Trans. Wireless Commun. **17**(10), 6958–6971 (2018)
6. Zhang, Y., Jiang, X., Zhong, C., Zhang, Z.: Performance of proactive eavesdropping in dual-hop relaying systems. In: 2017 IEEE Globecom Workshops (GC Wkshps), pp. 1–6. IEEE Press, Singapore (2017)
7. Ma, G., Xu, J., Duan, L., Zhang, R.: Wireless surveillance of two-hop communications. In: 2017 IEEE 18th International Workshop on Signal Processing Advances in Wireless Communications (SPAWC), pp. 1–5. IEEE Press, Sapporo, Japan (2017)
8. Hu, D., Zhang, Q., Yang, P., Qin, J.: Proactive monitoring via jamming in amplify-and-forward relay networks. IEEE Signal Process. Lett. **24**(11), 1714–1718 (2017)
9. Chen, Y., Huang, H., Lau, V.K.N.: Cooperative spectrum access for cognitive radio network employing rateless code. In: ICC Workshops-2008 IEEE International Conference on Communications Workshops (ICCW), pp. 326-331. IEEE Press, Beijing, China (2008)
10. Corless, R.M., Gonnet, G.H., Hare, D.E.G., Jeffrey, D.J., Knuth, D.E.: On the Lambert W function. Adv. Comput. Math. **5**(4), 329–359 (1996)

Determination of Membership Degree in Risk Assessment of Transportation Process

Chaozhou Chen, Guofang Wu, and Guoliang Dong

Abstract In the road passenger transportation information management system, the safety of the transportation process needs to be fuzzy evaluated before the departure of passenger vehicles. The data involved in the evaluation include data from many sources that are aggregated into the information management system through the Internet and wireless communication. In fuzzy evaluation, the determination of the membership function is important. A fuzzy evaluation method is adopted in the risk evaluation of road passenger transportation process. The shape of the membership function curve is observed by setting different values of the parameters in the membership function. According to the establishment principle of the membership function and the actual situation of the risk assessment of the transportation process, the parameters of the appropriate membership function are determined, and the membership function of each evaluation level of the transportation process is finally obtained.

1 Introduction

The road passenger transportation information management system includes transportation process safety management, vehicle management, driver management, passenger line management, and other management related to the transportation process. In order to improve the safety of the transportation process, the vehicle needs to be evaluated for safety during the transportation process before departure. Comprehensive analysis of many factors affecting vehicle safety using information technology can quickly complete the safety evaluation of the transportation process. The various factors involved in the safety evaluation are aggregated into the information management system through technical means such as the Internet and wireless communication, which greatly improves the real-time performance and the efficiency of the safety evaluation.

C. Chen · G. Wu · G. Dong (✉)
Research Institute of Highway Ministry of Transport, Beijing 100088, China
e-mail: gl.dong@rioh.cn

R. Kountchev et al. (eds.), *Advances in Wireless Communications and Applications*,
Smart Innovation, Systems and Technologies 191,
https://doi.org/10.1007/978-981-15-5879-5_15

Table 1 Transportation process risk assessment level

Risk classification, V	$v1$, very low	$v2$, low	$v3$, average	$v4$, high	$v5$, very high
Evaluation score, x	0–60	60–70	70–80	80–90	90–100

The safety of road passenger transport processes involves many factors such as driver, vehicle condition, road, environment, and business management. Evaluating the risk of vehicles, drivers, driving routes, and road environment before the vehicle departs, it is possible to detect accidents in the transportation process in advance and reduce the risk of transportation [1–4].

The fuzzy comprehensive evaluation method is a mature evaluation method and has applications in various fields [5–7]. A fuzzy evaluation method is applied in the risk assessment of road passenger transportation process. In the evaluation model construction process, the determination of the membership function is an important link. The different values of the parameters in the membership function affect the slope and coverage of the membership function curve. According to the establishment principle of the membership function, the changes of the curves when different parameters are observed, and the membership function of each evaluation level in the risk evaluation of the transportation process are determined.

2 Evaluation Level

Table 1 shows the risk assessment level of the transportation process. The risk assessment level of the transportation process is divided into five levels, and the risk level is very low, low, average, high, and very high. The risk assessment level corresponds to the evaluation score. The higher the evaluation score, the higher the risk.

3 Membership of Qualitative Indicators

For qualitative indicators during transportation, such as the driver's driving skills and physical fitness, the expert survey method is used to determine the degree of membership. The subjective scoring of the evaluation indicators is determined by experts to subjectively score the degree to which the evaluation indicators meet the rating. The expert survey method is a subjective evaluation method, and the evaluation results are related to the professional knowledge and subjective tendency of the experts [8, 9].

4 Membership of Quantitative Indicators

For the quantifiable indicators in the transportation process or the indicators that can be evaluated by the scoring method, the assignment function is used to determine the membership function. Quantitative indicators such as driving age, driver's age, vehicle mileage, and age can be obtained by the assignment method.

4.1 Principles for Establishing the Membership Function

The membership function should be consistent with people's understanding of the regularity of things and should abide by certain principles [10].

The fuzzy set represented by the membership function must be a convex fuzzy set. That is, the membership function is required to have a single peak. The membership function is usually symmetrical. Each element belongs to at least one area of membership function, but should not exceed two areas. The same element does not take the maximum value at the same time in the two membership functions. If the two membership functions overlap, the overlap and the maximum of the two membership functions should not intersect.

4.2 Commonly Used Membership Function

Commonly used membership functions mainly include rectangular distribution, trapezoidal distribution, gamma distribution, triangular distribution, normal distribution and Cauchy distribution. According to the shape of the membership function, it can be divided into Z-shaped function, S-shaped function and Π-shaped function, which are suitable for the case where the variable value is small, intermediate and large. In practical applications, the membership function of different distribution shapes should be selected according to the increasing or decreasing relationship of the function and the smoothness of the curve [11, 12].

4.3 Membership Function of Safety Evaluation of Transportation Process

The evaluation score of the quantitative indicator in the transportation process evaluation is set to x which is between 0 and 100 points. It is necessary to determine the membership function for each evaluation level separately.

4.3.1 Determine the Membership Function of the Evaluation Level v1

It can be seen from Table 1 that when the evaluation score is between 0 and 60, the risk evaluation level is “very low".

When x is larger, the membership degree to v_1 is smaller. The membership function of the Z-shaped distribution should be selected. In order to obtain a smoother function curve, the membership of v_1 is chosen to be a reduced half-Cauchy distribution.

$$u_{v_1}(x) = \begin{cases} 1 & x \leq c \\ \frac{1}{1+\alpha(x-c)^2} & x > c \end{cases} \tag{1}$$

When the score value $x \leq 60$, the membership value of v_1 is 1. From $u_{v_1}(60) = 1$, then $c = 60$. When $x = 100$, there should be $u_{v_1}(100) = 1$.

When $60 < x < 100$, the value of α determines the shape of the curve. According to the principle that x should fall on no more than two evaluation levels, there should be $u_{v_1}(70) = 0$. Considering that the range of the overall interval is narrow, the curve distribution should cover more intervals. Set α different values and observer the change of the shape of the curve.

When $u_{v_1}(90) = 0.01$, $\alpha = 0.110$ is calculated. When $u_{v_1}(80) = 0.01$, $\alpha = 0.248$ is calculated. When $u_{v_1}(70) = 0.01$, $\alpha = 0.990$ is calculated. Correct the remaining part to a straight line. The membership function curves of the three sets of different values are shown in Fig. 1.

Observe the three curves in the graph. When x is above 80, the value on the y-axis is approximately zero. When x is 70, the difference on the three curves is less than

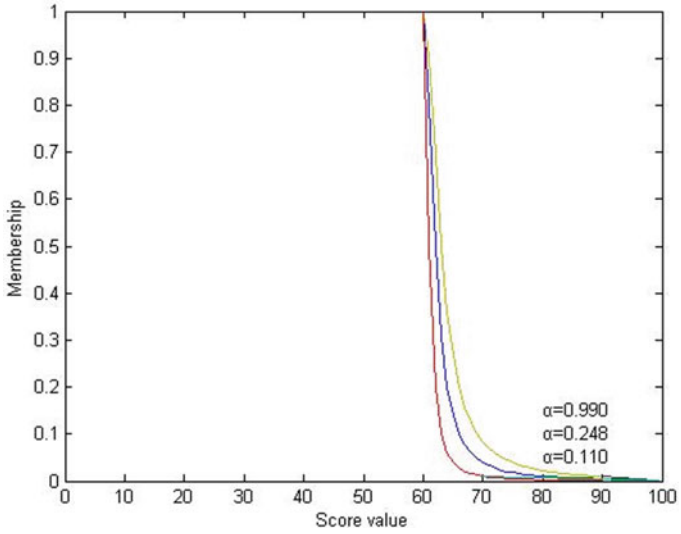

Fig. 1 $u_{v_1}(x)$'s membership for different rates

0.1. In order to smooth the value of the y-axis over the interval of 70 to 80, $u_{v_1}(90) = 0.01$ is selected, at which time $\alpha = 0.110$. Then, the determined membership function $u_{v_1}(x)$ of the evaluation level v_1 is:

$$u_{v_1}(x) = \begin{cases} 1 & 0 < x \leq 60 \\ \frac{1}{1+0.11(x-60)^2} & 60 < x \leq 90 \\ 1 - \frac{x}{100} & 90 < x \leq 100 \end{cases} \tag{2}$$

4.3.2 Determine the Membership Function of the Evaluation Level v2

When the evaluation score is between 60 and 70, the risk evaluation level is "low".

For the evaluation level v_2, the intermediate membership function (the Π-shaped function) should be selected. Choose a symmetric Cauchy distribution:

$$u_{v_2}(x) = \frac{1}{1 + \alpha(x - c)^2} \tag{3}$$

Taking the midpoint of the interval as the maximum point of membership, then $c = 65$.

When $u_{v_2}(60) = 0.9$, $\alpha = 0.004$ is calculated. When $u_{v_2}(80) = 0.01$, $\alpha = 0.01$ is calculated. When $u_{v_2}(50) = 0.1$, $\alpha = 0.04$ is calculated. When $u_{v_2}(55) = 0.1$, $\alpha = 0.09$ is calculated. The membership function curves of the four different values are shown in Fig. 2**.**

Observing the curve in the graph, when $\alpha = 0.004$ and $\alpha = 0.010$, the slope of the curve decreases slowly, and the response to the evaluation score is relatively slow. When $\alpha = 0.090$, the slope of the curve drops too fast and responds quickly to the evaluation score. When $\alpha = 0.040$ is selected, the determined membership function $u_{v_2}(x)$ of the evaluation level v_2 is:

$$u_{v_2}(x) = \frac{1}{1 + 0.04(x - 65)^2} \tag{4}$$

4.3.3 Determine the Membership Function of the Evaluation Level v3

When the evaluation score is between 70 and 80, the risk evaluation level is "average".

Select a symmetric Cauchy distribution. With the midpoint of the interval as the highest convexity of the membership, there is $c = 75$. The membership function $u_{v_3}(x)$ of the evaluation level v_3 is determined according to a similar method of the evaluation level v_2, and $\alpha = 0.040$ is taken. The determined membership function $u_{v_3}(x)$ of the evaluation level v_3 is

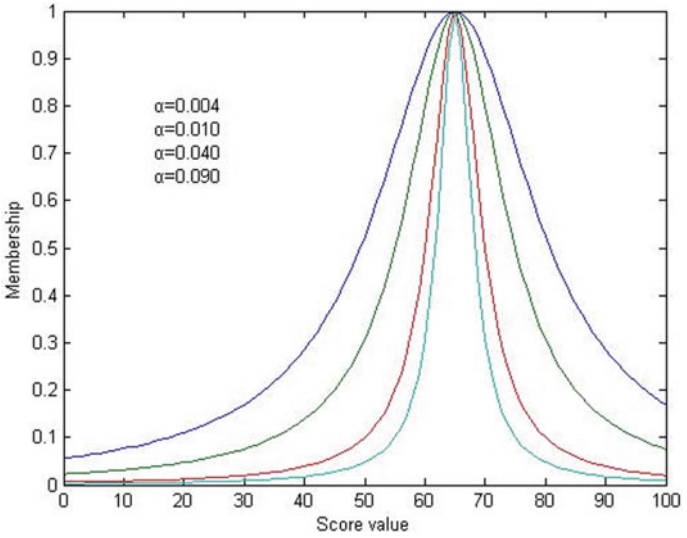

Fig. 2 $u_{v_2}(x)$'s membership for different rates

$$u_{v_3}(x) = \frac{1}{1 + 0.04(x - 75)^2} \tag{5}$$

4.3.4 Determine the Membership Function of the Evaluation Level v4

When the evaluation score is between 80 and 90, the risk evaluation level is "high".

Select a symmetric Cauchy distribution. With the midpoint of the interval as the highest convexity of the membership, there is $c = 85$. The membership function $u_{v_4}(x)$ of the evaluation level v_4 is determined according to a similar method of the evaluation level v_2, and $\alpha = 0.04$ is taken. The determined membership function $u_{v_4}(x)$ of the evaluation level v_4 is:

$$u_{v_4}(x) = \frac{1}{1 + 0.04(x - 85)^2} \tag{6}$$

4.3.5 Determine the Membership Function of the Evaluation Level v5

When the evaluation score is between 90 and 100, the risk evaluation level is "very high".

The larger x is, the greater the membership degree of v_5 is. The membership function of the S-shaped distribution should be selected. The membership of v_5 is

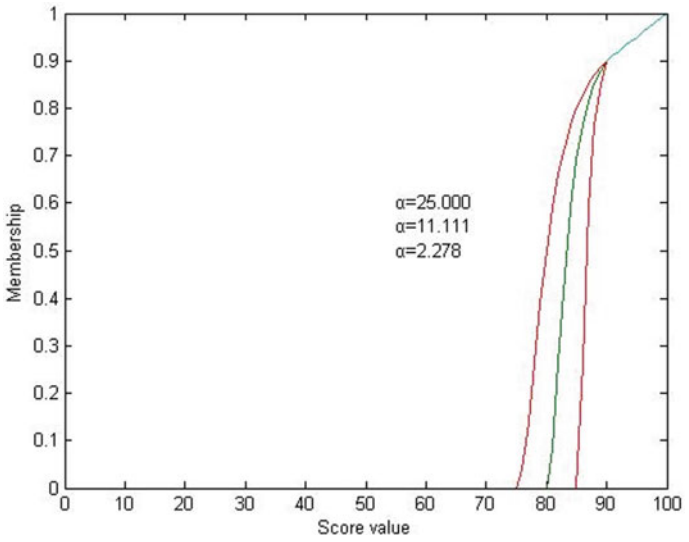

Fig. 3 $u_{v_5}(x)$'s membership for different rates

chosen to be a half-Cauchy distribution.

$$u_{v_5}(x) = \begin{cases} 0 & x \leq c \\ \frac{1}{1+\alpha(x-c)^{-2}} & x > c \end{cases} \tag{7}$$

Set $u_{v_5}(90) = 0.9$, select different values for c, and observe the change of the curve. When $c = 85$ is selected, $\alpha = 2.778$ is calculated. When $c = 80$ is selected, $\alpha = 11.111$ is calculated. When $c = 75$ is selected, $\alpha = 25$ is calculated. Correct the remaining part to a straight line. The membership function curves of the three different values are shown in Fig. 3.

In order to obtain a wider coverage interval, $c = 75$ is selected, at which time $\alpha = 25$. Then the determined membership function $u_{v_5}(x)$ of the evaluation level v_5 is:

$$u_{v_5}(x) = \begin{cases} 0 & 0 < x \leq 75 \\ \frac{1}{1+25(x-75)^{-2}} & 75 < x \leq 90 \\ \frac{x}{100} & 90 < x \leq 100 \end{cases} \tag{8}$$

5 Conclusion

In the fuzzy evaluation, the determination of the membership function is important. By discussing the influence of the degree of influence of different parameters in the process on the change of the membership curve, the membership function of each

evaluation level of the safety evaluation of the transportation process is determined. Reasonable membership function and detailed evaluation classification method can improve the accuracy and scientificity of the safety evaluation of transportation process.

Acknowledgement This paper is funded by the Special Fund Project for Science and Technology Innovation of Research Institute of Highway Ministry Transport (2018-E0030) and the Special Fund Project for Transfer of Science and Technology Achievements of Highway Science Research Institute of the Ministry of Transport (2018-F1001).

References

1. Shi, N.: Analysis of the frequency distribution of driver accidents and its influencing factors, Ph.D. thesis (2018)
2. Ding, Y.: Analysis of characteristics and influencing factors of heavy traffic accidents, Ph.D. thesis (2016)
3. Li, F.: Research on the cause mechanism and risk behavior of heavy traffic accidents, Ph.D. thesis, Chang'an University (2014)
4. You, D., Han, B., Juanjuan, Hu: Risk factors affecting traffic safety of long-distance passenger lines and tourist chartered drivers. Human Transp. Sci. Technol. **4**, 151–154 (2015)
5. Wu, J., Fan, W.: Research on risk assessment system for dangerous goods road transportation. J. Highw. Transp. Res. Dev. **32**(12), 6–11 (2015)
6. Guo, F., Meng, Y.: Research on coal quality grading evaluation based on fuzzy evaluation method. Math. Pract. Cognit. **7** (2019)
7. Zhu, W., Mei, S.: Application of fuzzy comprehensive evaluation method in hospital internal performance appraisal. Sci. Educ. Lit. (first issue) **454**(04), 115–118 (2019)
8. Gang, Wu, Li, C.: Application of analytic hierarchy process in safety risk assessment of CFST arch bridge construction. West. Transp. Sci. Technol. **132**(07), 123–127 (2018)
9. Wu, Y.: Technology foresight research in the energy field based on Delphi survey method. J. Wuhan Univ. Technol. (Inf. Manag. Eng. Edn) (2017)
10. Wang, J., Lu, Z.: Determination method of membership function in fuzzy control. Henan Sci. **18**(4), 348–351 (2000)
11. Wang, Y., Li, C., Huang, H., et al.: Selection of membership function of fuzzy controller based on adaptive Gaussian cloud transform. J. Northwestern Polyt. Univ. 171(03) **36**, 44–52 (2018)
12. Shi, X., Hao, T.: Fuzzy Control and Its MATLAB Simulation. Tsinghua University Press (2008)

Online Monitoring System for the Amusement Equipment Based on Wireless Sensor Network ZigBee

Jin-e Wang and Lechen Sun

Abstract Amusement parks are children's favorite places of entertainment. So, the safety of the equipment is very important. However, due to the backward management of many amusement parks, the fault of amusement equipment cannot be predicted in advance, and when a fault occurs, casualties occur sometimes. In order to solve this problem, the online monitoring system of the amusement equipment based on wireless sensor network ZigBee was proposed in this paper. It also discusses the overall architecture of the system, the composition of hardware, and the design method of software module. The overall architecture of the network is a tree structure, which is composed of host computer, coordinator, routers, and terminals. The host computer is responsible for managing and monitoring the running state of the equipment, analyzes and processes the information of the equipment states from the field, predicts the equipment fault, and can also give the alarm and the suggestions when the fault occurs. The experimental results show that the implementation of the system is feasible.

1 Introduction

With the improvement of people's living standards, the amateur life of them is becoming richer and richer. More and more people will go to amusement parks in their leisure time or holidays to enjoy the thrills and pleasures of all kinds of amusement equipment. At the same time, in order to attract more tourists, the amusement park has also introduced a variety of faster, higher, more exciting, and more realistic amusement facilities. The balance between supply and demand has contributed to the vigorous development of the entertainment industry.

J. Wang (✉)
School of Mechanical and Electric Engineering, Soochow University, Suzhou, China
e-mail: wangje213@126.com

L. Sun
Suzhou Paradise Development Co. Ltd., Suzhou, China

R. Kountchev et al. (eds.), *Advances in Wireless Communications and Applications*,
Smart Innovation, Systems and Technologies 191,
https://doi.org/10.1007/978-981-15-5879-5_16

However, while the amusement industry is developing rapidly, the safety of amusement equipment cannot be ignored. Because of the noisy surrounding environment and a large number of tourists, it is difficult for operators to accurately monitor the faults of the equipment with their eyes and ears when the equipment is running. Therefore, the online monitoring system for the running state of amusement equipment based on wireless sensor network ZigBee was proposed in this paper, which can monitor the running state of the equipment at any time. With the aid of this system, operators can know the running state of the equipment and carry out reasonable maintenance of the equipment.

2 Overall Architecture of the System

The system consists of coordinator, routers, terminals, and the computer as the host. The coordinator, the router, and the terminal are three types of network node devices. There must be a unique coordinator in ZigBee network, which is responsible for the startup, the configuration of the network and the allocation of the network address, i.e., PAN ID [1]. After the network was created, the function of the coordinator is equal to a router. Routers are responsible for network maintenance, routing management, and forwarding information, and they are also used to connect other devices to the network. The terminal node devices are responsible for the implementation of some specific functions and wireless data sending and receiving.

The ZigBee network composed of three kinds of the network nodes adopt a tree topology structure, as shown in Fig. 1.

In this structure, the depth of the network can be extended by the routers connected to the network in turn [2]. After the node devices are connected to the network by full function device, FFD for short, the parent–child relationship between the two

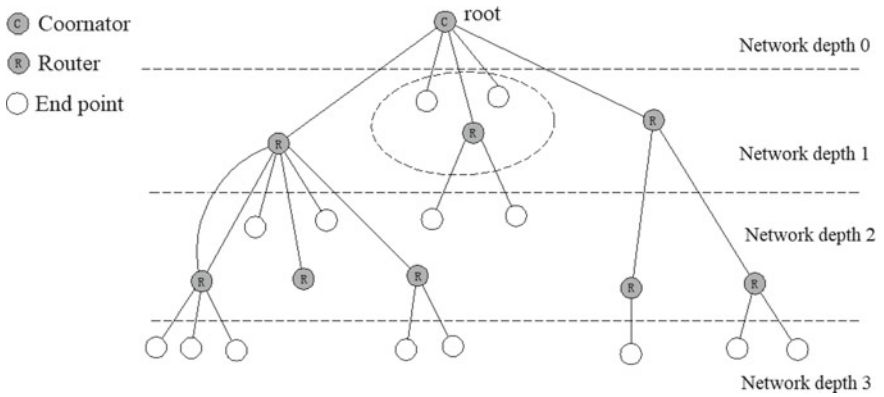

Fig. 1 Topological structure of the network

node devices is built. The child node device can only communicate with its parent node device. With the aid of the tree routing of the protocol stack, the communication between non parent–child node devices can also be implemented.

3 Hardware Design of ZigBee Network Nodes

All of the node devices of ZigBee network use CC2530 as the core processing unit. In order to carry out the data acquisition and the communication, ZigBee network can be built by combining CC2530, system-on-a-chip, with the peripheral auxiliary circuits and the sensor circuits based on modular design idea [3, 7].

The front-end RF module of CC2530 adopts monopole antenna. With Barron circuit, the differential signal RF-P and RF-N outputted by CC2530 which is an unbalance signal can be converted into a balance signal and then is transmitted to the antenna. In the power supply module, the voltage regulator converts a voltage of 5 V to a voltage of 3.3 V so as to provide a stable supply voltage for the system. ADXL345 produced by Analog Device Inc., ADI for short, is for the acceleration sensor. ADXL345 is a three-axis acceleration sensor with a maximum range of + 16 g and the highest resolution of 13 bits. The chip pins CS, SDA, SDO, and SCL of ADXL345 are connected to the pins P1_4– P1_7 of CC2530 for 4-wire SPI communication. PL2303HX is for the UART/USB converter to realize the communication between the coordinator and the host computer.

4 Programming of ZigBee Network Node Devices

4.1 Programming of the Coordinator

The coordinator can create the network and the network address (PAN ID) by scanning and detecting the channels in order to select the appropriate channel. All of the data acquired from the sensors are sent to the host computer by the coordinator. At the same time, the coordinator which is the main node of the network manages the other nodes of the network. The program flowchart of the coordinator was shown in Fig. 2.

The coordinator can automatically create the network after it was powered on, synchronize with the host computer and display the network states. And then, the coordinator will wait for the initiation of the host computer and the data acquisition instruction from the host computer.

After receiving the instruction, the coordinator commands the terminal nodes of the network to acquire the data. As soon as the coordinator receives the data required, it forwards the data to the host computer by the serial port with the aid of the DMA function of CC2530 [4]. The communication of the serial port is mainly

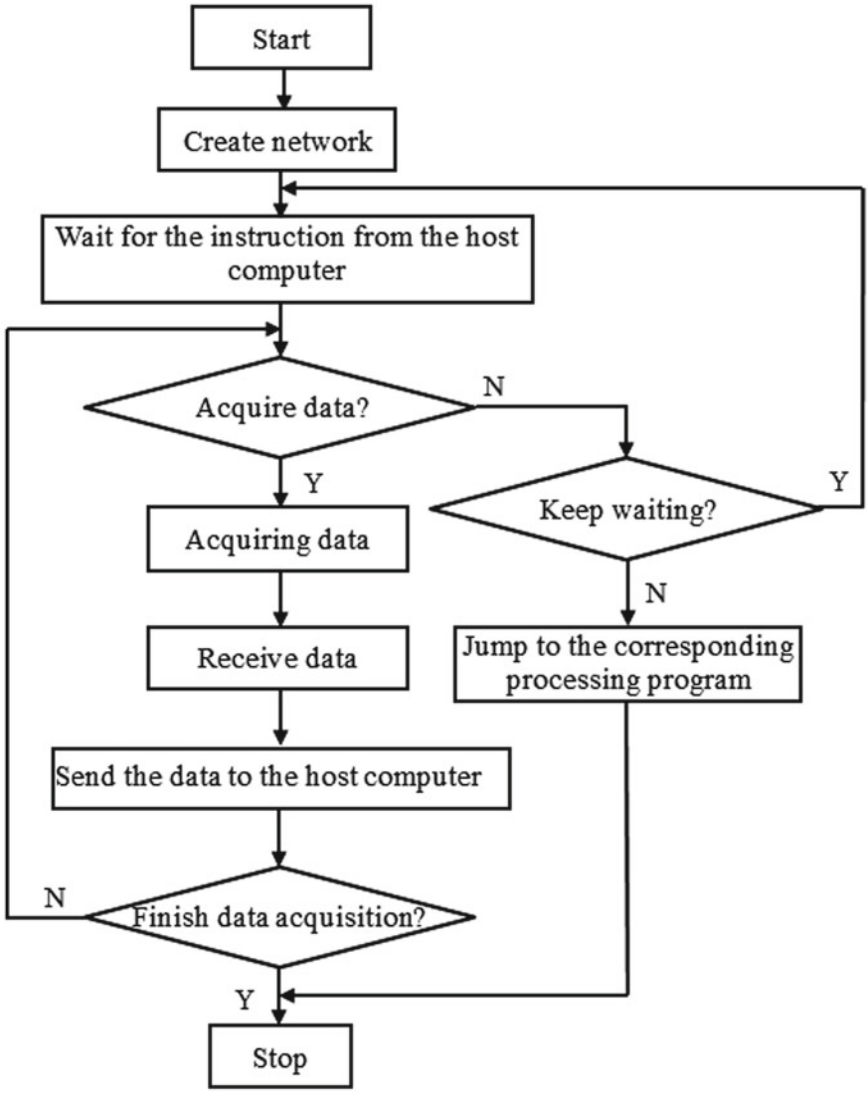

Fig. 2 Program flowchart of the coordinator

realized by three functions: serial port configuration function uint HalUARTOpen (uint8 port,halUARTCfg_t * config), serial port read function uint HalUARTRead (uint8 port,uint * buff,uint16 len), and serial port write function uint HalUARTOpen (uint8 port,uint * buff,uint16 len).

4.2 Programming of the Router

After the network is created, the router node applies to join the network, and the routing table is generated and maintained. While communicating, the router which acts as the relay of the remote node joins the remote node to the network and forwards the data for it. The program flowchart of the router is shown in Fig. 3.

After starting work, the router sends a beacon frame nearby so as to probe whether there is the coordinator or the router that has been previously connected the network according to the preset channel. If it exists, the router will apply to join the network. As soon as the router joins the network successfully, it sends the network address assigned to the coordinator, and which will be displayed on the host computer. At the same time, the router can also introduce the nearby nodes to join the network, which will become its child node, and forward the instructions from the coordinator to its child nodes so that they can acquire or forward data.

4.3 Programming of the Terminal Node Devices

After been powered on, the terminal node devices can search and join the network specified PAN ID [5]. The terminal node devices can be connected to the network not only by the coordinator directly but also by the relay router. After receiving the instruction of starting task from its parent node device, the terminal node device commands the sensor to acquire data and then transmits the data to its parent node devices, i.e., coordinator or router [6]. The program flowchart of the terminal node device is shown in Fig. 4.

5 Conclusion

The system has the characteristics of reliable link, energy saving, low cost, and extensibility [7]. The vibration sign temperature signals acquired from the node devices can be transmitted to the host computer and analyzed by building the ZigBee network and developing the application layer program, and the running state of the amusement equipment can also be monitored in real time.

Presently, the system is still in the research period in laboratories, since entertainment equipment need more safety and reliability requirements than others, and could not be put into practice without 100% guarantee. The research results show that the system successfully realizes the creation of the network, the data acquisition, the data sending, and the data display of the monitoring points of the amusement equipment. In theory, the number of devices that are joined the network is more than 60,000 [2]. At present, only four node devices which are used to measure the acceleration and the

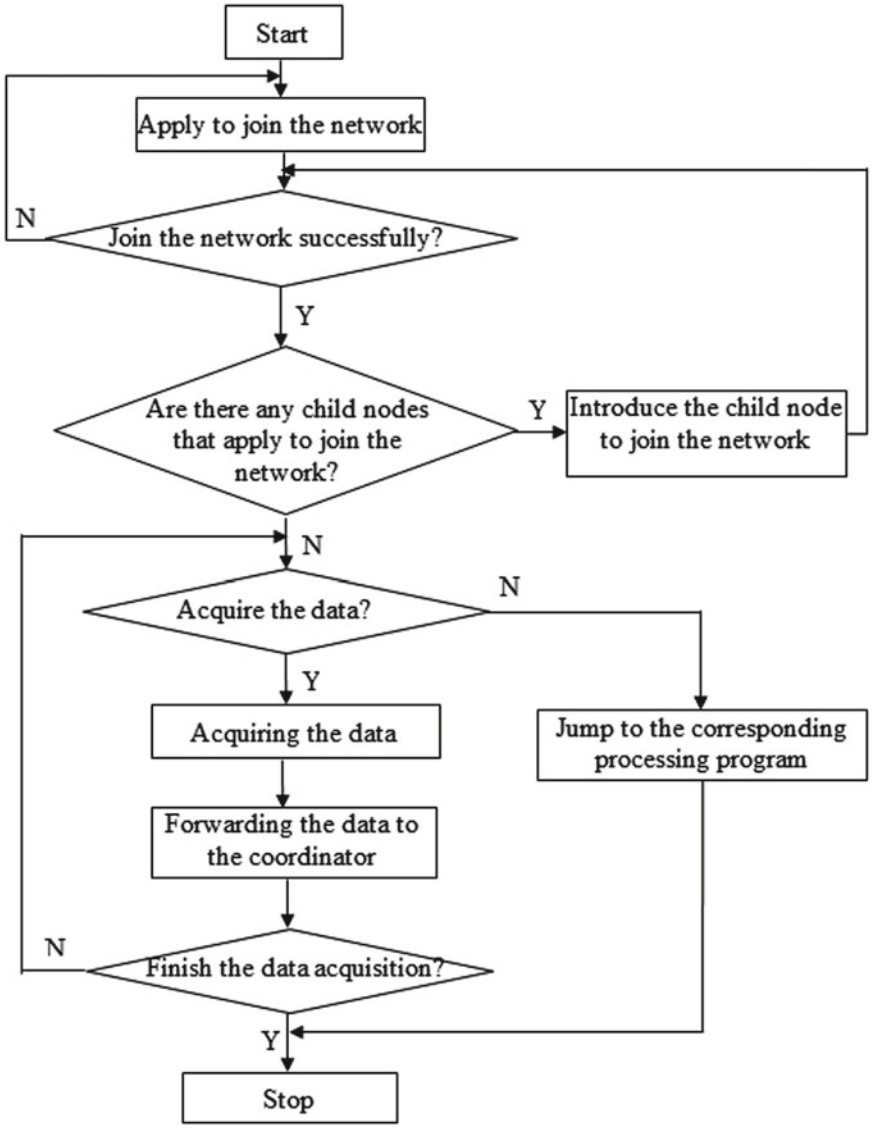

Fig. 3 Program flowchart of the router

temperature of the monitoring points are connected to the network. The permutation entropy algorithm is used to preprocess the signal [8]. With further development and improvement of the system, it is feasible to apply the system to practice.

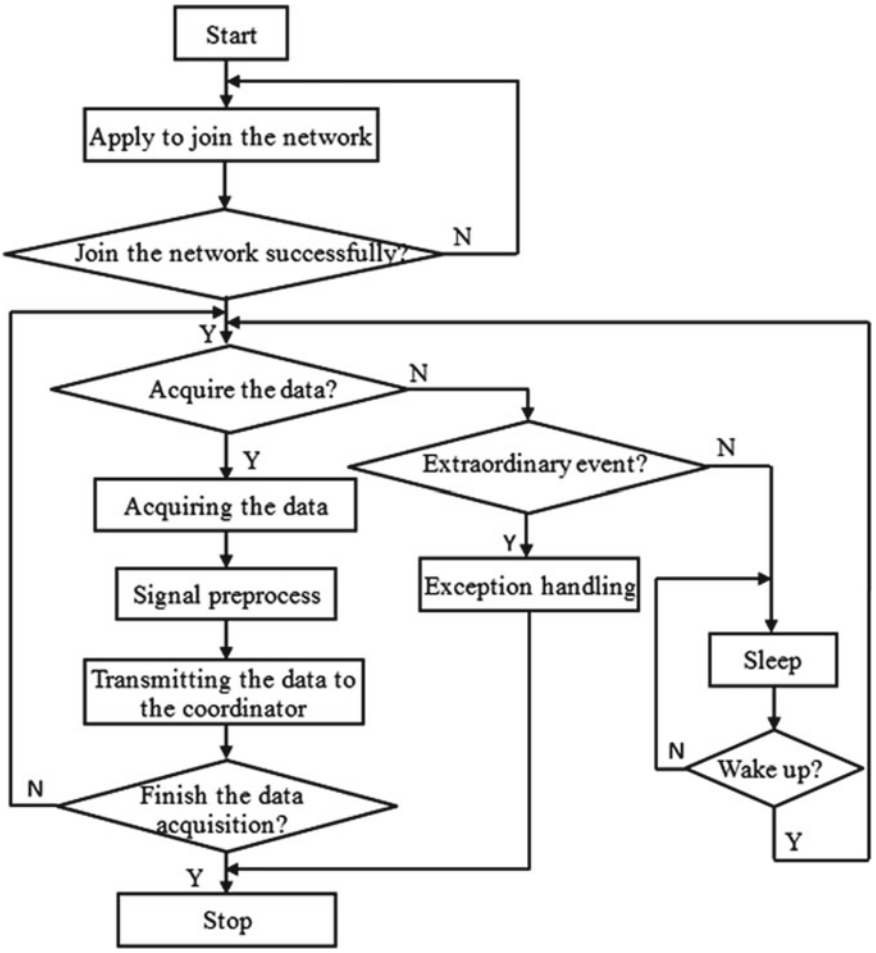

Fig. 4 Program flowchart of the terminal node device

References

1. Huo, P.J., Yang, F., Luo, H.B., Zhou, M.K., Zhang, Y.L.: Distributed monitoring system for precision management of household biogas appliances. Comput. Electron. Agric. **157**, 359–370 (2019)
2. Wadhwa L.K., Rashmi, S.D., Vishnu, P.: Extended shortcut tree routing for ZigBee based wireless sensor network. Ad hoc Netw. 295–300 (2016)
3. Salman, N., Kemp, A.H., Khan, A., Noakes, C.J.: Real time wireless sensor network (WSN) based Indoor air quality monitoring system. IFAC PapersOnLine 52–24, 324–327 (2019)
4. Wang, X.J.: Design of wireless medical monitoring system based on ZigBee. J. Changchun Univ. **29**(4), 14–18 (2019) (in Chinese)
5. Guo, N., Guo, K., Guo, X.R., Mao, X.D.: Design of temperature and humidity acquisition and monitoring system based on ZigBee. Measur. Control Technol. **36**(7), 101–104 (2017) (in Chinese)

6. Xia, Y.L., Zhou, Z.M., Wang, J., Du, L.L., Li, M.X., Xu, L.: ZigBee-based structural strain monitoring wireless sensing network design. Electron. Test **9**, 61–63 (2019) (in Chinese)
7. Zhao, Y.N., Bian, S.F., Wu, Z.M., Ji, B.: Design and realization of BDS position monitoring system based on ZigBee technology. Hydrogr. Surv. Chart. **36**(6), 62–64 (2016) (in Chinese)
8. Liu, R.Q., Zhou, Q.C., Xie, C.: Research on coal mine hoister hoist monitoring system based on embedded ZigBee. Coal Technol. **37**(2), 233–235 (2018) (in Chinese)

Design of Intelligent Seasoning Quantitative Device Based on Internet of Things Technology

Yi Liu, Danhong Chen, Qibing Yan, and Qiuya Song

Abstract Internet of things technology is an important technology after Internet and computer. A large amount of information can be obtained by controlling a variety of devices, and the trend of change in a certain period of time is predicted and adjusted accordingly after integration analysis. This technology is widely used in many fields. At present, how to achieve fast and high standard seasoning is a problem that cannot be ignored in the home cooking and catering industry. The intelligent seasoning quantitative device is proposed in this paper. It starts from the problem of storage and quantification, and combines the advantages of the Internet of things to propose an intelligent seasoning quantitative device. The purpose is to precisely adjust the amount of condiment, save time and man power, and greatly improve efficiency. Intelligent seasoning quantitative device solves the problem that people often meet with imperfect taste of dishes and will have a broader market.

1 Introduction

Internet of things technology belongs to the third generation of information technology, which is an important technology emerging behind the Internet and computers. Internet of things technology is widely used in many industries. Its ability to collect and process information is widely used, and its business types

Y. Liu · D. Chen (✉) · Q. Yan
School of Economics and Management, Shenyang Aerospace University, Shenyang, China
e-mail: Danhong1000@126.com

Y. Liu
e-mail: 1401109715@qq.com

Q. Yan
e-mail: 839515312@qq.com

Q. Song
School of Economics, Tianjin University of Commerce, Tianjin, China
e-mail: songqiuya@163.com

R. Kountchev et al. (eds.), *Advances in Wireless Communications and Applications*,
Smart Innovation, Systems and Technologies 191,
https://doi.org/10.1007/978-981-15-5879-5_17

are expanding continuously, facilitating the gradual integration of various fields. At present, whether in the home cooking or catering industry, there are often problems such as the salty taste of the dish and the imperfection of the "color and fragrance," which leads to various disputes [1]. Therefore, the Internet of things is applied to the catering industry to solve the above important problems. The involvement of Internet of things technology can mobilize all items and collect and analyze all information, which has become an opportunity for the development of small kitchen appliances.

The intelligent seasoning quantitative device is a device that automatically separates salt, chicken essence, sugar, and other seasonings by using the Internet of things technology, automatically or according to people's instructions. The intelligent seasoning quantitative device proposes a new hybrid field concept, which combines the Internet of things with catering to achieve cross-domain integration and solves the above problems. The intelligent seasoning quantitative device can save man power, improve safety, realize intelligent operation and data visualization, and it is therefore an advanced, fashionable, and high-tech kitchen equipment.

2 Working System

Intelligent seasoning quantitative devices can be divided into information systems, operating systems, and security systems. The working system is shown in Fig. 1.

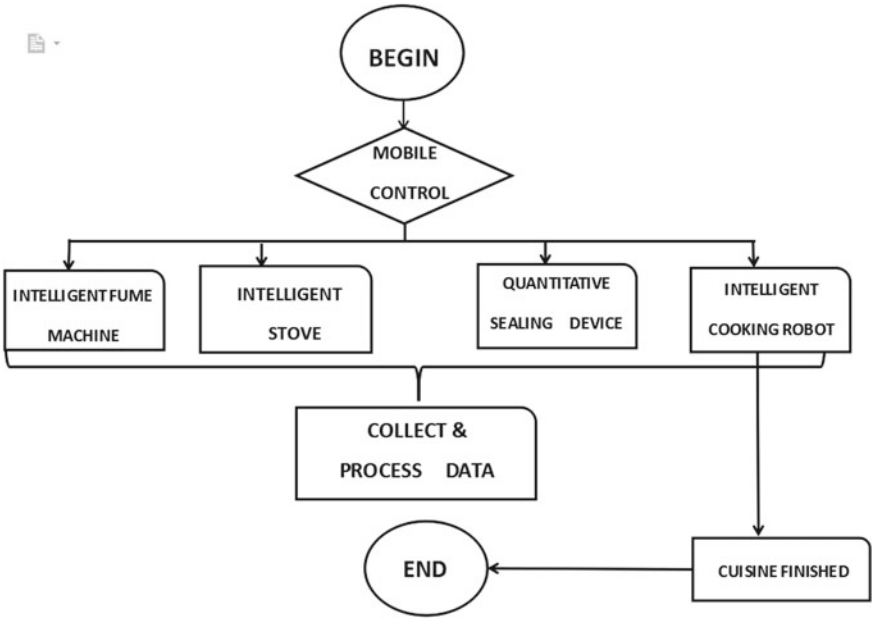

Fig. 1 Working system diagram of intelligent seasoning quantitative device

2.1 Information System

The intelligent seasoning quantitative device has its own information system. Firstly, it can make use of sensing technology and wireless communication technology to record the demand of different condiments for different dishes. Secondly, the information can be transmitted to the terminal through the Internet of things, and the intelligent terminal can conduct analysis, query, and mining, so as to finally analyze different requirements of different groups on condiments, give targeted analysis reports, and make corresponding decisions on the next output of condiments. The analysis report is given and the next decision can be given when the next seasoning is controlled. Common methods for predicting behavior of users in smart kitchen classes include association rule data mining, decision tree classification, artificial neural networks, and the like. The intelligent sealing device can use the association rule data mining method to use people to use different condiments as data sets, visually analyze the flavor varieties and dosages, and reasonably predict people's needs and characteristics. The intelligent seasoning quantitative device judges the needs of people at different times and different dates according to the simulation curve obtained by visual analysis. The next time you use it, you can directly call up the solution that is most likely to solve the problem in the database and feed it back to the mobile terminal. People will consider whether to adopt it. If not, fill in the corresponding reason and re-record it in the database. Then, organize the records and judge again if it is feasible. The mobile terminal can monitor the reflection of the relevant readings under any module in real time, and the four information ports finally collect the information into the processor in the information system [2].

2.2 Operating System

The intelligent seasoning quantitative device has its own operating system to achieve global control and change the original process. The intelligent seasoning quantitative device can also perform manual participation and refers to the database data to find similar processes. If the system determines that it is not feasible after manual participation, all operating systems are stopped, and the reason for not running is transmitted to the terminal together with the change suggestion, and the person judges. The intelligent seasoning quantitative device automatically performs the cleaning work after the operating system is finished and the dishes are output. At this point, the entire smart cooking is over. In addition, on the console side, you can also set login options to ensure that preferences are not adjusted. The intelligent seasoning quantitative device realizes safe operation through remote operation system [3].

2.3 Security System

The intelligent seasoning quantitative device has its own safety system. If there is a problem with the operating system, the terminal will automatically cut off the circuit if there is no terminal execution. Also, if there is a human intervention during normal operation, the entire operating system automatically disconnects from the server to ensure data security and personnel security. Before and after each use, automatically check whether the circuit, server, and other parts have security risks [4]. If there is a security risk, the smart prompt will indicate the location and cause of the error, thus ensuring the security of the entire system.

3 The Design of Device Structure

The design of intelligent seasoning quantitative device is shown in Fig. 2.

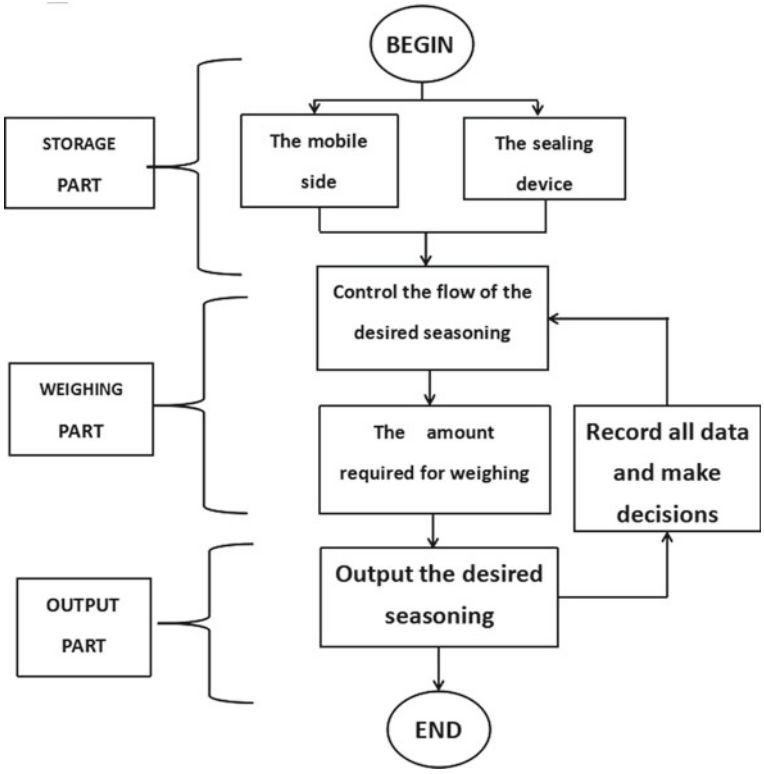

Fig. 2 Structure frame of intelligent seasoning quantitative device

3.1 Theoretical Design

At present, there is no relevant restriction on seasoning or relevant quantitative device in either the family or the restaurant. Therefore, the design theory of intelligent seasoning quantitative device is as follows: First, both the shell of the sealing device and the weighing device should use biodegradable and pollution-free food-grade material. Second, different seasonings put together will reduce the color and flavor of food, so according to demand should be placed separately; third, the precise use of condiments is a major reason for the deliciousness of the dishes. Intelligent seasoning quantitative device can control the quantity of seasoning by using piezoresistor and assembling reverse control circuit. Fourthly, the intelligent seasoning quantitative device uses mobile terminal control device to realize remote control and save time. Fifthly, data can be collected after each use of the intelligent seasoning quantitative device, and preferences can be analyzed to provide suggestions for the next use of intelligent device.

3.2 Structural Design

Traditional seasoning, although simple to operate, is relatively short in use, but the results are unsatisfactory. The structure of the intelligent seasoning quantitative device is clearly divided, and the three modules of storage, quantification, and output complement each other.

The storage part satisfies the storage needs of the condiment, ensuring that different condiments can be sealed well under different storage conditions, and there is no bad condition such as deterioration.

The quantitative part is controlled by the mobile end, or the front panel of the sealing device is controlled to control the amount of the seasoning. The control of the mobile end is automatically recorded, and the characteristics of the user are analyzed, intelligently summarized, and a reasonable prediction is made for the next use. In the early stage of making dishes, using mobile docking saves part of the time, preventing the bad conditions such as food scorching caused by the entanglement of spices [5].

The output section ensures that the output environment is clean and tidy, and the material is used to ensure fewer residues.

3.3 Volume Design

Whether it is a family or a restaurant, the amount of condiments required for each dish is almost constant and fluctuating. There are different requirements for liquid

seasonings and granular solid seasonings. No matter whether it is storage, quantification, or output, it cannot be too big, too big to meet the needs of the kitchen, and it is not practical. Therefore, for the three, the maximum volume of the liquid seasoning is 30 mL, and the maximum mass of the granular solid seasoning is 50 g.

3.4 Material Design

Considering the problem of placing the smart sealing device, it is necessary to use the material to have the heat preservation effect, the elastic deformation is small, and the heat is not easily decomposed. Therefore, intelligent seasoning quantitative device can choose thermoset plastic, aluminum hot alloy, and food-grade plastic assembly sealing device. In addition, the intelligent seasoning quantitative device can select the LCD to highlight the screen, that is, become the second operating environment except the mobile terminal.

3.5 Circuit Design

The circuit of the intelligent quantitative sealing device uses the American silicon piezoresistive pressure sensor code—27AND37 and code—MS4425 to ensure the accuracy of the seasoning. At the same time, the commonly used wires are replaced by batteries, and the number of circuits is reduced in the case of sufficient power supply, ensuring that the circuits are not wound in parallel after a long period of use, and the entire system is paralyzed.

4 Conclusion

The intelligent seasoning quantitative device can reasonably and effectively solve the problems of traditional cooking dishes, such as random control of the seasoning, unpleasant taste of the dishes, and long time consumption of the seasonings during cooking. Based on the intelligent seasoning quantitative device under the Internet of things, the mobile device can be used to control the sealing device at the moment, and the Wi-Fi connection can be used to save a large amount of time, while storing the usage record, intelligently analyzing the demand for the seasoning, and giving reasonable suggestions. The hermetic seal is designed to store condiments, eliminating the need for traditional unsanitary storage containers, as well as ensuring that the properties of the condiments do not change and that the taste is delicious. The intelligent seasoning quantitative device is healthy, environmentally friendly, and hygienic, and there is no contamination caused by the chemical reaction of the

container due to the change of temperature and humidity. Intelligent seasoning quantitative device solves the problem that the cooking or catering industry in the home often encounters the taste of the dish is not perfect, and will have a broader market.

Acknowledgement This research was supported by the college students' innovative entrepreneurial training plan of Shenyang Aerospace University under grant 201910143159. Professor Chen Danhong is the corresponding author and instructor of this paper.

References

1. Zheng, L.: Discussion on the status quo and application prospects of internet of things technology. Comput. Prod. Circ. **9**, 163 (2019)
2. Wei, Z.: Current status and application prospects of internet of things technology. Comput. Knowl. Technol. **12**, 49–50 (2016)
3. Condiment Association. China's compound seasoning industry overview and future development trends. https://www.China-condiment.com/interview/63543.2018/11/21
4. Chunyu, Z., We, C.: Research on the business model of condiment enterprises under the new retail background. Chin. Condiment **6**, 168–171 (2018)
5. Zhang, Y., Li, L.: Analysis of the status quo and development trend of condiment industry. Food Saf. Guide **3**, 51 (2018)

Analysis on Construction and Application of the Special Emergency Communication Systems in the Industries

Haitao Wang, Lihua Song, Jun Liu, and Lijun Liu

Abstract At present, the conventional emergency communication systems are becoming more and more perfect and new emergency communication technologies based on wireless ad hoc networks are becoming more and more advanced. In order to promote the popularization of emergency communication systems in various industries, the construction methods and application scenarios of the special emergency communication systems are discussed and analyzed according to the communication service demands of different industries in particular emergency environments, mainly including electric power, water conservancy, and railway industries. In addition, functional structures and network architectures of above three special emergency communication systems are expatiated. Finally, some opinions are proposed and conclusions are given.

1 Introduction

Emergency communication plays a crucial role in disaster relief, materials transportation, and disposal various urgent events. Emergency communication systems must utilize various communication techniques to offer reliable and flexible communication services for different user groups at the occurrence of unexpected events [1]. In practice, emergency communication involves many industries and sectors, such as telecommunication, electricity, water, petrochemicals, railways, public security, fire fighting and finance [2]. Different departments and industries should build their emergency communication systems based on their own characteristics to meet the industry demands and could take specific emergency communication support countermeasures when facing the accidents of different natures. This paper takes electric power, water conservancy, and railway industries as typical examples and

H. Wang · J. Liu · L. Liu
Nannjing Audit University Jinshen College, Nanjing 210027, Jiangsu, China

L. Song (✉)
College of Command Control Engineering, PLAAEU, Nanjing 210007, Jiangsu, China
e-mail: 1936241606@qq.com

R. Kountchev et al. (eds.), *Advances in Wireless Communications and Applications*,
Smart Innovation, Systems and Technologies 191,
https://doi.org/10.1007/978-981-15-5879-5_18

discussed and analyzed the construction and applications of emergency communication systems under special emergency environment for different industries. In particular, the design objects or requirements are given and the design ideas and methods are explained in order to offer some useful references and helps.

2 Construction of Power Emergency Communication System

2.1 Construction Objectives

Power emergency communication system is the important foundation to ensure the stable operation and reliable development of power network, but currently there is no perfect solution available. As the accidents are mainly uncertain and emergent, the time and location cannot be predicted in advance; the existing communication network is unable to satisfy the needs for emergency handling. Therefore, it is imperative to build an efficient and practical power emergency communication system which can support on-site video back-haul and voice communication and realize the visualization of the on-site commanding and disaster rescue in order to ensure the mobilization of different sectors within the shortest time for the coordinated collaboration and take orderly, rapid, and efficient responses to the accidents [3].

2.2 Construction Plan

2.2.1 Overall Plan

Power emergency communications usually contain two aspects: one is the emergency recovery of electric power communication fault and the other is the scene emergency command of electric power accident when the accident occurs. The communication system of the command vehicle can achieve the trunk communication and dispatch on the site and contact with the backstage command center via one specific backhauling technology in order to build a complete emergency commanding system. In order to address the drawbacks of the traditional emergency communication systems, the local integrated data network can be resorted, such as McWiLL [4]. By using video transmission in power emergency commanding system, the broadband wireless communication technology provides trouble-shooting and fault-repairing to the affected power facility in case of emergency and offers convenient ways of emergency communication to power production system and marketing system.

Due to the specific characteristics of power industry, the transmission of video signal has posed higher requirements on communication links. At present, power industry has basically realized the optical fiber interconnection between all the

offices, stations, and substations to provide the high-speed and broadband backbone transmission channels. Therefore, the construction of power emergency communication system based on the integration of fiber optic communication and wireless communication is the optimum solution for power industry. Specifically, McWiLL broadband wireless communication technology and COFDM wireless video transmission technology could be considered for employment to provide power emergency command communication in case of unexpected grid faults, bolstering the emergency-handling capability of power grid. In short, the power emergency wireless communications system is composed of point-to-point back-haul communications networks and broadband wireless access networks [5].

2.2.2 System Functional Structure

Power emergency communication system is a multi-tiered distributed information system, which contains four layers: network infrastructure layer, basic service layer, function module layer, and application system layer, and its system functional structure is depicted in Fig. 1.

The lowest layer is the communication network infrastructure, including public communication networks, private networks, and ad hoc networks. Basic service layer provides data management, communication support, GIS service, and information acquisition services in which communication services is the core service. The functional module layer is responsible for resource management and scheduling, information retrieval, transmission and processing, and report and display functions. At the top are the three major subsystems: command center subsystem, on-site emergency command subsystem, and on-site emergency communication subsystem and they run on different hardware platforms.

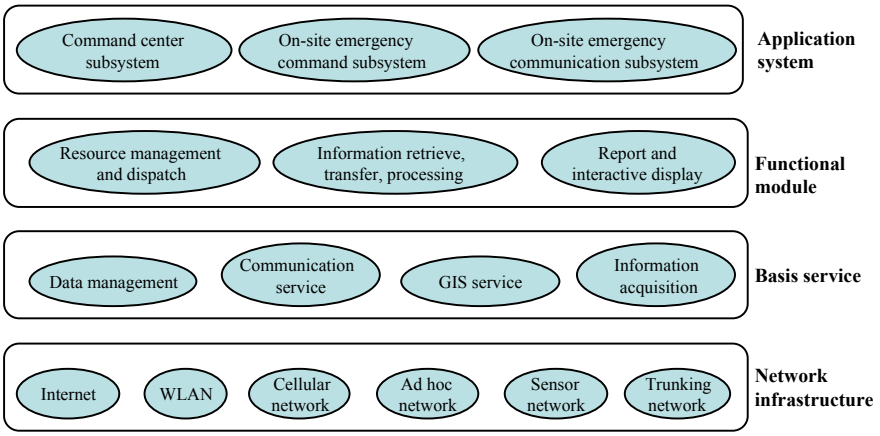

Fig.1 Functional structure of power emergency communication system

2.2.3 Point-To-Point Back-Haul Network

The emergency command vehicles are connected to the command center via back-haul networks, which guarantees the on-site communication terminals to access to servers and related database located in the command center. In the back-haul network, Coded Orthogonal Frequency Division Multiplexing (COFDM) technology is a priority solution, which is currently the most advanced and most potential modulation technology and it can make full use of the radio spectrum resource. The back-haul access point may choose the nearby substations with optical fiber. COFDM is able to realize the real-time transmission of high-speed wireless data under fast-moving conditions, and delivers the voice, data, and image one-way or two-way integrated transmission services under sever conditions.

2.2.4 On-site Broadband Wireless Access Network

In the emergency site, the high-speed and secure Multi-Carrier Wireless Information Local Loop (McWiLL) broadband wireless access technology based on SCDMA with wide coverage should be adopted to provide high access rate easily in multi-path interference environment. In particular, the on-site emergency command vehicle is equipped with McWiLL and the broadband wireless access network is built on the emergency site. So, the voice-, video-, and data-integrated access communications channels can be available on the site to quickly get the site information back to the emergency command center. Another applicable technique is to adopt World Interoperability for Microwave Access (WiMAX) to construct backbone network for power emergency communication. The main reasons for choosing WiMAX are: easy to deploy, support high mobility, large coverage, and high transmission capacity [6]. In Table 1, performances of several wireless technologies including McWill, WiMAX, WiFi, UMTS, and HSDPA are compared to show their technology characteristics.

Table 1 Performance comparisons of several wireless technologies

Wireless technology	Mobility (km/h)	Data rate (Mbps)	Coverage (km)	Spectrum type
McWiLL	120	20	13	Licensed/unlicensed
WiMAX	100	70	6.5	Licensed/unlicensed
WiFi	10	54	0.03	Unlicensed
UMTS	500	Uplink (0.4) Downlink (2)	30	Licensed
HSDPA	500	Uplink (0.4) Downlink (14)	30	Licensed

3 Construction of Water Emergency Communication System

3.1 Construction Objectives

Water emergency communication system plays a vital role in flood control, drought relief, and disaster alleviation [6]. Water emergency communication system is mainly used to deliver the dispatching calls in the disaster rescue scenes, the transmission of live images in the flood control and disaster rescue scenes, and the transport of live images recording the disaster situation and rescue progress. Through the water emergency communications systems, the commanding officers can perform efficient and accurate decision making, which could protect people's life and property safety to maximum extent and improve the integrated capability of disaster control and disaster alleviation.

3.2 Construction Strategies and Methods

The planning and construction of the water emergency communications must follow the fundamental rules of being proactive, safe, scientific, and realistic. In this regard, no matter from market, technological innovation or institutional competition aspects, the comprehensive investigations should be carried out, and from the central government to local, from technology to function, and from system to equipment, in order to meet the minimum requirements of the National Emergency Response Plan for the water emergency communication system. The construction of water emergency communications has to correctly deal with the relationship between public and private networks and construction of the flood-control communication network has to follow the basic principles of integrating the wireline networks and wireless networks closely. During the construction of the flood-control communication networks, meeting the needs of flood control is the first priority, while it also provides communication services to the water office automation and other departments. In addition, according to the needs for flood control and considering geographical conditions, dedicated radio channels according to local situation should be built and the communication options include VHF, microwave, and satellite [7].

Water emergency communications network use IP protocol to link various heterogeneous networks, including wired LAN in rear command post, various wireless networks within emergency scene, and wide area network (WAN) between rear command post and emergency scene, as shown in Fig. 2. Water emergency communications are facing complex situations with many uncertainties, which require to use a variety of advanced communication and information processing technologies, including satellite communication, wireless broadband access communication, and

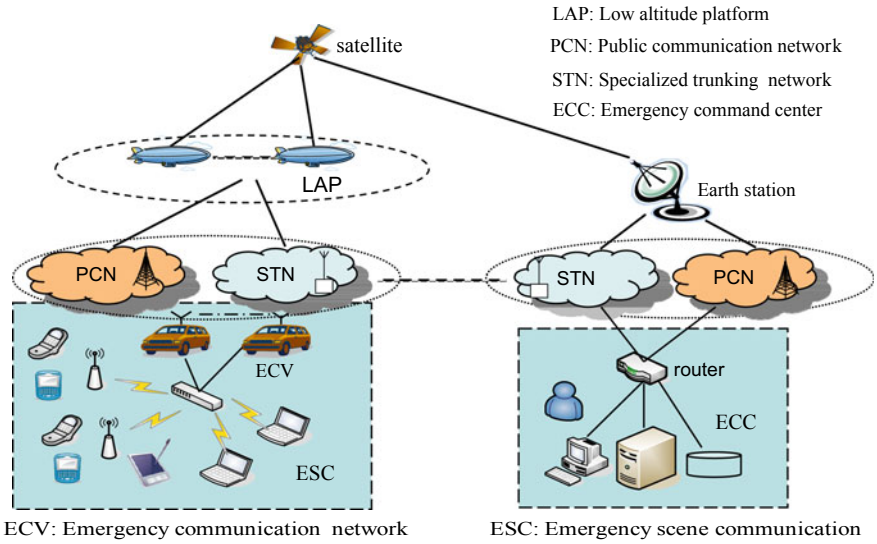

Fig. 2 Network structure of water emergency communication system

digital trunking communication technologies, in order to guarantee the smooth operation of the on-site commanding, to improve the scientific and effective decision making on flood control and achieve the goals of flood control and disaster relief.

4 Construction of Railway Emergency Communication System

4.1 Construction Requirements

When the railway accidents or severe natural disasters occur, the railway emergency communication system should be able to quickly send on-site information to the command center in time, allowing supervisors to comprehend the situation immediately [2]. In recent years, with the leap-forward development of the railway construction, the needs for emergent response and rapid handling to the accident were put forward. The railway emergency communication system must deliver the image, voice, and data recorded in the field to the emergency command center in time. In addition, the railway emergency communication has posed many requirements for the on-site access equipments including modular design, sturdy packaging, easy to carry and maintain, convenient installation, and debugging for various working environments.

4.2 Design Plans and Schemes

The railway emergency communication system is mainly composed of three parts: emergency rescue command center, transmission network, and on-site emergency access. The emergency command center includes center control console, display, and recording equipments. The transmission network may make advantage of the existing railway communication network resources. By virtue of its technical and cost advantages, IP networks should become the main framework of the railway emergency communication transmission network, conveying the real-time business in the fields, such as voice, video, and data [8].

Emergency rescue and command center equipment is the core of the entire emergency communications system, integrating TDM switching and IP switching altogether and possessing powerful access capability and operational capacity. The central access equipment mainly fulfills the service access, processing and switching between the center and stations, as well as the management and scheduling of the rescue command centers. The on-site emergency access firstly conveys the field information to the nearby stations optical access points, and transmits information to the emergency sub-centers by the existing transmission networks. The emergency center performs decoding, display, recording, and control of the uploaded images and voices from the field, and achieves the real-time surveillance and commanding in the field. The on-site mobile individual equipments are primarily composed of cameras, video encoders, wireless transmitter, and other components. It is noted that as the railway emergency communication has not applied for specific wireless channel so far, the wireless transmitter has to be able to sweep entire 300–900 MHz band and confirms the usages of wireless channel in the field, in order to avoid the frequency overlapping with the existing railway wireless communication systems [9].

To achieve the real-time transmission of information to the emergency command center function, wired and wireless access can be used to provide voice, video, and data services. As shown in Fig. 3, the landline railway emergency communication access mainly uses the twisted-pair lines reserved in the communication poles between railway spans and converts the analog signals into IP data packet by digital

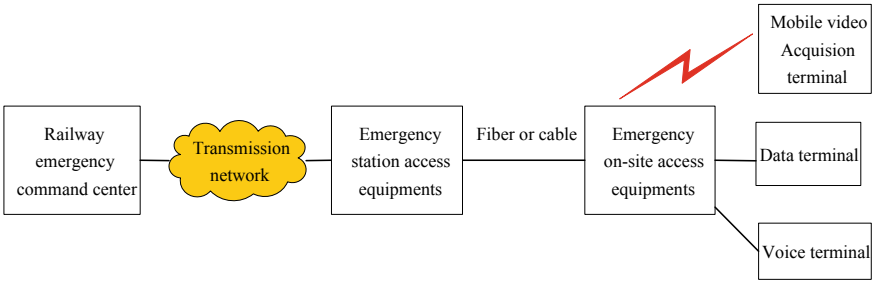

Fig. 3 Landline railway emergency communication access manner

modulation technologies, conveying the site information to the station, then further forwarding to the emergency command center.

Due to complex environment and excessive obstacles along the railway, it requires the distance of the equipment located between the site broadband wireless access and the station wireless access be more than 3 km, and its available channel bandwidth no less than 1 Mbps in order to meet the transmission of the CIF-resolution real-time images and multi-channel voice communications. The Inmarsat system access technology has been long developed and widely employed at home and abroad, and its access equipment and terminals are well designed, but its cost is high, and voice communication is an international business, video communication is limited by the bandwidth, and so the image quality is not high.

5 Conclusions

The emergency communications system is an organic and important part of national emergency management system and underlining the emergency communication supporting work is an important and complex task. At present, all important industry sectors have established their corresponding special emergency communication systems according to their respective service needs, but still face many problems and challenges during the course of construction. For example, these emergency communication systems lack unified planning and interoperability standards, and the emergency command platforms are unlikely interconnected, resulting in low efficiency of inter-departmental collaboration. In this article, several typical industry sectors are selected, and the construction objectives, construction plans, and existing issues of the industry-specific emergency communication systems for power, water, and railway industries are elaborated. Additionally, useful advice on the improvement and development of the specific emergency communication systems are put forward in the future.

References

1. Liu, Y.C., Zhu, Z.L.: Research on intelligent networking platform for emergency communication command system. Fire Sci. Technol. **9**(12), 901–903 (2012)
2. Zhong, B., Li, B., Cheng, Q.: Improve the ability of anti disaster emergency wireless communication system. Commun. Inf. Technol. **7**(1), 44–47 (2015)
3. Lin, R.: Emergency measures for electric power communication. Power Inf. Syst. **6**(3), 21–22 (2016)
4. Cao, Y.: Emergency communication service on public telecommunication network. Mod. Telecommun. Technol. **15**(8), 27–30 (2015)
5. Li, W., Li, W.H.: A novel multi-mode electric power emergency communication system. In: ICCCBDA 2019, pp. 24–30. IEEE, Chengdu, China (2019)
6. Liu, J., Xu, M.: Application of wireless ad hoc network in public security emergency communication. J. Chin. People's Pub. Secur. Univ. **17**(1), 55–57 (2017)

7. Wang, W., Gao, W.D., Bai, X.Y.: A framework of wireless emergency communications based on relaying and cognitive radio. In: PIMRC 2007, pp. 432–436. Springer, Greece (2017)
8. Zhang, X., Wang, R.: New Technology and System Application of Emergency Communication. Mechanical Industry Press, Beijing (2015)
9. Wang, Y., Liu, X.: An emergency communication platform based on vehicle communication system. Telecom. Eng. Tech. Std. **12**(7), 15–19 (2018)

Research on the VR Platform Construction of Intangible Cultural Heritage of Li Nationality in Hainan

Xi Deng

Abstract In this paper, we build a virtual reality platform to display intangible cultural heritage. Taking the intangible cultural heritage (ICH) of Li nationality in Hainan as the research object, from the angle of virtual reality interaction experience, the paper explored the possibilities of establishing a virtual reality platform to inherit and develop the Hainan Li ICH in the ICH digital environment. The corresponding smart services and application construction strategy are also discussed, which are expected to play a reference role in the development of China's Li intangible cultural heritage.

1 Introduction

Digital research on intangible cultural heritage (ICH) has now entered a mature stage, mainly focusing on digital collection, storage, protection, database resource construction, realizing the protection, development and utilization of ICH through digital technology, information technology, network technology, and other modern scientific and technological means. The related technologies such as digital development and protection, system development and application, and cultural creative products of virtual reality are also in a period of rapid development, whereas domestic digital research and practice remain in the stage of exploration and exploration. There is still a lack of systematic solutions in the research of public digital display, communication platform, development and utilization, and other aspects. The Hainan Li nationality is the concentrated embodiment of Hainan culture. In the investigation of the Li nationality, it is found that the Li nationality's culture contains the unique marine culture of Hainan. In history, the maritime "silk road" centered on the South China Sea once presented the prosperity of maritime cultural exchanges. Archeologists found ancient tombs and burial objects of the Han dynasty in Le Dong, Chang Jiang, Dong Fang, and other places where Li people lived. Therefore, based

X. Deng (✉)
College of Art and Design, Hainan University, Haikou, China
e-mail: dengxi@hainanu.edu.cn

R. Kountchev et al. (eds.), *Advances in Wireless Communications and Applications*,
Smart Innovation, Systems and Technologies 191,
https://doi.org/10.1007/978-981-15-5879-5_19

on the research of the integration of Hainan's ICH and VR technology, our platform explored the methods and paths of digital display and development of intangible cultural heritage for mobile intelligent terminal platform via digital technologies and information technologies such as computer graphics, multimedia, digital animation, and network communication.

2 Domestic and Foreign Research

China is in the exploration stage in digital acquisition, protection, storage, digital protection technology, digital display, digital communication, digital development and utilization and other aspects. There are several influential projects in the field of material and cultural protection. One is the "Cooperative research on digital Dunhuang frescoes" jointly carried out by the DunHuang research institute and northwestern university in the USA. The "digital Dunhuang" includes three parts: virtual reality, augmented reality, and interactive reality [1]. The other is the "digital Old Summer Palace" project, which aims to reproduce the Old Summer Palace in a comprehensive, three-dimensional, and exquisite way on the basis of keeping the site intact with the latest technological means, such as augmented reality technology. It also launched a mobile app, allowing visitors to see the original appearance of the restored Old Summer Palace and its background information in different historical periods through handheld mobile devices [2]. The third project is the "Luoyang paradise ruins" protection demonstration project. The newly opened ruins is a tower building that integrates protection and display functions, which uses the advanced digital protection technology of project-based spatial augmented reality to display and protect the "paradise" ruins [3].

Since the birth of computer-aided design systems in foreign countries, digital technology has become a favorable tool for design, creation, and communication in developed countries. The USA, Japan, and the UK are the first countries to adopt digital technology to protect cultural heritage. These countries have widely applied digital technology to the restoration, reproduction, architectural roaming, and digital film and television exhibition of intangible cultural heritage landscape.

The "American memory" project, a national virtual library in the USA, aims to "provide free and open access to written and oral text, audio recordings, static and dynamic images, prints, maps, music, and other resources to record the impression of the USA through the Internet. It is the digital record of American history and creativity" [4]. The researchers in University of Geneva, Switzerland [5], studied the use of animation, virtual reality, and other digital technologies to digitally present the living traditional culture and cultural events of Pompeii, an ancient city with European cultural characteristics. The contents of this project include visualization, contextualized three-dimensional characters, 3D animation, virtual ancient architecture, and scenes key live events and embody the characteristic culture elements of dress, hairstyle, virtual reconstruction, and reproduction. Finally, the virtual digital

cultural content information is superimposed in the real Pompeii cultural relic environment by using augmented reality technology, so that users can experience the historical situation behind the relics in the real cultural relic site environment.

3 Present Status of Li nationality's ICH in Hainan

The Li nationality is the major ethnic minorities in Hainan. After thousands of years of exploration and inheritance, the Li nationality has created their unique civilization and culture. At present, there are ten intangible cultural heritages have been included in the national intangible culture list and more than ten provincial intangible cultural heritages (as shown in Table 1). From the current situation of intangible cultural heritage development in Hainan, it is generally developed and utilized through three ways. First, carry out industrial development and management of the transformation of handicrafts, souvenirs, and other products of Hainan intangible cultural heritage resources, such as traditional crafts, traditional fine arts, folk literature, coconut carving, and textile craft, to achieve the development-type protection of intangible cultural heritage. Second, realize the function of education and propagate through the concentrated display and communication of Li culture in the intangible cultural heritage museum, such as Hainan Museum. Third, build cultural tourism scenic spots such as ecological museum, folk village, and ethnic customs garden to develop cultural tourism for intangible cultural heritage, such as BingLang valley.

4 Virtual Reality Platform Construction Scheme for the Hainan ICH (ICH VR Platform)

4.1 The Content of the ICH VR Platform

ICH VR platform is to digitalize the ICH of Li nationality in Hainan, which combined computer graphics, computer animation, network communications, cloud storage services, and other modern means of science and technology [6], based on VR technology of Hainan Li intangible digital display, transmission, established theoretical methods, and practical path of ICH protection in Hainan. The aim of this platform is to solve the current dilemma that Hainan's ICH cannot be inherited, unable to experienced, hard to spread, and to realize the integration on culture, science, and technology of intangible cultural heritage. The following three aspects are elaborated:

Constructing the digital framework of Hainan's ICH based on virtual reality technology, which can providing a systematic and integrated new model for the digital development of ICH. Nowadays, there are many kinds of ICH in Hainan which are rather messy, the preservation status is not ideal and there is a tendency to gradually disappear. The primary task of the platform is to sort out the ICH of Hainan (as shown

Table 1 Representative list of Li intangible cultural heritage in Hainan Province

Items	Name	Level
Folk literature	Li folk tales	Provincial
	Li Cong Liu's song	Provincial
	Li folk songs (Qiongzhong Li folk songs)	National
	Bamboo and wood instrumental music of Li nationality	National
	Li sai dialect long tone	Provincial
Traditional dance	Li firewood dance	National
	Li Qian Ling double sword dance	Provincial
	The Li pound rice dance	Provincial
	Li people dance together	Provincial
	Li mask dance	Provincial
	Li old dance	Provincial
Traditional skill	Li traditionally dyed spun silk embroideries skills (including linen textile weaving, Beng dye, double-sided embroidery, the dragon was)	Provincial
	Li bark cloth making skills	National
	Li bone ware making skills	Provincial
	The original pottery making skill of Li nationality	National
	Li's skill of drilling wood and making fire	National
	Li ganlan construction skills	Provincial
	Li boat building skills	National
	Li rattan and bamboo weaving skills	Provincial
	The craft of making single wood utensils of Li nationality	Provincial
	Li Jin spinning, dyeing, and embroidering tool-making skills	National
Traditional sports	Traditional sports and entertainment of Li nationality	Provincial
Traditional medicine	Li medicine (bone injury therapy and snake wound therapy)	Provincial
Traditional custom	"March 3rd" festival of the Li and Miao nationalities in Hainan	National
	Li clothing	National
	Li traditional wedding	Provincial
	The custom of crossing the river by Yao boat	Provincial

in Table 1), list each intangible cultural heritage digitization idea and how to implement it with virtual reality to form a systematic and integrated digital development framework. Each intangible cultural heritage item is built into a virtual platform in the form of a module for reproduction or reconstruction.

For example, in the list of intangible cultural heritage, the traditional textile, dyeing and embroidery skills of Li nationality are mainly in four steps. Step 1: hand-twist spinning, the oldest human spinning technique. Step 2: dyeing. All the dyes come from natural plants, mainly using mountain wild or domestic plants as raw materials.

Fig. 1 Four steps of Li textile skill

Step 3: Li Jin Beng dye. Beng dyeing craft is Li nationality's unique ancient dyeing techniques. It is a living fossil of Chinese dyeing skills. Step 4: brocade. The loom at the waist is a very old loom, and Li women use it to weave beautiful and gorgeous complex patterns (as shown in Fig. 1). In this platform, we will have an immersive and close understanding of the production process of Li Jin. In addition to showing the production process, we can also have interactive experience, so that the audience can fully understand this technology through the virtual reality platform and achieve the function of teaching and inheritance. Various patterns and styles of Li Jin can be viewed and people can virtually dressed in the clothes of Li nationality.

(2) Research and design a virtual reality cultural digitization platform using virtual reality technology to provide a specific application development solution for the future digital development of ICH under the digital framework of ICH in Hainan.

Based on the real scene, beforehand by camera to collect material texture map and build 3D model, users can use the modeling module [7] to process the texture and build a real three-dimensional model Li's living scene. Then, import it into virtual reality software such as Unity 3D to build a virtual platform, implant sound effects, graphical interface, plug-in, and light setting rendering. Add gesture interaction through Leap Motion's sensors to complete the user's gesture detection thereby giving feedback to the user in real time. The overall research process is shown in Fig. 2.

Realize the combination of virtual reality technology and computer animation art. Taking the living environment of Hainan and some humanistic materials as examples, combined with the technology of virtual reality and the art of computer animation, the experimental development and design of application examples were carried out.

There are three aspects need to be balanced on this virtual reality platform: the artistry of animation, the interaction of virtual reality technology, and the inheritance of intangible cultural heritage. Animation is a technique of expression of art. It is a kind of artistic processing through hand-drawing or three-dimensional form and continuous frame playing and combines some traditional art forms to show a charm different from traditional art. In the performance of intangible cultural heritage, animation is particularly applicable to oral myths and historical stories. However,

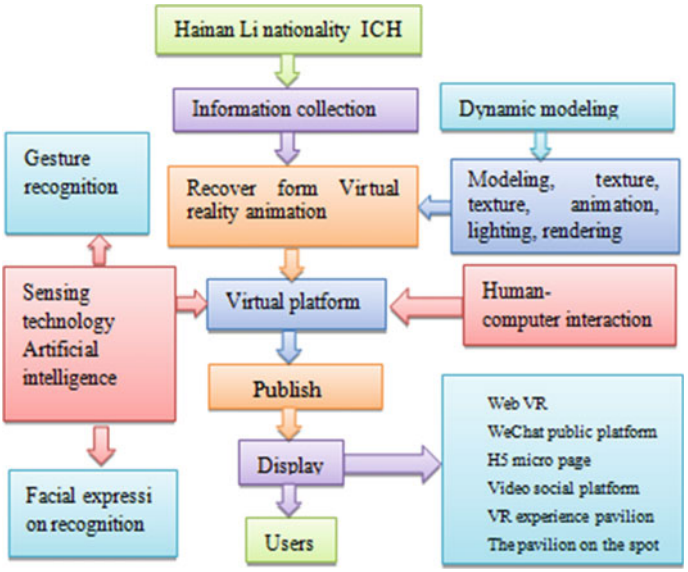

Fig. 2 Virtual reality flow chart of intangible cultural heritage in Hainan

animation lacks interactivity, which can be compensated by virtual reality technology. The inheritance of traditional skills, sacrificial activities, dances, music, legends, and so on in the ICH is difficult to preserve. The remaining documents, video, and other documents are also poorly preserved and difficult to meet people's evaluation standards, so they are basically abandoned, resulting in the loss of many traditional folk customs. The inheritance of ICH cannot only rely on the teachings of the older generation and their precarious status to attract people's attention. If it wants to be accepted and loved by modern people, it must be in line with the development of modern society. Only by displaying the charm of intangible cultural heritage in modern ways can it be accepted by modern people, especially the younger generation. With the expansion of animation market, the rise of artistry and the addition of new virtual reality technologies, the expression of intangible cultural heritage can be accepted by modern people and thus be inherited.

This platform applies the virtual reality technology to the protection and development of Hainan ICH, which is an innovative form in the development of Hainan. ICH's cultural heritage belongs to "invisible, intangible, and unable to experience." To solve this problem, we can construct a virtual platform, which uses virtual reality technology to create an immersion environment by VR glasses equipment. Through the platform, user will experience the feature of Hainnan ICH in real time and dynamically. For example, Hainan Li folk tales have always been marginalized in the development and protection process of digitization. In many researches and practical operations, no effective specific digital development and protection measures have been taken. Using digital technologies and information technology like VR and animation

to dig the cultural connotation and spiritual value in folk stories, folk legends and folk literature, we can develop abundant VR digital culture creative products which combined with traditional culture, educational, and entertaining.

4.2 Technical Routes of ICH VR Platform

This project belongs to interdisciplinary research, which integrates digital technologies and information technologies such as augmented reality, computer graphics and images, digital animation, multimedia, network communication, and cloud storage system and combines many cutting-edge theoretical knowledge in ICH. In this project, we propose a system in which virtual reality and experience sense are integrated to allow agents to interact with virtual environments in real time [8]. Segmented object and scene date are used to construct a Li national's living scene within Unreal Rngine4. In terms of research methods, literature review, cross research, case analysis, and application case study are mainly adopted.

Virtual reality technology is currently researching and developing technology in virtual electronic media, driving, education, virtual reality sports, virtual video conference, entertainment, game mode application, medical technology, tourism industry application, etc., and has achieved certain effects, whereas the use of virtual reality to restore the intangible heritage of the original ecosystem still needs the support of the mainstream of the virtual reality technology.

The virtual reality platform is mainly composed of five parts: users, activators, scene generators, presenters, and sensors. The key part of the research is scene modeling and rendering (Fig. 3). Modeling includes geometric modeling, dynamic modeling, and behavior modeling. Rendering includes modeling simplification, multi-resolution, and hardware acceleration. For virtual reality scene construction, modeling and rendering are a pair of inseparable problems, that is, scene modeling needs to consider its rendering efficiency, while scene rendering also needs to pay attention to the third dimension of modeling.

5 Conclusion

Virtual reality technology has already demonstrated its advantages and values in the protection of intangible cultural heritage, although virtual reality technology is affected by hardware equipment and the speed of network transmission today, which has certain limitations on industrial promotion. In tracking technology and eye wearable equipment, highly integrated portable devices are the future. 5G technology will break the barrier of transmission speed and bring greater possibility of comprehensive promotion of VR and AR, using smart devices to realize the digital application of intangible cultural heritage. In the future promotion of intangible cultural heritage, virtual reality technology will expand the field of vision and hearing, maintain the

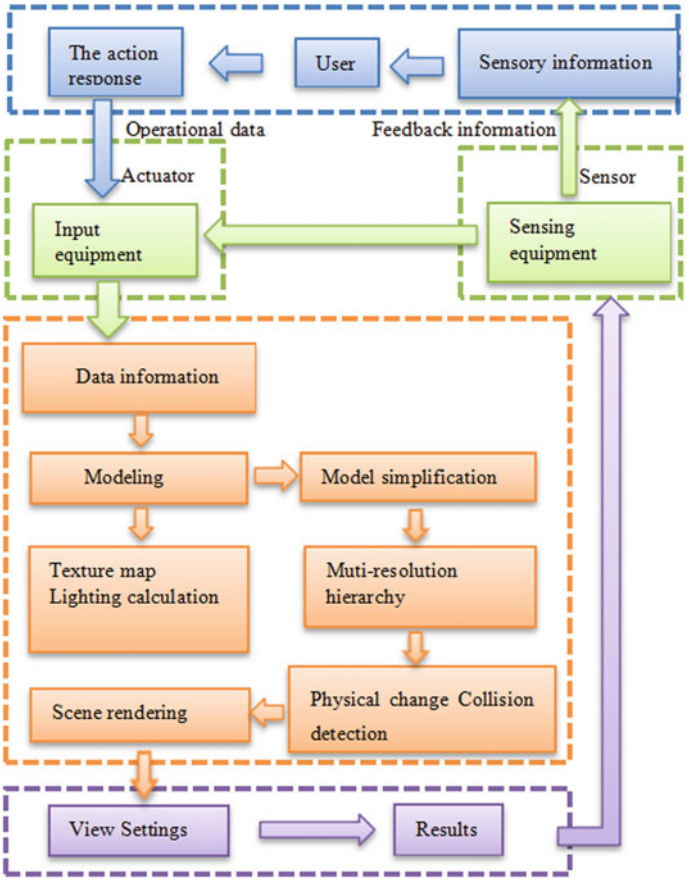

Fig. 3 Function module of virtual reality system

integrity of the world, simulate the cultural and historical environment to the greatest extent, break the limitation of time and space, and bring the audience a stronger sense of reality, so that the image and the real world can be seamlessly connected. The establishment of virtual reality platform will provide a more effective way to protect the intangible cultural heritage of Li nationality thus achieving the protection of human spiritual wealth and the inheritance of spiritual civilization.

Acknowledgements This paper is one of the results of key research and development projects in Hainan Province. Digital research on the intangible cultural heritage of Li nationality in Hainan by virtual reality technology. No. ZDYF2019017.

References

1. Chao, B.L.V.: Analysis of virtual reality technology and the intangible culture heritage protection. J. Dalian Univ. **36**(4), 80–83 (2015)
2. Kurillo, G., Bajcsy, R.: 3D teleimmersion for collaboration and interaction of geographically distributed users. In: Proceedings of Virtual Reality, pp. 29–43 (2013)
3. Maimone, A., Fuchs, H.: Encumbrance-free telepresence system with real-time 3D capture and display using commodity depth cameras. In: Proceedings of IEEE International Symposium on Mixed and Augmented Reality, Seoul, pp. 137–146 (2011)
4. Zhou, Z., Zhou, Y., Xiao J.J.: Survey on augmented virtual environment and augmented reality. Sci. China Press **45**(2), 157–180
5. Beck, S., Kunert, A., Kulik, A., Froehlich, B.: Immersive group-to-group telepresence. IEEE Trans. Visual. Comput. Graph. **19**(4), 616–625 (2013)
6. Chen, G.F.: Intangible cultural heritage preservation: an exploratory study of digitization of the historical literature of Chinese Kunqu opera librettos. ACM J. Comput. Cult. Herit. **7**(1), Article 4 (2014)
7. Dou, M., Davidson, P., Fanello, S.R., Khamis, S., Kowdle, A., Rhemann, C., Tankovich, V., Izadi, S.: Motion2Fusion: real-time volumetric performance capture. ACM Trans. Graph. **36**(6), 246:1–246:16 (2017)
8. Lin, J., Guo, X., Shao, J., Jiang, C., Zhu, Y., Zhu, S.-C.: A virtual reality platform for dynamic human-scene interaction. In: SA '16 SIGGRAPH ASIA 2016 Virtual Reality meets Physical Reality: Modelling and Simulating Virtual Humans and Environments. Article No. 11 (2016)

Design of Control System for Reinforcing Bar Thread Processing Equipment

Hongyu Wang and Huijun Sun

Abstract In order to overcome the shortage that has been existing in both semiautomatic and manual operation devices of processing thread at home and abroad, an automatic processing thread technology is developed. It consists of the technology of electric drive, hydraulic transmission and PLC controls, which realizes the automatic processing thread tech from loading material, feeding material to processing thread. Ipc, as the upper computer, is used for man–machine interaction and processing information storage. Wireless communication between ipc and PLC is realized through wireless router. The conclusion is that it improves the production efficiency.

1 Introduction

Since the reform and opening up, with the rapid and sustainable development of the national economy, high-rise buildings and large industrial plants have been built in large quantities, and the thick and dense steel bar has been widely used, which puts forward high requirements on the steel bar connection technology. The reinforcing bar connection technology often used on the construction site mainly includes manual arc welding, cold extrusion connection of reinforcing bar and screw connection of reinforcing bar.

The basic principle of manual arc welding is the welding method with manual operating electrode. The stable burning arc between the electrode and the welded part is used to melt the electrode and the welded part, so that the solid welded joint can be obtained. The advantages are flexible operation and wide weldable metal materials. The disadvantages are the low welding productivity and the fact that weld quality highly depends on the welder's operating skills and the situation of field.

The basic principle of cold extrusion connecting steel is to put a steel sleeve on the end of two ribbed steel bars and use ultra-high-pressure hydraulic equipment to squeeze the steel sleeve radial along the steel sleeve. Under the action of squeeze

H. Wang (✉) · H. Sun
North China Institute of Aerospace Engineering, 065000 Lang fang, China
e-mail: 7666287@163.com

R. Kountchev et al. (eds.), *Advances in Wireless Communications and Applications*,
Smart Innovation, Systems and Technologies 191,
https://doi.org/10.1007/978-981-15-5879-5_20

clamp, the steel sleeve produces plastic deformation and tightly combines with the steel bar. The advantages are high joint strength and reliable performance as well as simple operation, fast construction speed, energy and materials saving and comprehensive economic benefits. The disadvantage is that the cost of it is high and it is especially suitable for the structure and position of high demand. Due to heavy equipment and labor intensity of workers, once the equipment maintenance is poor, it is likely to produce oil leakage, pollute rebar and affect the effectiveness of normal production [1].

The basic principle of rebar thread connection technology is to make the joint of rebar to be connected upsetting, then process thread on the upsetting part and finally connect the rebar with thread sleeve at the construction site. The advantage is that the production of connecting sleeve and reinforcing bar thread has been realized in the factory. In the construction site, only the sleeve connection is needed, and the installation of the threaded sleeve is also very convenient, which only needs to be screwed into place with a wrench. It is because only the sleeve is rotated instead of the steel bar, and the advantages of installing large-diameter steel bar and arc steel bar are more obvious, which reduces the construction difficulty on site and improves the production efficiency [2].

The last one of the three technologies mentioned above has dominated the relative area due to its advantages. And thread processing machine is the key equipment of this technology.

At present, most of the thread processing machines used at home and abroad adopt manual operation mode and some companies use semiautomatic control. But whether manual or semiautomatic control, there are certain safety risks and the processing quality is not stable.

In order to realize man–machine interaction, storage processing information and other functions, the industrial computer is applied. Considering the complexity of the processing site, it is not convenient to use wired communication between ipc and PLC, so the wireless switch is used to realize the wireless communication between ipc and PLC.

The successful development of the rebar screw thread processing equipment with this scheme fills the gap of the domestic and foreign non-automatic rebar screw thread processing equipment, and the popularization and application of this equipment in the construction industry will obtain considerable economic and social benefits.

2 Design Requirement

According to the core connotation of reinforcing bar thread processing technology, the design requirements of automatic feed and automatic return during thread cutting are put forward.

The details are as listed in terms:

After the system starts, the status detection is carried out automatically.

If the fault is found, the fault status alarm will be carried out. At this time, the power supply will be turned off to eliminate the fault. If there is no fault, the material test is carried out to check whether there is material of steel bar on the material feeding rack [3].

If no material is detected on the material feeding rack, the flipping process is carried out which takes the rebar to the rack. At the same time, the signal that represents whether or not the process is finished successfully is generated. If mistakes occur, there is an alarm of fault status.

When the material is detected on the material feeding rack, it will start feeding. At the same time, the retaining iron that restricts the feeding position of materials starts to swing upward and stops when the retaining iron is placed in the limited position.

When the material reaches the limited position of the retaining iron, the movement of the material feeding rack is stopped. The three cases listed below happen simultaneously: (1) The retaining iron swings downward until it reaches the limited position of the bottom. (2) The vises that fix the position of the material are clamped. (3) The cooling pump acts.

When the vises are clamped, the process of cutting thread starts that provides both manual and automatic shifts. The specific details are as listed in terms: [4]

Oil feeding cylinder drives the main motor that is of cutting thread to rotate at high speed.

When the oil feeding cylinder reaches the limitation of the back, the main motor starts smoothly.

When the oil feeding cylinder reaches the limitation of the one, feeding speed is modified to be low.

When the oil feeding cylinder reaches the limitation of the two, feeding speed is modified to be middle. And the main motor is at high speed.

When the oil feeding cylinder reaches the limitation of the three, feeding speed is modified to be high.

When the oil feeding cylinder reaches the limitation of the four, feeding speed is modified to be middle.

When the oil feeding cylinder reaches the limitation of processing thread, the feeding is stopped.

When the delay of three seconds is finished, the oil feeding cylinder moves back quickly.

When the oil feeding cylinder backs to the initial position, the three cases listed below happen simultaneously: (1) The oil feeding cylinder stops to back. (2) The vises start to be loose. (3) The main motor stops.

After the delay of three seconds, the vises loose completely. At the same time, the material feeding rack moves back quickly.

When the rebar moves back to the limitation of position, the rebar that has been processed is moved out. At the same time, the next rebar is loaded. Up to now, it has finished a circle.

3 Design of Hardware

Control system consisting of PC and PLC control system, industrial computer as the upper machine is used to realize the human–computer interaction, storage, processing information; PLC control system to realize the automatic processing of reinforced thread control, through the wireless router to realize wireless communication between industrial PC and PLC. The structure of the control system is shown in Fig. 1: [5]

General system schematic diagram is shown in Fig. 2.

According to the overall design of the process, the whole control system involves the hardware part that includes one material feeding motor, one flipping motor, one vise, one main motor, one hydraulic pump, one water pump, two hydraulic cylinders, one PLC, several contactors, several relays, several hydraulic valves, several buttons, wires and other related materials. The functions of the main related devices are as listed in terms:

The main motor is to drive the cutting device for fast thread rolling and rib stripping.

The material feeding motor is to drive the rack to move forward and backward so that the material accurately feeds and backs.

Fig. 1 Structure of the control system

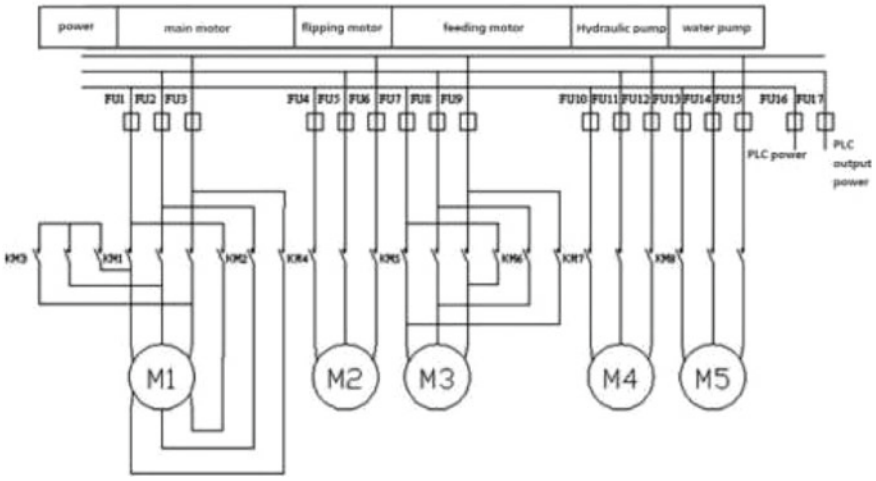

Fig. 2 General system schematic diagram. It explains to the electrical structure of hardware

Table1 Input and output pins

Input	Annotation	Output	Annotation
I0.1	Material ready	Q0.1	Rack feeding
I0.3	Retaining iron upward completed	Q0.2	Rack flipping
I0.4	Rack feeding completed	Q0.3	Alarm
I0.5	Vise clamped	Q0.4	Retaining iron upward
I0.6	Iron downward completed	Q0.5	Vise starts to clamp
I0.7	Feed limit 1	Q0.6	Retaining iron downward
I1.1	Feed limit 2	Q0.7	Water pump
I1.2	Feed limit 3	Q1.0	Oil feeding cylinder fast
I1.3	Feed limit 4	Q1.1	Oil feeding cylinder low
I1.4	Processing thread limit	Q1.2	Oil feeding cylinder starts
I1.5	Oil feeding cylinder backward limit	Q1.3	Oil feeding cylinder backward limit
I1.6	Rack backward limit	Q1.4	Main motor high speed
I1.7	Manual/auto switch	Q1.5	Oil feeding cylinder backs
I2.0	Auto-processing starts	Q1.6	Vise loosed
I2.1	Auto-processing stops	Q1.7	Rack backward
I2.2	Manual processing starts	Q2.1	Indicator of auto-form
I2.3	Manual processing stops	Q2.2	Indicator of manual form
		Q2.6	Intermediate relay of manual form

The flipping motor is to drive the material rack to rotate in order to take the rebar onto the rack, and when the whole process is finished, take the rebar away from the rack.
Hydraulic pump, hydraulic valve and hydraulic cylinder function together to complete the movement of the retaining iron and main motor.
PLC, contactor and relay function together to complete the automatic control of the system.
Vise is to fix the material so that the process is precise.

The assignment of input and output pins is listed in Table 1.

4 Design of Software

Through the ladder diagram of PLC programming, the software is finished. The procedure flow is as follows:

The working mode of steel bar threading machine can be switched between “automatic” and “manual.” Under the automatic mode, the processing equipment can realize the whole process from sending to returning materials. Every time the

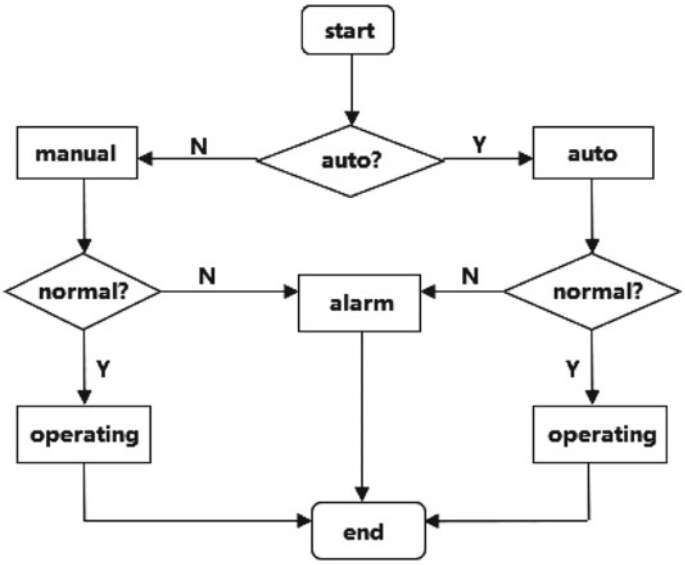

Fig. 3 General flow of the program

processing is completed, the system will automatically turn over and change materials, realizing the continuous processing without manual intervention. In the manual mode, because the accuracy of manual operation is difficult to ensure, therefore the entire process is not required to be manual, but in the key part of process PLC automatic control is needed and the feeding and refueling process are completed by workers. When the process of a bar is finished, manual control is needed to realize refueling and start the processing of the next rebar [6].

The general flow of the program is shown in Fig. 3.

The part of the program is shown in Fig. 4.

5 Conclusion

Construction steel bar screw connection technology is a kind of fast and convenient mechanical connection technology, because its joint performance is reliable and easy to manage, and it has a broad application prospect. The adoption of reinforcement thread connection technology is primarily concerned with the choice of reinforcement thread processing method. With the extensive application of reinforcement thread connection technology, the original manual machining method can no longer meet the needs of production. Now, the reinforcement thread processing equipment is mainly semiautomatic equipment. Although it makes up for the huge shortage of manual processing, it still does not meet the needs.

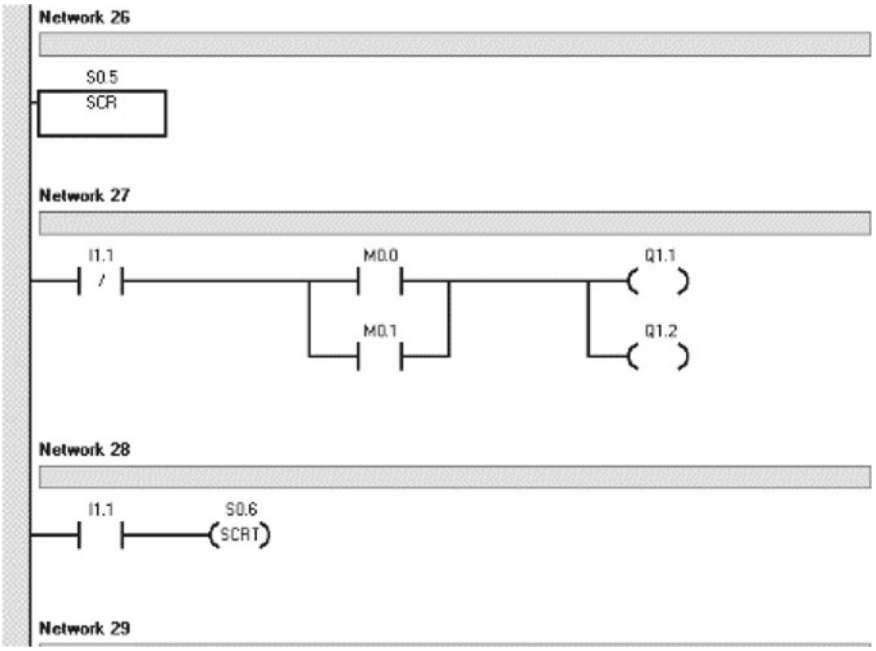

Fig. 4 Part of the program

This paper designs a set of automatic reinforcement thread processing equipment control system. In the choice of control method, because the relay control system hardware cost is high, its wiring is complex, it is difficult to maintain and update, and the advanced PLC control method is chosen. Through PLC program control, coupled with advanced sensor detection technology, the system can achieve the reinforcement thread processing of full automation from sending, processing and returning new material which does not need manual intervention and the realization of circular processing. In addition, it provides the traditional semiautomatic processing mode.

Besides, ipc is used to deal with the bad environment of the industrial site, frequent vibration, dust, large load and even a variety of electromagnetic interference. And the wireless communication between ipc and PLC can reduce the construction cost, shorten the construction project cycle and better deal with the complex environment of the construction site, so that the later equipment maintenance and function expansion become easy.

The system designed in this project has been applied to the production site. Under the control of this system, the reinforcing bar thread processing equipment can work normally according to the design requirements, and the control effect is good. But there are some problems, such as the cost of the whole control system is relatively high, not conducive to the promotion and application of the equipment, and reinforcement screw processing parameters are not easy to change. In the future, efforts should be made to reduce the production cost of the fully automatic steel bar thread

processing equipment, so as to better promote the application of the equipment in the construction industry. In addition, the steel bar screw thread processing equipment developed at present can change the screw thread processing parameters of the steel bar by manually changing the position of the position detection sensor. In the future research, it can be considered to automatically change the position of the detection sensor according to the processing needs, so as to further improve the efficiency of the system.

Acknowledgements This work is supported by National Key Science Research Program under Grant 2017YFC0704001-03. All the persons and organizations that have supported the work are sincerely appreciated.

References

1. Li, F., Liu, S., Shi, A.: Research on laser thread form bending of stainless steel tube. Int. J. Precis. Eng. Manuf. **6** (2019) (China)
2. Midha, V.K., Gupta, V., Mukhopadhyay, A.: Impact of positive thread feeding for high-speed industrial lockstitch sewing machines: part I development of device. J. Institut. Eng. Ser. E (2019) (India)
3. Zhou, Q., Yang, P.: Design of semi-automatic feed mechanism for rebar thread sheathing machine. Construct Mach. **8** (2005) (China)
4. Ye, X.: GK type conical threaded joints with equal strength reinforcement. Build. Technol. **5**, 340 (1999) (China)
5. Tang, M., Lou, Z., Rui, S., et al.: Study on terminal crack in single welding. J. Weld. **7**(3), 123–132 (1987) (China)
6. Sun, Z., Xiong, Z.: Comparison and selection of several reinforcing bar mechanical connection technologies. Construct. Technol. **5** (2003) (China)

Simulation Experiment Research of Applying Superconducting Receiving Technology to Satellite Payload

Jun Zhi, Wei Ji, Yu- Dong Pei, and Shan Huang

Abstract Firstly, the paper analyzes the principle of applying superconducting receiving technology to satellite payload. Combined with the advantages of superconducting receiving technology, it establishes the circuit model of single-antenna receiving system. Secondly, it sets the relevant parameters reasonably according to the application requirements and simulates the performance of conventional devices and superconducting devices accurately, then finishes the comparison. Simulation results show that the application of superconducting receiving technology can effectively improve the sensitivity of satellite payload. Under the condition of keeping the gain basically unchanged, the noise coefficient and suppression performance are improved after adding the superconducting receiver.

1 Introduction

There are two advantages of superconducting receiving technology applied to satellite systems:

1. The superconducting receiver has very low noise coefficient. Replace normal temperature low-noise amplifier with superconducting receiver; it can improve the sensitivity of the satellite and improve the ability to acquire weak signals [1]. Noise performance comparison between superconducting receiver and traditional receiver is shown in Fig. 1. The X-axis denotes the P, L, S, W band. The Y-axis denotes the noise performance.
2. Superconducting filters have the ability of very low insertion loss and very high out-of-band rejection [2]. It is well suited as a preselected filter before a low-noise amplifier. The anti-out-of-band suppression capability of the satellite system is greatly improved without affecting the sensitivity of the system. At the same time, it can reduce the interference of adjacent channel and reduce bit error rate.

J. Zhi (✉) · W. Ji · Y.-. D. Pei · S. Huang
Beijing Institute of Remote Sensing Information, Beijing, China
e-mail: njzhijun@163.com

R. Kountchev et al. (eds.), *Advances in Wireless Communications and Applications*,
Smart Innovation, Systems and Technologies 191,
https://doi.org/10.1007/978-981-15-5879-5_21

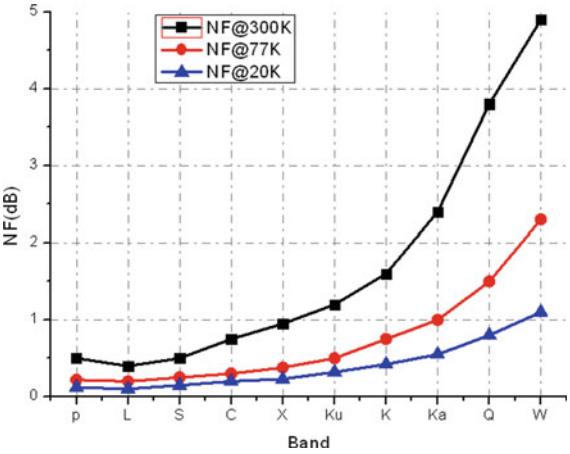

Fig. 1 Noise performance comparison between superconducting receiver and traditional receiver

2 Experimental Principle

Single-antenna receiving system of certain satellite and its schematic diagram are shown in Fig. 2. After the signal passes through the antenna, the signal is filtered out by the standby preselected filter, and then low-noise amplification (LNA) is carried out. After passing through the numerical control attenuator and power splitter, the signal is divided into multi-channel equivalent in-phase signals, which are, respectively, entered into multiple receivers.

The core components of superconducting receiver are superconducting filter and low-temperature low-noise amplifier. The satellite's receiving system consists of bandpass filters and low-noise amplifiers that function like superconducting receivers [3]. Therefore, the idea of applying superconducting receiving technology to satellites is to replace the bandpass and LNA in the principle block diagram with a superconducting receiver. As shown in Fig. 3, the superconducting receiver's extremely low-noise characteristics and excellent out-of-band suppression capability can improve the sensitivity and anti-interference capability of the system.

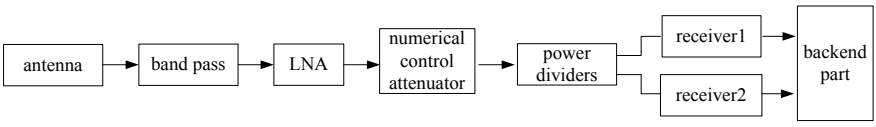

Fig. 2 Schematic diagram of satellite signal receiving system

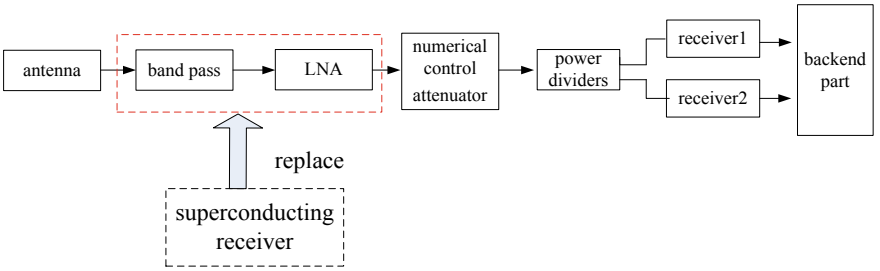

Fig. 3 Method of superconducting receiving technology applied to signal receiving system

3 Process of Simulation Experiment

We establish the circuit model of single-antenna receiving system and run the simulation, and the simulation results are obtained. The single antenna system consists of antenna, bandpass filter, low-noise amplifier, numerical control attenuator, power divider, and receiver, etc. The antenna does not belong to the front part and can be ignored [4]. Finally, the system simulation model is obtained as follows (Fig. 4; Table 1).

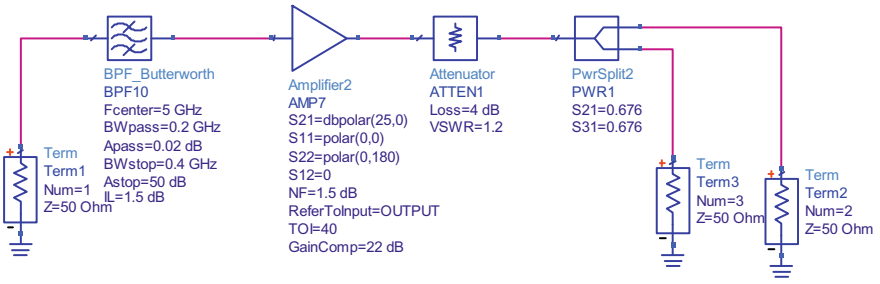

Fig. 4 Simulation model of front end of single-antenna receiving system

Table 1 Key parameters of the simulation model

Module	Normal temperature parameters	Superconducting parameters
Bandpass filter	Losses: 1.5 dB Restraint outside the band: 50dBc@ out-of-band 100 M	Losses: 0.25 dB Restraint outside the band: relate to bandwidth
Low-noise amplifier	Gain: 25 dB Noise: $\leq$1.5 dB	Gain: 25 dB Noise: $\leq$ 0.35 dB
Numerical control attenuator	Losses $\leq$ 4 dB	Losses $\leq$ 4 dB
Power dividers	Losses $\leq$ 3.4 dB	Losses $\leq$ 3.4 dB

The system has multiple components, and the bandwidth varies from 200 MHz to 2 GHz. In the simulation process, it is necessary to carry out simulation according to different bandwidth. The bandwidths are set as follows: 200 MHz, 500 MHz, 1 GHz, and 2 GHz. Simulate them, respectively, the results are listed in the following table (Table 2).

The above simulation results show that the variation of gain and noise coefficient is not related to bandwidth, and they, respectively, promote 1.25 dB (mainly because of the loss reduction of superconducting filter) and improve 2.5 dB. The inhibition degree at 100 MHz outside the band is related to the bandwidth. The wider the bandwidth, the lower the inhibition degree improvement at 100 MHz outside the band. At 200 MHz bandwidth, 40 dBc can be raised by suppression at 100 MHz outside the band. When the bandwidth reaches 1 GHz and above, the suppression at 100 MHz outside the band hardly improves. But at 50% of the out-of-band bandwidth, the inhibition can still increase 40 dBc.

Table 2 Simulation results

Serial number	Bandwidth		Gain	Noise factor	Suppression at 100 MHz out of band	Suppression at 50% of out-of-band bandwidth
1	200 MHz	Normal temperature	16.1 dB	3.07 dB	7.07 dBc	7.07 dBc
		Superconducting	17.35 dB	0.57 dB	47.38 dBc	47.38 dBc
		Benefit	Promote 1.25 dB	Improve 2.5 dB	Promote 40 dBc	Promote 40 dBc
2	500 MHz	Normal temperature	16.1 dB	3.07 dB	0.45 dBc	9.45 dBc
		Superconducting	17.35 dB	0.57 dB	10.44 dBc	52.44 dBc
		Benefit	Promote 1.25 dB	Improve 2.5 dB	Promote 10 dBc	Promote 42.09 dBc
3	1 GHz	Normal temperature	16.1 dB	3.07 dB	0.104 dBc	11.1 dBc
		Superconducting	17.35 dB	0.57 dB	0.958 dBc	58.3 dBc
		Benefit	Promote 1.25 dB	Improve 2.5 dB	Promote 0.854 dBc	Promote 47.2 dBc
4	2 GHz	Normal temperature	16.1 dB	3.07 dB	0.044 dBc	16.44 dBc
		Superconducting	17.35 dB	0.57 dB	0.133 dBc	69.23 dBc
		Benefit	Promote 1.25 dB	Improve 2.5 dB	Promote 0.089 dBc	Promote 52.79 dBc

4 Sensitivity Analysis

Although the sensitivity cannot be measured directly, it can be analyzed by combining theoretical calculation with simulation results. Firstly, according to the sensitivity formula [5]:

$$S = -174 + \mathrm{NF} + 10\log \mathrm{BW} + \mathrm{SNR}$$

where S is the receiver sensitivity, the measure is dBm; BW is the operating bandwidth of the receiver, the measure is MHz; SNR is the minimum signal-to-noise ratio (SNR) required to satisfy a certain condition of bit error rate, the measure is dB; NF is the noise factor of the receiver, the measure is dB. The noise factor of a single-antenna system receiver is mainly determined by the filter amplifier module, and the influence of the latter part is negligible, namely:

$$\mathrm{NF}_{\text{single antenna receiver}} = \text{loss of preselected bandpass filter} + \text{noise factor of low} - \text{noise amplifier}$$

Therefore, the preselected filter loss of the original system is 1.5 dB, and the noise coefficient of the low-noise amplifier is 1.5 dB, so the noise coefficient of the original system receiver is about 3 dB. After the superconducting receiver is installed, the difference loss of the superconducting filter is 0.2 dB at 5 GHz, and the noise coefficient of the low-temperature low-noise amplifier is 0.3 dB, so the noise coefficient of the superconducting receiver is about 0.5 dB.

According to the sensitivity calculation formula and simulation, the system sensitivity can be improved by 2.517 dBm after superconducting receiver is installed.

5 Conclusion of Simulation Experiment

The sensitivity of satellite payload can be improved by 2 ~ 2.5 dBm when superconducting technology is applied to the receiver of single-antenna system. If the superconducting device technology is further improved, the sensitivity can be increased by 3 dBm in the limit case. Superconducting receiving technique is applied in single-antenna structure (bandpass filter), and the out-of-band suppression is related to bandwidth. With the development of superconducting receiving technology, if the feeder can be combined with the superconducting receiver for an integrated design, the feeder can also be placed in a low-temperature environment, the lead can be shortened, and at the same time, the difference loss of the feeder can be reduced at low temperature, further improving the sensitivity of satellite payload. In addition, the influence of the cooling time and vibration of the superconducting receiver on the satellite will be reduced, and the limited sensitivity increase will be improved.

References

1. Meng, X.M.: Study on application of superconducting receiver front-end in L-band radar. Fire Control Radar Technol. **47**(1), 58–62 (2018)
2. Zuo, T.: Superconducting filters for deep space stations. J. Spacecr. TT&C Technol. **33**(5), 382–386 (2014)
3. Zhang, M.: Development of a high temperature superconducting(HTS) composite filter. Superconductivity **46**(3), 38–42 (2017)
4. She, S.G.: Application of high-temperature superconductive filter in space technology. J. Astronaut. **35**(7), 857–862 (2014)
5. Fan, C.H.: Principles of Communications, 7th edn. National Defense Industry Press, Beijing (2012)

Python Teaching Research and Practice from the Perspective of Computational Ecology

Lina Wang and Ying Ren

Abstract In view of the current teaching practice of Python, combined with the characteristics of Python language, this paper expounds the teaching concept of Python language from the perspective of computational ecology and based on the theory of learning motivation. Under the guidance of the teaching concept, it organizes "useful" + "interesting" teaching cases, from the initial understanding of Python ecology, in-depth understanding of Python ecology to the application of Python ecology, and pays attention to the gradual progress of knowledge. It is a contemporary tool to stimulate students' learning motivation and cultivate students' habits of calculation thinking and engineering thinking, and explore a new perspective of the application of computer theory.

1 Introduction

In 2016, the Guiding Committee of the Ministry of education for the teaching of computer courses in colleges and universities issued the basic requirements for the teaching of basic computer courses in colleges and universities (hereinafter referred to as the basic requirements) [1]. According to the situation of computer teaching in colleges and universities in China, Python is recommended for the first time. Under this impetus, domestic universities have gradually carried out Python language teaching. Among the top 30 universities in the USA, 90% of American universities teach Python in the computer science (CS) introductory course. At the same time, Python is also the most popular introductory programming language in the computer science department of American universities. Choosing different languages as the entry language of programming not only reflects the concept of computer education in different schools but also affects students' first impression of computer science. As an ecological language, Python plays an important role in training students' ability in computing thinking and engineering thinking habits.

L. Wang (✉) · Y. Ren
Naval Aviation University, Yantai 264000, China
e-mail: wanglina5677@163.com

R. Kountchev et al. (eds.), *Advances in Wireless Communications and Applications*,
Smart Innovation, Systems and Technologies 191,
https://doi.org/10.1007/978-981-15-5879-5_22

2 Python from the Perspective of Computational Ecology

2.1 Computational Ecology

The concept of "ecology" originates from biology. It studies the relationship between organisms and between organisms and non-biological environment. Since the origin of life on the Earth billions of years ago, after a long development and evolution, a variety of life forms have been bred, with natural selection and dependence. In the field of computer, the first electronic digital computer ENIAC was born at the University of Pennsylvania in 1946. With the development of modern science and technology and information technology, an open and open-source information form has gradually emerged in the computer neighborhood, such as various open-source software covering many neighborhoods, open-source operating system represented by Linux, and Arduino. Beaglebone, raspberry, PI are the three major open-source hardware, which constitute the "computing ecosystem." Like biological ecology, there are many participants in the computing ecosystem. They compete, depend on and develop in a free environment, which provides an important source of innovation for the progress of information technology.

2.2 Features of Python

In the field of Python development, there is a popular saying "life is short, you need Python". This seemingly joking remark actually reflects the language features of Python and its value in the minds of developers.

Python is characterized by fast problem solving. Simple and elegant are its most intuitive features, using less code to complete more work. To implement the same task, C language needs 1000 lines of code, Java only needs 100 lines, and Python may only have 20 lines.

Python is an easy to learn, free, and open-source high-level language. Although it is an explanatory language, compared with other compiled languages, the efficiency of program execution will be reduced. However, the processing speed of the processor completely offsets the cost of program execution efficiency in most application scenarios, and Python language achieves a balance between program development speed and running efficiency.

In view of these characteristics of Python, it is easier for students to learn. It allows students to focus on programming without paying attention to the underlying details. Even beginners of programming can easily start Python learning journey. This will help to cultivate students' calculation thinking and engineering thinking habits. In addition, there are many options for the job opportunities, positions and work contents of learners, and there is also a large space for future development.

2.3 Python's Computing Ecology

Python has been committed to open source since its birth, establishing the world's largest programming and computing ecosystem [2]. Python has built more than 200 standard libraries, which are rich in types and powerful in functions, and can meet general needs, including input and output, numerical calculation, file processing, etc. After users install the program, they can use it directly without downloading it separately. As a result, Python has the nickname "built-in battery". In addition, Python enthusiasts all over the world have contributed a large number of third-party libraries for a long time. At present, the number of Python third-party libraries is nearly 120,000, covering data processing, artificial intelligence, system operation and maintenance, network programming and so on, almost covering all computing fields. Python's computing ecosystem is quite strong.

Python is extensible. The second nickname of Python is "glue language". The so-called glue language refers to the functional modules that can be glued and called in other languages, and the code that cannot be compatible can be glued. The advantages of other languages can be organically combined to form an efficient new program. Python can easily combine the modules written by C++ and Java, so that the advantages of C++ at the bottom and the characteristics of java object-oriented can be unified into a complete program. It is the role of "glue" that makes Python stand out in the language rankings.

3 Python Teaching Concept from the Perspective of Computational Ecology

Guided by the understanding and application of Python's computing ecosystem, we divide the teaching content into two parts: Python basic ecosystem and Python advanced ecosystem. At the same time, we combine the motivation model to divide the teaching stage.

Psychology believes that it can form effective teaching to arouse and maintain learners' learning motivation. In the 1980s, Professor John M Keller of Florida State University put forward an incentive model for teaching design, i.e., ARCS model. The model is an acronym for four English words: attention, relevance, confidence, and satisfaction [3]. This model focuses on how to mobilize learners' learning motivation through teaching design.

Under the guidance of the arcs teaching model, combined with Python's computing ecology characteristics, we divide the teaching process into the following stages.

Understand Python basic ecology. The basic ecology of Python is programming in a general sense. At this stage, we pay attention to the explanation of Python's basic syntax and elements, highlight the methods of high-level language programming, from problem abstraction to algorithm to program implementation. Take the standard

library provided by Python as "building blocks" guide students to use building blocks to organize programs, and help students build modular solutions.

Relate to the Python ecosystem. Python language has a huge computing ecosystem. The solution of any problem depends on the computational nature of the problem. When constructing teaching cases, the third-party library is taken as the basic module to solve problems, and the vision of students' programming is expanded. In addition, there are dependencies among some third-party libraries of Python. When using these related libraries, we should understand their dependencies and train students to solve problems with the perspective of connection.

Understand Python's ecological value. Compared with C, Java, and other traditional languages, Python has a simple syntax, but it has its own complete syntax logic. It is a simple, easy to learn, and powerful programming language. In terms of artificial intelligence, machine learning, and data mining, Python has powerful third-party libraries to support. By using these libraries, students can achieve some powerful functions without writing huge code, enhance their confidence in solving problems, and at the same time, make students focus on the analysis of problems in the learning process, rather than wasting their time on complex languages. In the aspect of error correction, it improves students' interest in learning and cultivates students' ability of calculating thinking.

Implement Python ecological functions. Taking the scientific computing libraries Numerical Python (NumPy) and SciPy as examples, NumPy supports multidimensional array and matrix operations, and also provides a large number of mathematical function libraries for array operations. SciPy is based on NumPy and provides many scientific algorithms. For example: optimization, interpolation, Fourier transform, etc. These functions and algorithms are closely related to higher mathematics, linear algebra, and mathematical modeling, so that students can realize that the knowledge they have learned can be useful, and then maintain a higher learning motivation.

4 Python Teaching Practice from the Perspective of Computational Ecology

Under the guidance of Python teaching concept, we organize "useful" + "interesting" teaching cases, from initial understanding of Python ecology, in-depth understanding of Python ecology to using Python ecology, paying attention to the gradual progress of knowledge, stimulating students' learning motivation, and cultivating students' computing thinking.

4.1 Get to Know Python Ecology

In the initial stage of understanding Python, this paper introduces the basic concepts of Python language and establishes a basic understanding of programming methods, so that students can write about ten lines of Python programs. Python's basic knowledge points mainly include: Python basic elements, Python sequences, and control statements. These knowledge points are consolidated through some interesting classic cases, such as: "one hundred money, one hundred chickens," "narcissus number," "body mass index BMI," and other interesting cases. Initially contact Python's third-party library, and consolidate cycle statements, selection statements and the use of nested statements enables students to feel the fun of Python.

4.2 Go Deep into Python Ecology

In this stage, functions and object-oriented are explained in order of code reuse and abstraction. Through the military-related cases to realize the learning of the relatively difficult knowledge points, such as carrier equipped with carrier aircraft, pilot flight training, and other cases related to their own career development, so that students can realize that the learned knowledge points can be learned to use. On this basis, the application field of Python is gradually expanded. Using Python to build von Neumann architecture, to realize the use of operating system, to realize the operation of database, etc., expands the vision of students' programming, and maintains students' learning motivation. Through the use of *psutil* module and *pymysql* module, students can deeply understand the characteristics of Python "glue" language.

4.3 Using Python Ecology

This stage focuses on training students to use the characteristics of Python ecological language to solve practical problems, which belongs to Python's advanced ecosystem. In the process of teaching, we should pay attention to the actual problems as teaching cases, use socket programming to realize network communication, use Web crawler to crawl Web site information, use NumPy and SciPy to realize optimization, linear equation, integration, interpolation, special function, fast Fourier transform, and other commonly used calculations in science and engineering, and use Matplotlib library to realize data visualization. Train students to use engineering thinking habits to solve problems.

5 Conclusion

From the point of view of computational ecology, Python knowledge points can be explained. On the one hand, it can make students better understand and use Python language. On the other hand, this kind of teaching idea is also in line with the learning idea of Python as an ecological language. At the same time, under the guidance of the theory of learning motivation, to explain Python's knowledge context with the thinking of computational ecology, can cultivate students' Computational Thinking Ability and engineering thinking habits, which are the core competencies necessary for the information society.

References

1. Huang, T., Li, X.: Python language: an ideal choice for the teaching reform of programming course. Teaching of China University, vol. 2, pp. 42–47 (2016)
2. Song, T., Huang, T.: Fundamentals of Python Programming. Higher Education Press, Beijing (2019)
3. Liu, S., Zheng, Y., Ruan, S.: Research on micro curriculum design from the perspective of ARCS model. China Audio Visual Education, vol. 2, pp. 51–56 (2015)

Detection of Compromised Devices Based on Alert Logs in Smart Grid

Zhengping Jin, Ye Liang, Yifan Zhou, Xueqi Jin, Piaohong Kong, Zhengwei Jiang, and Lisong Shao

Abstract Detecting compromised devices helps to evaluate the security threats and reduce the security risks in the smart grid. Compared with the alert data in the general sense, the alert data in the smart-grid monitoring system has the features of higher alert aggregation level and lower alert aggregation threshold, which makes it difficult to detect the compromised devices with the existing detection methods. To solve the problem that there is no suitable detection scheme to find the compromised devices based on alerts log in smart grid, in this paper, a compromised device-detection model based on statistical analysis of alert data is proposed. This model is divided into three modules, namely pre-processing module, roof-detection module, and peak-detection module. The experimental results show the validity of the proposed model for real alert logs in smart grid, and its average accuracy can be close to 90%.

1 Introduction

The emergence of industrial Internet and smart grid has brought great opportunities to the world's industrial upgrading and development, while it also brings new challenges to its security [1].

In order to possibly prevent potential threats, the security equipments have been deployed in smart grid. Compared with the alert data in the general sense, the alert information in smart grid has the following uniqueness: (1) Before the alert information being reported, it is usually aggregated based on the frequency of the same alert

Z. Jin (✉) · Y. Zhou
State Key Laboratory of Networking and Switching Technology, Beijing University of Posts and Telecommunications, Beijing 100876, China
e-mail: zhpjin@bupt.edu.cn

Y. Liang · L. Shao
NARI Group Corporation, Nanjing 211106, China

X. Jin · P. Kong · Z. Jiang
State Grid Zhejiang Electric Power Co. Ltd., Hangzhou 310007, China
e-mail: zhpjin@bupt.edu.cn

R. Kountchev et al. (eds.), *Advances in Wireless Communications and Applications*,
Smart Innovation, Systems and Technologies 191,
https://doi.org/10.1007/978-981-15-5879-5_23

in a period; (2) When the alert frequency exceeds a certain threshold, a high-level alert is generated. The alert information at this time is very abstract, and the threshold is often set to be very low.

How to accurately find the useful information and concerned devices in large and abstracted alert information is an urgent problem to be solved [2, 3]. In response to this challenge, the alert information should be filtered, aggregated, and analyzed to discover possible attacks on the system [4]. We call the device with a number of such alerts which is far beyond the normal state, the compromised device.

The existed methods of analyzing alerts information are mainly based on learning methods [5, 6] and statistical analysis [7, 8], which are usually used in Internet security analyzing, but not suitable for alerts log in smart grid to find the compromised devices. For example, the e-divisive with medians (EDM) algorithm [8] uses the law of large numbers to find the median over a period to define the state. Because the time sequence for alert logs in smart grids has noise and the length of time sequence for different states is short, its accuracy will be significantly reduced when the EDM algorithm is applied for this case.

In this paper, a compromised device-detection model based on alert logs in smart grid is proposed, which includes the pre-processing module, the roof-detection module, and the peak-detection module. The abnormal states are output by integrating with the results from the roof-detection module and the peak-detection module, and the corresponding devices with respect to causing the abnormal alerts are also returned, which are compromised devices and will help the maintenance expert and system manager to analyze the security risks and threats existed in smart grid.

1. A particular threshold training module is given to automatically calculate the threshold. The module takes the alert time sequence and the number of manually labeled start roofs as input. Three different ratio parameters are set in advance within the module. As the alert time sequence is different, the module calculates three different thresholds based on the three ratio parameters. Based on these three thresholds, three different start roof quantities are detected. By comparing these three different start roof numbers which are close to the number of manually marked start roofs, the output of the threshold training model is the threshold closest to the manual annotation as the final threshold. It avoids manually setting the threshold and also makes the threshold closer to reality.
2. For the transition features between the normal state and the abnormal one, the roof-detection module and the peak-detection module are proposed, which detect the sudden increase and reduce the alert number by the variation range between adjacent time sequence points to determine the change point between states. The roof-detection module is used to detect the roof-type abnormalities, which is divided into two sub-modules: start roof-detection module and end roof-detection module. The peak-detection module is used to detect the peak-type abnormal state, which is caused by a sudden increase. A new decision indicator *acc(accuracy)* is set in our peak-detection module to solve this problem. It has been proved by experience that our proposal can more effectively reflect the relative growth rate of alerts.

3. The parameters of the detection method are determined as the comprehensive optimal parameters under the smart grid alert data set, that is, the threshold is selected at 20%, and the surge rate and the ratio of inflection point are both doubled. Finally, verified with these adjusted parameters, our proposed model's average accuracy can be close to 90%.

2 Compromised Device-Detection Model

In order to get a detecting method which is suitable for alerts log information in smart grid, a compromised device-detection (CDD) model is proposed. The model aims to find the compromised device by analyzing the input alerts logs and outputting the abnormal state for each corresponding device, which is executed by the system manager or maintenance expert to analyze the security risks and threats existing in the smart grid. The CDD model consists of three modules, as shown in Fig. 1, which mainly includes the pre-processing module, the roof-detection module, and the peak-detection module.

Alert logs are the original alert information, which is obtained by reading the central database through the application programming interface (API) interface, and then they are processed into dense alert number sequences via the pre-processing module. The alert logs are divided into many parts according to its source Internet Protocol (IP) address and destination IP address, respectively. For each part, the alerts are counted by some fixed interval time, e.g., day by day, and then the alert number is deleted when it is zero. Finally, the left alert numbers are formed to be a time sequence, which is called the *alert number sequence*.

Consequently, according to above characteristics of the alert number sequence, it is divided into two cases. In our framework, the roof-detection module and the peak-detection module detect these two types of abnormal states, respectively.

In order to detect the roof-type abnormal state, we designed the roof-detection module to capture its start and end boundaries. The module includes two sub-modules, the start roof-detection module and the end roof-detection module.

The details are as follows.

2.1 Pre-processing Module

The pre-processing module takes the original alert information as input, as shown in Table 1 for example, and processes it into a dense sequence which consists of alert numbers within fixed interval time. The alerts are counted by fixed interval time, e.g., day by day, and then the alert numbers for each day are recorded which compose an alert number sequence, and finally, the alert number sequence is reduced by eliminating the zero items to get the outputted dense sequence.

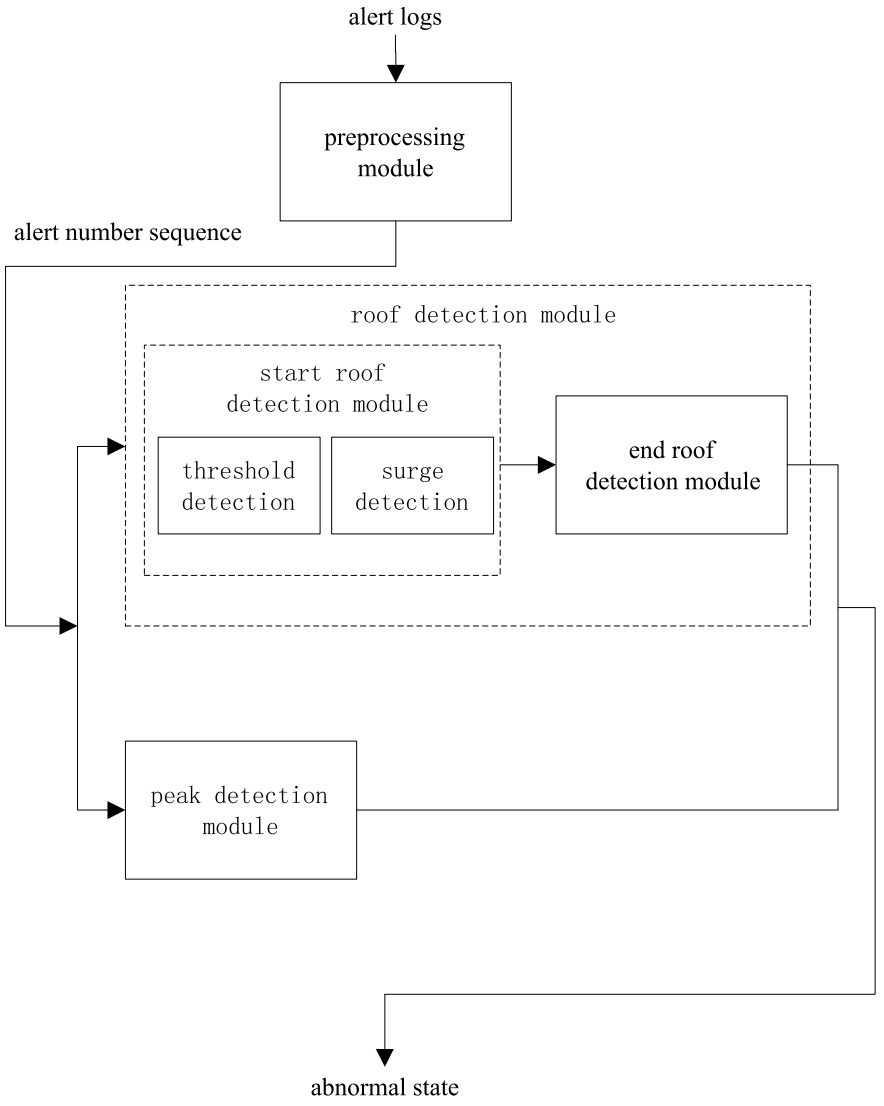

Fig. 1 Model framework

Table 1 An example of original alert information

Warningtime	Content
2018–03–12 19:14:44	There is a large amount of DHCP (Dynamic Host Configuration Protocol) service access or port scan: access from the host such as [*.*.*.*] to the ** port of the destination host [*.*.*.*]
2018–03–09 17:17:30	There is a DDoS event: a DDoS event from the host such as [*.*.*.*] to the **** port of the destination host [*.*.*.*]

2.2 Roof-Detection Module

The roof-detection module is used to detect the roof-type abnormal state. This abnormal state has the characteristic that it will rapidly rise to a much higher number than the steady value, and will continue to stabilize at a higher level for a period of time, and then quickly fall to a stable value. Its framework is shown in Fig. 2 as follows.

Roof detection uses time sequence as the input of the whole module, and passes the time sequence to two detection modules, threshold detection and surge detection. These two sub-modules are responsible for detecting the start boundary of the roof-type abnormal state.

The sequence detected by the start roof-detection module is the input to the end roof-detection module, and the start boundary of roof-type abnormal state is also input. According to the start roof, the end roof-detection module finds the end boundary corresponding to each start roof, and finally outputs the abnormal state set in the form of (*StartRoof*, *EndRoof*).

The roof-detection module detects a roof-type abnormal state for each input time sequence, which contains threshold detection and surge detection. Below, we will expand on the three main modules involved in the roof-detection module: threshold detection, surge detection, and end roof detection.

2.3 Threshold Detection

The threshold detection first detects each element in the sequence with a threshold. If the element is larger than the threshold, the date of the element is considered to be an abnormal start time. The determination of the threshold is obtained by checking the ip-threshold table by the threshold_selection() function. Threshold selection()

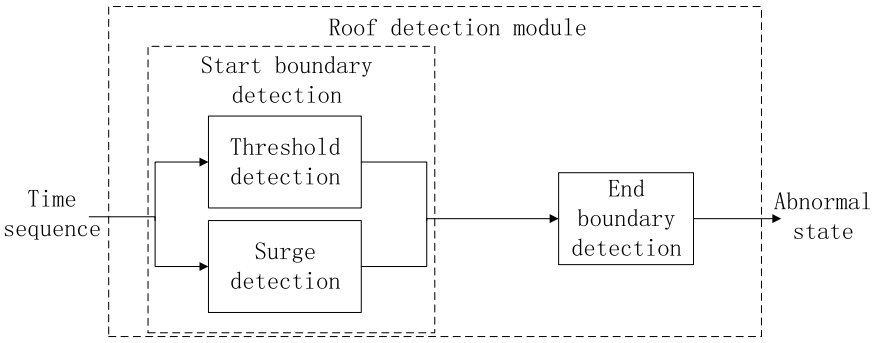

Fig. 2 Framework of roof-detection module

takes the IP address as the input, and searches the threshold corresponding to the IP address through the ip-threshold table.

This ip-threshold table is obtained by training a part of the manual labeling sequence in advance through the threshold training module. This part of work is performed offline.

The threshold training module firstly selects the first half of the alerts total data to generate an alert time sequence, and then, manually marks the number of start roofs in these sequences. This part of the manually marked alert time sequence is the input to the threshold training module. The threshold training module relies on this part of the alert sequence to learn the thresholds for distinguishing between normal and abnormal states.

Three threshold ratios a_1, a_2, and a_3 are selected in advance in the threshold training module. These three ratios are derived from the results of the repeated experiments on alert data. According to a large number of experiments, 10, 15, and 20% are generally taken.

Algorithm 1 threshold training module

Input:sequences S[1…N], corresponding IP IP_set[1…N], the number of start roof n[1…N], threshold ratio a_1,a_2,a_3
Output:threshold t
i ← 0
For s,ip in S,IP_SET:
  i ← i+1
    S_{sort} ←sort the sequence s
    Length ← len(s)
    $threshold_1$←S_{sort}[Length * a_1]
    $threshold_2$←S_{sort}[Length * a_2]
    $threshold_3$←S_{sort}[Length * a_3]
    // Get the number of start roofs for the sequence based on threshold and sequence
    $test\_number_1$[i]←get_roof($threshold_1$, s)
    $test\_number_2$[i]←get_roof($threshold_2$, s)
    $test\_number_3$[i]←get_roof($threshold_3$, s)
    select_threshold[i] ←min_index($test\_number_1$[i], $test\_number_2$[i], $test\_number_3$[i])
    // Select the threshold that is closest to the number of manually marked startroofs and save the threshold in the select_threshold table.
return select_threshold

The threshold training module uses the manually labeled alert sequence and three thresholds as an input to the module. Firstly, the alerts are sorted from large to small and the number of alerts at positions a_1, a_2, and a_3 before the sequence is selected as the threshold. This threshold is entered into *get_roof*(). The get_roof() is used to calculate the number of start roofs for the sequence based on this threshold. The

threshold training module compares the number of manual annotations with the number of start roofs calculated by *get_roof* () based on three thresholds, and selects the result that is closest to the number of manual annotations. The corresponding threshold is recorded in the table for use by the *threshold_selection*() query in the roof-detection module.

2.4 Surge Detection

Similarly, the alert number sequence is sent to the surge-detection module. The module calculates the growth rate of each element and the two elements before and after it. If the growth rate satisfies a small increase and then follows a large increase mode, it is considered to meet the start boundary condition of the roof-type abnormal state. The elements are added to the start roof collection, and then the end roof corresponding to each start is detected.

The outputs of the threshold detection and the surge detection are the start-roof set of the current-detection sequence. There will be a certain number of coincident start boundaries between these two sets. When these two modules are detected, respectively, the outputs are combined and the results are input to the end roof-detection module.

2.5 End Roof-Detection Module

The end roof-detection module finds the corresponding end roof for each start roof in the input sequence. When the end roof detection identifies a start boundary in the sequence, it begins monitoring each subsequent time sequence element, and adds the increment of each element afterwards. If the current element's increase is much larger than the previous increase and decrease mean, then the element is considered to be an end boundary. Because the end boundary has such a feature, its drop in the roof-type abnormal state will remain at a small fluctuation, and when it ends this state, it will end with a large drop. The end roof-detection module is designed to capture such large drops. This large reduction is relative to the previous small fluctuations, so we need to calculate the average of the small fluctuations before determining this large decline. Finally, combined with the start boundary, the end boundary is added to the array of outputs.

Algorithm 2 End roof detection module

```
Input: time sequences S[1…N],start roof B[1…N]
Output: abnormal AB
For s in S:// Take each sequence in the sequence set
    For e in s:// Take each element of the sequence
        If e.date in B: // If the date of finding an element in sequence S is included in B
            st ← e.date
                    n←1
                    avg_acc = e.value – pre(e).value // Take the increase of the current
                    point as the first item of the average increase
                    for j in rest of s:
                        n ← n + 1
                Avg_acc = [avg_acc * (n-1) + j.value – pre(j).value]/n
                If avg_acc << e.value – pre(e).value: // If the increase is much larger than
the average increase and decrease, then it is considered to have reached an end state.
                    For i in B :
                        If i in (st, e.date): // Eliminate the start roof between this set of ab-
normal states
                            Put i out of B
                Put (st, e.date) into AB // Put the combination into the abnormal state
                                Break
return AB
```

2.6 Peak Detection

The peak-detection module is used to detect the peak-type abnormal state, which exhibits a rapid decline after a rapid rise. Unlike the roof-type abnormal state, the peak-type abnormal state does not remain in an abnormal state for a long period.

The peak-detection module detects the time points at the peak in the alert sequence based on the characteristics of the peak-type abnormal state. To choose the rate of increase but not the increase itself to consider the inflection point is because the value of the increase does not reflect the relative situation of this increase in the overall environment. For a different number of IP alerts, this situation may happen: for an IP, the increase is small on a global scale, but it is a large increase for another IP. Therefore, we choose the rate of the increase, which avoids the subjectivity of determining a certain increment as an indicator by a single IP. A new decision indicator *acc(accuracy)* is set in our peak-detection module to solve this problem. To calculate such a point, we propose the following formula:

$$\mathrm{acc} = \frac{|y3 - y_2|}{|y_2 - y_1|} \tag{1}$$

where y_1, y_2, and y_3 are ordinate values for three points $A(x_1, y_1)$, $B(x_2, y_2)$, and $C(x_3, y_3)$, which are three consecutive points in the time sequence, with $x_1 + 2 = x_2 + 1 = x_3$.

3 Experimental Analysis

3.1 Implementation

3.1.1 Data Set

Taking the smart grid real data as an experimental sample, which totally contains 95 items, such as INDEXID; The CONTENT field contains a total of seventy-one types of alerts, such as "sql statement execution time exception," "there are a large number of non-TCP (Transmission Control Protocol)/UDP (Transmission Control Protocol) exception access packets, which may be Internet Control Message Protocol (ICMP) or other application protocol packets," "webcast or Broadcast storms".

3.1.2 Model Effectiveness and Efficiency

From Figs. 3 and 4, we can see that only a small amount of computing resources is needed, except for the initial requirements for system resources. At the peak state, the model also requires less memory resources, and at most, only 45 Mb of capacity. Therefore, the proposed algorithm has a low overall requirement for machine performance and a small burden on the server.

Finally, we test a total of 6155 IPs across the network and collected the results. And then, we compared the results obtained by the proposed algorithm with the

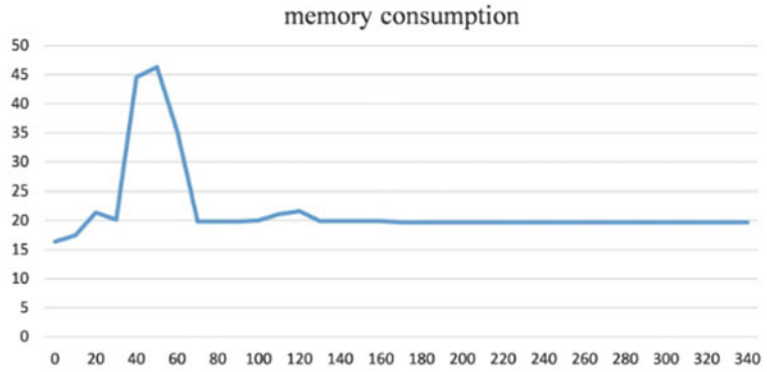

Fig. 3 Memory consumption

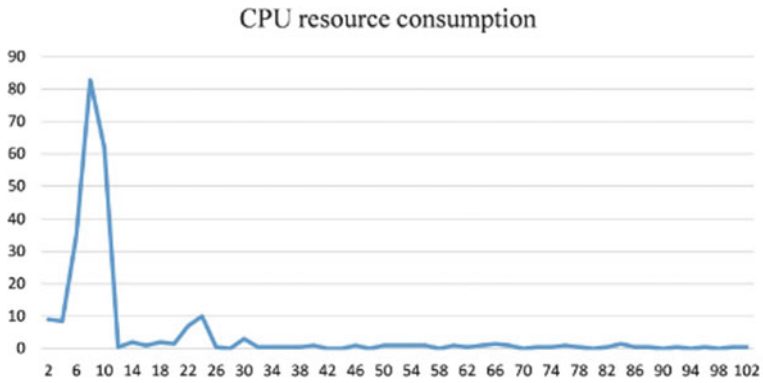

Fig. 4 Central processing unit (CPU) resource consumption

abnormal states which we marked manually. The average detection accuracy of the algorithm is 44,465/50,864 = 87.42%, the recall is 26,184/30,062 = 87.1%, and the precision is 26,288/28,819 = 91.22%.

4 Conclusion

We have analyzed the features of alert data in smart grid and proposed the compromised device-detection model based on statistical analysis. This model, respectively, calculated all the abnormal states of the alert time sequence. Among them, we have designed the threshold training module in order to obtain the threshold better. Three different ratio parameters are set in advance within the module. Moreover, we have made a full experiment to confirm the various parameters in the proposed model and given the comprehensive accuracy under the optimal parameters. In the future, we will conduct further research in the following aspects: analyzing time sequence, modeling different time sequence, extracting features, and implementing automatic analysis of time sequence with different parameters.

Acknowledgements Thanks to State Grid for their support for the data and funding of this project. This research was funded by the Science and Technology Project Funding of State Grid Corporation of China (Research and Application of Network Security Situation Awareness Technology in Power Monitoring System in 2018–2019).

References

1. Li, X., Liang, X., Lu, R., Shen, X., Lin, X., Zhu, H.: Securing smart grid: cyber attacks, countermeasures, and challenges. IEEE Commun. Mag. **50**(8), 38–45 (2012)
2. Zang, T., Yun, X., Zhang, Y.: A survey of alert fusion techniques for security Incident. In: 2008 The Ninth International Conference on Web-Age Information Management. IEEE, pp. 475–481 (2008)

3. Wu, J., Ota, K., Dong, M., Li, J., Wang, H.: Big data analysis-based security situational awareness for smart grid. IEEE Trans. on Big Data **4**(3), 408–417 (2018)
4. Salah, S., Maciá-Fernández, G., Díaz-Verdejo, J.: A model-based survey of alert correlation techniques. Comput. Netw. **57**(5), 1289–1317 (2013)
5. Feng, W., Han, C.: A novel approach for trajectory feature representation and anomalous trajectory detection. In: 2015 18th International Conference on Information Fusion (Fusion), pp. 1093–1099 (2015)
6. Raimondo, M., Tajvidi, N.: A peaks over threshold model for change-point detection by wavelets. Stat. Sinica **14**(2), 395–412 (2004)
7. Chakraborty, G., Kamiyama, T., Takahashi, H., et al.: An efficient anomaly detection in quasi-periodic time series data—a case study with ECG. In: International Work-Conference on Time Series Analysis, pp. 147–157 (2017)
8. Matteson, D.S., James, N.A.: A nonparametric approach for multiple change point analysis of multivariate data. J. Am. Stat. Assoc. **109**(505), 334–345 (2014)

Design and Realization of Trunk Amplifier at 2.5–2.6 GHz

Shiwen Li and Licong Li

Abstract In view of the difficulty of gain control and the problem of self-excitation, a trunk amplifier with automatic gain control and anti-self-excitation is proposed. The system has a high operating frequency, with an uplink operating frequency band of 2500–2570 MHz, a downlink operating band frequency of 2620–2690 MHz, a downlink gain of 45 dB, an uplink gain of 55 dB, a passband ripple of less than 6 dB, a noise coefficient of less than 6 dB, and a voltage standing wave ratio (VSWR) of less than 2. We introduce the main circuits of the system, which includes low-noise amplifier (LNA) circuit, power drive amplifier circuit, power amplifier (PA) circuit, automatic gain control (AGC) circuit, and surface acoustic filter (SAW) circuit. Then, we carried out production and testing of the system. The test results show that the system basically meets the expected requirements. At the same time, it has the characteristics of low cost, controllable gain, and anti-self-excitation. It has great advantages in reducing operation and maintenance costs.

1 Introduction

The trunk amplifier is mainly used to make up for the line loss, which requires small distortion, low reflection loss, and the gain cannot be too high. It mainly includes three parts: a uplink radio frequency circuit, a downlink radio frequency circuit, and a control circuit.

At present, many scholars have conducted in-depth research on the related fields of trunk amplifiers. For example, some scholars have conducted related research on cable television trunk amplifiers [1]. As a key component in the field of mobile communications, many scholars have discussed the research and design of 4G related

S. Li (✉)
Department of Electronics and Information Engineering, Heyuan Polytechnic, Heyuan, Guangdong, China
e-mail: lishiwen1015@126.com

L. Li
Shenzhen Jiams Technology Co., Ltd., Shenzhen, Guangdong, China

R. Kountchev et al. (eds.), *Advances in Wireless Communications and Applications*,
Smart Innovation, Systems and Technologies 191,
https://doi.org/10.1007/978-981-15-5879-5_24

devices [2]. The LNA circuit is the key to achieve high gain and low noise [3, 4]. The trunk amplifier has a high-frequency band, so the system itself is very prone to self-excitation [5]. At the same time, in order to effectively transmit the signal to the terminal, the impedance matching of the system needs to be considered [6]. Based on the consideration of system impedance matching and anti-self-excitation, this paper has designed a low-cost, self-excitation-resistant small trunk amplifier.

2 System Overall Design

The overall block diagram of the trunk amplifier is shown in Fig. 1. This system mainly includes three parts: an upstream radio frequency (RF) circuit, a downstream RF circuit, and a single-chip microcomputer control circuit. The downstream circuit mainly includes LNA, diplexer (DPX), attenuator (ATT) and AMP, on the other hand, the upstream circuit mainly includes ATT, DPX, AMP, and AP. The LNA, PA, and AMP are mainly used to amplify signals, especially LNA has a wide bandwidth, which can effectively suppress noise and improve system gain. Because there is no LNA in the uplink, after the uplink signal enters the main line amplifier through the feeder line, the signal is then sent to the base station by the antenna after being amplified AMP and PA.

There is no PA in the downlink, and the downlink signal is amplified by LNA and AMP. After the signal passes through the multi-stage AMP, the signal is sent to each coverage area through the feeder. The uplink operating frequency band of this system is 2500–2570 MHz, and the downlink frequency band is 2620–2690 MHz. So we choose SAW as our filter, whose center frequency is 2535 and 2655 MHz, respectively. Due to the high gain of the mains amplifier, a single SAW cannot achieve the required out-of-band suppression. Therefore, multi-stage filtering is selected in the uplink and downlink circuits to meet the system index requirements.

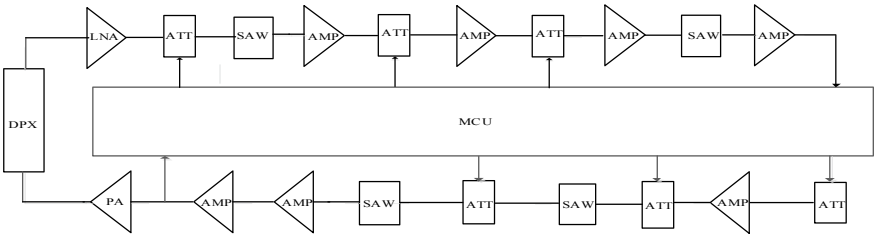

Fig. 1 Overall system diagram

3 Circuit Design

The trunk amplifier circuit mainly includes a low-noise amplifier circuit, a power amplifier circuit, an AMP circuit, an attenuation circuit, an AGC circuit, and a control circuit. We introduce each circuit in detail below.

3.1 Design of LNA Circuit, Drive Amplifier Circuit, and ATT Circuit

The LNA, AMP, and ATT circuits shown in Fig. 2. In this system, LNA selects SGA8343, AMP selects SGA-6489, the upstream SAW filter selects NDF9201, and the downstream SAW filter selects SF9659. The system noise figure is a key index that needs to be considered. We know that the overall noise of the system is mainly determined by the parameters obtained by the selected amplifier, and the noise figure of the first-stage amplifier has the largest influence on the total noise of the system. In our system, the noise figure is less than 6 dB, so we need to choose a better LNA element. Due to the high requirements of the first-level LNA circuit, we selected RF Micro Devices (RFMD)'s low-noise amplifier SGA8343. The operating frequency bandwidth of SGA8343 is 0–6 GHz, the maximum gain at 2.6 GHz is 17 dB, and its noise figure F is 1.1 dB. The specific circuit is shown in Fig. 2, where Q30 is a low-noise amplifier SGA8343, with a total of 4 pins. The LNA's pin 1 is the RF input, pins 2 and 4 are grounded, pin 3 is the RF output and direct current (DC) bias.

The driving circuit is U91 where there are 4 pins in the AMP circuit. The AMP's Pin 1 is the RF input, pins 2 and 4 are ground, and pin 3 is the RF output and DC bias. Q31 and q32 are analog attenuation circuits. When the output power is too large, the power attenuation is realized by controlling the pins LU-AGC and UL-AGC-DC by single-chip microcomputer. UL-RFSAW is surface acoustic wave. The center frequency of its uplink is 2535 MHz, and its downlink center frequency is 2655 MHz.

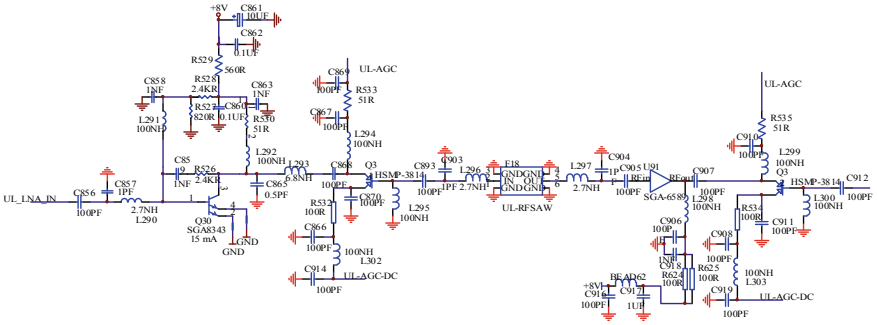

Fig. 2 Low-noise amplifier, drive amplifier, and attenuation circuit

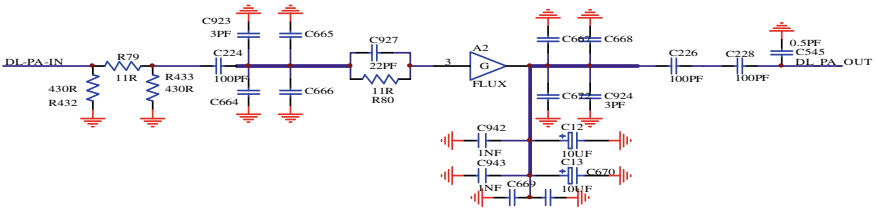

Fig. 3 Power amplifier circuit

3.2 Power Amplifier Circuit

Figure 3 shows a power amplifier circuit. The chip is FLUX, manufactured by Fujitsu Japan. R111, R455, and R456 are π-shaped resistors, and C305, C925, C695, C694, C696, C928, and R112 are input impedance matching networks.

The capacitors C667, C668, C667, C672, C924, C545, C942, C12, C13, C943, C669, and C670 mainly complete high-frequency filtering. C226 and C228 are mainly used to isolate DC.

3.3 The Design of Automatic Gain Control Circuit

Power control technology is mainly accomplished through a feedback mechanism. Automatic level detection compares the output power of the system with a threshold set by the system. If the output power is greater than the threshold, a controllable program is starting to control. It attenuates the circuit by reducing the output power. The attenuation circuit used in this system includes an analog attenuation circuit and a digital attenuation circuit, which cooperate with each other to realize power adjustment. The digital attenuation circuit is mainly used to control the output power of the system. The analog attenuation circuit is mainly used to precisely control the output power of the system.

The system AGC circuit is shown in Fig. 4, and the RF output signal is converted into a DC signal through a detection diode at the RF output terminal, and then the DC signal is sent to the DL-DEC terminal of the LM393. LM393 is a comparator, which can judge whether the voltage of RF signal reaches the threshold value. If the output RF level reaches the threshold value, the signal UL-PD is high. When the microcontrol unit (MCU) detects the signal, it adjusts hsmp-3814 to attenuate the signal, so as to reduce the output power. In addition, the signal fed back from the RF output terminal is sent to another comparator LM1000A, and then the comparator is used to compare whether the RF output signal is large enough. When the signal is large enough, the signal is transmitted to the attenuation circuit through dl-agc-att and f-dl-agc. In this way, the microcontroller and hsmp-3814 can control the output power accurately.

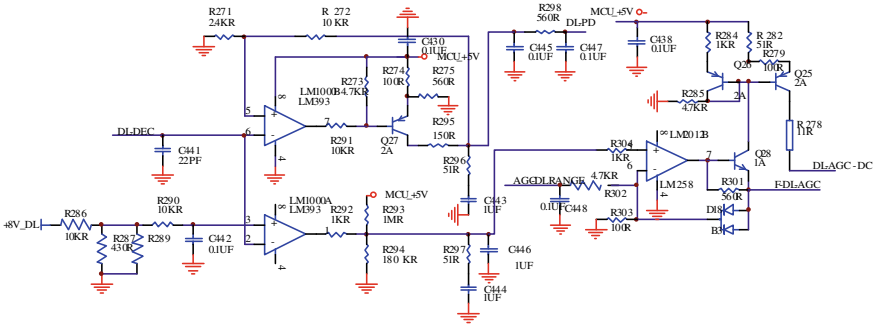

Fig. 4 Automatic gain control circuit

4 Measurement Results

We produced the physical object of the system based on the above circuit diagram. The main modules are divided by separate chambers, which can better prevent self-excitation caused by signal transmission. Each amplifier is bonded to the Cu plate, which provides the good heat dissipation through the heat sink at the bottom of the module. The physical object of the system is shown in Fig. 5 and relevant tests were performed. The test results are shown in Table 1. In the test, the instruments we mainly used were a spectrum analyzer (model: Agilent E4440A), a signal generator (model: Agilent E4436B), a network analyzer, a power supply, and a multimeter.

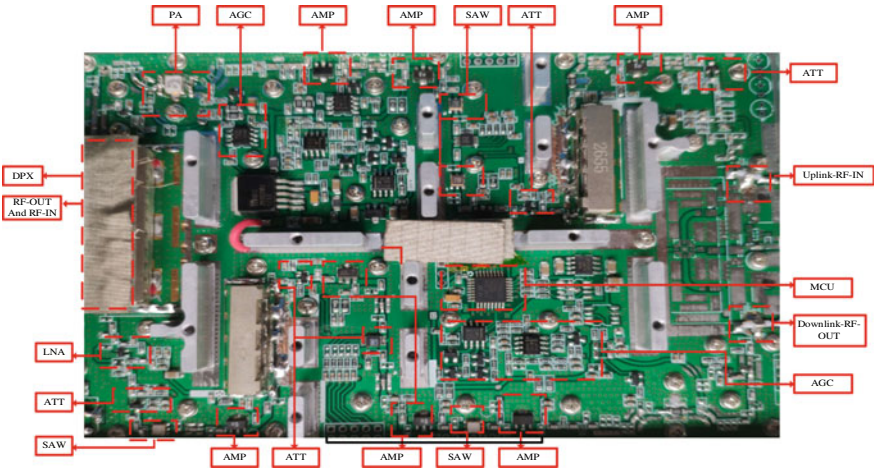

Fig. 5 Photograph of trunk amplifier

Table 1 Test results of trunk amplifier

Test content	Gain (S21)	Passband ripple	Standing wave ratio	Output power
Uplink (2500–2570 MHz)	47.5–54 dB	6.5 dB	1.23–1.78	37 dBm
Downlink (2620–2690 MHz)	39.7–45 dB	5.3 dB	1.72–2.3	28.5 dBm

4.1 Measurement of System S21 Parameters

In this paper, the measurement of parameters mainly includes system S21 parameters, output power, and standing wave ratio. When measuring the parameters of the system S21, you first need to calibrate the network analyzer. During the calibration, the input and output cables are connected to each other. When measuring downlink parameters, the center frequency is set to 2655 MHz and the measurement bandwidth is 180 MHz. In the test, the starting frequency of the network analyzer was set to 2.62 GHz, and the ending frequency was set to 2.69 GHz. The test parameters are the forward transmission channel S21 parameters, and then are adjusted the instrument parameters so that the gain displayed on the screen to be 0 dB. After calibration, the trunk amplifier is connected to the network analyzer.

The downlink test results are shown in Fig. 6. Four marker points are set during the test. The frequency of the first marker is 2.62 GHz, and the gain is 41.785 dB.

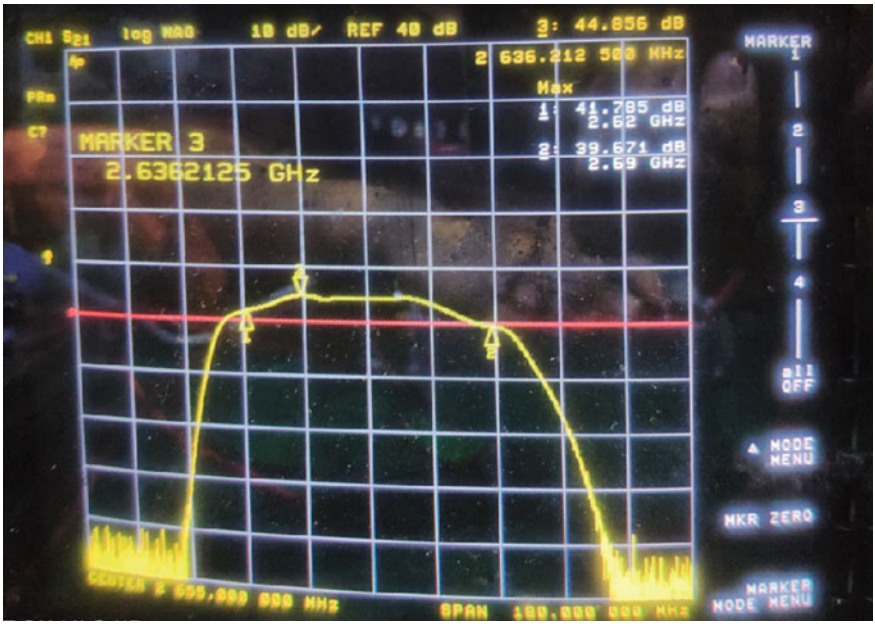

Fig. 6 Downlink S21 parameter

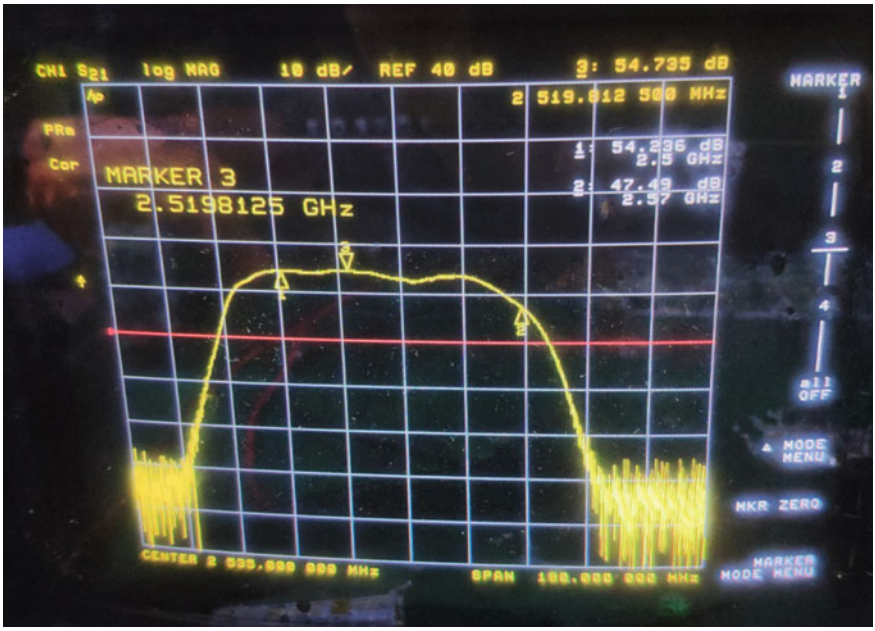

Fig. 7 Uplink S21 parameter

The frequency of the second marker is 2.69 GHz, and the gain is 39.671 dB. The frequency of the third marker is 2.64 GHz, and the gain is 44.856 dB. The maximum gain is about 45 dB, while the minimum gain is 39.7 dB in the frequency range of 2.62–2.69 GHz. The in-band fluctuation is less than 6 dB, so the downlink S21 parameter meets the design requirements.

When measuring the uplink parameters, the center frequency is set to 2535 MHz and the measurement bandwidth is 180 MHz. The uplink test results are shown in Fig. 7. Three marker points were set during the test. The frequency of the first marker is 2.5 GHz and the gain is 54.236 dB. The frequency of the second marker is 2.57 GHz and the gain is 47.49 dB. The frequency of the third marker is 2.52 GHz and the gain is 54.735 dB, the maximum gain of this trunk amplifier in the frequency range of 2.5–2.57 GHz is about 54 dB, while the minimum gain is 47.5 dB. The in-band fluctuation is about 7 dB, and the system gain can basically meet the design requirements.

4.2 System Standing Wave Ratio Measurement

According to relevant requirements, we measured the standing wave ratio of the system by a network analyzer.

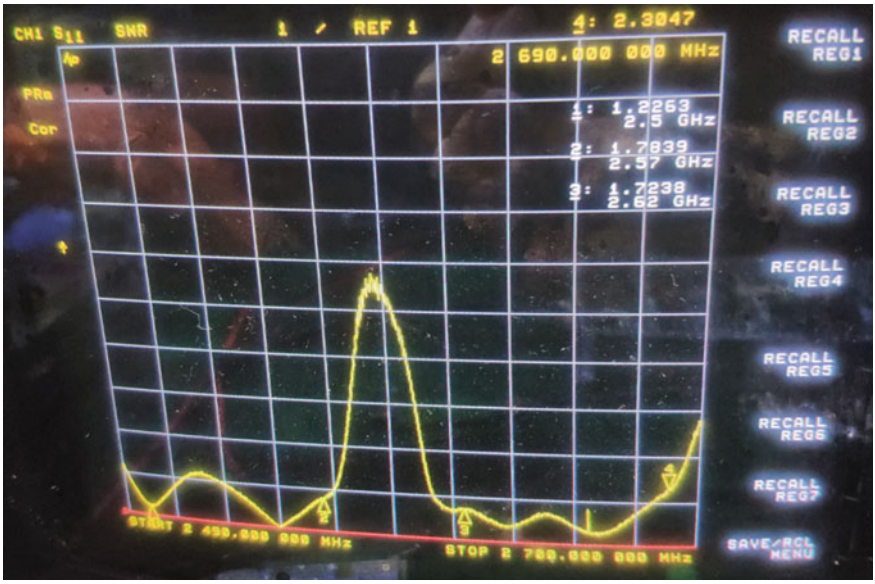

Fig. 8 Standing wave ratio measurement results

The measurement results are shown in Fig. 8. During the test, four marker points were set together. Markers 1 and 2 measure the downlink standing wave ratio, and the markers 3 and 4 measure the uplink standing wave ratio. From the measurement results, it can be seen that the frequency of the first mark is 2.5 GHz, and the standing wave ratio is 1.23. The frequency of the second mark is 2.57 GHz, and the standing wave ratio is 1.78. The frequency of the third mark is 2.62 GHz, and the standing wave ratio is 1.72. The frequency of the fourth mark is 2.69 GHz, and the standing wave ratio is 2.3. It can be seen from measurement results that the standing wave ratio is slightly higher, especially the fourth point. The main reason is that we did not add a cover plate during the test. After we have added a cover plate, if the standing wave ratio is then too high, we can adjust it with proper resistance or inductance.

4.3 Measurement of Downlink Output Power

Finally, the output power of the output system is tested. During downlink power measurement, the signal generator generates a signal with a frequency of 2.655 GHz and its output amplitude is −6 dBm. The test is performed by a spectrum analyzer. The output power is approximately 28.5 dBm by test, which is the maximum output power. If we increase the input power by adjusting the signal generator at this time, we will find that the output power is no longer increasing depending on increases of the input signal. It means that the power has been controlled to a fixed value.

During uplink power measurement, the signal generator generates a signal with a frequency of 2.535 GHz. The output power is about 37 dBm, which is the maximum uplink output power.

5 Conclusion

In this paper, a trunk amplifier is designed. The system consists of RF circuit, MCU control circuit, AGC control circuit, and ATT circuit. The whole system uses LNA, SAW, and MCU to prevent self-excitation. At last, we make and test the trunk amplifier. From the test results, the system achieves our initial design goal and can be directly applied in the actual project.

References

1. He, T.P., Wen, G.J.: Design of high-performance broadband CATV trunk amplifier. Video Eng. **35**(24), 42–44 (2011)
2. Lu, Y.W.: A novel harmonic suppression compact power amplifier for 4G wireless LTE system. Chin. J. Electr. Dev. **41**(5), 412–415 (2018)
3. Rajendiran, P., Srinivasan, R.: Single-event radiation performance analysis of junction and junctionless FET-based low-noise amplifiers. J. Comput. Electron. **18**(4), 1162–1172 (2019)
4. Ahn, C.H., Kim, Y.H.: Design and realization of low cost 10 W power amplifier module at 7.9–8.4 GHz. IEICE Electron. Exp. **19**(15), 1–9 (2018)
5. Wang, P., Wang, M.Q.: Research on echo cancellation algorithm of adaptive repeater based on LMS. Telev. Technol. **37**(11), 155–158 (2013)
6. Saberkari, A., Ziabakh, S.: Active inductor-based tunable impedance matching network for RF power amplifier application. Integ. VLSI J. **52**(C), 301–308 (2015)

Automated Home Safety Through IoT

Sangam Malla, Prabhat Kumar Sahu, Priyam Patnaik, and Srikanta Patnaik

Abstract The life of every person is getting simplified by the continuous development of different technologies. The age of using manual systems is gone. Now, everyone is dependent on automatic systems. For this, nowadays, the Internet of thing (IoT) is playing a vital role in making things easier and simpler for us. It acts as a developing network by considering a number of objects which can share information among each other and fulfill our work. A huge number of applications are coming forward in this technology. One of the applications of IoT is home-automated system. IoT works more efficiently to save electric consumption. It uses many wireless devices for controlling the functioning of wireless devices used in it. All the gadgets or nodes used in home automation are controlled remotely. All the home appliances were controlled using this automation technology. A large number of wireless sensors are used to detect the room temperature, leakages of gas, short circuit, etc. All these sensors work together and communicate with each other using messages by GSM and then send it to the local-based server installed in the house. Thus, the server coordinates all the sensors to make the home fully automated.

S. Malla · P. K. Sahu · P. Patnaik · S. Patnaik (✉)
Department of Computer Science and Engineering, Siksha O Anusandhan University, Bhubaneswar, Odisha, India
e-mail: srikantapatnaik@soa.ac.in

S. Malla
e-mail: sangam.malla2015@gmail.com

P. K. Sahu
e-mail: prabhatsahu@soa.ac.in

P. Patnaik
e-mail: priyamdaspatnaik@gmail.com

R. Kountchev et al. (eds.), *Advances in Wireless Communications and Applications*,
Smart Innovation, Systems and Technologies 191,
https://doi.org/10.1007/978-981-15-5879-5_25

1 Introduction

The concept of home-automated system was heard only theoretically in around 1970s. But this concept came practically by using the concept of IoT. IoT helped to bring this concept fully implemented in real world where the people will not only imagine it but also can experience the real implementation. Even IoT brought up several methods of current safety standards. The flexibility, safety issues, energy consumption issues, etc., made the use of IoT more popular.

In this paper, we have discussed of communicating with the home appliances through some messages when we are at some far distance from home. We have also discussed of how to save the home from any accidents like fire, gas leakage, etc. The project objective is to detect and inform the owner if there will be any chances of accidents inside the home. It mainly emphasizes on room temperature, detecting fire, or gas leakage like LPG, etc. [1]. It works by taking the help of many sensors who will detect any abnormality and will inform the owner through SMS and if possible will take necessary action. For example let us say if the sensors detect that there is any increase in temperature, then it will check for what reason the temperature is increasing and if the sensors will find a drastic increase in room temperature then it will send a SMS to the registered mobile number. The owner after receiving the alert message can switch off the appliances of the house through the cell phone no matter wherever may be the owner at any location. So the main objective of the paper is to examine different criteria's like temperature, any gas leakages or fire then it will take preventions to save the house as well as people as compared to other older systems.

2 Literature Review

A lot of research has been done on home-automation systems, a number of techniques had been used for making a number of improvements in automating the home appliances. The motive behind making home automation is to control the home appliances remotely irrespective of the distance. By taking the help of Internet, the appliances are connected to each other and communicate with each other [2]. And through this project, we can also monitor and control the accidents that are likely to occur in our daily life like fire in house, gas leakages, etc. Through the help of sensors, the abnormality of the home is detected and informed to the owner to take necessary action. The people of modern era want everything under their fingertips. And the security of home and its appliances are very important for the owners. They always try to monitor and control their home appliances being at any location [3]. The common problem of people is that they forget to switch off the appliances when they are going out somewhere. So by using IoT technologies, we can easily switch on or switch off the home appliances through our cell phone using Internet.

3 Proposed System

The system works by taking the help of different sensors installed at different places inside or outside the house to monitor the changes or check for any abnormality in the house. All the sensors are connected to a server which is installed locally. The sensors communicate with each other within the network and work accordingly [4]. The maximum and minimum values of the sensors are set and displayed on the monitor. If the values exceed the set values of the sensors, then it is estimated that there is some abnormality faced by the sensors of the network. And the SMS regarding the abnormality is sent to the owner, and the owner can take necessary action [5] as shown in Fig. 1.

Sensors for monitoring and controlling temperatures: The system contains some sensors that will monitor the temperature of the appliances. The output of the device is given in terms of resistance current or voltage. To connect the sensors with the microcontroller, the sensor's output is converted to digital form [6]. One of the most common and well-known temperature sensors is LM35. This sensor gives the result in degree Celsius. So the voltage output of the device or sensors increases with the increase in degree Celsius and decreases with the decrease in degree Celsius.

Sensors for monitoring and controlling fire: The system contains some fire sensors that will detect the weak DC signals of the appliances that were sent to the igniters through the AC power. These sensors consist of some IR sensors, some comparators, and LED. At a range of about 700 nm or more, the flame or wavelength can be

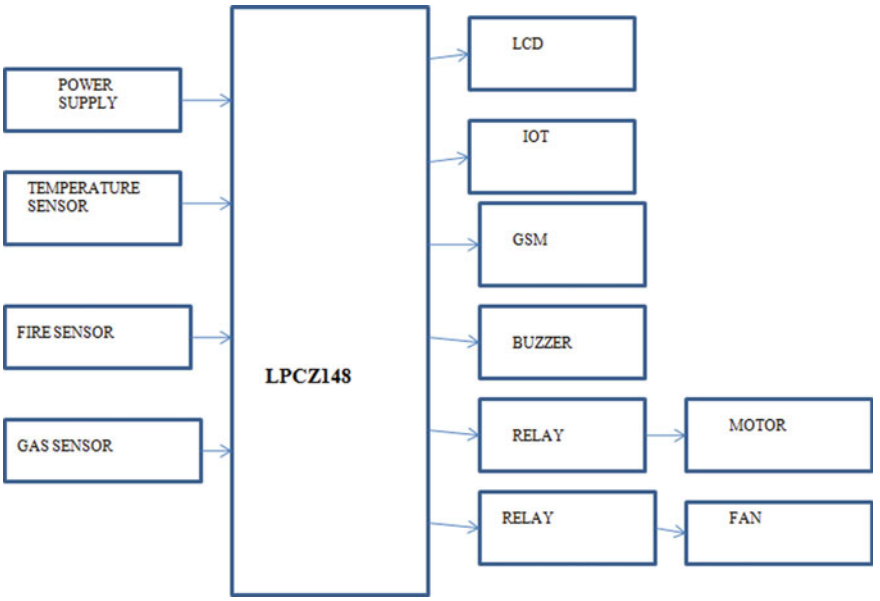

Fig.1 Block diagram of proposed automated security system

detected. The more the distance, lighter is the flame, which means they are inversely proportional. The sensors connected to the microcontroller will direct the signal to a motor which will get ON when any fire is detected and at the same time, an alert message is sent to the registered mobile number [7].

Sensors for detecting GAS leakages: The system contains some sensors which are used to detect any type of GAS leakages, as it is the more important area for safety system. These sensors are able to detect LPG, some propane, smokes, and H2 gases within a very quick response time. These sensors are used to detect some of the dangerous or flammable gases. When the gas leakages are detected, it delivers an alarm for informing the owners about the accidents that can happen. Some of the sensors are also used to detect the concentrations of different gases which are volatile in nature.

Communicating through GSM: One of the globally recognizable standard in digital data communication is GSM. GSM is widely used to transfer data among each node through voice. As in this project, we have used around 51 numbers of frames and around 26 number of frame structure. And the data rate used in their communication is around 9.6 kilobits per second. The microcontroller communicates with each other by sending messages. Time division multiple access is used to break the frequencies into different time slots. The benefit of using GSM is that multiple users can use the same frequency channel for their communication without any traffic congestion. GSM also takes the help of SIM card for Internet connection so that they can communicate with the microcontroller as shown in Fig. 2. Wireless devices like Wi-Fi: As we are dealing with a system that runs wirelessly, so there must be a powerful wireless device that can help the electronic gadgets of the system to communicate with a broad bandwidth without any traffic congestion. In this case Wi-Fi brings a solution for a smooth flow of data among the devices. Wi-Fi works together with Bluetooth to bring forward a new dynamic system.

4 Simulation Result

The entire system was designed and installed as per the flowchart we have designed. All the stimuli were taken under a controlled surrounding to avoid any type of accidents. According to our flowchart as shown in the flowchart figure, first the temperature of the room is tested and checked whether the devices are working properly or not, similarly fire and LPG are also tested for checking the working of the devices. The abnormalities were detected by the sensors and messages were sent to the user for necessary action. The microcontrollers attached in the system also worked properly and the values were displayed accordingly in the LCD. Detector abnormalities like motor sprinkler and buzzer worked perfectly at the time of their action.

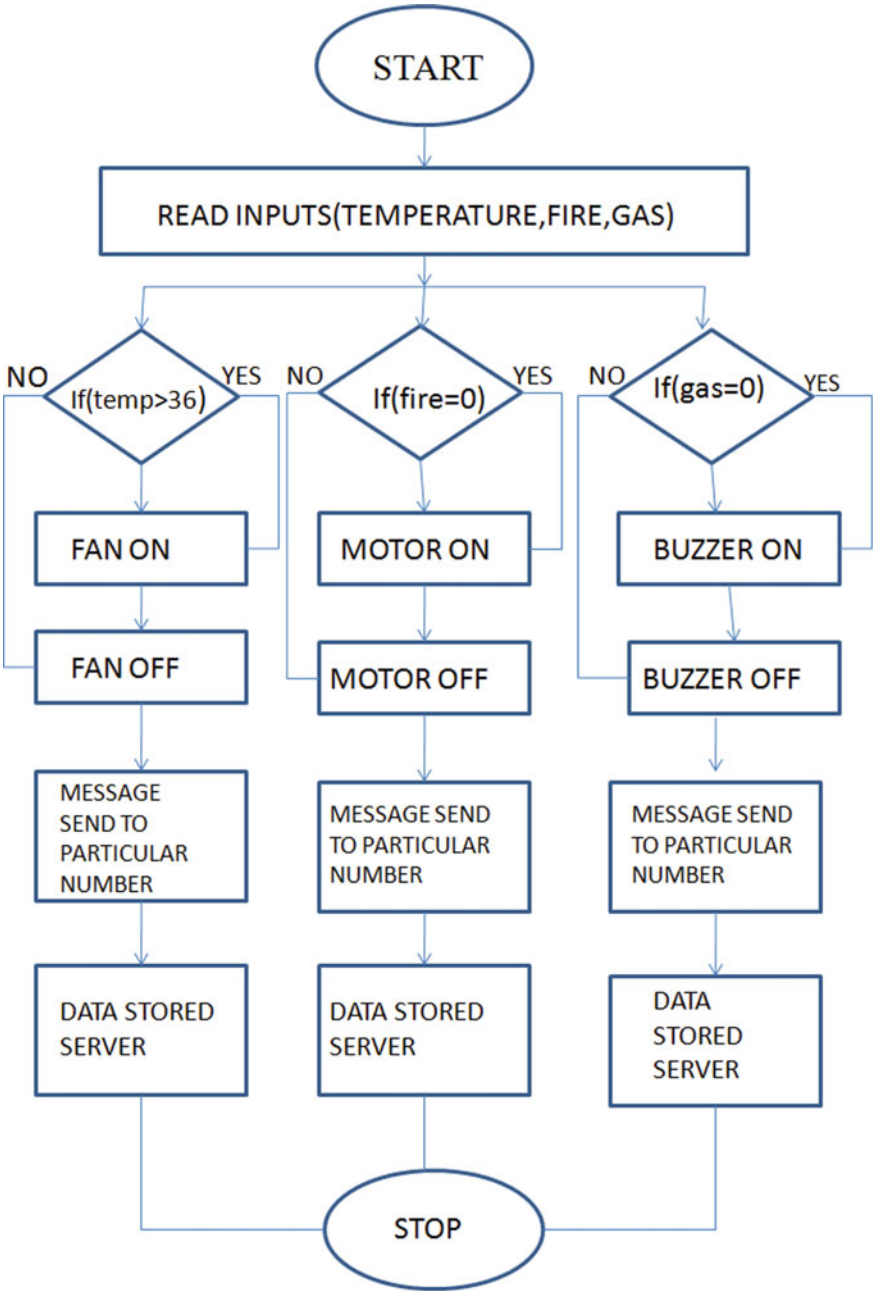

Fig. 2 Flowchart of the proposed system

5 Comparison with Other Systems

a. As compared to previous home-based automatic systems like "Smart Gas Level monitoring," this project can not only detect the gas leakages but can also take necessary action to prevent fire.
b. If we will compare the "wireless home automation system using IoT algorithm," then in that system, the home automation is not carried out by taking so many sensors to prevent any mishaps. But, in this system, we have taken temperature sensor, gas sensor, and fire sensor to prevent any mishaps.
c. In comparison with the system of "Home Automation using Cloud Network and Mobile Devices," our system has local servers installed in nearby areas so that it will not take much time to save and retrieve the data from the cloud. Thus, our system will work faster.
d. If we will compare with other systems older than 2016, then the sensors used in our system are quite better, faster, and cheaper. Our system sensors work much accurately and perfectly than older systems.

6 Conclusion

Through this paper, we have discussed about many safety issues that can occur in a home. We tried to find out some solutions regarding the accidents that may happen inside the house. We included a number of devices in our project in order to bring safety smartly. Devices like detectors, microcontrollers, communicating devices, and techniques were used to bring out the safety issues solution through this paper. The advantages of the proposed system were already discussed, comparison with other systems was also done which will have definitely a good impact on the researchers.

References

1. Keshamoni, K., Hemanth, S.: Smart gas level monitoring, booking & gas leakage detector over IoT. Int. Adv. Comput. Conf. IEEE (2017)
2. Mihalache, A.: Wireless home automation system using IoT. Informatica Economica. Academy of Economic Studies—Bucharest, Romania **21**(2), 17–32 (2017)
3. Dhole, S.N.S., Mohire, P.S., Naik, N.P., Ratnaparkhi S.C.: Home automation using cloud network and mobile devices. N.S Department of Computer Engineering, 44. Vidyanagari, Parvati, Pune-411009, India University of Pune
4. Nakamura, Y., Arakawa, Y., Kanehira, T., Fujiwara, M., Yasumoto-SenStick, K.: Comprehensive sensing platform with an ultra tiny all-in-one sensor board for IoT research. J. Sens. **2017**, 16 Article ID 6308302 (2017)
5. Kodali, R.K., Jain, V., Bose, S., Boppana, L.: IoT based smart security and home automation system. In: International Conference on Computing, Communication and Automation (ICCCA)'2016, pp. 1286–1289 (2016)

6. Matlak, S., Bogdan, R.: Reducing energy consumption in home automation based on STM32F407 microcontroller. IEEE (2016)
7. Win, S.Z., MinHtun, Z.M., Tun, H.: Smart security system for home appliances control based on internet of things. IJSTR **5**(6) (2016)

The Forecast Study of Sanya Tourism Income Based on Fuzzy Time Series Forecasting Model F5

Wang Haifeng, Hu Yaqi, Li Jinxia, and Wang Hongxu

Abstract Using the data that include the past data, the different rate of past data and the different rate of past data's different rate and relying on the inverse fuzzy number function and the predictor function we built, we preliminarily establish the theoretical framework of the F5, the set of fuzzy time series forecasting model. F5(μ) is one common element of the F5, and also it is the predictor function. We used F5(0.000001), a common prediction model, to study the problem about the forecast of tourism income in Sanya. F5(0.000001) offers a new approach to the problem about the forecast of the fuzzy time series.

1 Introduction

Fuzzy set theory provided a new and powerful tool for studying the uncertainty problem in 1965 [1]. In 1993, in [2] was established the first fuzzy time series forecasting model using fuzzy set theory, and a classic case was studied by using it was a prediction problem about the registrations number studied by University of Alabama from 1971–1992. In 2007, in [3] was proposed and used inverse fuzzy number to build fuzzy time series forecasting model, and in 2009, in [4] was improved [3] and was increased the prediction accuracy to a certain extent. In 2012, in [5] was further improved the fuzzy time series forecasting model based on the inverse fuzzy numbers and was proposed a highly accurate prediction model; then taking into account the classic cases was got that AFER = 0.3406% and MSE = 9169, which led to an unprecedented level of accuracy. Wang et al. [6, 7] proposed a fuzzy time series forecasting model based on inverse fuzzy numbers, one of which (the prediction model) [7], had some prediction accuracy improvement. On the basis of them, the concepts of the fuzzy number function, the inverse fuzzy number function, and the predictive function were proposed. F5(μ) ($\mu \in (0,1)$) is the general element

W. Haifeng (✉) · H. Yaqi · L. Jinxia · W. Hongxu
College of Computer Science and Technology,
Hainan Tropical Ocean University, Sanya 572022, China
e-mail: wyfxxz@163.com

R. Kountchev et al. (eds.), *Advances in Wireless Communications and Applications*,
Smart Innovation, Systems and Technologies 191,
https://doi.org/10.1007/978-981-15-5879-5_26

of F5 and is also the predictor of the model; F5(0.000001) is a common forecasting model for F5.

The Fuzzy set theory and time series prediction model are widely used in all aspects [8, 9], and have achieved good results. In this paper, the forecasting model was used to study the forecast of tourism income in Sanya from 2006 to 2018, and the prediction accuracy of AFER = 0.000083% and MSE = 0.000001 is obtained. When we treated 2018 as an unknown year, we used forecasting rules of F5(0.000001) and F5(3-3-1-4) to forecast the tourism income for 2018, and the smallest predicted error rate of the predictive value and real data was 9.81%. Therefore, when applied to study the forecast of Sanya tourism income of the unknown year 2019, the prediction accuracy should have higher expectations.

2 Basic Concepts

This article uses the following basic concepts and formulas.

Definition 1: If the past data domain is $Z = \{Z_1, Z_2, \ldots, Z_n\}$, then the formula of the different rate in the year i is $U_i = (Z_i - Z_{i-1})/Z_{i-1}$.

Definition 2: If the different rate domain is $U = \{U_2, U_3, \ldots, U_n\}$, then the formula of the different rate of different rate in the year i is $V_i = (U_i - U_{i-1})/U_{i-1}$.

Definition 3: If the different rate domain is $U = \{U_2, U_3, \ldots, U_n\}$, and the different rate domain of different rate is $V = \{V_1, V_2, \ldots, V_n\}$, then $\beta_i(\mu) = \frac{\mu+1}{\mu/U_{i-1}+1/V_i}$, $\mu \in (0, 1)$ is defined as the fuzzy number function on the domain U and V, where U_{i-1} is the different rate of year $(i-1)$, and V_i is the different rate of the different rate of the year i; μ is defined as the membership rate of the different rate U_{i-1}, and 1 is the membership rate of the different rate V_i of the different rate.

Definition 4: If the different rate domain is $U = \{U_2, U_3, \ldots, U_n\}$, and the different rate domain of the different rate is $V = \{V_3, V_4, \ldots, V_n\}$, then

$$\alpha_i(\mu) = \frac{\mu + 1}{\beta_i(\mu)} = \frac{\mu + 1}{\mu/U_{i-1} + 1/V_i}, \quad \mu \in (0, 1) \tag{1}$$

is defined as the inverse fuzzy number function of the fuzzy number function $\beta_i(\mu)$ on the domain U and V, where U_{i-1} is the different rate of year $(i-1)$, and V_i is the different rate of the different rate of the year i; μ is defined as the membership rate of the different rate U_{i-1}, and 1 is the membership rate of the different rate V_i of the different rate.

Definition 5: We use the following test formula: Mean Square Error (MSE) = $\frac{1}{n}\sum_{i=1}^{n}(X_i - Z_i)^2$; Prediction Error Rate: $|X_i - Z_i|/Z_i$; Average Forecasting Error Rate (AFER) = $\frac{1}{n}\sum_{i=1}^{n}|X_i - Z_i|/Z_i$, where X_i is the predicted value of year i, and Z_i is the past data value of the year i.

3 The Set of Prediction Models Represented by F5

1. Establishment of the predictive function F5(μ).

Definition 6: We define the predictor function on $U = \{U_2, U_3, \ldots, U_n\}$ of the past data, and $V = \{V_3, V_4, \ldots, V_n\}$ of the different rate:

$$X_i(\mu) = Z_{i-1} \times \left[1 + (1 + \alpha_i(\mu))U_{i-1}\right] \tag{2}$$

where $\alpha_i(\mu)$ is the inverse fuzzy number function of year i, as the inverse fuzzy number function (1), and $U_{i\text{-}1}$ is the different rate of the past data for year $(i - 1)$, and V_i is the different rate of the different rate of year i, and μ is called the membership rate of the different rate $U_{i\text{-}1}$, and $X_i(\mu)$ is the predictor function of past data for year i, and $Z_{i\text{-}1}$ is the past data for year (i-1).

2. Application steps of F5(μ). For the one value of the membership μ, $\mu \in (0, 1)$, we can establish the predictive function F5(μ), as (1) and (2), then we can use F5(μ) to perform time series analysis as follows:

   Step 1: Enter the past data of the time series prediction;
   Step 2: Enter the domain system (enter Z, U, V);
   Step 3: Write the predictive function F5(μ);
   Step 4: Apply F5(μ) to calculate the predicted value of past data;
   Step 5: Use prediction rules of F5(μ) for the predicted values for the unknown years;
   Step 6: Use the prediction rules of F5(μ) for the predicted values for the unknown year and F5(μ) to calculate the predicted value for the unknown year;
   Step 7: Decision (get a sort of predictions of unknown year's data).

   In fact, when a value of $\mu \in (0, 1)$ is determined, a time series prediction model F5(μ) with the application steps above can be obtained, so we get that:

Theorem 1: When determining a value of $\mu \in (0, 1)$, the predictive function F5(μ) is also a time series prediction model.

3. F5 represents a set of fuzzy time series prediction models. Theorem 1 suggests that when we determine a value of $\mu \in (0, 1)$, we can get a time series prediction model F5(μ). So, we further get that:

Definition 7: When determining a value of $\mu \in (0, 1)$, a time series prediction model F5(μ) can be obtained. If we take each value in the interval (0,1), we obtain a series of time series prediction models F5(μ). The sum of all the time series prediction models F5(μ) is defined as the set of Fuzzy Time Series Forecasting Model 5 (FTSFM 5), which is abbreviated as F5 and its general element is F5(μ). F5(μ) represents not only the time series prediction model but also the predictive function of the model.

Because the prediction function F5(μ) is based on the inverse fuzzy function (1), FTSFM 5 is a set of time series prediction models based on inverse fuzzy functions.

FTSFM 5 is the general forecast about time series prediction. Thus, FTSFM 5 is actually a set of time series prediction models.

4 Predictive Rule of F5(0.000001) for Unknown Years

Because there is a lack of the difference rate of the difference rate of the unknown historical data in the domain system, the prediction formula cannot be used directly to predict the historical data of the unknown years. Assuming that the historical data of the unknown year are related to the historical data of the previous years, the prediction rule of F5(0.000001) is established on the basis of the historical data of the unknown years.

1. F5(3-h-1-h + 1) Predictive Rule.

Definition 8: (F5(3-h-1-h + 1) Predictive Rule) Suppose the historical data of the unknown year are related to the historical data of the previous years, and it is necessary to calculate the forecast value of the data in year K.

From the historical data, the difference rate of the difference rate in the first 3 years k-3, k-2, k-1 of k were found out as $V_{\boldsymbol{k\text{-}3}}$,$V_{\boldsymbol{k\text{-}2}}$,$V_{\boldsymbol{k\text{-}1}}$.

Calculate:ρ=$\{\max\{V_{k\text{-}3}, V_{k\text{-}2}, V_{k\text{-}1}\} - \min\{V_{k\text{-}3}, V_{k\text{-}2}, V_{k\text{-}1}\}\}/h$; use parameters separately, $U_{k\text{-}1}$ and $V_1 = \min\{V_{k\text{-}3}, V_{k\text{-}2}, V_{k\text{-}1}\}$; $U_{k\text{-}1}$ and $V_2 = \min\{V_{k\text{-}3}, V_{k\text{-}2}, V_{k\text{-}1}\} + \rho$; $V_{k\text{-}1} = \min\{V_{k\text{-}3}, V_{k\text{-}2}, V_{k\text{-}1}\} + (h\text{-}1)\rho$; $V_k = \max\{V_{k\text{-}3}, V_{k\text{-}2}, V_{k\text{-}1}\}$;

And for $Z_{k\text{-}1}$, using the predicted formula of F5(0.000001), the obtained values are in small to large order, which is the smallest forecast value and the smaller forecast value of the historical data of the unknown year,… the bigger forecast value, the biggest forecast value. Where the value of the parameter h is standard: in all the predicted values, the predicted error rate between the real data and the predicted value should be less than 1%. This predicted rule is called F5(3-h-1-h + 1) predicted rule.

2. Decision-making method of the predictive value. The first decision-making method: It is same sort of smallest, smaller,…, larger, largest that the recommended sort of forecasted values of unknown year k and the prediction error rate of the predictive value and the actual historical data in the known year $(k - 1)$.

The second decision-making method: a sort is determined by decision makers themselves according to experience or objective situation.

5 The Forecast Study of Sanya Tourist Income

This section uses F5(0.000001) to study the forecast of Sanya tourist income from 2006 to 2018.

1. Enter historical data: The historical data of the tourist income in Sanya from 2006 to 2018 are shown in Table 1.
2. Input domain system: According to Table 1, tourist income domain: Z is the different rate domain of the tourist income and U is the different rate domain of the difference rate of the tourist income V.
3. Show the predictive formula for F5(0.000001). As F5(0.000001) is the element of F5, the predictive formula is:

$$X_i = Z_{i-1} \times \left[1 + (1 + \alpha_i)U_{i-1}\right], \alpha_i = \frac{0.000001 + 1}{\frac{0.000001}{U_{i-1}} + \frac{1}{V_i}} \tag{3}$$

where X_i is the predicted value of the annual tourist income in year i, $Z_{i\text{-}1}$ is the tourist income in year (i-1), α_i is the inverse fuzzy number, $U_{i\text{-}1}$ is the different rate of tourist income in year $(i - 1)$, V_i is the different rate of the different rate of the tourist income; $= \mu 0.000001$ is the membership degree of the different rate $U_{i\text{-}1}$.

4. Forecasting Sanya Tourism Income from 2006 to 2018 with F5(0.000001). Applying formula (3) of F5(0.000001), calculate the forecast value of the tourist income in 2008 ~ 2018, test $(X_i - Z_i)^2$ and $|X_i - Z_i|/Z_i$ to fill in Table 1. We see the MSE is only 0.000001, the AFER of only 0.000083% is very small, and the accuracy is very high.
5. Apply prediction rule of F5(3-3-1-4) to Forecast Sanya Tourism Income

Table 1 Forecasting tourist income of Sanya with F5(0.000001) (billion yuan)

Years	Z_i	U_i	V_i	X_i	$(X_i - Z_i)^2$	$\lvert X_i - Z_i\rvert/Z_i$
2006	65.40					
2007	80.11	0.2249				
2008	91.05	0.1366	-0.3929	91.0500	0.000000	0.000000
2009	103.77	0.1397	0.0230	103.7700	0.000000	0.000000
2010	139.64	0.3457	1.4743	139.6398	0.000000	0.000001
2011	160.71	0.1509	-0.5635	160.7099	0.000000	0.000000
2012	192.22	0.1961	0.2994	192.2200	0.000000	0.000000
2013	233.33	0.2139	0.0908	233.3300	0.000000	0.000000
2014	269.73	0.1560	-0.2706	269.7300	0.000000	0.000000
2015	302.31	0.1208	-0.2257	302.3100	0.000000	0.000000
2016	322.40	0.0665	-0.4498	322.3999	0.000000	0.000000
2017	406.17	0.2598	2.9099	406.1673	0.000007	0.000007
2018	514.73	0.2673	0.0287	514.7300	0.000000	0.000000
AFER						0.000083%
MSE					0.000001	

(a) Forecast tourism income of 2018. If 2018 is assumed as an unknown year, we take $h = 3$, apply the prediction rule of F5(3-3-1-4) to forecast the tourism income of the unknown 2018. From Table 1, we take $Z_{2017} = 406.17$, and apply the formula (3) of F5(0.000001) to calculate. The obtained values are ranked from small to big, which is the predicted value (PV) of the tourism income in the unknown 2018, as shown in Table 2. According to Table 2, the forecasted value of the 2018 tourism income and the forecasted error rate with real data are sorted from small to large as follows:

(b) Forecast tourism income of 2019. Year 2019 is really unknown. We take $h = 3$, and apply the prediction rule of F5(3-3-1-4) to forecast the tourism income of 2019. From Table 1, according to 4.1, is calculated ρ=1.1199. The parameters are used separately: $U_{2018} = 0.2673$ and $V_1 = -0.449819$, $V_2 = 0.670089$, $V_3 = 1.7899969$, $V_4 = 2.909904$, and is taken $Z_{2018} = 514.73$; then we apply the formula (3). The obtained values are ranked from small to big, which are the predicted values of the tourism income in the unknown 2019, as shown in Table 3.

According to the first decision-making method (Table 2), the rank of the predicted value of the tourist income is got. It is the recommended rank of the tourist income for 2019. According to the second decision-making method, the rank is determined by decision maker themselves, according to experience or objective situation.

Table 2 Apply F5(3-3-1-4) to forecast tourism income of 2018 in Sanya

The predicted type	The predicted value	The real value	$\lvert X_{2018}-Z_{2018}\rvert/Z_{2018}$ (%)	Rank
Smallest	464.23	514.73	9.81	1
Smaller	582.42	514.73	13.15	2
Larger	700.61	514.73	36.11	3
Largest	818.80	514.73	59.07	4

Table 3 Apply F5(3-3-1-4) to forecast tourism income of 2019 in Sanya

The predicted type	The predicted value in 2019	The real value in 2018	$\lvert X_{2019}-Z_{2018}\rvert/Z_{2018}$ (%)	Rank
Smallest predicted value	590.42	514.73	14.71	1
Smaller predicted value	744.49	514.73	44.64	2
Larger predicted value	898.56	514.73	74.57	3
Largest predicted value	1052.63	514.73	104.50	4

6 Conclusions

The fuzzy number function, the inverse fuzzy number function, and the prediction function are put forward. The basic theoretical framework of F5 is preliminarily established. F5 is a set of fuzzy time series forecasting models. F5(0.000001) is one of the commonly used prediction models. The faced historical data of forecasting problem of the time series can be used without any rule. It has the forecast function of historical data and has the function of predicting the unknown year data when combined with F5(3-h-1-h + 1) prediction rules. For each prediction value of an unknown year data, a method of recommended sorting and a sort of self-determination are given. It is a direction of future research to establish what is the more practical forecasted rule of the unknown year data. F5(0.000001) gives a new method for the problem of forecasting time series.

Acknowledgements This work was financially supported by the 2019 Research Project on Education and Teaching Reform in Universities of Hainan Province (No. Hnjg 2019–78, Hnjg 2019–73).

References

1. Zadeh, L.A.: Fuzzy set. Fuzzy Sets Syst. **8**, 338–353 (1965)
2. Song, Q., Chissom, B.S.: Forecasting enrollments with fuzzy time series-part I. Fuzzy Sets Syst. **54**, 1–9 (1993)
3. Jilani, T.A., Burney, S.M.A., Ardil, C.: Fuzzy metric approach for fuzzy time series forecasting based on frequency density based partitioning. In: Proceedings of World Academy of Science, Engineering and Technology, vol. 34, pp. 333–338 (2007)
4. Stevenson, M., Porter, J.: Fuzzy time series forecasting using percentage change as the universe of discourse. In: Proceedings of World Academy of Science, Engineering and Technology, vol. 55, pp. 154–157 (2009)
5. Saxena, P., Sharma, K., Easo, S.: Forecasting enrollments based on fuzzy time series with higher forecast accuracy rate. Int. J. Comput. Technol. Appl. **3**(3), 957–961 (2012)
6. Wang, H.X., Guo, J.C., Feng, H., et al.: A fuzzy time series forecasting model based on percentages. Front. Comput. Educ., 11–14 (2015)
7. Zhang, K., Wang, H.X., Wang, H.F., et al.: The time series prediction algorithm of enrollment based on the hesitancy degree correction rule of vague sets. ICIC Exp. Lett. **09**(05), 1311–1318 (2015)
8. Zhang, K., Shen, C., Gao, Q., et al.: Research on similarity metric distance algorithm for indoor and outdoor firefighting personnel Precision wireless location system based on vague set on UWB. IEEE ICCT **2017**, 1162–1165 (2017a)
9. Zhang, K., Shen, C., Gao, Q., et al.: Research on UWB precise indoor positioning in ship based on intuitionistic fuzzy. Adv. Eng. Res. **131**, 285–291 (2017b)

A Just-In-Time Private-Cloud Mobile-App-Based Announcement Portal (AP): A Hong Kong Case Study with Broad Application for Academic, Commerce, Government

Brian Siu

Abstract This paper describes how easy it is to generate a Just-in-Time (JIT) Private-Cloud Mobile-App-based Announcement Portal (AP) suitable for broad application in academic, commerce, and government organization. The AP enables speedy update by non-IT personnel of an organization. Viewing by organization staff using mobile phone is convenient through placing AP as a Mobile Phone App, for instant viewing of JIT Announcements. Administering user access can be made by non-IT staff who has remote access connection to the server for easy adding/deleting users using pre-set simple-to-use screens in mobile phone format. The paper shows the ease of development based on the Make-To-Order (MTO) methodology, the ease of testing using mobile phone with 4G or iPad with WIFI; and answers the question: "Why can't we use our Company Announcement Portal (CAP)?", by pointing out that reading CAP may be time consuming using multiple levels of access from company login to reaching the CAP, while the announcements are not placed in permanent storage (drop box) for easy reference. The paper describes production of nine AP for nine public funded academic institutions with immediate usability as a case study. The paper proposes further work in three areas of: workplace contribution, technology innovation, and community contribution with focus on mobile app innovation perspectives through the MTO methodology: with tools and techniques.

1 Introduction

1.1 Motivation for a Just-In-Time Announcement Portal (AP)

During June 2019 to October 2019, the Hong Kong's extradition bill proposal raised by the HK Government resulted in series of social events covering road block, mass transit railway disturbance, take-to-street confrontations with law enforcing body,

B. Siu (✉)
School of Continuing and Professional Education, City University of Hong Kong, Tat Chee Avenue, Kowloon Tong, Hong Kong, China
e-mail: dcbksiu@cityu.edu.hk

R. Kountchev et al. (eds.), *Advances in Wireless Communications and Applications*,
Smart Innovation, Systems and Technologies 191,
https://doi.org/10.1007/978-981-15-5879-5_27

and vandalism of commercial business and catering business outlets [1]. In this situation, organization chiefs, whether academic, commerce or government, need to inform their employees through daily announcements in order to ensure a safe working environment for employees' travel-to-work or work-from-home planning. Players in different socio-economic-political roles (district councilors, company directors, small and medium enterprise, catering companies etc.) also felt the need for a kind of Announcement Portal that provides similar function in a easy-to-use, efficient, and value-for-money solution. In addition, some organizations felt the need for a separate Announcement Portal that can provide a value-added service to their organization's Legacy Announcement Portal (such as the City First Bus Announcement Portal—CFBAP, or ABC College's College Announcement Portal—ABCAP) which provide discrete daily announcements, but which are not consolidated into a persistent (private-cloud drop box) store for easy reference; and which involve multiple steps of login to the organization's email system to read the message then losing sight of the message after some days. Therefore, some proposed for a database (persistent data) store of announcements where different levels of staff in the organization can trace the time series of announcements when needed. They also emphasize the need for immediate usability, best through smart phones.

1.2 The MTO Methodology Helps Make a Success with Speed and Efficiency

The MTO methodology was devised during mid 2016–mid 2019 [2–4] when SCOPE [5] proposed research activity to innovate mobile app systems to support eLearning for self-financing institutions programme (Figs. 1, 2). The MTO infrastructure consists of latest Microsoft tools covering Integrated Development Environment using the Visual Studio tool, Visual C# programming, Microsoft SQL Database Management, Microsoft Expression 4 Web design tools, which together leverage on

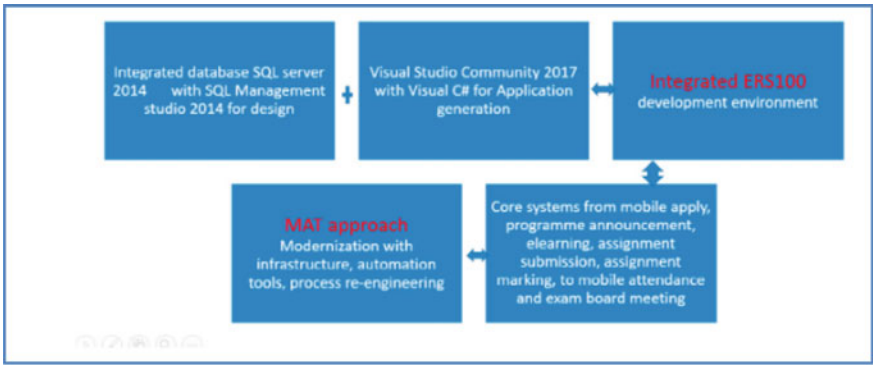

Fig. 1 MTO infrastructure [3]

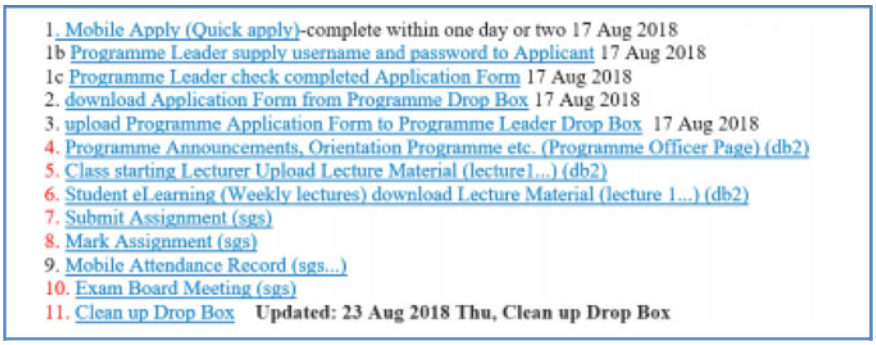

Fig. 2 Mobile-app generation using the MTO methodology [3]

the new technologies of HTML5, CSS 3, ASP.NET, PHP, JavaScript, XML + XSLT (their technical merits are beyond the scope of this paper).

The innovation by the MTO methodology resulted in a set of 11 core education systems (Fig. 2), from mobile apply to eLearning support, to assignment submission, to exam board meeting. These form a set of master templates which in simple terms are folders in the C: drive of the Windows 10 server. These template systems can be extended (Make-To-Order) for other mobile app.

1.3 The Make-To-Order Process for AP

The MTO environment is a Private Cloud Windows 10 server environment, running Microsoft SQL Server Database Management system, Visual Studio 2017 with Visual C#, and an Integrated Development Environment (which offers tools like button with programming logic inside). For mobile app user-interface design, Microsoft Web Expression 4 provides the mobile phone user-interface for entry. These, together with Microsoft's Remote Desktop Connection (plus the Cisco AnyConnect Secure Mobility Client) [6], enable work-from-home, thus helping to speed up development work. AP is created by modifying the core education systems in Fig. 2. AP access is made through https://144.214.178.236/ap then registering it as a mobile phone app.

The AP user interface is shown in Fig. 3. On the left, Upload Function by Organization Staff; View Announcement by Organization Employees. On the right, it shows viewing the Announcement Drop Box after login. The Announcements Drop Box is a folder in Windows 10 server's C drive. It stores word, pdf, audio (3 min or less), and video (30 s or less), where the audio size and video size was set by the Microsoft programming tools.

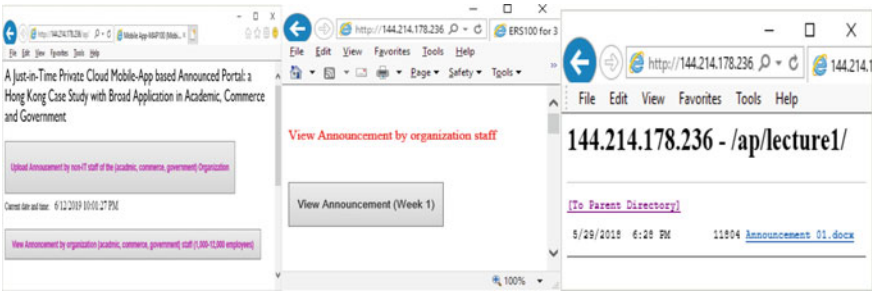

Fig. 3 Upload and view function

2 Testingate Usability of AP

2.1 Testing AP Using Mobile Phone (4G) and iPAD (WIFI)

We made an audio file (within 3 min), connected it to AP, uploaded the audio file using the username password of a Secretary, then viewed the announcement using the username password of an organization employee. Testing using an iPaD using WIFI in the Hong Kong Admiralty MTR station during lunch time shows it is fast, and easy to use. The behind technology is simple: login button, folder access (folders holding the Announcements as drop box in the C: drive storing PDF, word, audio, and video files).

2.2 Immediate Usability Case Study: Tailoring 10 AP for 10 Public Funded Academic Institutions

The Upload Function and View Function enable an organization to deliver announcement, let the employees view them through registering the Web address of AP (https://144.214.178.236/ap) on a mobile phone. AP's Immediate Usability is ready for extending to different organizations too. As a case study, the AP master set is duplicated to 10 AP (Table 1) for 10 academic institutions, with each institution having its own folder in windows server's C drive, while managing all database access through a central Microsoft Database Management System with different sets of username password for different institutions. It takes around two days in testing out the work.

Table 1 APs for 10 institutions

Institution	Mobile App Link
Hong Kong Baptist University	https://144.214.178.236/apbu
The Chinese University of Hong Kong	https://144.214.178.236/apcu
City University of Hong Kong	https://144.214.178.236/apcity
The Education University of Hong Kong	https://144.214.178.236/apedu
The University of Hong Kong	https://144.214.178.236/aphku
Lingnan University	https://144.214.178.236/apln
The Open University of Hong Kong	https://144.214.178.236/apopen
The Hong Kong Polytechnic University	https://144.214.178.236/appoly
The Hong Kong University of Science and Technology	https://144.214.178.236/apust
The Hong Kong Academy for Performing Arts	https://144.214.178.236/apapa

2.3 Discussion—The Choice Versus Speed of Access and Persistent Drop Box Storage

University and College Presidents might ask: "Why can't we use our own Company Announcement Portal (CAP)?". The answer is yes, but AP offers Speed and Efficiency plus Persistent Storage of Announcements in a Private Cloud Drop Box Persistent Storage environment, with instant access as compared to the multiple steps needed to connecting to a traditional CAP. Readers may try the link to the master AP https://144.214.178.236/ap.

To get a feel (through getting the username and password from the author), OR refer to the Videos—in YouTube Channel:

https://www.youtube.com/channel/UCclr6GAftYq0DNpOtuoVMXQ
OR Weibo Channel (for viewing in China)
https://www.weibo.com/siub12.

3 Conclusion and Further Contribution

3.1 Conclusion

The versatile feature of this AP is that the announcement format can be audio, PDF, word, video (though with limitations set by Microsoft tools, i.e., audio within 3 min, video within 30 s), there is ease of making extra copy of the app for different organization, and there is ease of modifying the app for different functions.

3.2 Further Work

With MTO, AP can be extended to form new mobile apps for other work (Table 2).

Table 2 Extending MTO and AP for other work areas

Work area	For whom?	What mobile app/task	Internal/external
(a) Workplace contribution	Internal colleagues of different job roles: IT, clerical support, programme admin. in SCOPE and university	(i) Workflow system for communications channel for cross team meeting (ii) User training and technology transfer to other Colleagues (iii) Facility office mobile app	For internal workplace: SCOPE [7], and university e.g., Facility office alert management mobile app (FOAM) [6]
(b) Technology innovation	Use case for Student I.T. Project, Possibility of joint study on setting up Mobile App Laboratory in college	(iv) Using AP as training material (v) Support Degree Program Practical Project (vi) Setting up mobile app computer room facility to promote practical usage of new technology	Possibility of Microsoft new product support, Joint investigation with colleagues in sister institution [8, 9]
(c) Community contribution (spare-time work)	Government, Political Party, OUR Hong Kong Foundation	(vii) Government survey system (viii) Political party survey (ix) Survey system for OUR Hong Kong Foundation	Survey platforms using Cloudflare [10–14]

Acknowledgements Thanks to the following who contributes to this paper: SCOPE initiation of mobile app research (Louis, Jason, Raymond, Patrick), SCOPE Network Administrator (Patrick) [5], Computing Services Centre Security Officer and Hot Line support on Remote Desktop Connection and Cisco Remote client work-from-home (Tsui and Tony) [6]; the inspiring discussions with Fred [8, 15] and Brian [9, 15].

References

1. Instant News on smart phone on Hong Kong's Social Events: HK TVB, Cable TV, RTHK Hong Kong 32. Accessed Jun–Nov, 2019
2. Brian SIU, Invited Presentation (on topic of Drop Box systems supporting eLearning for academic staff and students) to Federation for Self-Financing Tertiary Education and Hong Kong Council for Accreditation of Academic and Vocational Qualifications Conference (theme: Enhancing Student Learning Experience) November 2016
3. Brian SIU, Modernizing I.T. Applications. In: 9th Annual International Congress of Information and Communication Technology, Jan 11–13: Nanning. Guangxi, China (2019)
4. Brian SIU (2018) Developing drop box systems for non-eLearning based tertiary programmes—a Hong Kong case study with broad relevance. In: 8th international congress in information and communications technology, Xiamen, Jan 27–28
5. SCOPE. School of Continuing and Professional Education, City University of Hong Kong
6. City University of Hong Kong, Computing Services Centre, Cisco Remote Connect software; proposed Facilities Management Function, FOAM-Facility Office Alert Management Mobile App linking all Security staff who can upload with smart phone messages to the system, while Director of Facilities Management can view the messages instantly online with smartphone, a process similar to the function of AP
7. Strategic Workshop of SCOPE, 25 October 2019 Hotel Alva, Shek Mun. (Workshop Outcome—Process and Quality Improvement, Communications Channel for Cross-Team Meeting)
8. Fred S, Microsoft National Technology Officer, in Applied Education Forum
9. Brian L, Hong Kong College of Technology, in Applied Education Forum
10. Richard LAU. Assistant Researcher. OUR Hong Kong Foundation
11. Gibson LAU. Senior Officer, Advocacy. OUR Hong Kong Foundation
12. Victor Kwok. Researcher Head, Education & Youth. OUR Hong Kong Foundation
13. OUR Hong Kong Foundation, United Hong Kong Fund, a Hong Kong non-profit think tank established in 2014 by former chief executive
14. Cloudflare, with Security and Internet Availability service. https://www.cloudflare.com/
15. Applied Education Forum, 5 Dec 2019, Grand Standford Hotel, Hong Kong

Development and Application of Multi-functional Intelligent Robot Motion Chassis

Sun Hao, Liu Yongcheng, Ma Xiaolin, Wang Jing, Wang Mingrui, Chen Tao, and Wang Chao

Abstract Motion mechanism of mobile robot was studied and analyzed deeply in this paper. Based on this, two general chassis for omnidirectional mobile robot were designed, including a wheeled chassis and a crawler chassis. These two kinds of chassis can meet the functional requirements of all kinds of mobile robots because of the design idea of modularization and serialization. Then, dynamic vibration characteristics of the chassis were proposed. Afterward, the dynamic performance was analyzed after the robot which was impacted and vibrated by various uncertain factors, which could provide the basis for the arrangement of sensors and the damping. Finally, these two kinds of chassis were applied to the indoor live-working robot and the substation fire-fighting robot. The application results show that there was a good application effect on these two kinds of chassis, which can meet the actual needs.

1 Introduction

Mobile robots have been increasingly used in different fields such as industrial manufacture, military organizations, and public service communities [1–4]. High mobility on various environments is the critical requirement of a mobile robot [5, 6]. As a result, how to improve the passing ability of chassis in complex terrain environment has been a hot topic for experts and scholars both at home and abroad. According to the complex road conditions, the current mobile chassis can roughly be divided into wheeled, tracked, and legged chassis [7–9].

S. Hao · L. Yongcheng (✉) · M. Xiaolin · W. Mingrui
Shandong Dalai Intelligent Technology Co., Ltd., Zaozhuang, Shandong Province, China
e-mail: 892856420@qq.com

S. Hao · L. Yongcheng · M. Xiaolin · W. Jing · W. Mingrui · C. Tao · W. Chao
Shandong Industrial Technology Research Institute of Zhejiang University, Zaozhuang, Shandong Province, China

S. Hao · L. Yongcheng · M. Xiaolin · W. Mingrui
Shandong Reapdaro Automation Technology Co., Ltd., Jinan, Shandong Province, China

R. Kountchev et al. (eds.), *Advances in Wireless Communications and Applications*,
Smart Innovation, Systems and Technologies 191,
https://doi.org/10.1007/978-981-15-5879-5_28

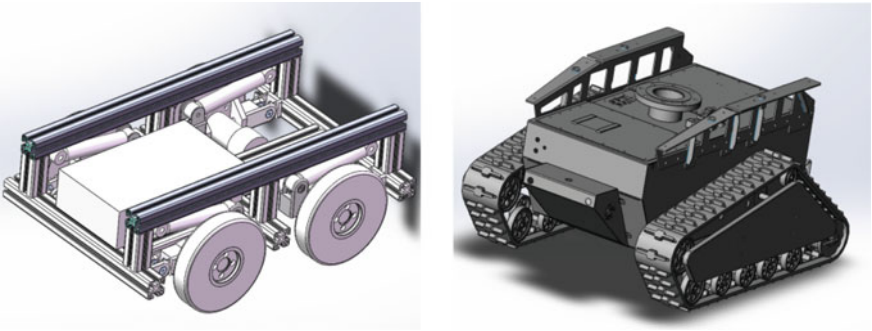

a. Wheeled chassis b. Crawler chassis

Fig. 1 Two chasses

With the progress of science and technology, more and more attention has been paid to the research of robot technology, especially in-service robot, inspection robot, detection robot, and other robot fields [10].

2 Chassis Structure

Two kinds of universal chassis were designed in this paper, including wheel type and track type, which are shown in Fig. 1.

The chassis mainly included motor assembly, power supply system, damping system, frame, control system, etc. The motor assembly provided the driving force for the chassis, and the control system integrated the robot sensor, signal receiving, and processing functions.

3 Research of Random Vibration Theory

The excitation of random vibration is an aperiodic load, which has an uncertain function relationship with time. Therefore, the excitation of the system needs to be described by the probability and statistics characteristics of the load. The ground unevenness, like the random vibration waveform, can be regarded as the sample function of the stationary random process, and the frame can be excited by applying the power spectral density [9, 11–13].

The power spectral density is the statistical result of the response of the structure under the random dynamic load excitation, and it is the distribution of the total root mean square of the random variable in the frequency domain, and meanwhile, it is a measure of the vibration power size in the unit frequency band. The expression is [9]:

$$G_q(n) = G_q(n_0)\left(\frac{n}{n_0}\right)^{-w} \tag{1}$$

where n is the space frequency (reciprocal of wavelength λ), m^{-1}, indicating how many wavelengths are included in the length per meter; n_0 is the reference space frequency, $n_0 = 0.1\ ^{\mathrm{m}-1}$; $G_q(n_0)$ is the road roughness coefficient (value of road spectrum when frequency value is n_0), which is usually taken according to the statistical results; w is the frequency index (slope of oblique line on double logarithmic coordinate), and value of w is two usually [14].

According to the literature [9], power spectral density can be expressed as:

$$G_q(f) = \frac{1}{u}G_q(n_0)\left(\frac{n}{n_0}\right)^{-2} = G_q(n_0)n_0^2\frac{u}{f^2} \tag{2}$$

where u is the velocity of the robot.

According to the first derivative and second derivative of longitudinal length I of through unevenness function $G_q(f)$, velocity power spectrum and acceleration power spectrum of space frequency can be expressed as follows:

$$\begin{cases} G_{\dot{q}}(f) = (2\pi f)^2 G_q(f) = 4\pi^2 G_q(n_0)n_0^2 u \\ G_{\ddot{q}}(f) = (2\pi f)^4 G_q(f) = 16\pi^4 G_q(n_0)n_0^2 u f^2 \end{cases} \tag{3}$$

In order to simplify the calculation, the excitation of each wheel is simplified to the same, and the power spectral density value input by each roller is the same. In the literature, the pavement roughness coefficient $G_q(n_0)$ is taken as the value of grade C pavement when calculating the power spectral density [14, 15], while in another literature, the pavement roughness coefficient $G_q(n_0)$ is taken as the weighted value of asphalt road, gravel road, and rural soil road [14, 16].

4 Calculation Method of Chassis Input Excitation

The input of ground excitation was shown in Fig. 2 when the chassis was moving, 1, 2, 3, and 4, respectively, represented the four supporting wheels or wheels of the machine. $q_i(I)$ was the ground unevenness. $x(I)$and$y(I)$ were the ground unevenness function of the left and the right track. I was the length coordinate of the road surface. Self-spectrum and mutual generalization of $x(I)$, $y(I)$ were $Gxx(n)$, $Gyy(n)$, $Gxy(n)$, $Gyx(n)$.

The unevenness functions of the two front rollers were $q_1(I) = x(I)$, $q_3(I) = y(I)$; Since the lag distance of the two rear rollers is the wheel base L in the coordinate direction of the ground, we can get the following relational expression: $q_2(I) = x(I - L)$, $q_4(I) = y(I - L)$. Therefore, the Fourier transform of the ground roughness function of the four rollers were as follows [11]:

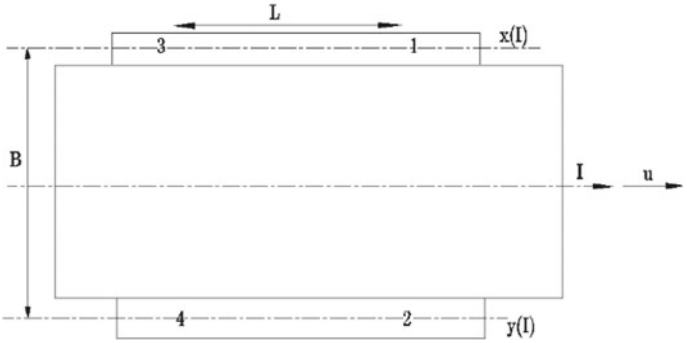

(L was the tread, B was the width of wheel centerline, $x(I)$ and $y(I)$ were the ground unevenness function of the left and the right track, I was direction of datum plane, u was the speed)

Fig. 2 Input excitation in operation

$$\begin{cases} F_1(n) = F[q_1(I)] = F[X(I)] = X(n) \\ F_2(n) = F[q_2(I)] = F[X(I-L)] = X(n)e^{-j2\pi nL} \\ F_3(n) = F[q_3(I)] = F[Y(I)] = Y(n) \\ F_4(n) = F[q_4(I)] = F[Y(I-L)] = Y(n)e^{-j2\pi nL} \end{cases} \tag{4}$$

where $F_i(n)$ were the Fourier transform of space frequency n; $X(n) and Y(n)$ were the Fourier transform of $x(I)$ and $y(I)$, which were marked as $F[x(I)]$, $F[y(I)]$.

The self-spectrum of four roller input and the cross spectrum of four roller could not be ignored when four input vibration transmissions were considered in the chassis [2, 7, 10]. As a result, there were 16 spectral quantities in total, labeled as $G_{ik}(n)(i, k = 1, 2, 3, 4)$, and 12 of them were conjugated [16].

$G_{ik}(n)$ was represented as follows:

$$G_{ik}(n) = \lim_{T\to\infty} \frac{1}{T} F_i^*(n) F_k(n) \tag{5}$$

As a result:

$$\begin{cases} G_{11}(n) = G_{22}(n) = G_{xx}(n) \\ G_{33}(n) = G_{44}(n) = G_{yy}(n) \\ G_{12}(n) = G_{21}^*(n) = G_{xx}(n)e^{-j2\pi nL} \\ G_{34}(n) = G_{43}^*(n) = G_{yy}(n)e^{-j2\pi nL} \\ G_{14}(n) = G_{41}^*(n) = G_{xy}(n)e^{-j2\pi nL} \\ G_{32}(n) = G_{23}^*(n) = G_{yx}(n)e^{-j2\pi nL} \\ G_{13}(n) = G_{31}^*(n) = G_{xy}(n) \\ G_{42}(n) = G_{24}^*(n) = G_{yx}(n) \end{cases} \tag{6}$$

The cross spectrum between left and right wheel traces could be expressed as [9]:

$$G_{xy}(n) = \left|G_{xy}(n)\right| e^{-j\varphi_{xy}(n)} \tag{7}$$

where $\left|G_{xy}(n)\right|$ was the cross-spectrum amplitude of $x(I)$ and $y(I)$; $\varphi_{xy}(n)$ was the phase spectrum of $x(I)$and$y(I)$.

From formula (7), the coherence function of two-wheel traces could be expressed as:

$$\mathrm{coh}_{xy}^2(n) = \frac{\left|G_{xy}(n)\right|^2}{G_{xx}(n)G_{yy}(n)} \tag{8}$$

The linear correlation degree between components with frequency n was described by the coherence function in the frequency domain $x(I)$and$y(I)$. If the value of $\mathrm{coh}_{xy}^2(n)$ was 1, which was indicated in $x(I)$and$y(I)$, the amplitude ratio and phase difference between components with frequency n will always remain unchanged, namely linear complete correlation; when value of $\mathrm{coh}_{xy}^2(n)$ is 0, indicating linear independence, that is to say random change. The difference of the amplitude and phase difference of the left and right track unevenness will lead to the roll angle vibration.

From formula (8), we can get the relationship as follows [9],

$$G_\theta(n)/G_q(n) = \frac{2}{B^2}\left[1 - \mathrm{coh}_{xy}(n)\right] \tag{9}$$

when $G_{xx}(n) = G_{yy}(n) = G_q(n)$ and $\phi_{xy}(n) = 0$, we could get the formula: $G_{xy}(n) = G_{yx}(n) = \mathrm{coh}_{xy}(n)G_q(n)$ according to the definition expression of coherence function.

Finally, the input spectrum matrix of the road to the machine can be expressed as:

$$G_{ik}(n) = G_q(n)\begin{bmatrix} 1 & e^{-\mathrm{j}2\pi nL} & \mathrm{coh}(n) & \mathrm{coh}(n)e^{-\mathrm{j}2\pi nL} \\ e^{-\mathrm{j}2\pi nL} & 1 & \mathrm{coh}(n)e^{-\mathrm{j}2\pi nL} & \mathrm{coh}(n) \\ \mathrm{coh}(n) & \mathrm{coh}(n)e^{-\mathrm{j}2\pi nL} & 1 & e^{-\mathrm{j}2\pi nL} \\ \mathrm{coh}(n)e^{-\mathrm{j}2\pi nL} & \mathrm{coh}(n) & e^{-\mathrm{j}2\pi nL} & 1 \end{bmatrix} \tag{10}$$

From the above formula (10), it could be seen that there was a certain theoretical relationship between the excitation input of the four wheels. This modified formula provides a theoretical basis for the subsequent optimization of the chassis. During the research process, we can test the vibration of one of the wheels and deduce the vibration of other wheels according to this relationship. So, the test time can be reduced.

a. Indoor live-working robot b. Fire-fighting robot

Fig. 3 Field application

5 Field Application

Finally, the above two kinds of chassis were applied in the field. The wheeled chassis was applied in the field of indoor live working in Zaozhuang 220 kV Xizhong substation. The crawler chassis was applied in the field of substation fire-fighting robot, as shown below. The fire-fighting robot developed in this project has improved the fire prevention and emergency response capacity of the substation, which presented a good prospect of promotion and application. This fire-fighting robot has reached the international advanced level (Fig. 3).

After three months of trial operation, there was no abnormal condition occurred such as structural vibration caused by bolt looseness and vibration. From the application on these two kinds of robots above, it was proved that the universal chassis design in this paper was reasonable and has good damping effect. On the other hand, the vibration characteristics of these two chassis could meet the requirements.

6 Conclusion

The universal chassis of omnidirectional mobile robot for narrow space was designed, including a wheeled chassis and a crawler chassis;

This paper analyzed the dynamic characteristics of chassis in the course of driving and then discussed the dynamic performance of the chassis after the robot was impacted or vibrated by various uncertain factors, which could provide the basis for the arrangement of sensors and the damping for the robot.

Finally, two kinds of chassis were applied to the indoor live-working robot and the substation fire-fighting robot. The application results show that there is a good application effect on these two kinds of chassis, which can meet the actual needs.

Acknowledgements Fund projects: Joint fund of industry, university and research of Zaozhuang, *Research and application of key technologies for indoor live working robot*; Key R & D plans of Shandong Province (Public science and Technology) (2019GGX104061).

References

1. Li, K., Voicu, R.C., Kanhere, S.S., et al.: Energy Efficient legitimate wireless surveillance of UAV communications. IEEE Trans. Veh. Technol. **68**(3), 2283–2293 (2019)
2. Ye, W., Li, Z., Yang, C., et al.: Vision-based human tracking control of a wheeled inverted pendulum robot. IEEE Trans. Cybern. **46**(11), 2423–2434 (2016)
3. Zhu, Y., Fei, Y., Xu, H.: Stability analysis of a wheel-track-leg hybrid mobile robot. J. Intell. Robot. Syst., 1–14 (2017)
4. Li, L., Yan, S., Yu, X ., et al:. Robust multiparton detection and tracking for mobile service and social robots. IEEE Trans. Syst. Man Cybern Part B (Cybern.) **42**(5), 1398–1412 (2012)
5. Jung, S., Kim, et al.: Improvement of step-climbing capability of a new mobile robot RHyMo via kineto-static analysis. In: Mechanism and Machine Theory: Dynamics of Machine Systems Gears and Power Transmissions Robots and Manipulator Systems Computer-Aided Design Methods, vol. 114, pp. 20–37 (2017)
6. Li, Z., Ma, S., Li, B., et al.: Analysis of the constraint relation between ground and self-adaptive mobile mechanism of a transformable wheel-track robot. Sci. China Technol. Sci. **54**(3), 610–624 (2011)
7. Jiang, H., Xu, G.Y., Zeng, W., Gao, F.: Design and kinematic modeling of a passively-actively transformable mobile robot. In: Mechanism and Machine Theory, vol. 142, p. 103591 (2019)
8. Wang, M.D., Zhao, Y.Q., Zhu, J.G.: Principle of tank driving. National Defense Industry Press, Beijing (1983)
9. Yu, Z.S.: Automobile Theory. China Machine Press, Beijing (2009)
10. Ciciliano.: Robot Manual (2013)
11. Luoyang Tractor Research Institute: Ministry of Mechanical and Electronic Industry: Tractor Design Manual, Vol. I. China Machine Press, Beijing (1994)
12. Editorial board of mechanical engineering material performance data manual: Mechanical engineering material performance data manual. Mechanical Industry Press, Beijing (1995)
13. Pu, L.G.: Mechanical Design, 8th edn. Higher Education Press, Beijing (2006)
14. Yang, F.Z., Lu, Y., Liu, Y.C., Lan, Y.B., Chen, Z., Wang, Z.: Research and design of tiny and remotely controlled electric tractor used in greenhouse. M.A.C.E., 969–972 (2012)
15. Marklund, P.O., Nilssom, L.: Optimization of a car body component subjected to side impact. Struct. Multidisc. Optima **21**, 383–392 (2001)
16. Ao, K., Niiyama, J., Matsui, T., Hara, K., Nakamura, M.: Analysis of torsional stiffness share rate of truck frame. SAE Technical Paper Series **19**, 18–21 (1991)